Author:
Zhao, Xingjie

Title:
Stress and failure analysis of adhesively bonded joints.

STRESS AND FAILURE ANALYSIS OF ADHESIVELY BONDED JOINTS

by

XINGJIE ZHAO

A dissertation submitted for the Degree of Doctor of Philosophy at the University of Bristol,
Department of Mechanical Engineering
June 1991

SUMMARY

This thesis presents the results of a study into the mechanics of stresses in adhesive layer and the failure of adhesively bonded lap joints.

A brief survey was made of the existing methods on the stress analysis of adhesively bonded lap joints. Following this is a discussion of the mechanics of adhesively bonded lap joints. The existence of stresses and factors affecting these stresses are presented in physical terms.

A new method is presented for the determination of bending moments at the ends of the overlap for single lap joints. This method is accurate for joints with either identical or different adherends.

A new procedure combining the analytical and numerical methods was proposed to obtain stresses in the adhesive layer accurately and efficiently. The reason why analytical methods yield somewhat *half* the real *peel* stresses in the adhesive layer in double lap joints has been established. Some improvements in the determination of peel stresses in the adhesive layer in double lap joints have been made.

A three dimensional stress analysis was carried out to study the stress distribution across the joint width.

An intuitive and numerical study was made into the mechanics of the longitudinal stresses in the adhesive layer.

An elastic-plastic stress and strain analysis has been performed with FEM on joints bonded with radii adherends to study the effect of the rounding of the adherend corners on the stress distribution in the adhesive layer.

Some study into the failure process and failure modes were performed. Tests were made on both double and single lap joints.

Finally, the failure criteria concerning strength predictions of adhesively bonded joints were reviewed. A new criterion was proposed for the prediction of joint strength.

List of Tables

List of Figures

Memorandum

The accompanying dissertation entitled "Stress and failure analysis of adhesively bonded lap joints" is submitted in support of an application for the degree of Doctor of Philosophy in Engineering at the University of Bristol.

The dissertation is based on independent work by the candidate - all contributions from other workers have been acknowledged fully within the dissertation. The supervisor's contributions were that normally made in a British University.

None of the work described has been, or is being, submitted for any other degree or diploma to this or any other University. A part of the work has formed the basis of two conference papers.

I hereby declare that the above statements are true.

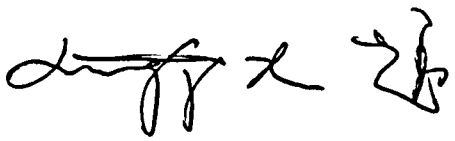

X. Zhao

Acknowledgements

I would like to thank Prof. R. D. Adams for his supervision and encouragement throughout this work. I am grateful to the other academic and technical staff of the Department of Mechanical Engineering who provided advice and assistance, particularly Mr. J. Skinner for producing the adhesive and joint specimens. I also wish to thank Dr. V. Mallick for many helpful discussions.

I would like to acknowledge the financial support from the Ministry of Education of the Chinese Government and the British Council.

Finally, I would like to thank my parents for their enormous encouragement, without which this work would not have been completed.

Notation

E	-	Young's Modulus
G	-	Shear Modulus
μ	-	Poisson ratio
M	-	Bending moment
P	-	Tensile load
T	-	Tensile load
Q	-	Shear force or generalised forces
k	-	Bending moment factor
c	-	Half overlap length
D	-	Flexural rigidity
ζ	-	$\sqrt{(P/D)}$
h	-	Adherend thickness
w	-	Displacement normal to joint load plane
W	-	Strain energy integration
σ	-	Tensile stress tensor
τ	-	Shear stress tensor
ϵ	-	Normal strain tensor
γ	-	Shear strain tensor
Θ	-	Adherend rotation
U	-	Strain energy
J	-	Sum of hydrostatic stress components
Y	-	Yield stress derived from uniaxial tests
Π_c	-	Complementary energy
[K]	-	Stiffness matrix
[K]	-	Stiffness matrix
[N]	-	Modulus array
[D]	-	Modulus array
$[\sigma]$	-	Stress array
$\{\beta\}$	-	Generalised stress tensor

[P]	-	Matrix defining stresses
[F]	-	Applied forces
F	-	Nodal forces
V	-	Volume
[H]	-	Matrix defining strain energy in terms of stresses
{u}	-	Displacements
{q}	-	Generalised displacements
{Q}	-	Generalised displacements for the whole structure.
[L]	-	Containing coordinates of element surface
S	-	Surface force components
S	-	The ratio of the yield stress in compression and tensile
[S]	-	Matrix containing surface force components
[R]	-	Matrix containing coordinates of the surface
[T]	-	Matrix in defining complementary energy
T	-	Tensile load
P	-	Complementary energy
l	-	Adherend length
L	-	Total length of the joint
a	-	Angle between load line and joint central line
n	-	Direction cosine of surface normal
{f}	-	Force vector
{F}	-	Force vector for the whole structure
A	-	Surface area

SUBSCRIPTS

1	-	Upper adherend sheet or horizontal direction
2	-	Lower adherend length or vertical direction
x	-	Parallel direction to joint loading plane
y	-	Transverse direction to joint loading plane
z	-	Transverse direction across the joint width

a	-	Adhesive
GR	-	Goland and Reissner
HS	-	Hart-Smith
VM	-	von Mises
max	-	Maximum value

Chapter 1

INTRODUCTION

1.1 BACKGROUND

Structural adhesives have been becoming increasingly important in engineering applications. This is not only because of advances in adhesive manufacturing technology, but also in the engineering demands which the conventional joining technologies cannot always fulfil. In order to explore fully joining technology based on adhesives, basic research is essential to understand the properties of adhesives, the adhesion mechanisms, and the properties of bonded joints. The science of adhesion is generally an inter-disciplinary subject, involving chemistry, physics, and mechanics. Because the present work is mainly concerned with the mechanical aspects, no attempt is made here to address in depth the chemical and physical aspects. More information can be found in recently published reviews (Wake, 1982, Matthews *et al*, 1982, Adams and Wake, 1984, and Kinloch, 1987) covering all the disciplines.

Structural adhesives, commonly epoxies, are generally organic materials. The characterisation of their mechanical properties is essential before they can be considered in engineering applications. Adhesives are usually used as a thin layer between two stiff substrates. This makes material tests extremely difficult and leads to the fact that there are no satisfactory standardized methods to test adhesives (Kinloch, 1988).

There are many adhesion theories concerning the mechanisms of two different separate materials joined together. In order for the adhesion between the two materials to take place, at least one of the materials must be in liquid state initially so that intimate contact can be achieved. The liquid must be cured later so as to form a stable structure and to carry loads. Normally, the adhesive is used to fill the gap between two substrates. Once the adhesive is cured, the bond is made.

Bonded joint tests are extremely important in assessing the performance of joints before their engineering usages. There are two types of joint test, one to determine the material

properties and the other to evaluate joint strength. Most tests *in situ* do not permit the basic engineering properties of the adhesive to be deduced. However, tests *in situ* are widely used to assess the joint strength and to verify various theories with regard to failure predictions. In order to understand what is actually tested, stress and strain analyses are necessary. Various theories exist to model the test specimen, ranging from analytical to numerical methods, all of which are based on continuum mechanics. The analysis methods will be discussed in detail in Chapter 2. It will be shown that the stress state can be easily obtained with the existing methods. However, there are still some unsolved debates involving the modelling of bonded joints. First, what material properties should be used? Although the material properties in the bulk form are well known, whether or not they are the same as *in situ* especially near the ends of joints, is still under investigation. Furthermore, the material properties at or near the interface between the adhesive and the substrates have received little attention. Secondly, stress analysis methods fail to give solutions at the ends of the joints where the stresses or strains can be singular. Physically, these stresses or strains cannot be singular and therefore it is argued that at what distance away from these singular points the stresses or strains given by these analysis methods truly represent the stress state. This is particularly important for the subsequent failure predictions based on stresses or strains.

1.2 OBJECTIVES

From the above discussions, it may be seen that stress analysis is extremely important in predicting joint performance because of the difficulties involved in the experiments. With the available analysis techniques, proper modelling of the joints is essential in order to analyse and understand the performance of the joints satisfactorily. Finally, an understanding of the failure process and therefore failure predictions are required in engineering applications. The objectives of the present work are thus:

(a). Improvements in the stress analysis method;

(b). Improvements in the modelling of a joint;

(c). Understanding of the mechanics of stresses in lap joints

(c). Understanding of the failure process;

(d). Failure predictions of joints.

1.3 OUTLINE OF THE WORK

The relative ease of preparation and its application in engineering has made the single lap joint one of the most widely used test specimens. It has therefore been chosen for this work. Two adhesives have been used, one brittle (MY750 see Chapter 8) and one ductile (CTBN see Chapter 8). The properties of the two adhesives, typical of those used in industry, are shown in Chapter 8. The adherends used are an aluminium type T4014 whose properties are also given in Chapter 8.

Chapter 2 presents a literature review, in which the mechanics of lap joints is discussed.

Up to this time, most of analytical methods have concentrated on the determination of stresses in the adhesive layer. The research on the bending moments required at the ends of the overlap has largely been ignored. Little work has been done so far on the bending moments at the ends of the overlap for joints with different adherends. A new method, which can be used for either identical or different adherends, is proposed and demonstrated in Chapter 3.

All the analytical methods for the stress analysis of single lap joints are a two-step procedure, the whole joint being analysed followed by the determination of the stresses in the adhesive layer. In the numerical FE approach, only one-step is used, in which large displacements are usually included. A new method, which utilises the two-step analytical method combined with FE, is developed in Chapter 4.

Most of the analyses in this field make the plane strain assumption, which is generally applicable to the centre of the joint across the joint width. To improve the modelling of the joint, a 3D analysis based on FE has been undertaken in Chapter 5. New features absent in the 2D analysis are presented there.

Chapter 6 studies the Poisson's ratio effects on the longitudinal stresses in lap joints. It explains the existence of longitudinal stresses in lap joints.

Chapter 7 presents a study of the effects of radiused corners of adherends on the stress and strain distributions in the adhesive layer for brittle and ductile adhesives.

Material characterisation of the adherends is presented in Chapter 8. Failure studies on both single and double lap joints are given. Tests on the strength are also included.

In Chapter 9, various failure criteria have been assessed and a new failure criterion is proposed with which strength predictions can be made.

In the final Chapter, Chapter 10, some general discussions are presented and suggestions are made for future work.

Chapter 2

NATURE OF STRESSES IN LAP JOINTS

2.1 APPROACHES TO STRESS ANALYSIS FOR LAP JOINTS

The nature of stresses or strains in an adhesively bonded joint is essential for the understanding of joint performance. Based on the stresses or strains, a failure study can reveal the underlining parameters which govern the failure and an appropriate failure criterion may be developed to predict joint strength. Such information is extremely important for engineering applications, especially at the present time when such information is very limited in industry. Stress distributions are also necessary in joint tests to provide the information as to what is actually tested. Stress distributions in an adhesively bonded joint can be determined either experimentally or theoretically. Experimental measurements in real adhesively bonded joints are extremely difficult, particularly when the adhesive layer is thin. Because of these experimental difficulties, theoretical analysis is an effective alternative for the determination of stresses or strains in the adhesive layer and the analysis does give some ideas on the performance of joints.

2.1.1 Experimental Approach

Experiments on the determination of stresses or strains have been performed with various techniques. McLaren and MacInnes (1958) performed a photoelastic study on a lap joint. They showed that the highest peel and shear stresses are near the ends of the overlap of the joint. More work has been done later to determine the stresses in the adhesive layer with this technique (e.g. Hahn, 1960, Harborne and Howard, 1989). However, this technique is too crude to measure the strains in the adhesive layer quantitatively. Another optical technique, termed Moiré Interferometry pioneered by Post (1987), offers the potential for the measurements in the whole adhesive layer (Post *et al*, 1988). It is effective and a quantitative study may be undertaken by using this technique. However, the measurements can only be made at the surfaces of the joint. More recently, new measuring technology has been developed to measure peel strains in single lap joints by using etched KYNAR

piezoelectric film sensors (Dillard, 1989). However, all the experimental techniques face the problem that strain concentrations are very difficult to measure, although they are essential to verify the various stress analysis theories reviewed later.

Another simple model was proposed by Adams *et al* (1973) who used a rubber model to represent the adhesive. The experimental results of displacements agreed well with the corresponding FE analysis. They also showed that the stress concentration at the adherend corner was significant and the directions of the maximum principal stresses were about 45^0 to the applied load.

2.1.2 Theoretical Approach

Theoretical stress analysis is based on continuum mechanics which requires the satisfaction of force equilibrium, displacement compatibility, constitutive equations, and given boundary conditions for the whole structure under analysis. Solutions satisfying the above conditions are termed analytical. However, such solutions are extremely difficult to obtain, except for simple structures. Numerical methods, which are generally approximate in nature, have therefore gained ground in engineering applications. For lap joints, which have simple geometry but may have dissimilar materials, analytical solutions are obtainable for linear-elastic materials with some assumptions on the stress state in the adhesive and adherends. Obviously, they encounter some difficulties when non-linear materials or complex geometry, such as tapered adherends, are present. They also suffer from the inherent simplifications made before the solutions are attempted. Numerical methods, on the other hand, have developed dramatically with advances in computer technology. FEM, one of the various numerical methods in engineering, has been well developed and has gained universal acceptance since it facilitates more complete analyses than are otherwise possible. However, FEM usually needs a powerful computer and experienced personnel. Because both analytical and FE methods have advantages and disadvantages and have been used parallel in practice, both of them are reviewed below.

Numerous reviews have been conducted in this literature by Sneddon (1961), Kutscha (1964), Grant *et al* (1983), Adams and Wake (1984), and Kinloch (1987), etc. No attempt is

made here to repeat these reviews. However, the mechanics of lap joints is emphasized, which is felt to be somehow ignored by most of the reviews.

2.2 ANALYSIS OF AN ADHESIVE JOINT: THE PROBLEM

The basic geometry of a lap joint is shown in Figure 2.1. The two adherends are joined together by a thin layer of adhesive. The joint is subjected to tensile forces as shown in the Figure. The basic problem is to determine the stress state in the adherends and, in particular, in the adhesive layer. Because of the load eccentricity, the overlap will rotate under load. Because the transverse deflection of the joint is caused by the lateral tension, a stress-stiffening model with large displacements is required and the tensile stresses in the adherends play an important role in determining the rotation of the overlap. Also two or more than two materials are used in a joint and these materials may deform plastically under load. All of these factors make an analytical solution extremely difficult, if not impossible. By studying the experiments on lap joints, it may be seen that large rotations usually occur at the ends of the overlap. The adherends are stretching and bending due to tensile stresses in them and the overlap does not deform much compared with the adherends outside the overlap. This observation much simplifies the analysis, which can then be separated into a two-step procedure. Firstly, the overlap may be treated as a rigid solid with the adherends as elastic plates under bending and stretching. Once the stresses at the ends of the overlap have been approximated with good accuracy, the overlap can then be treated as a two dimensional problem with small displacements. Even so, exact solutions to the stresses in the adhesive layer are still very difficult to obtain because the overlap has dissimilar materials and the boundary conditions applied to the ends of the overlap are complicated. Further assumptions are needed to simplify the governing differential equations in order to seek solutions. All the analytical methods currently available are based on the above process, although different methods have different assumptions. The deriving of the stresses applied to the ends of the overlap is presented in Chapter 3. Discussion here are then made on the solutions of the stresses in the overlap region.

Exact solution to the state of stresses in a lap joint is very difficult, if not impossible. This is because the joint has different materials, complicated geometry and the transverse deflections resulting from the tensile forces. Assumptions are therefore inevitable in order to seek simple analytical solutions.

2.3 ANALYTICAL SOLUTIONS

2.3.1 Volkersen's solution

Volkersen (1938) was among the first to develop a solution to the stress state in the adhesive layer. By studying the behaviour of a single lap joint, he assumed that the adherends are simply in tension, whilst the adhesive is in pure shear. Based on this assumption he developed an analytical solution to the shear stress state in the adhesive layer. Although initially his method was meant for single lap joints, the method is actually only applicable to double lap joints. In single lap joints, the adherend bending introduces a large amount of peel stress in the adhesive and the adherends cannot be in simple uniform stretching. Also, Volkersen's theory predicted that the adhesive shear stresses are maximum at the ends of the overlap, while the shear stresses should in fact be zero because of the free-shear surfaces at the ends of the overlap.

2.3.2 Goland and Reissner

The peel stresses in the adhesive of a single lap joint were first analysed by Goland and Reissner (1944) where they took the effect of bending moments and joint rotation into account. They showed that there were net bending moments at the ends of the overlap because of the load eccentricity applied to the joint as shown in Figure 2.1. They further demonstrated that the bending moments were reduced from the initial values due to the rotation of the joint. They used a cylindrically bent plate theory, combined with axial loading, to develop a formula for the evaluation of the bending moments at the ends of the overlap. Having obtained the bending moments at the ends of the overlap, there are two types of stress solution in the adhesive layer for very stiff and for very flexible adhesives, respectively. For very stiff adhesives, they used plane strain elasticity theory, assuming that

the joint is homogeneous with the stiffness of the adhesive being the same as the adherends. For very flexible adhesives, however, they treated the adherends as cylindrically bent plates and the adhesive as a system of infinitesimal coil springs positioned between the two adherends. It should be noted, for reasonably long overlaps, that their theory is still applicable, although they did not consider the rotation of the overlap region in the derivation of the internal stresses as pointed out by Benson (1969). The reason is that the stiffness of the overlap is much larger than either adherend, and therefore the effect of the rotation is weak in the overlap region for reasonably long overlaps. They showed that large peel stresses existed in the adhesive layer for single lap joints. This is easy to understand because the net bending moment at the end of either adherend needs to be balanced by the moment introduced by the shear stresses, acting at the interface between the adherend and adhesive, and by the peel stresses. It should also be noted that their two-step procedure is the foundation of later analytical solutions for single lap joints. However, in their second approximation, their method has strong limitations. The following two criteria need to be satisfied to use their solutions.

$$\frac{tE}{hE_a} \leq 0.1, \quad \frac{tG}{hG_a} \leq 0.1 \tag{2.3a}$$

$$\frac{hE_a}{tE} \leq 0.1, \quad \frac{hG_a}{tG} \leq 0.1 \tag{2.3b}$$

where t and h are the adhesive and the adherend thickness, E & G and E_a & G_a are the adherend and adhesive Young's and shear moduli. Adhesives satisfying the first criterion are generally used in wooden joints, whereas the second criterion is applicable to metal joints. For a typical lap joint, $h_1=h_2=1.62$ mm, $t=0.125$ mm, $G_1=G_2=26.316$ GN m^{-2}, $E_1=E_2=70$ GN m^{-2}, $G_a=1.0$ GN m^{-2}, $E_a=2.8$ GN m^{-2}, so

$$\frac{hE_a}{tE} = 0.512, \quad \frac{hG_a}{tG} = 0.486 \tag{2.4}$$

are beyond the bounds (2.3) and therefore it is not strictly applicable for most of structural adhesives in common use. However, Lubkin and Reissner (1956) stated that the bounds (2.3) were too conservative. Peppiatt (1974) showed that Goland and Reissner's second

theory was still applicable to joints with similar materials and geometry in the above example. Owing to the assumption that the peel stress is constant across the adhesive layer, the zero-shear condition at the ends of the overlap cannot be met as shown in Figure 2.2. Because the adherends surrounding the adhesive layer are bent in different directions, the shear strains cannot be zero if the peel strains are constant across the adhesive layer. Finally, it should be noted that the bending moments derived by Goland and Reissner are not very accurate at the ends of the overlap as shown in Figure 2.3a. They assumed that the overlap acted as a whole plate. But in fact the stress distribution across the thickness of the adherend is as shown in Figure 2.3b, which was pointed out by Hart-Smith (1977). It can be seen that the stress distribution across adherend thickness is dramatically different from Goland and Reissner's assumption. However, as will be shown in Chapter 3, the bending moments from Goland and Reissner's method at the ends of the overlap are not as dramatically far away from the true values as the stress distribution across the adherend.

2.3.3 Later developments

In later work, Volkersen (1965), treating the adhesive in the same way as Goland and Reissner, attempted to set up a set of differential equations to obtain the peel and shear stresses in the adhesive of a double lap joint. He also included the free shear stress in the adhesive at the ends of the overlap. However, as explained by Peppiatt (1974), there were several errors in the paper, particularly in the assumed boundary conditions, and an analytical solution was not possible.

Recently, several authors have developed the classical theories to take account of adherend bending, shearing and normal straining. Renton and Vinson (1975) modelled the adherend with stretching, shear and bending, whilst Allman (1977) used a two dimensional model to analyse the overlap region. Hart-Smith (1973) included plastic deformation of adhesives, which had been ignored in most of the analytical methods.

Another notable analysis was given by Adams and Peppiatt (1975) to study the Poisson's ratio effect. They found that stresses across the joint width were significant. Because 3D analysis is presented in Chapter 5, a review on this aspect is given there.

2.3.3.1 Renton and Vinson

Renton and Vinson (1977) have produced a solution for a single lap joint between orthotropic sheets by including adherend shear, bending and normal stresses. However, there is no coupling between bending, stretching or shearing, which is significant for unbalanced composites. Also, it is assumed that the shear and peel stresses are constant across the adhesive thickness. In addition, they set the adhesive shear stresses to zero at the overlap ends, but by forcing the shear stresses at the adhesive ends to be zero still violates the stress equilibrium at the adhesive ends as explained by Harris (1983), because their shear and peel stresses are constant across the adhesive layer. Such assumptions cannot accommodate the zero shear stresses as shown physically in Figure 2.2. Their modelling of the adherends is partly concerned with anisotropic materials, so their methods are applicable for composite materials. From their numerical example of a single lap joint with thick adherends as reproduced in Figure 2.4, it can seen that the inclusion of transverse normal and shear stresses in the adherends significantly reduces the peel stresses in the adhesive. However, they have little effect on the shear stresses except at the ends of the overlap. It may be seen that the adherend shearing enhances the peel concentration as shown in Figure 2.5, although the effect may be small. The inclusion of adherend transverse stretching reduces the peel stress concentration, because this reduces the stiffness of the adherend in the transverse direction. These two factors work in opposition to each other. The net effect depends on the magnitudes of the two factors. In thick adherends, the adherends shearing is almost neglected. The transverse stiffness of the adherend depends on the thickness of the adherend. Thus, in thick adherends, the transverse normal stretching is much more significant than the adherend shearing effect, thus reducing the peel stresses at the ends of the overlap. However, the complexity of the solution is such that it is necessary to resort to digital computers to ease the burden of calculations.

2.3.3.2 Allman

From the above discussion, it may be concluded that more realistic solutions come closer and closer to the full continuum mechanics solution. As pointed out earlier, the full field

problem is extremely difficult to solve analytically because of the different materials and complicated boundary conditions. The most realistic analysis so far is probably that due to Allman (1977). The analysis includes the effect of bending, stretching and shearing of the adherends and accounts for the shearing and peeling of the adhesive. Because both stress equilibrium and displacement compatibility need to be satisfied (which is normally very difficult), stress functions may be used in which the stress equilibrium will be automatically satisfied. The problem will then be simplified to satisfy the displacement compatibility. This process was adopted by Allman who defined two stress functions $f_1(x)$ and $f_2(x)$ throughout the joint. To satisfy the displacement compatibility, a complementary energy function for the joint is derived in terms of the two unknown stress functions and their derivatives. The function is then minimised, using the Euler-Lagrange equations of variational calculus, to yield two fourth order differential equations for the stress functions. For an unbalanced joint, the equations are coupled and a closed form solution is not possible. Instead, Allman suggested an approximate numerical method, which is similar to the Finite Element Method. For a balanced joint, the equations uncouple and can be analytically solved to give the stress functions.

The method is thought to be the most thorough closed form solution available as it includes all the factors that the other analyses use. It accounts for the shear stress free edges with stresses at the edges in equilibrium because it allows a linear variation of peel stress through the adhesive thickness as shown in Figure 2.6. Allman's method gives accurate results for both shear and peel stresses except at the ends of the overlap as will be shown in Chapter 3.

Mallick (1989a) has extended Allman's method to include the longitudinal stresses along the overlap and to model elastic-plastic adhesives. Thermal loadings has also been included. A friendly-used software running on desktop personal computers has also been developed by Mallick (1989b).

2.3.3.3 Hart-Smith

Although there has been so much development in the closed form solutions, all the methods follow Goland and Reissner's first step to obtain the bending moments at the ends of the overlap. It was Hart-Smith who physically pointed the error in the determination of the bending moments by Goland and Reissner's method as shown in Figure 2.3. He then developed a new equation for determining the bending moments. However, as will be shown in Chapter 3, his bending moment equation underestimates the true values for long overlaps, although it is accurate for short overlaps.

All the closed form analyses discussed above assume that the joint materials are elastic. It is, however, well known that modern adhesives are usually toughed epoxies which are very ductile and can withstand large plastic deformation. Hart-Smith (1981) was among the first to model material non-linearities by using continuum mechanics. The first difficulty of modelling elastic-plastic materials is the characterisation of the adhesives. To simplify the mathematical process, he used a bi-linear curve as his elastic-plastic model as shown in Figure 2.7. The principle is that the area under the curve is equal to that under the true stress-strain curve and that the failure stresses or strains are the same for the two curves as shown in Figure 2.7. The basic solution itself is similar to Goland and Reissner's except for the introduction of an iterative procedure to model plasticity.

However, it should be noted that Hart-Smith only considered the elastic-plastic shear properties of adhesives, the adherends still being kept elastic.

2.3.3.4 Adams and Peppiatt

Adams and Peppiatt (1973) studied the Poisson's ratio effects on the shear stresses in the adhesive layer and longitudinal stresses in the adherends acting at right-angles to the direction of the applied load. Because Chapter 5 presents the results of a 3D stress analysis, more details concerning Adams and Peppiat's solution can be found there.

2.4 NUMERICAL METHODS

It has been shown that a full field solution is extremely difficult, if not impossible, for a lap joint. This is only concerned with elastic materials. If complicated constitutive relations such as elastic-plastic materials, creep, visco-elasticity, are included, the mathematics will be too complicated to be soluble. Also, complex geometry such as spew fillets, will prohibit any closed form solutions. Instead, numerical methods are needed. FEM is a very effective numerical means of solving continuum problems and has gained widespread acceptance in most of the engineering fields. It fills the gaps left by the analytical methods to model complex situations, such as adhesively-bonded lap joints, accurately and efficiently.

The FE procedure is as follows (Zienkiewicz and Taylor, 1988):

(a) the continuum is divided into a finite number of parts (elements), the behaviour of which is specified by a finite number of parameters, and

(b) the solution of the complete system as an assembly of its elements follows precisely the same rules as those applicable to standard discrete problems.

The basic theory is presented in Appendix 1, where displacement-type elements are used. A hybrid element is introduced in Chapter 4.

The FEM has long been used to model adhesively bonded joints. All the restricting assumptions in the closed form solutions can be withdrawn, thus producing an accurate model for a joint. Non-linear material properties, creep, viscoelasticity, thermal effects, and any joint geometry, can be effectively handled with FEM. FEM has successfully been used by Adams *et al* (1984) to analyse the nature of stresses in joints and to predict joint strength. They have, in their FE models, included either elastic or elastic-plastic materials in both adhesives and adherends (Adams *et al*, 1974 and Harris and Adams, 1984). It is noted that the yield criterion they use is a modified version of that due to von Mises (Raghava *et al*, 1973 and Raghava and Caddell, 1973). In modelling single lap joints, they used a large displacement procedure to model the rotation of the joints (Crocombe and Adams, 1981). They have included spew fillets and various joint configurations. They have

also modelled realistic boundary conditions in their analyses (Zhao and Adams, 1989). Composite materials have been included, too (Adams *et al*, 1986). Different loadings such as static, impact, thermal and residual stresses have been analysed. It has been demonstrated that FEM is a very powerful tool in modelling joints and in predicting joint strength.

2.5 CONCLUSIONS ABOUT THE MODELLING AND ANALYSES OF LAP JOINTS

The stresses and strains in the adhesives and adherends are very important for understanding the joint behaviour. If joint strength is to be predicted, then it is essential to know the magnitudes and directions of the stresses and strains at the ends of the overlap. Closed form solutions are accurate for most of the overlap except at the ends. Experiments have shown that it is these regions at the ends of the overlap where failure always starts. FEM is the only method which provides reliable technique of stress evaluation in this region. It is well known that stress or strain concentration occurs at these regions. FEM involves a large amount of mesh refinement and curve fitting if the stresses or strains are to be accurately analysed in these regions. Such a process is difficult and time-consuming. Even though the stress or strain concentrations may be accurately evaluated theoretically, such concentrations are still difficult to correlate to the joint strength. In engineering applications, a general state of stress is needed and, for this reason, closed form solutions are often used. With closed form solutions, it may be said that the important factors to be included in the model are the shear, peel stresses in the adhesive and the stretching and bending of the adherends.

2.6 FACTORS INFLUENCING THE STRESSES IN THE ADHESIVE LAYER

Double and single lap joints are often used to test adhesives. The stress state in the adhesive layer has been well discussed. It is felt that the physical insight into the nature of the stresses has, however, been little mentioned. For engineering applications, the physical understanding is at least as important as the numbers from an analysis in that some underlining parameters affecting the strength of a joint need to be carefully controlled. In this review, emphasis is therefore placed on the physical insight in order to discuss the factors influencing the stresses in the adhesive layer with simple mechanics. To simplify the

discussions, only square-ended lap joints are included here. However, it is believed that joints with spew fillets have similar features.

2.6.1 Factors influencing shear stresses

Shear stresses have been calculated since Volkerson's work in 1938 and it is well known that the shear stress distribution is not uniform along the overlap but is as shown in Figure 2.8. The physical explanation for this distribution is shown in the Figure. It can be seen that a nonuniform shear stress is introduced by the uneven stretching of the adherends (shear lag). The larger the difference in stretching, the more uneven is the distribution of shear stress. Because the sum of the shear stresses along the overlap is equal to the applied loads, the larger the difference in stretching, the higher the shear stress near the ends of the overlap. Bearing this in mind, it is easy to understand that the stiffer the adherends, the lower the shear stresses at the ends of the overlap, because stiffer adherends stretch less and therefore produce a smaller difference in stretching (shear lag effect). The same argument can be applied to the explanation of the effect of adhesive stiffness on the shear stress distribution. Flexible adhesives results in lower stresses at the ends of the overlap and therefore decrease the unevenness in adherend stretching.

Thicker adhesive layers decrease the shear stress near the ends of the overlap in the adhesive layer. The reason is that a thicker adhesive layer has less shear strains at the ends of the overlap in the adhesive than thin adhesive layer if adherend stretching is the same as illustrated in Figure 2.9. Therefore the shear stress is smaller because shear stress is proportional to the shear strain. But it should be noted that the difference between the shear strains for thick and thin adhesive layers is small because the change in adhesive thickness is usually small. Adams *et al* (1978) has showed that the effect of the adhesive thickness on double joint strength is small for adhesive thickness varying between 0.1-0.4 mm.

The explanation of the effect of adherend thickness on the shear stress is fairly simple. Increasing adherend thickness is simply to raise the stiffness of the adherend. As a result, the shear stresses in the adhesive layer decrease.

The effect of the overlap on the shear stresses is shown in Figure 2.10. It can be seen that the highest shear stress decreases significantly with the increase in the overlap for short overlaps. But the change in shear stresses become small for long overlap. The reason is as follows. The peak of the shear stresses happen near the ends of the overlap, which depends on the relative movement of the two adherends near the ends of the overlap. For short overlaps, the increase in the length of the overlap is simply to enlarge the area which supports the applied load and therefore the shear stresses decrease. But when the overlap length reaches a certain distance, the peak of the shear stresses become almost constant because the relative movement of the two adherends near the end of the overlap are almost constant. This is because the relative movement of the two adherends near the ends of the overlap is mainly dependent on the local area near the end of the overlap for very long overlaps. Other regions away from the ends of the overlap have little effect on the shear stresses near the ends of the overlap.

From Volkersen's solution, the shear stresses should be the same for single and double lap joints provided that the material properties, loads and geometry (half of the double lap joint and a single lap joint) are the same. But in fact there is a large difference in shear stresses between single and double lap joints. The reason is that the inner and outer sides of the loaded adherend of a single lap joint stretch in a different manner. The inner side stretches much more than the outer side. But the sum of the stresses across the thickness of the adherend is the same for both single and double lap joints equal to the applied load. Consequently, the inner side of the single lap joint elongates much more than that of the double lap joint. This enhances the shear lag effect and therefore results in higher shear stresses in single lap joints than in double lap joints as shown in Figure 2.11.

2.6.2 Factors influencing peel stresses

Having discussed the factors influencing the shear stresses in lap joints, the influences of these factors on peel stresses are presented here. First, it has been demonstrated by Adams and Peppiatt (1973) that peel stresses exist in double lap joints even though there is no net bending moment on a symmetric double lap joint. The reason is that the shear stresses

applied to the outer adherend through the adhesive layer are not at the neutral axes of the adherend as shown in Figure 2.12. Examining a double lap joint under load carefully may confirm that there is NO net bending moment in the adherends. But where are the peel stresses from? It will be shown that the peel stresses are because of the shear stresses applied to the inner side of the outer adherend. It is noted that the shear stresses acting at the outer adherend introduce a bending moment to the neutral axes of the adherend. This bending moment needs to be balanced. The uniform (or nearly uniform) longitudinal stresses acting on the cross section of the adherend cannot balance the bending moments induced by the shear stresses. Therefore, the bending moment needs external forces in order to be balanced. It is the peel stresses acting on the adherend which balance the bending moment as shown in Figure 2.12, because the peel stresses are the only external forces left acting on the adherend. The effect of the peel stresses acting on the adherend is to produce a pure bending moment at the neutral axes without introducing any net forces in the vertical direction so that the adherend is in equilibrium in the vertical direction. This results in a compressive stresses at a small distance away from the end of the overlap and the sum of the peel stresses and that of the compressive stresses should be equal but having opposite signs. The compressive stresses at the other end of the overlap can be explained in the same way.

Peel stresses are very significant for single lap joints. It is shown in Chapter 3 that an increase in the adherend stiffness increases the bending moments at the ends of the overlap. It therefore seems that stiffer adherends increase the peel stresses in the adhesive layer because of the larger bending moments at the ends of the overlap. However, it has been shown (Crocombe, 1981) that stiffer adherends decrease the peel stresses in the adhesive layer. This may be explained as below. There are two factors affecting the peel stresses in the adhesive. The first one is the bending moments acting at the ends of the overlap. If the materials are the same, the larger the bending moments, the higher the peel stresses in the adhesive layer. Secondly, the adherend stiffness plays an important role in the determination of the peel stresses in the adhesive layer for a given bending moment. To determine the effect of the stiffness of the adherends on the peel stresses, an extreme case

is considered first. It is supposed that rigid adherends are used as adherends. With the rigid adherends, the peel stress will be very small close to zero in the adhesive layer of a single lap joint. This is because the single lap joint is anti-symmetric with regards to the joint centre. As a result, the bending moments at the ends of the overlap will have no effect on the peel stresses in the adhesive layer as illustrated in Figure 2.13a. Figure 2.13a shows that the bending moments at the ends of the overlap induce both peel and compressive stresses in the adhesive layer at different ends of the overlap. These peel and compressive stresses induced by the two bending moments cancel each other resulting in zero peel stresses. The peel stresses in the adhesive layer are caused by the transverse shear forces only and the shear forces are small. It may therefore be concluded that almost no peel stresses are induced by the bending moments for the joint with rigid adherends. Consequently, the peel stresses are due to the adherend *deformation*. The dominant deformation of the adherends is stretching, which varies linearly across adherend thickness, thus giving rise to the bending of the adherends. Therefore, the degree of adherend bending can be used to assess the peel stresses in the adhesive layer. The larger the adherend deformation bending), the higher the peel stresses. To further demonstrate this point, the effect of the deformation of an elastic adherend is examined here. It may be seen that the change in peel strains along the overlap, for a given bending moment will be much smoother for stiffer adherend than for flexible one, as is shown in Figure 2.13b. As a result, larger peel stresses will occur at the ends of the overlap for flexible adherends. To investigate the overall effect of the bending moments and the stiffness of the adherends, the following equation (see Chapter 3) for the rotation of the normal of the neutral surface of the cylindrically bent plate may be used,

$$\Theta = \frac{12M(1-\mu^2)}{Eh^3} = \frac{6(1-\mu^2)}{Eh^3}\,\frac{Th}{1+\varsigma c}$$

$$= \frac{6(1-\mu^2)}{Eh^2}\,\frac{T}{1+\sqrt{(12T(1-\mu^2)/Eh^3)}c}$$

$$= 6T(1-\mu^2)\,\frac{1}{Eh^2+\sqrt{(12ET(1-\mu^2)h)}c} \qquad (2.5)$$

where c is half of the overlap length.

From Eq. 2.5, it can be seen that the stiffer the adherend, the smaller the rotation of the normal (smaller bending) caused by the bending moments. Larger bending of the adherend gives rise to the unevenness of the peel stresses and therefore increases the peel stress at the ends of the overlap.

Decreasing the stiffness of the adhesive has the same effect as increasing the stiffness of the adherend. A flexible adhesive results in a more gradual change in the peel stresses and therefore these peel stresses are lower than for a stiff adhesive.

The adhesive thickness has the same effect as the adherend thickness. A thicker adhesive layer implies a more flexible adhesive. Therefore, the same transverse displacements mean smaller strains for a thicker adhesive layer. As the strains are smaller, so are the peel stresses.

2.6.3 The effect of plasticity

All the above discussions are concerned with linear materials of both adherends and adhesives. Modern adhesives are usually toughed epoxies, which are quite ductile, so that their elastic-plastic properties need to be taken in account when predicting joint strength. Also, metals such as aluminium are used as adherends in joint tests and real applications, and such adherends normally yield before the joint fails. To predict the joint strength accurately, the elastic-plastic behaviour of the adherends needs also to be included.

Firstly, the elastic-plastic behaviour of the adherends will be discussed. It is often said that the yielding of the adherends enhances the rotation of the overlap, thus reducing the bending moments at the ends of the overlap. However, it should be noted that the reduction in the bending moments does not necessarily mean a decline in the peel stresses. In fact, yielding of the adherends increases the stresses (both peel and shear) in the adhesive layer since yielding of the adherends decreases the stiffness of the adherends. The overall effect of the adherend yielding on the peel stresses is to increase the peel stresses as discussed above with Eq. 2.5. In addition, the adherend yielding enhances the shear straining at the end of the overlap, thus increasing the shear stresses. This argument is supported by the

fact that joints with stiff adherends have higher strength than those with flexible adhesives (Harris, 1983).

Adhesive yielding has the opposite effect on the stresses as adherend yielding. Adhesive yielding is preferred, and this can increases the joint strength dramatically. There are two factors which make adhesive yielding beneficial. First, adhesive yielding is equivalent to decreasing the stiffness of the adhesive. As discussed above, a reduction in the stiffness of the adhesive lowers the stresses in the adhesive layer. Secondly, adhesive yielding means a large local elongation of the adhesive, so that a larger proportion of the adhesive layer will carry the load, thus increasing the strength of the joint.

2.6.4. Spew fillet effect

All the above discussions are concerned with "square ended" adhesive joints as shown in Figure 2.14a. In reality, adhesives are squeezed out to form spew fillets when they are manufactured shown in Figure 2.14b. It has been demonstrated that the spew fillets are beneficial for joint strength (Adams and Wake, 1984). Physically, there are two factors which make the spew fillets preferred. In the first place, the spew fillets reinforce the area around the loaded adherend, reducing the stress concentration there. The stress concentration is moved to the end of the unloaded adherend, where the stresses are much reduced because it is not on the main path of the loading. Secondly, the spew fillets transfer some load, which therefore increases the area of the load path. However, it should be noted that too large spew fillets, such as that in Figure 2.14c, make the spew fillets transfer too much load. Because the stress state at the ends of the adherends is largely in tension and adhesives in tension are the weakest, failure may initiate at the ends of the adherends if the spew fillets are too large, thus causing premature failure and reducing the joint strength. This phenomenon has been noticed before (Chen, 1985, Moult, 1986) and was experienced by the present author. As is shown in Figure 2.14c, the failure tends to start at the ends of the adherend, and then enter the adhesive layer causing premature failure.

2.7 CONCLUSION

From the above discussions, it may be seen that some factors, influencing the stresses and therefore the strength of lap joints, are very important whilst some are not. Some conclusions may be drawn from the discussions. The most important factors are the stiffnesses of both adherends and adhesives. Stiff adherends are beneficial while a flexible, preferably ductile, adhesive increases joint strength dramatically. Another important factor is the length of the overlap. A rise in the length of the overlap increases the joint strength. But this benefit is limited because once the length of the overlap exceeds some values, no further increment in joint strength can be obtained by further increasing the length of the overlap. Adherend thickness is also important; the thicker the adherends, the higher the strength of the joint. Spew fillets should not be removed, because they can increase joint strength and removing the fillets may introduce extra cracks at the ends of the overlap. Such cracks will lower the strength of the joint. Too large fillets may, however, cause premature failure at the unloaded adherend ends.

Chapter 3

A NEW METHOD FOR THE DETERMINATION OF BENDING MOMENTS FOR SINGLE LAP JOINTS

3.1 SUMMARY

This chapter presents a new method of determining bending moments at the overlap ends of single lap joints. It is based on the assumption that the overlap region does not deform under load. This assumption is supported by the observation that for an overlap of up to 50 mm the large deformation occurs only at the ends of the overlap. Physical insight into the mechanics of the overlap rotation shows that the rotation is merely a geometric effect, which tends to align the load path during the loading process. Finite element analysis confirms that the bending moments hardly change with variations in overlap properties for given loads.

Examples show that this method is better than those of Goland and Reissner (1944) and of Hart-Smith (1973) for overlaps up to 25 mm long. It is more useful for unbalanced joints, where Goland and Reissner's method fails to work and Hart-Smith's method involves difficult mathematics. This method may also be easily extended to deal with non-linerities in the adherends.

3.2 INTRODUCTION

A knowledge of the state of stresses inside the adhesive layer of an adhesively bonded joint is essential for joint strength prediction and joint design. There are two methods for the stress analysis of lap joints, namely analytical and numerical methods. The analytical methods (closed form) employ classical linear theories in which some simplifications are used. The Finite Element Method (FEM), on the other hand, is a well-established numerical technique, which can handle complex structures and non-linear material properties, where classical methods generally fail to work. Although the closed form solutions have their limitations, they are easy to use, especially for parametric studies. The FEM needs large computer power and experienced personnel. Consequently, the former is widely used for

joint design and the latter for research. The aim of this chapter is to improve the analysis of the closed form solutions and therefore the classical method is mainly used. The FEM is only used to verify the closed form solutions.

Analytical solutions for single lap joints have been developed since 1938 when Volkersen (1938) analysed the shear-lag problem in single lap joints. However, he ignored the bending moments applied to the joint because of the eccentricity of the load. It was Goland and Reissner (1944) who were among the first to produce solutions for peel stresses as well as for shear stresses. In their method, there are two steps. The first is to determine bending moments at the ends of the overlap. The bending moments are then used as boundary conditions to analyse the overlap region. They considered only two cases, in which the adhesive layer is either very stiff or very soft. To overcome the limitations involved in the work of Volkersen, Goland and Reissner and other earlier workers, extensive development has been made since then, notably by Renton and Vinson (1975) and Allman (1977). All of the methods attempt to improve the analyses of the stresses inside the overlap, but they follow the first step in Goland and Reissner's method to determine the bending moments. It was Hart-Smith (1973) who first recognized the limitation in Goland and Reissner's determination of the bending moments. He stated that Goland and Reissner overestimated the bending moments. To improve the determination of bending moments, he developed a new bending moment factor, which involves complicated mathematics. Unfortunately, his bending moment factor underestimates the true value compared with FEM predictions. It should be noted that both Goland and Reissner's and Hart-Smith's bending moment factors are only applicable to identical adherends. Joints with different adherends (e.g. composite and aluminium) are widely used in industry and this requires the determination of bending moments at the ends of overlap if analytical methods are to be used. Brooker (1980) extended Goland and Reissner's bending moment factor to deal with non-identical adherends, but a 6 X 6 matrix needs to be solved and no results are given. Hart-Smith (1973) also gave an expression to obtain the bending moments. However, the solution can only be obtained by numerical iteration. It can be concluded from the above that a more accurate and convenient determination of bending moments is required for both identical

and, in particular, non-identical adherends. In this Chapter, a new method is proposed for determining the bending moments for single lap joints with either identical or non-identical adherends. It is based on the assumption that the overlap region does not deform during loading. Numerical examples are given to compare the results from the present method and that from Goland and Reissner's and Hart-Smith's methods. Comparison is also made with FE results, which are believed to be most accurate and reliable and which can be used to assess the accuracy of other methods.

3.3 THEORY

The proposed method is based on the assumption that the overlap region does not deform under load. The assumption is made by realising that the stiffness of the overlap is much higher than that of either adherend (since bending stiffness is proportional to the cube of the thickness). Experiments also show that the overlap region does not deform much during the loading process. More evidence is given in Fig. 3.1, where the results are calculated using FEM for joints with a 12.7 mm overlap and 1.6 mm thick adherends. Other parameters are listed in the Figure. It can be seen that the stiffness of both the adherends and the adhesive and the thickness of the adhesive (in the range of 0.125 - 0.3 mm) in the overlap region (the stiffness of adherends outside the overlap is kept constant) have little effect on the bending moments. With this assumption, the following analysis is able to utilise basic cylindrically bent plate theory.

Figure 3.2 shows the geometry of a single lap joint and its material properties. The overlap length of the joint is l, the lengths of the two sheets outside the joint are l_1 and l_2, and their thicknesses are t_1 and t_2. The joint width is assumed to be large enough compared with the sheet thickness so that only the cross section need be considered. The joint is loaded with tensile forces T per unit of joint width. The overlap is assumed to be rigid so that only the two sheets need to be analysed. The coordinate system is shown in Figure 3.2. The w coordinate represents transverse deflection of the two sheets from their undeformed positions. The effects of the sheet deflections are included in the determination of the bending moments.

The bending moments per unit width in the sheets may be expressed as follows:

$$M_1 = T\,[\alpha_n x_1 - w_1], \qquad 0 \le x_1 \le l_1, \tag{3.1}$$

$$M_2 = -\,T\,[\alpha_n (l_2 - x_2) + w_2], \qquad 0 \le x_2 \le l_2, \tag{3.2}$$

where α_n is the angle between the x_1 (or x_2) axis and the line of the load path as shown in Figure 3.2 and is given by

$$\alpha_n = (t_1+t_2)/2(l_1+l_2+l) = (t_1+t_2)/2L, \tag{3.3}$$

where $L = l_1+l_2+l$, w_1 and w_2 are the defections of the two sheets from their undeformed shape, and the thickness of the adhesive is ignored.

According to the classical theory of the small bending of thin, cylindrically bent plates, the differential equations for the transverse deflections of the two sheets can be written as

$$d^2w_1/dx_1^2 = -\,M_1/D_1 = -\,T[\alpha_n x_1 - w_1]/D_1, \tag{3.4}$$

$$d^2w_2/dx_2^2 = -\,M_2/D_2 = T[\alpha_n(l_2-x_2) + w_2]/D_2, \tag{3.5}$$

where D_1 and D_2 are the flexural rigidities of the two sheets respectively, i.e. $D_1 = E_1t_1^3/12(1-\mu_1^2)$ and $D_2 = E_2t_2^3/12(1-\mu_2^2)$.

Writing $\zeta_1^2 = T/D_1$ and $\zeta_2^2 = T/D_2$, then

$$d^2w_1/dx_1^2 - \zeta_1^2 w_1 + \zeta_1^2\alpha_n x_1 = 0, \tag{3.6}$$

$$d^2w_2/dx_2^2 - \zeta_2^2 w_2 - \zeta_2^2\alpha_n(l_2-x_2) = 0 \tag{3.7}$$

These are standard, second-order, linear differential equations and have solutions of the form

$$w_1 = A_1\cosh \zeta_1x_1 + B_1\sinh \zeta_1x_1 + \alpha_n x_1, \qquad 0 \le x_1 \le l_1 \tag{3.8}$$

$$w_2 = A_2\cosh \zeta_2x_2 + B_2\sinh \zeta_2x_2 - \alpha_n(l_2-x_2), \qquad 0 \le x_2 \le l_2. \tag{3.9}$$

The four constants can be determined from the following four boundary conditions as shown in Figure 3.3,

$$w_1 = 0, \qquad \text{at } x_1 = 0, \tag{3.10a}$$

$$w_2 = 0, \qquad \text{at } x_2 = l_2, \tag{3.10b}$$

$$dw_1/dx_1 = dw_2/dx_2, \qquad \text{at } x_1=l_1,\ x_2=0, \tag{3.10c}$$

$$w_1 - w_2 = -ldw_1/dx_1, \qquad \text{at } x_1 = l_1,\ x_2 = 0, \tag{3.10d}$$

where Eqs.(3.10c) and (3.10d) are from the assumption that the overlap is rigid.

By applying the boundary conditions, the deflections of the two plates can be written as

$$w_1 = (-\alpha_n L\zeta_2 \cosh \zeta_2 l_2 \sinh \zeta_1 x_1)/(\zeta_2 \sinh \zeta_1 l_1 \cosh \zeta_2 l_2 + \zeta_1\zeta_2 l \cosh \zeta_1 l_1 \cosh \zeta_2 l_2 + \zeta_1 \cosh \zeta_1 l_1 \sinh \zeta_2 l_2) + \alpha_n x_1, \quad 0 \le x_1 \le l_1, \tag{3.11}$$

$$w_2 = (\alpha_n L\zeta_1 \sinh \zeta_2 l_2 \cosh \zeta_1 l_1 \cosh \zeta_2 x_2)/(\zeta_2 \sinh \zeta_1 l_1 \cosh \zeta_2 l_2 + \zeta_1\zeta_2 l \cosh \zeta_1 l_1 \cosh \zeta_2 l_2 + \zeta_1 \cosh \zeta_1 l_1 \sinh \zeta_2 l_2) - (\alpha_n L\zeta_1 \cosh \zeta_2 l_2 \cosh \zeta_1 l_1 \sinh \zeta_2 x_2)/(\zeta_2 \sinh \zeta_1 l_1 \cosh \zeta_2 l_2 + \zeta_1\zeta_2 l \cosh \zeta_1 l_1 \cosh \zeta_2 l_2 + \zeta_1 \cosh \zeta_1 l_1 \sinh \zeta_2 l_2) - \alpha_n(l_2 - x_2), \quad 0 \le x_2 \le l_2. \tag{3.12}$$

The moments at the left end of the overlap become

$$M^L = (M_1)\Big|_{x_1=l_1} = -D_1(d^2w_1/dx_1^2)\Big|_{x_1=l_1}$$

$$= 0.5T(t_1+t_2)\zeta_2 \cosh \zeta_2 l_2 \sinh \zeta_1 l_1/(\zeta_2 \sinh \zeta_1 l_1 \cosh \zeta_2 l_2 + \zeta_1\zeta_2 l \cosh \zeta_1 l_1 \cosh \zeta_2 l_2 + \zeta_1 \cosh \zeta_1 l_1 \sinh \zeta_2 l_2) \tag{3.13}$$

and the moments at the right end of the overlap

$$M^R = (M_2)\Big|_{x_2=0} = -D_2 (d^2w_2/dx_2^2)\Big|_{x_2=0}$$

$$= 0.5T(t_1+t_2)\zeta_1 \cosh \zeta_1 l_1 \sinh \zeta_2 l_2/(\zeta_2 \sinh \zeta_1 l_1 \cosh \zeta_2 l_2 + \zeta_1\zeta_2 l \cosh \zeta_1 l_1 \cosh \zeta_2 l_2 + \zeta_1 \cosh \zeta_1 l_1 \sinh \zeta_2 l_2) \tag{3.14}$$

In practice, the values of $\zeta_1 l_1$ and $\zeta_2 l_2$ are sufficiently large to permit taking

$$\sinh \zeta_1 l_1 \simeq \cosh \zeta_1 l_1 \simeq 1/2\ \mathrm{EXP}(\zeta_1 l_1) \tag{3.15a}$$

and

$$\sinh \zeta_2 l_2 \simeq \cosh \zeta_2 l_2 \simeq 1/2\ \mathrm{EXP}(\zeta_2 l_2). \tag{3.15b}$$

Then we have

$$w_1 = (-\alpha_n L\zeta_2 \sinh \zeta_1 x_1)/(\zeta_2 \sinh \zeta_1 l_1 + \zeta_1\zeta_2 l \cosh \zeta_1 l_1 + \zeta_1 \cosh \zeta_1 l_1) + \alpha_n x_1,$$

$$0 \le x_1 \le l_1; \qquad (3.16)$$

and

$$w_2 = (\alpha_n L\zeta_1 \cosh \zeta_2 x_2)/(\zeta_2 + \zeta_1\zeta_2 l + \zeta_1) - (\alpha_n L\zeta_1 \sinh \zeta_2 x_2)/(\zeta_2+\zeta_1\zeta_2 l+\zeta_1) - \alpha_n(l_2 - x_2),$$

$0 \le x_2 \le l_2$. (3.17)

The moments at the left end of the overlap become

$$M^L = (M_1)\Big|_{x_1=l_1} = -D_1 \quad (d^2w_1/dx_1^2)\Big|_{x_1=l_1}$$

$$= 0.5T(t_1+t_2)\zeta_2/(\zeta_2 +\zeta_1\zeta_2 l+\zeta_1). \qquad (3.18)$$

Similarly,

$$M^R = (M_2)\Big|_{x_2=0} = -D_2 \quad (d^2w_2/dx_2^2)\Big|_{x_2=0}$$

$$= 0.5T(t_1+t_2)\zeta_1/(\zeta_1+l\zeta_1\zeta_2 +\zeta_2). \qquad (3.19)$$

For identical adherends, $\zeta_1 = \zeta_2$, then we have

$$M^R = M^L = 0.5Tt\ 1.0/(1+0.5\zeta l) = 0.5Tt\ 1.0/(1+\zeta c) = 0.5Tt\ k, \qquad (3.20)$$

where $\zeta=\zeta_1=\zeta_2$, c is the half overlap length, i.e. 2c=l and k is defined as the bending moment factor, which is

$$k = 1/(1 + \zeta c). \qquad (3.21)$$

Hart-Smith's result can be written as

$$M = 0.5T(t+t_a)\ 1/(1+\zeta c+\zeta^2 c^2/6), \qquad (3.22)$$

where t_a is the thickness of the adhesive. Therefore his bending moment factor is

$$k_{HS} = 1/(1 + \zeta c + \zeta^2 c^2/6). \qquad (3.23)$$

Comparison of Eq. (3.21) with Eq. (3.23) shows that the difference between the present result and Hart-Smith's is the term $\zeta^2 c^2/6$. Hart-Smith's form includes the thickness of the

adhesive, which is ignored in the present method. It is known that Hart-Smith's result underestimates the bending moment factor. Therefore, the present method is believed to be more accurate than Hart-Smith's. In order to compare the results of the present method with Goland and Reissner's, their formulae have been used in the following forms

$$M = 0.5Tt\ k, \tag{3.24a}$$

and

$$k_{GR} = 1/[1 + 2(\sqrt{2})\tanh \varsigma c/(2(\sqrt{2}))]. \tag{3.24b}$$

3.4 RESULTS

3.4.1 Identical adherends

3.4.1.1 Different lengths of overlap

To verify and demonstrate the use of the new formula presented above, numerical examples are presented in this section. First, identical adherends of single lap joints are used and calculations are made with different overlap lengths and loads. To compare with Goland and Reissner's and Hart-Smith's methods, corresponding results from their methods are also shown in the figures. Comparison has also been made with results from FEM. In the FE analysis, an adhesive with a Young's modulus of 2.8 GPa has been used, which represents the real conditions in a typical lap joint using an epoxy adhesive. The FE results are believed to be the most accurate and reliable and therefore they can be used to assess the accuracy of the different analytical methods. A 2D plane strain FE research programme FELDEP (Crocombe, 1981) was used throughout this study. 8-noded isoparametric elements were used and a large displacement linear model was included. A typical mesh is shown in Figure 3.4. The boundary conditions used for the FE analysis are shown in Figure 3.2. These are not typical boundary conditions used in testing, in which the ends are restrained from rotation. Chen (1985) has showed that the effects of boundary conditions on the bending moments at the ends of the overlap are significant with small displacement FE analysis, but the effects are very small with large displacement FE analysis. For single lap

joints, the large displacement analysis is essential to model the eccentricity of the load. Therefore, all the analyses with large displacement FE are applicable to any kind of boundary conditions. For different lengths of overlap, the adherend length outside the overlap was kept constant (= 87.3mm). For different lengths of the overlap, it is obvious that the ratio of the length of the adherend outside the overlap to that of the overlap (l_1/l) varies significantly. To analyse this effect, calculations were made with different lengths of the adherends outside the overlap for 12.7mm and 100mm overlaps. Results are shown in Figure 3.5. It can be seen that the bending moments are insensitive to the adherend lengths outside the overlap, although short adherends outside the overlap have some small effect on the bending moments for short overlaps. The adherend length (= 87.3mm) outside the overlap used here was long enough not to have any effect on the calculations of the bending moments. The bending moments were calculated by numerical integration with stresses available at the Gauss points from the FE results and then the bending moments were extrapolated to the edges of the overlap.

The results of the bending moment factors and bending moments for joints with varying lengths of overlap from 6mm to 100mm are shown in Figures 3.6 - 3.15 inclusive. For joints with short overlaps (6 mm), although all the three methods (Goland and Reissner's, Hart-Smith's and the present) underestimate the bending moment factors for the whole range of the load, the bending moments from the three methods are very close as shown in Figs. 3.6 and 3.7. It is noted in passing that Hart-Smith's method produces lower bending moment factors but higher bending moments for high load. The reason is that the adhesive thickness is included in Hart-Smith's method (see Eq. 3.22). For joints with a 12.7 mm (half inch) overlap, all the three methods yield almost identical results for the bending moments within the whole range of the load, although there is slight discrepancy in the bending moment factors as shown in Figures 3.8 and 3.9. Figures 3.10 and 3.11 show the bending moment factors and bending moments for joints with a 25mm overlap. It can be seen that the present method agrees best with FEM of all the methods for bending moment factors and bending moments. Goland and Reissner's method overestimates both bending moment factors and bending moments, and the larger the load, the larger the overestimating. Hart-

Smith's method, however, underestimates both bending moment factors and bending moments, giving large errors at large load. It may be concluded that either the present method or Goland and Reissner's method should be used, because Hart-Smith's method does not err on the safe side. For long overlap joints (50mm), none of the three methods gives satisfactory results, as is clearly shown in Figures 3.12 and 3.13. Hart-Smith's method yields too large an error to be of any practical use. Goland and Reissner's method and the present method produce the same order of error, with the former overestimating and the latter underestimating the true bending moment factors and bending moments. However, the large error appears only at high load. For medium load, e.g. 10kN for a joint with a width of 25mm, the present method introduces an error of about 10%, which can still be used for engineering applications. For very long overlap joints (100 mm), neither Hart-Smith's method nor the present method gives accurate results, although the Hart-Smith's method is worse than the present method as shown in Figures 3.14 and 3.15. Goland-Reissner's method, however, is the most accurate, even though the error is quite large for high load. But it is on the safe side.

As can be seen from above discussion, the present method agrees best with FEM of the three methods for joints with reasonably long overlap. The present method is in any circumstances superior to Hart-Smith's method, although the latter involves much more complicated analysis. For very long overlap joints, however, only Goland and Reissner's method gives reasonably accurate results. As pointed out by Hart-Smith (1973), Goland and Reissner's method suffers from the assumption that the overlap region is taken as a whole plate with double the thickness of the individual adherends and the elastic axis has a discontinuity of amount t at the joint edges. It is in these regions of the joint edges that the error is a maximum. But the bending moments are required at these regions. Thus, Goland and Reissner's method does not give exact results. Hart-Smith's method, on the other hand, assumes small displacements in the overlap region and many assumptions are made in the process of deriving the bending moments. The present method ignores any deformation of the overlap region. Therefore, Hart-Smith's and the present methods will have large errors for long overlaps. Large displacements are included in Goland and Reissner's method.

Consequently, it is superior to Hart-Smith's and the present methods for very long overlaps. It is felt that the rigid-overlap assumption is acceptable for joints with up to 50 mm overlap. However, it should be noted that the employment of closed form solutions for very long overlap joints may not be accurate enough anyway in that the solution procedure in the second step, following the determination of bending moments, is based on small displacement theories. This will therefore introduce errors in the stress analysis. As a result, large-displacement FEM is the only tool which should be used for very long overlap joints.

3.4.1.2 The change in the thickness of the adherends

It has been shown that all the joints analysed have 1.6mm adherends. In joint testing, thick adherends are often used, such as the so-called thick adherend shear test. To assess the accuracy of the present method for thick adherends, analyses have been done with 12.7mm and 50mm overlaps for 3.2mm and 6.35mm adherends. Figures 3.16 and 3.17 show the results with 12.7 mm overlap for 3.2mm and 6.35mm adherends. It can be seen that all the methods give accurate predictions of the bending moments for the thick adherends. This is also true for the 50mm overlap as shown in Figures 3.18 and 3.19. It can be seen that more accurate results are given with the analytical methods for thick adherends than for thin ones. The reason is that thick adherends have larger stiffness and thus bend less than thin ones. As a result, the rigid overlap assumption holds more for thick adherends than for thin ones.

3.4.1.3 Variation in the stiffness of the adherends

It has been shown that the analytical methods are more accurate for thick adherends than for thin ones. It may be argued that the method should be more accurate for stiff adherends than for flexible ones. In fact, this is true as shown in Figures 3.20, in which the adherend properties are those of a typical steel with a 1.6 mm thickness and a 50 mm overlap. It clearly shows that the methods are much more accurate for stiff adherends than for flexible ones as shown in Figure 3.13. Consequently, it may be concluded that the stiffer the adherends (either high Young's modulus or large thickness), the more accurate the analytical methods.

3.4.2 Non-identical adherends

3.4.2.1 Adherends having different material properties

Having discussed results for balanced single lap joints, the unbalanced single lap joints are calculated below. First, the geometry of the joints is kept the same as that of balanced joints. But material properties are changed as shown in Figure 3.2, which is typical of a steel/aluminium joint. A joint with a 12.7mm (half inch) overlap is used followed by a joint with a 25mm overlap. Bending moments are shown in Figures 3.21 and 3.22. Results from FEM are also shown in the Figures, which are used to assess the accuracy of the analytical methods. It can be seen that the present method is accurate for the whole range of the load for the 12.7 mm overlap. The present method overestimates the bending moments at the stiff end but underestimates the bending moments at the flexible end. The bending moments at the stiff adherend are higher than that at the flexible one. It should be pointed out that the error at the flexible adherend is a little larger than that at the stiff one. The reason may be that the flexible adherend bends more than the stiff one and therefore the rigid assumption holds more at the stiff end than at the flexible one. However, they are accurate enough to be used practically. For joints with a 25mm overlap, the present method is accurate for up to 400 N/mm load. The errors became larger as the load increased as shown in Figure 3.22. Again, the present method overestimates the bending moments at the stiff end but underestimates the bending moments at the flexible end. However, for medium load, typically 10 kN for a joint with a 25 mm width, the error is about 10 %, which is still acceptable for engineering applications. Although Goland and Reissner's method is not applicable to joints with different adherends, their method has been used to calculate the bending moments for joints with different adherends. The procedure is as follows. When calculating bending moments for joints with different adherends, the joint is so treated as to consist of identical adherends for each of the adherends. Thus, two bending moments may be calculated by inputting the material properties of either adherend into their formula. Surprisingly, the bending moments so calculated agree well with the FE results as is shown in Figure 3.22. More research is needed to establish this procedure.

The above discussion is mainly concerned with 1.6 mm adherends. To model the effect of the thickness of adherends on the accuracy of the determination of bending moments, analyses are made with 3.2 mm and 6.35 mm adherends with the material properties kept unchanged. Figures 3.23 to 3.26 show the bending moments for 3.2 mm and 6.35 mm adherends with 12.7 mm and 25 mm overlaps. It can be seen that the present method is more accurate for thick adherends than for thin ones as discussed above, especially for the 50 mm overlap. However, it should be noted that for very thick adherends (6.35 mm) with stiff materials (E=207 GPa), the assumption in Eq. 3.15 is not valid as can be seen in Figure 3.27. Figure 3.27 shows that large difference exists between the two curves, which, according to the assumption in Eq. 3.15, should be very close to each other. Figures 3.28 and 3.29 show the results by using Eqs. 3.13 and 3.14 and the simplified Eqs. 3.18 and 3.19. The results from FEM are also shown in the Figures. They clearly show that there is a big difference between the results from Eqs. 3.13 and 3.14 and the simplified Eqs. 3.18 and 3.19. As a result, Eqs. 3.13 and 3.14 should be used instead of Eqs. 3.18 and 3.19 for stiff and thick adherends. In fact, the predictions in Figures 3.23 to 3.26 are based on Eqs. 3.13 and 3.14. The invalidity of assumption in Eq. 3.15 was neither addressed by Goland and Reissner (1944) nor by Hart-Smith (1973). From this analysis, it may be concluded that care needs to be taken with thick and stiff adherends (e.g. the thick steel adherend) when using Eqs. 3.18 and 3.19. The conditions in Eq. 3.15 need to be satisfied to use Eqs. 3.18 and 3.19. Otherwise, Eqs. 3.13 and 3.14 should be used. This will be further demonstrated below.

3.4.2.2 Different thickness of adherends

To model the second type of unbalanced joint, the material properties are kept the same (aluminium), but the thickness of one of the adherends is increased to five times larger than that of the other one as shown in Figure 3.2. Joints with 12.7mm and 25mm overlaps are used. Again, comparison is only made with FEM as shown in Figures 3.30 and 3.31. It is clearly shown that the present method with the simplified equations yields accurate results for both thick and thin adherends for the two overlaps. It can also be seen that the bending moments in the thick adherend are much higher than in the thin one. The bending

moments increase almost linearly with the applied load. The effect of the stiffness of adherends on the accuracy of the calculations of the bending moments is shown in Figure 3.32, in which the stiffness of both the adherends is 207MPa and the length of the overlap 25mm. It can be seen that the present method for the stiff adherends give more accurate results than for flexible ones as shown in Figure 3.31. This is in line with the above discussions that the stiffer the adherends, the more accurate the present method. It should also be noted that the results shown in Figure 3.32 are based on Eqs. 3.13 and 3.14 rather than the simplified Eqs. 3.18 and 3.19. The reason is the same as that given above. Here for the stiff and thick adherends, the conditions for the assumptions in Eq. 3.15 are seriously violated. Therefore, Eqs. 3.18 and 3.19 produce a large error for the stiff and thick adherends as shown in Figure 3.33. Figure 3.33 shows the results by using Eqs. 3.13 and 3.14 and the simplified Eqs. 3.18 and 3.19. Results from FEM are also shown in the Figure. In this case, the results based on Eqs. 3.18 and 3.19 have too large errors to be any use. As a result, care must be taken when using the simplified Eqs. 3.18 and 3.19. The conditions must be checked before deciding which equations should be used.

3.5 CONCLUSIONS

It has been shown that the new method is accurate for single lap joints with reasonably long overlaps. It can be used either for identical adherends or, in particular, for non-identical ones for which the present method is very simple but accurate. The bending moments are found to be insensitive to the length of the adherend outside the overlap. The thicker and stiffer the adherends, the more accurate the present method. An important conclusion here is that the bending moments at the ends of the overlap are induced by the eccentric geometry effect and have little to do with the stiffness of the overlap. Care must be taken to use the appropriate equations when analysing stiff and thick adherends.

Chapter 4

A TWO-STEP PROCEDURE FOR THE STRESS ANALYSIS OF LAP JOINTS

4.1 SUMMARY

In this chapter, a two-step procedure, based on the analytical methods and FEM, is proposed for the analysis of lap joints. The basic idea is to take advantage of the analytical and numerical methods so as to develop an accurate and effective method for obtaining the stress state in lap joints. A special package based on this procedure may be written which may be used in the same way as analytical methods (Mallick, 1989). It is well known that analytical solutions are easy to use, while numerical methods such as FEM can accurately model the joints. To keep the advantages and discard the disadvantages of both methods, it is proposed to use the analytical method to determine the bending moments at the ends of the overlap of a lap joint, and then to analyse the overlap region with FEM to calculate the stresses in the adhesive layer with the bending moments from the first step as boundary conditions. In the first step, the new method given in Chapter 3 may be used to obtain the bending moments at the ends of the overlap. In the FE process, a program based on a hybrid element has been developed in order to obtain accurate calculations with a modest number of elements. Such an element is the most effective of 4-noded linear elements for bending problems (Zienkiewicz and Taylor, 1988). The procedure is effective and may be used on a personal computer.

4.2 INTRODUCTION

Analytical solutions and numerical methods have long been used in parallel, having their advantages and disadvantages as discussed in Chapter 2. All the analytical approaches require a two-step solution procedure, but the FE solution is achieved in one step. For single lap joints, the two-step procedure significantly reduces the complexity involved in the mathematical process and most of the work can then be devoted to the overlap region. It has been shown in Chapter 3 that the bending moments obtained with the new method are accurate. FEM, however, treats the joint as a whole structure and, inevitably, requires

large displacements analysis. This can only be undertaken iteratively and requires a large amount of computing time even for an elastic solution. Because the bending moments at the ends of the overlap have been accurately evaluated with a simple equation, the adherends outside the overlap need not be included in the stress analysis of a single lap joint. It seems that the two approaches differ from each other so much that they have never been combined to generate an effective and user-friendly method. In this chapter it is intended to take advantage of both methods to form an effective and accurate procedure. A four node linear element is implemented which is the most effective of 4-noded elements for bending problems. However, it will be shown that the two-step procedure is not effective for double lap joints, although they are much easier to analyse than single lap joints. Thus, for the double lap joint, the present method can easily be used, whilst the analytical methods involve large errors. Two proposals are put forward to analyse the double lap joint with the present method.

From the author's point of view, the two-step procedure in the closed form solutions is an excellent idea and this should be utilised in the FE analysis. The large displacements or stress-stiffening need not be included so that computing time can be much reduced if the two-step procedure is adopted. On the other hand, the FE modelling of the overlap region is very accurate and therefore this should be used to analyse the bond stresses. The whole chapter is based on this idea and the results from this procedure is demonstrated in comparison with both the analytical and FE analyses.

It is noted that the analysis of the overlap region is a plane strain bending problem. It is well known that the best 4-noded element for plane bending problems is the so-called hybrid elements (Pian, 1964 and Zienkiewicz and Taylor, 1988). The hybrid element is adopted here and a program has been written to solve lap joint problems. It is noted that there are many hybrid elements in the FE literature (Atluri *et al*, Ed., 1982). To demonstrate the procedure proposed above, the earliest hybrid element (Pian, 1964) has been incorporated in the program and it is accurate enough for bond stress analyses. More complicated hybrid elements can be found in the FE literature (e.g. Pian, 1987). It should be pointed out that the above proposed procedure can also use either displacement type (see

Appendix 1) or stress type elements (Allman, 1977 and Mallick, 1989). However, they require more elements for the same accuracy. In this chapter, the basic theory is introduced first, followed by the discussion of computing aspects. Two methods are proposed to analyse double lap joints, where analytical methods result in large errors. Finally, some results from the current procedure are presented to demonstrate the accuracy of the method.

4.3 THEORY

Generally speaking, there are three types of elements in the FE literature, displacement, stress and hybrid or mixed elements. The displacement elements have been extensively developed and widely used. They are convenient and easy to program, but they suffer from the fact that they tend to make a structure stiffer because of the assumed limited degrees of freedom of the given structure. Elements based on the stress assumption in the elements have been largely ignored, although this type of element can be very useful in engineering applications (Robinson, 1983). However, structures modelled by stress elements tend to be softer, because the displacement compatibility is not generally satisfied. It was Pian (1964) who was the first to propose a new type of element which combines the displacement and stress element: this was later termed a hybrid element. Results from hybrid elements lie between the displacement and stress types of element and therefore they are more accurate than either the displacement or stress elements in most circumstances.

The basic idea is that stresses are assumed inside the element but displacements on the boundaries of the element. It is clear that two field parameters are assumed independently initially. The assumed stresses satisfy equilibrium inside the element and the displacements compatibility on the element boundaries. The above assumption that stresses are in equilibrium have been extended (Pian, 1984), but this assumption is still made here. Elasticity requires that stresses are in equilibrium and displacements are compatible. According to these requirements, the above independently assumed stresses and displacements are then constrained to best satisfy the basic equations in elasticity. In this process, two energy principles in elasticity are used which best satisfy the basic equations in

elasticity with the assumed stresses and displacements. The stiffness matrix can then be derived after this process. Below are the details of this process.

The stress distribution $\{\sigma\}$ ($= \{\sigma_{11}, \sigma_{12}, \ldots\}$) inside the element is expressed as

$$\{\sigma\} = [P]\{\beta\}, \tag{4.1}$$

where the terms of the matrix [P] are functions of the coordinates x_i (i=1,2,3). The number of elements in $\{\beta\}$ is unlimited. It should be noted that the stresses in Eq. 4.1 should satisfy equilibrium equations. This condition has been eliminated later (Pian, 1984). However, for the element used here, this condition is still satisfied. Assuming that the stress and strain relations are linear, we have

$$\{\epsilon\} = [N]\{\sigma\}, \tag{4.2}$$

where [N] is a matrix of elastic constants. For plane strain, [N] are

$$[N] = \frac{1+\mu}{E} \begin{bmatrix} 1-\mu & -\mu & 0 \\ -\mu & 1-\mu & 0 \\ 0 & 0 & 2 \end{bmatrix} \tag{4.3}$$

where E is Young's modulus and μ is Poisson's ratio.

Then the internal strain energy can be written as

$$U = \frac{1}{2} \int_V \{\sigma\}^T [N] \{\sigma\} \, dV \tag{4.4}$$

or

$$U = \frac{1}{2} \{\beta\}^T [H] \{\beta\} \tag{4.5}$$

where

$$[H] = \int_V [P]^T [N] [P] \, dV \tag{4.6}$$

It may be seen that [H] is symmetric.

Having assumed the stresses inside the element, the displacements at the boundary of the element are also prescribed as

$$\{u\} = [L]\{q\} \tag{4.7}$$

where {q} are the n generalized displacements and the terms in the matrix [L] contain coordinates of the element surface.

Now two field variables exist independently and the next step is to combine them. It is clear that the final solution to the problem must to attemt to satisfy both displacement compatibility and stress equilibrium. Now the stresses in Eq. 4.1 have satisfied equilibrium inside the element and the displacements in Eq. 4.7 have satisfied the displacement compatibility on its boundary. If the displacement compatibility inside the elements and the stress equilibrium on the element boundaries can be satisfied, the solution will be exact. However, this will be extremely difficult if not impossible. However, an approximation can be made here which will best satisfy the displacement compatibility and stress equilibrium with the given stresses in Eq. 4.1 and the assumed displacements in Eq. 4.7. This can be done with the complementary energy principle (Washizu, 1982) and the potential energy principle. The complementary energy density is defined as the area between the stress-strain curve and the stress axis in a stress-strain curve. The complementary energy is the integral of the complementary energy density over all the volume of the body. Before the complementary energy principle is used, the tractions at the element boundary are first determined. The traction components can be related to the stress components by

$$S_i = \sigma_{ij} n_j \tag{4.8}$$

where n_j is the direction cosine of the surface normal. By using Eq. 4.1, the tractions {S} on the surface of the element can be expressed in terms of the stresses {β} as

$$\{S\} = [R]\{\beta\} \tag{4.9}$$

where the terms in [R] also contain the coordinates of the surface. The total complementary energy is then

$$\Pi_c = \tfrac{1}{2} \{\beta\}^T [H]\{\beta\} - \{\beta\}^T [T]\{q\} \tag{4.10}$$

where

$$[T] = \int_A [R]^T[L]\, dA \tag{4.11}$$

The complementary energy principle states that the complementary energy is minimum when displacement compatibility is satisfied. Applying this principle, we have

$$[H]\{\beta\} = [T]\{q\} \tag{4.12}$$

or

$$\{\beta\} = [H]^{-1}[T]\{q\} \tag{4.13}$$

The displacement compatibility for individual elements has been best approximated based on the assumed stresses inside the elements and displacements on their boundaries. Also, it is clear that the displacements on the common boundaries between adjacent elements are compatible. Only the stress equilibrium for the whole structure needs to be satisfied. This can be done in the usual way in the FEM, that is, by minimising the strain energy. Substituting Eq. 4.13 into Eq. 4.5, we have

$$U = \tfrac{1}{2}\{q\}^T[T]^T[H]^{-1}[T]\{q\} \tag{4.14}$$

Thus, the stiffness matrix can be written as

$$[k] = [T]^T[H]^{-1}[T] \tag{4.15}$$

It should be noted that the above stiffness matrix is for an element. To derive the stiffness of the whole structure, these elements may simply be assembled as is done in the general FE procedure. The same is true for nodal forces which need to be assembled too.

Having laid down the basic theory, the element in Fig. 4.1 is discussed here. For this element, the stresses which satisfy the equations of equilibrium can be expressed as

$$\sigma_x = \beta_1 + \beta_2 y \tag{4.16a}$$

$$\sigma_y = \beta_3 + \beta_4 x \tag{4.16b}$$

$$\tau_{xy} = \beta_5 \tag{4.16c}$$

The traction matrix consists of eight elements representing the x and y components of the tractions along the four edges. These are as follows

$$\{S\} = \begin{bmatrix} (S_x)_{AB} \\ (S_y)_{AB} \\ (S_x)_{BC} \\ (S_y)_{BC} \\ (S_x)_{DC} \\ (S_y)_{DC} \\ (S_x)_{AD} \\ (S_y)_{AD} \end{bmatrix} = \begin{bmatrix} -\tau_{AB}(x) \\ -\sigma_{yAB}(x) \\ \sigma_{xBC}(y) \\ \tau_{BC}(y) \\ \tau_{DC}(x) \\ \sigma_{yDC}(x) \\ -\sigma_{xAD}(y) \\ -\tau_{AD}(y) \end{bmatrix} \tag{4.17}$$

where the notations can be found in Figure 4.1. Substituting Eqs. 4.16 into Eq. 4.17, we have

$$\{S\} = \begin{bmatrix} 0 & 0 & 0 & 0 & 1 \\ 0 & 0 & -1 & -x & 0 \\ 1 & y & 0 & 0 & 0 \\ 0 & 0 & 0 & 0 & 1 \\ 0 & 0 & 0 & 0 & 1 \\ 0 & 0 & 1 & x & 0 \\ -1 & -y & 0 & 0 & 0 \\ 0 & 0 & 0 & 0 & -1 \end{bmatrix} \begin{bmatrix} \beta_1 \\ \beta_2 \\ \beta_3 \\ \beta_4 \\ \beta_5 \end{bmatrix} \tag{4.18}$$

Here, the matrix which precedes the $\{\beta\}$ vector is [R]. The displacements on the boundary of the element can be written as

$$\{u\} = [L]\{q\} = \begin{bmatrix} 1-x/a & 0 & x/a & 0 & 0 & 0 & 0 & 0 \\ 0 & 1-x/a & 0 & x/a & 0 & 0 & 0 & 0 \\ 0 & 0 & 1-y/b & 0 & y/b & 0 & 0 & 0 \\ 0 & 0 & 0 & 1-y/b & 0 & y/b & 0 & 0 \\ 0 & 0 & 0 & 0 & x/a & 0 & 1-x/a & 0 \\ 0 & 0 & 0 & 0 & 0 & x/a & 0 & 1-x/a \\ 1-y/b & 0 & 0 & 0 & 0 & 0 & y/b & 0 \\ 0 & 1-y/b & 0 & 0 & 0 & 0 & 0 & y/b \end{bmatrix} \begin{bmatrix} q_1 \\ q_2 \\ q_3 \\ q_4 \\ q_5 \\ q_6 \\ q_7 \\ q_8 \end{bmatrix} \tag{4.19}$$

The [T] matrix can be evaluated according to Eq. 4.11 as follows

$$[T] = \begin{bmatrix} -b/2 & 0 & b/2 & 0 & b/2 & 0 & -b/2 & 0 \\ -b^2/6 & 0 & b^2/6 & 0 & b^2/3 & 0 & -b^2/3 & 0 \\ 0 & -a/2 & 0 & -a/2 & 0 & a/2 & 0 & a/2 \\ 0 & -a^2/6 & 0 & -a^2/3 & 0 & a^2/3 & 0 & a^2/6 \\ -a/2 & -b/2 & -a/2 & b/2 & a/2 & b/2 & a/2 & -b/2 \end{bmatrix} \tag{4.20}$$

To build up the [H] matrix, the constitutive equations are needed. For lap joints, it is common practice to model joints assuming two-dimensional plane strain. Plane stress analysis follows the same procedure. The constitutive equations for plane strain is given in equation 4.3.

For this element, the [H] matrix can be explicitly expressed as

$$[H] = \frac{(1+\mu)ab}{E}\begin{bmatrix} 1-\mu & & & & \\ (1-\mu)b/2 & (1-\mu)b^2/3 & & S & \\ -\mu & -\mu b/2 & 1-\mu & & \\ -\mu a/2 & -\mu ab/4 & (1-\mu)ab/2 & (1-\mu)a^2/3 & \\ 0 & 0 & 0 & 0 & 0.5 \end{bmatrix} \tag{4.21}$$

where a and b are the lengths of the element.

Having obtained the matrices required in Eq. 4.15, the stiffness matrix can then be evaluated for each element. The stiffness matrix for the whole structure can be assembled by normal FE procedures, as is the force vector, to form the equations of equilibrium for the whole structure as

$$[k]\{q\} = \{f\} \tag{4.22}$$

which can be easily solved by Gaussian elimination. Once {q} has been calculated for each element, the stress coefficients (β) for the element can be obtained by using Eq. 4.13 and then the stresses (σ) using Eq. 4.16. It should be noted that the [H] matrix needs to be inverted for each element, which may take a large amount of computing time and may introduce some computational errors. However, the order of the [H] matrix is only five, which can be easily handled on a small computer. Also, a special pivoting procedure is used below to invert the [H] matrix so that the error in inverting [H] is made small.

4.4 IMPLEMENTATION

A program called HYBRID was written to implement the above procedure. At this stage, the program can only be run on mainframe with FORTRAN compilers. Ideally, the program should be adapted to run on a personal computer according to the aim of the present method proposed in the above introduction. However, no effort was made to write a PC version, because the present work was to demonstrate the method rather than writing a package. More work needs to be done to implement such a program on a personal computer.

Element stiffness matrices as in Eq. 4.15 are calculated first. The element stiffness matrices are then assembled to form the stiffness matrix for the whole structure and the equations of equilibrium are solved by Gaussian elimination. Finally, the stresses in each element are calculated. A time consuming part is the inversion of the [H] matrix for each element. In

the present program, a fully pivoting procedure is used (Collar and Simpson, 1986), which is thought to be accurate enough not to introduce extra errors in the formulation of element stiffness matrices. This pivoting scheme is accurate but time consuming. Another pivoting procedure called diagonal pivoting (Sehmi, 1985, Zhao and Simpson, 1987) may be used which is more efficient but less accurate. Here the fully pivoting procedure is adopted. Having inverted the [H] matrix, the stiffness can be formed by matrix multiplications. After the element stiffness matrix has been obtained, these are assembled and solved by Gaussian elimination. A semi-automatic mesh generating program (Chen, 1982) has been modified to generate 4-noded elements and nodes. The stresses for each element are calculated by using Eqs. 4.13 and 4.16. These stresses are then averaged at the nodes, which may be more accurate than stresses calculated in individual elements (Zienkiewicz and Taylor, 1988). All the above procedures are included in the program HYBRID. The program was tested with simple structures before it was applied to the analysis of lap joints.

4.5 RESULTS

The program described above was used to analyse both single and double lap joints with the two-step procedure. The geometries of the single and double lap joints, 25.4 mm in width, are shown in Figures 4.2 and 4.3. The material properties are as follows

Adherend Young's modulus	70 GPa
Adherend Poisson's ratio	0.33
Adhesive Young's modulus	2.8 GPa
Adhesive Poisson's ratio	0.4

A load of 12 kN was applied throughout the analyses. The method in Chapter 3 was used to determine the bending moments so that the boundary conditions for the overlap region of a single lap joint were obtained according to the plate bending theory as shown in Figures 4.2 and 4.3. Boundary conditions were applied to the overlap region to remove the rigid-body motion. The mesh used is shown in Figure 4.4. The stresses in the adhesive layer are at the central line of the adhesive layer, averaged at the nodes with stresses in the two layers of the elements below and above the central line.

4.5.1 Single lap joint

Before any results are presented, the boundary conditions in the adherends at the ends of the overlap are discussed. In analytical analyses, it is assumed that the longitudinal stresses in the adherends at the ends of the overlap are linear across adherend thickness, while the shear stresses are quadratic, as shown in Figure 4.2. To verify this assumption, the longitudinal and shear stresses in the adherends at the ends of the overlap were calculated with FEM on the whole joint. Figures 4.5 show the longitudinal and shear stresses at one end of the overlap from FEM. The assumed stresses in analytical methods are also shown in the figures. They clearly show that the longitudinal stresses in the adherend are almost identical for the two analyses. However, large difference is apparent for the two shear stresses. The results from FEM are thought to be accurate and reliable. The analytical methods involve large error in shear stresses. However, it should be noted that the magnitude of the shear stress is much smaller than that of the longitudinal stress. In addition, the sums of the shear stresses of the two models are equal. Therefore, the shear stresses play a less important role in the analysis of the overlap region than the longitudinal stresses in the adherends. It may be concluded that the method presented in Chapter 3 may accurately represent the true situation.

The present results are compared with those from conventional FEM and Allman's method. Analyses based on FEM have been carried out by using FELDEP and ANSYS with similar meshes. Allman's method has been extended by Mallick (1989) to include longitudinal stresses in the adhesive layer and the extended version was used. All the results are plotted at the middle of the adhesive layer.

Figure 4.6 shows the peel stresses plotted against the overlap length from one end of the overlap for a single lap joint. It can be seen that all three methods give almost identical results for the majority of the overlap, except at the ends of the overlap. The present method agrees very well with the FE analysis on the whole joint, which proves that the two-step procedure is accurate for the single lap joint. At the ends of the overlap, Allman's solution gives lower peel stresses, whilst the peel stresses from FE analysis using FELDEP

are little higher than the that using ANSYS. The present method yields very close results with the FE analysis with ANSYS.

Figure 4.7 shows the shear stress distribution along the overlap. It may be seen that the FE analyses predict higher shear stresses than Allman's method. The present method and the FE analysis from FELDEP yield almost identical results, these being a little lower than that from ANSYS. For the majority of the overlap, all the methods produce almost the same results.

The longitudinal stresses are plotted in Figure 4.8. Large difference exists between the FE analysis from ANSYS and all the other analyses. The FE analysis from ANSYS gives much higher longitudinal stresses than other analyses at the ends of the overlap. Slight differences exist between the other three analyses. It should be noted that the longitudinal stresses are of the same order as other stresses and therefore they need to be taken into account in failure criteria.

It may be concluded from the above analysis that the present method predicts all the stresses in a single lap joint accurately.

4.5.2 Double lap joints

It seems that double lap joints are much easier to analyse than single lap joints in that no large rotation of the overlap is involved. As a result, all the analytical methods employ uniform longitudinal stresses as shown in Figure 4.2 as boundary conditions for the stress analysis of the overlap region. Initially, this was followed in the present method. To verify the validity of the stresses at the ends of the adherends, FE analysis has been performed for the whole joint utilising the symmetric property of the double lap joint with reference to the central line of the central adherend. The longitudinal and shear stresses at the ends of the overlap are shown in Figures 4.9 and 4.10, respectively. It may be seen that the longitudinal stresses at both ends of the overlap are approximately uniform, which indicates that uniform longitudinal stresses can be used for the input of the overlap region. However, large shear stresses exist at the ends of the overlap as is shown in Figure 4.10. The shear

stresses in the central adherend are significant, whilst the shear stresses in the outer adherend are negligible. Because of the large shear stress in the central adherend, some error in the stresses in the adhesive layer may be induced with the two-step procedure without taking account of the shear stresses in the centre adherend. In fact, this is so for all the stresses, especially the peel stresses, in the adhesive layer, which will be discussed below.

Peel stresses at the central line of the adhesive are shown in Figure 4.11 by assuming uniform longitudinal stresses across the adherend thickness. It is clear that a large discrepancy exists between the two-step methods and the FE analysis based on the whole joint. The FE analysis on the whole joint yields nearly twice the peel stress as the two-step methods at the tensile end. Little difference was found at the compression end. The present method and the Allman's method give almost identical results. The large variations in the peel stresses between the two-step methods and FE on the whole joint are thought to be due to the shear stresses in the centre adherend at the ends of the overlap. As discussed in Chapter 2, the shear stress at the end of the adherend will introduce a large amount of shear strain and therefore corresponding stresses in the adhesive layer.

Figure 4.12 shows the shear stresses at the middle of the adhesive layer. Again, the FE analysis on the whole joint gives the highest shear stress near the ends of the overlap. However, the variation in shear stresses is much reduced compared with the peel stresses. For engineering applications, the shear stress predictions with the two-step method are accurate enough. Also, the shear stresses are not symmetric with respect to the centre of the overlap, the shear stress at the tensile end being a little higher than at the other end.

Finally, the longitudinal stresses vary in almost the same way as the peel stresses. It should be noted that the longitudinal stresses are quite significant as shown in Figure 4.13. It is therefore necessary to include these stresses in the failure prediction.

It may be concluded from the above results that closed-form analytical methods cannot be used to predict the peel and longitudinal stresses in a double lap joint accurately. Only the shear stress may be predicted by the analytical methods. Because the present method uses

the same boundary conditions at the ends of the overlap, it cannot be used to predict the peel and longitudinal stresses either. Unless the shear stresses in the central adherend at the ends of the overlap can be determined accurately without resorting to analysis of the whole joint, a full FE analysis on the whole joint is recommended. However, the present method can be easily extended to analyse the whole joint without any difficulty. This may make the mesh generating process a little more difficult, but because of the simple geometry, this should not be difficult.

4.5.3 Comparison of single and double lap joints

As discussed above, the present method is more suitable to the analysis of single lap joints than to that of double lap joints. Although a double lap joint seems simpler to analyse than a single lap joint, there are no analytical methods available to determine the shear stresses in the central adherend at the ends of the overlap. Although the two-step method can predict the shear stresses quite accurately, large errors exist for the peel and longitudinal stresses. It is the peel stresses which are most responsible for the failure of a joint. Therefore, two-step methods are not recommended for the stress analysis of a double lap joint. Instead, a full FE analysis on the whole joint or the methods presented below are essential.

4.6 IMPROVED ANALYSES FOR DOUBLE LAP JOINTS

As discussed above, the two-step method is unable to obtain peel and longitudinal stresses accurately in the adhesive layer for a double lap joint. As a result, more research is needed to improve the analysis. A straightforward method is to use a full FE analysis as mentioned above to include the central adherend, but the outer adherend outside the overlap is ignored. This method gives the most accurate results, as will be presented below. Another improvement may be made by analysing the overlap region with the aid of analytical methods. The first analysis is the usual procedure in all the analytical methods. The shear stresses in the adhesive from analytical methods are then used as boundary conditions acting at the central adherends at the ends of the overlap. This method is based on the fact that the shear stresses in the adhesive layer and in the adherends are equal at the interface

between them. The shear stresses so obtained in the adherends at the ends of the overlap may not be exact in the real situation. However, it has been shown that the analytical methods give fairly accurate shear stresses in the adhesive layer. Therefore, the error may be small enough for engineering applications. The second method is very easy to implement in the present method, which does not need to include the centre adherend outside the overlap.

4.6.1 FE analysis including the centre adherend outside the overlap

In the first place, the above hybrid finite element method has been extended to include the central adherends outside the overlap. This method is straightforward, and it only requires a little more effort in the mesh generating process. Because the geometry is very simple, the mesh generating process may be easily included in the mesh generating process. Figures 4.14 to 4.16 show the peel, longitudinal, and shear stresses at the central layer of the adhesive. It may be seen that they give accurate results.

4.6.2 Analysis without the centre adherend outside the overlap

The second improvement in the stress analysis is based on the observation that the shear stresses at the central adherend surfaces adjacent to the adhesive are equal to that in the adhesive layer. With this observation, the analysis was divided into two steps. The overlap region was first analysed with the usual process as demonstrated above with uniform tensile stresses as input data, or more effectively, with analytical methods. The shear stresses in the adherends were then assumed to be equal to that in the adhesive layer at the interface at the ends of the overlap. The shear stress distribution in the centre adherend was then assumed to be linear across the thickness, with the shear stresses at the middle of the centre adherend being zero. The shear stresses and the uniform tensile stresses were then used as boundary conditions for a re-analysis of the overlap. Because the peel stresses in the adhesive layer are under-estimated with the normal procedure and the shear stresses drop sharply across the central adherend thickness, the shear stresses were applied at the interface between the central adherend and the adhesive. This may cause some error in the stress analysis. However, it is felt that the error may be small enough for the stress analysis.

The results are shown in Figures 4.14 to 4.16. It may be seen that this method is very accurate for all the stresses. This confirms that this improvement may be used for the stress analysis of double lap joints.

4.7 CONCLUSIONS

A new two-step method based on the bending moment determination in Chapter 3 and a hybrid element has been developed. It has been shown that this method is very accurate for the stress analysis of a single lap joint, but errors exist for the stress analysis of a double lap joint. It is therefore essential to perform a full FE analysis on the whole of a double lap joint. This can be easily included in the present method. However, in order to avoid the full FE analysis on the whole joint, another method has been put forward, which utilises the shear stress in the adhesive layer from analytical methods as input for the current method. Hybrid elements are the best elements in bending problems. Consequently, many fewer elements are needed to fulfil the same task as other elements. The present method is especially useful for a non-linear stress or strain analysis, because FEM has well been developed to include non-linear material properties, whilst the development of analytical methods is very difficult. However, more work is needed to implement the current method on a PC.

Chapter 5

THREE DIMENSIONAL STRESS ANALYSIS OF LAP JOINTS

5.1 INTRODUCTION

It has been discussed that stress concentrations at the ends of the over-lap are extremely high. The areas around the ends of the over-lap are critical to the determination of the joint strength. A detailed stress analysis at the critical area is essential in predicting joint strength. There are two approaches to this problem, analytical (closed form) and numerical, mainly FEM. FEM is widely used in research because it can model joints accurately, whilst the closed form solution is generally used in joint design as it is simple to use, even though inaccurate. Most of the closed form and FE analyses are based on the two-dimensional plain strain assumption, which in fact only applies to the middle of the joint width (Adams and Wake, 1984). Experimentally, most of the joint specimens have finite width, in which the effect of the finite width on the stresses in the adhesive layer may be large. Also, it was found experimentally, that the failure locus across the width at the ends of the overlap of an joint was so complicated that it was needed to know where across the width cracks started. Furthermore, many small cracks were found to be present at the ends of the over-lap running parallel to the applied load. These cracks may be caused by stresses across the width. In order to understand the failure nature across the width, a stress analysis across the width is necessary.

Little work has been done concerning the stress distribution across the width. Hahn (1960) showed, by performing a photoelastic analysis on a single lap joint, that the shear stresses in the adhesive were highest at the corners. It was thought that the high shear stresses at the corners were caused by anti-clastic bending of the adherends. Basing his idea on this supposition, Kutscha (1964) drew a qualitative picture of the distribution of longitudinal shear stress in the adhesive of a single lap joint. Adams and Peppiatt (1973) modelled the Poisson's ratio effect on the stresses in a double lap joint. They showed that the shear stress in the adhesive and the direct stress in the adherend at right angles to the applied load were significant. Amijima *et al* (1976) performed a special FEM study on the width and

Poisson's ratio effects on the shear stresses in the adhesive layer. They also showed that longitudinal shear stresses were maximum at the edges of a lap joint. By studying the literature, it can be seen that little work has been done on the distribution of peel stress across the joint width, which is felt to be more important than the shear stress in determining joint strength. Furthermore, the direct and shear stresses at right-angles to the direction of the applied load may play an important role in predicting joint strength. All of these motivated the author to carry out a 3D stress analysis in order to obtain a clear understanding of the state of stresses in lap joints.

5.2 PROBLEM STUDIED

There are two types of joint widely used to test adhesives, single and double lap joints. The single lap joint is easy to make but large bending moments are involved because of the load eccentricity. On the other hand, double lap joints are stronger than single lap joints because no external bending moments exist. In stress analysis, large displacements have to be included in single lap joints with large loads, whereas small displacements analyses are accurate enough for double lap joints. In this study, both single and double lap joints are studied. For single lap joints, the two-step procedure outlined in Chapter 4 is used. The reason is that a large amount of computing time is involved in large displacement analysis, especially for 3D stress analysis. But by following the procedure in Chapter 4, only a small displacement analysis is needed and the two-step procedure yields accurate results (see Chapter 4). For double lap joints, the two-step procedure is also used here, although this procedure produces large error in stresses at the tension end of the double lap joint (see Chapter 4). The geometry of the lap joints studied are shown in Figures 5.1 and 5.2, in which there are no spew fillets.

5.3 FINITE ELEMENT ANALYSIS

A commercial package ANSYS was used throughout this study. It was running on the University of Bristol mainframe IBM3090. The 8-noded isoparametric block element was used for both adherends and adhesive. There were two steps in the analysis. First, the whole joint was analysed with the closed form solution (two dimensional) to obtain the

bending moments applied to the edges of the overlap as shown in Chapter 4. The bending moments were then used as boundary conditions for the analysis of the overlap region. Because of the symmetry of the joint with respect to the middle line through the joint width, only half of the joint across the width needs to be analysed. Adherends and adhesives were all modelled with two layers of elements across the thickness, twenty layers across the width and twenty layers along the overlap. A typical mesh is shown in Figure 5.3. There was slight difference between the analyses for single and double lap joints. For single lap joints, the whole region of the overlap was modelled, provided that some constraints were applied to eliminate rigid-body motions. For double lap joints, however, the problem was further simplified by analysing a quarter of the whole overlap because of the symmetry with respect to the central line of the central adherend. Again, the rigid-body motions were constrained. Also, any motions in the Y direction were restrained at the centre line of the central adherend. The material properties were the same as those in Chapter 4. A load of 12 kN was applied to the single lap joint and to each of the outer adherends of a double lap joint. Only linearly elastic materials were included here and no spew fillets were introduced.

5.4 RESULTS

5.4.1 Comparison of the FEM solution with the approximate analytical solution developed by Adams and Peppiatt (1973)

Adams and Peppiatt (1973) developed an analytical method to model the shear stresses in the adhesive layer and direct stresses in the adherends acting at right-angles to the direction of the applied load. These were shown to be significant and to be caused by Poisson's ratio strains in the adherends. Although their method was developed for single lap joints, the method was only applicable to double lap joints, because they did not consider the large rotation involved in single lap joints. Although their method is not applicable to single lap joints, some comparison is made here to assess the accuracy of their method for both single and double lap joints.

First, tensile stresses in the adherends of both single and double lap joints (σ_x) are plotted against the distance from one end of the overlap in Figure 5.4. It should be noted that the stresses in the central adherend of the double lap joint have been plotted from the other end of the overlap to compare with stresses in the outer adherend. Also, it should be noted that the stresses from 3-D FEM are at the middle plane across the adherend thickness. The stresses at the middle plane are thought to be most comparable to the results of Adams and Peppiatt's, because the longitudinal stresses in the FE analysis vary linearly across the adherend thickness. Some conclusions may be drawn from the Figure. Adams and Peppiatt's analytical method accurately predicts the tensile stresses in the adherends along the overlap for both single and double lap joints as shown in Figure 5.4. There is very little difference between the tensile stresses in the adherends for single and double lap joints, bearing in mind that the stresses are plotted at the centre line of the adherend across the thickness. It should be pointed out that the stresses from the FE analysis are those at the centre line of the adherends across the width. Later, it was found that the stresses across the width hardly changed for both double and single lap joints. Although Adams and Peppiatt successfully predicted the average tensile stresses along the overlap, their method only applies to the outer adherends of the double lap joint for the tensile stresses (σ_z) applied at right-angles to the applied load at the adherend centre across the width as shown in Figure 5.5. Next, the tensile stresses (σ_z) at right-angles to the load at a short distance from the end of the overlap (x=0.95mm) are plotted across the width in Figure 5.6. Because Adams and Peppiatt's results are only accurate for the outer adherend of the double lap joint, the stresses in the outer adherend of the double lap joint are shown here. It can be seen that Adams and Peppiatt's results agree well with the FE analysis, giving a maximum value at the centre the adherend across the width and dropping to zero at the edges of the adherend.

Having discussed the results for the adherends, the stresses in the adhesive are presented next. First, the longitudinal shear stresses (τ_{xy}) at the centres of the joint are plotted in Figure 5.7. The shear stresses from Adams and Peppiatt's method agree more with those in double lap joints than in single lap joints. This is because their method allows the central adherend to move in transverse direction (which is constrained in double lap joints) but without the inclusion of the joint rotation as in single lap joints. Shear stresses at right-

angles to the load in the adhesive (τ_{ys}) are compared in Figures 5.8 and 5.9. The transverse shear stresses at the edges of the joint along overlap from Adams and Peppiatt's method agree quite well with the FE analysis as shown in Figure 5.8, although the shear stresses for single lap joint are little higher than the other two, because joint rotation enhances the shear stresses in single lap joints. This is also so for the transverse shear stresses (τ_{ys}) in the adhesive varying across the width as shown in Figure 5.9. It can be seen that the stresses for double lap joint agree well with that from Adams and Peppiatt's.

To sum up the above results, it may be concluded that there is a significant difference in stresses between the analyses for double lap joints and for single lap joints with small displacements. This is because the centre plane is restrained in double lap joints, while it is kept free in single lap joints. This is evident in the shear stresses along the overlap in the adhesive. The shear stresses from small-displacement analysis for a double lap joint lie between those of the single and double lap joints. Therefore, the small-displacement model of a single lap joint cannot be used to analyse a double lap joint. Adams and Peppiatt's method may be used to calculate the shear stresses at right-angles to the applied load in the adhesive caused by Poisson's ratio effects. Their method is also reasonably accurate for calculating the tensile stresses (σ_x) in the adherends for both double and single lap joints.

5.4.2 General results from the FE analysis

5.4.2.1 Single Lap Joints

Results for single lap joints are shown first. Having obtained the bending moments applied to the overlap according to Eqs. 3.20 and 3.21 in Chapter 3, the longitudinal stresses in the adherends are then obtained from the thin plate theory as shown in Figure 4.2. It is supposed that the longitudinal stresses across the width are constant. Also, the longitudinal stress is assumed to vary linearly across the thickness of the adherend, while the shear stress is quadratic across the thickness as discussed in Chapter 4. It should be noted that the shear forces are obtained according to the equilibrium of the overlap as

$$Q = P/4c(h_1+h_2+2t)-(M_1+M_2)/2c \qquad (5.1)$$

There is slight difference between this shear force and that from the plate theory as discussed by Chen and Cheng (1982). It should be pointed out that a slight error is introduced by using this formula. The shear stress distribution across the thickness of the adherend from FEM is shown in Figure 4.5b. However, the shear forces are found to be small compared with the longitudinal ones and this will have little effect on the stress state in the adhesive layer.

Some results from the FE analysis are presented in this section. First, the peel stresses at the adhesive central line across the joint width in the adhesive layer are shown in Figure 5.10, in which the peel stresses in the adhesive across the width are at different positions along the overlap. It can be seen that the peel stresses remain unchanged for most of the width. They attain a maximum slightly near the edges of the joint before they decrease sharply at the edges. The reason is thought to be the anti-clastic effect in plate bending. For lap joints, peel stresses are the most critical for joint failure. From this analysis, it may be concluded that the failure initiates inside the width or near the edges rather than at the edges. The tensile stresses in the adhesive layer at right-angles to the load enhance the failure of the adhesive at the interior part of the width, because it is in the interior region (rather than the joint edges) where the tensile stresses are a maximum (above analyses and below). Close examination of failed specimens shows that small pieces of adhesive are usually left at the edges. Also, the crack front is normally as shown in Figure 5.11. This shape of the crack front can also be explained by this analysis because stresses are higher in the interior parts of the joints than those at the joint edges. Therefore, much attention needs to be paid to the interior part across the width rather than at the edges when examining the failure locus. Some misleading conclusions may be drawn by examining the failure locus at the joint edges. It seems that cracks do not run at or very close to the adherend corners if the cracks are examined at the edges as shown in Figure 5.12 (the stress distribution is believed to have the same features across the width if spew fillets are included).

Longitudinal shear stresses (τ_{xy}) across the width are shown in Figure 5.13. As Hahn (1960) and Kutscha (1964) reported, the maximum longitudinal shear stresses are at the edges of

the joint. The figure shows that the shear stresses have a large peak near the edges, while for the majority of the width, the shear stresses are almost constant. This is in line with peel stresses distribution across the joint width, because the anti-clastic effect is significant only at or near the edges of the joint. The tensile stresses (σ_z) at right-angles to the load across the width are shown in Figure 5.14. Again, the z-stresses remain constant for the majority of the width. They drop to zero at the edges because of the free surfaces at the edges. The stresses in the figure are not zero at the edges because of the coarse mesh used here. The z-stresses are caused by the Poisson's ratio effects. It should be noted that the magnitude of the z-stresses is large, being of the same order as the longitudinal stresses. Therefore in failure predictions, the z-stresses have to be included, because tension is the worst stress state as far as the joint strength is concerned. Bulk material tests usually give material properties in uniaxial tension, but the behaviour in tri-axial tension also needs to be determined. The shear stresses across the width (τ_{yz}) are shown in Figure 5.15. Maximum values appear to be at the edges of the joint, where the shear stresses should be zero because of the free surfaces there (complementary shear). The reason is that the mesh used here is quite coarse and the shear stresses (τ_{yz}) change sharply near the joint edges. A finer mesh would be necessary to see the zero shear stresses. The longitudinal stresses (σ_x) along the X axis across the width are shown in Figure 5.16. Similar to the peel stresses, the longitudinal stresses remain unchanged for most of the width, but they decrease sharply near the edges of the joint. Maximum principal stresses are often used as a failure criterion. Therefore, a clear understanding of their distribution across the width is necessary. Figure 5.17 shows the maximum principal stresses across the width at different positions along the overlap. It can be seen that they vary similarly to the other stresses, being unchanged for most of the width and peaking slightly before decreasing sharply near the edges of the joint.

5.4.2.2 Double Lap Joints

It has been pointed out in Chapter 4 that the two-step procedure is not exactly applicable to double lap joints, in which lower stresses are predicted at the tension end. However, the pattern of the distribution of stresses is still, to some extent, useful. Therefore, the two-step

procedure is also used here, bearing in mind that the stresses from this analysis are lower than the true values. With this two-step procedure, double lap joints are easier to analyse than single lap joints. Because of the symmetric property with respect to the central line, the bending moments applied to the ends of the overlap are negligible. As a result, the boundary conditions applied to the ends of the overlap are pure uniform tension similar to that in Figure 4.3. Again, the x longitudinal stresses across the width at the boundaries are assumed to be constant. A quarter of the joint needs to be analysed with all the degrees of freedom along the Y axis at the central plane of the joint being constrained. The mesh is shown in Figure 5.3 and the material properties are the same as used for the single lap joints. The applied force of 12 kN is the same as in the single lap joint. Therefore, some results from the two analyses are comparable.

First, the variation in the peel stresses in the adhesive across the width at the central and outer adherends and at the centre of the adhesive are shown in Figure 5.18. This is similar to the distribution for single lap joints, although the magnitude is much smaller; the peel stress distribution across the width remains unchanged for most of the width. These peak slightly before decreasing sharply near the edges of the joint. As for single lap joints, from the peel stress distribution it may be argued that the interior part across the width is more likely to fail than the edges. Therefore, attention needs to be given to the interior part when examining joint failure loci for double lap joints. The shear stresses (τ_{xy}) in double lap joints change across the width similarly to those in single lap joints, as shown in Figure 5.19. Again, the peak values across the width exist at the edges and the shear stresses remain unchanged before increasing sharply very near to the edges of the joint. The distribution of z-stresses across the width for double lap joints is similar to that of single lap joints as can be seen in Figure 5.20. The z-longitudinal stresses should be zero at the edges of the joints. However, because of the coarse mesh used here, they are not zero. The longitudinal stresses in the loading direction are shown in Figures 5.21. Figures 5.22 shows the stresses across the width at the compression end. It can be seen from Figure 5.22 that the compression peel stresses inside the width are much larger than at the edges. The z-stresses (σ_z) across the width are also in compression with the peak compression values in the central part across the width. The compression stresses are because of the Poisson's ratio

effect associated with the plane stresses σ_x, τ_{xy} and σ_y. The shear stress distribution is similar to that at the other end of the overlap.

5.5 CONCLUSIONS

Some conclusions may be drawn from the above analyses. Tensile stresses such as peel, x-stress and z-stress are almost constant for most of the joint width. Much lower values appear at the edges of the joint. As a result, the interior part of the width is important when examining failures. Z-stresses have been found to be significant and they need to be included in the yielding criteria and failure criteria. It has been shown that stresses vary significantly near the edges of a lap joint. However, the peel and maximum principal stresses, which are most responsible for the failure of lap joints, peek slightly near the joint edges. Therefore, it may be concluded that the 2D plane strain modelling for a lap joint is sufficient enough to calculate the stresses in a lap joint.

Chapter 6

THE MECHANICS OF LONGITUDINAL STRESSES IN LAP JOINTS

6.1 INTRODUCTION

It has been shown in the last two chapters that the longitudinal stresses along the overlap are significant in lap joints. As a result, they should be taken into account when joint strength is to be predicted. By studying the literature, it may be found that the existence of the longitudinal stresses has not been explained well. Analytical methods largely ignore the longitudinal stresses along the overlap, although Mallick (1989) has recently included the longitudinal stresses in his implementation of Allman's method. FEM, on the other hand, gives the longitudinal stresses automatically, but the existence of the stresses has not been physically discussed as has been done for peel and shear stresses. Possibly this was because of the emphasis of the through-thickness or peel stresses which were first emphasised by Goland and Reissner (1944). It was Adams *et al* (1978) who were among the first to include the longitudinal stresses in the study of the strength of lap joints with spew fillets. They have used failure criteria concerned with maximum principal stresses, which implicitly take into account the longitudinal stresses. The mechanics related to the longitudinal stresses have, however, not been addressed fully, even though the longitudinal stresses are important in the understanding of the state of stress in the adhesive layer, particularly for joints with rounded adherend corners as will be discussed in Chapter 7. By studying this literature, it may been found that nearly all the stresses, even the stresses across the width because of the Poisson's ratio effect in the adhesive layer, have been well discussed except the longitudinal stresses. Chapter 5 has shown that the magnitudes of the longitudinal stresses are much larger than that of the stresses across the width and Chapter 7 will show that the magnitudes of longitudinal stresses are the largest among all the stresses components for joints with radiused adherend corners. Therefore, the longitudinal stresses need to be studied in some detail if we are to have a better understanding of the state of stress in the adhesive layer. This chapter is therefore intended to fill this gap and is devoted to the study of the longitudinal stresses. Special attention is given to the discussion of the mechanics involved in the existence of the longitudinal stresses.

This chapter starts with a simple physical argument concerning the nature of the longitudinal stresses. This physical reasoning is the basis for the understanding of the existence of, and the nature of the longitudinal stresses. FEM is used to verify the intuitive proposal for both single and double lap joints. FE analysis has also been performed for lap joints with spew fillets. Some difference in the longitudinal stresses between joints with and without spew fillets is also discussed.

To verify the proposal for the nature of the longitudinal stresses, an imaginary Poisson's ratio of very low value of 0.04 has been included in the stress and strain analysis of lap joints. Although this value was not realistic, it provided the explanation of the existence of the longitudinal stresses. Finally, it should be mentioned that the geometries in this study were not the same for joints with and without spew fillets, because the FE meshes in the previous chapters are used here in order to save some analysis effort.

6.2 AN INTUITIVE REASONING OF THE STATE OF THE LONGITUDINAL STRESSES IN THE ADHESIVE LAYER

In a lap joint, the tensile forces applied to the adherends are transferred through the shearing of the adhesive layer, no matter what is the stress state in the adhesive layer. Because the tensile forces are applied at the ends of the lap joint, the forces along the overlap at any cross section across the whole joint thickness, including the overlap, along the lap joint are roughly equal to the applied forces. It is common in industry that the ratio of the stiffness of the adherends is about or more than 20 times that of the adhesive in a normal lap joint. Therefore, most of the applied forces along the overlap are carried by the stiff adherends inside the overlap. Because the averaged forces at any cross section are roughly equal to the applied forces, the averaged strains across the joint thickness at these sections will be roughly constant along the overlap, because they are controlled by the adherends, especially in the middle of the overlap. In the region around the middle of the overlap, the forces inside the two adherends are almost equal for identical adherends as shown in Figure 6.1. The strains may be easily determined by the following equation,

$$\epsilon = \frac{2P}{EA} \tag{6.1}$$

where ϵ, P, E, and A are the strain, applied force, Young's modulus and the cross section across the whole joint thickness. Towards the ends of the overlap, the forces in the two adherends are not equal and therefore the strains or stresses in the adhesive will vary across the adhesive layer. The sum of the longitudinal forces in the two adherends, however, are still roughly equal to the applied force. As a result, the strains in the adhesive layer still approximate to the strains expressed with the above equation. This is especially true for double lap joints in which the peel stresses are less significant than that in single lap joints. The situation at the ends of the overlap will be much more complicated, because the bending of the adherends enhances the longitudinal strains in these regions as discussed in Chapter 2.

Because of the large difference in the stiffness between the adherends and the adhesive, the longitudinal stresses in the adhesive layer will be very small if the Poisson's ratio effect of the other stresses are not taken into account. However, earlier chapters have shown that the longitudinal stresses are significant. This leads to the questions: where do the longitudinal stresses come from and how do they affect the strength of the lap joints? Based on the analyses in earlier chapters and the above arguments, this section introduces a new proposal on the existence of longitudinal stresses and this is followed by a numerical analysis based on FEM to verify this proposal.

For joints with spew fillets, it has been shown in Chapter 2 that the spew fillets carry some loads through the ends of the adherends. In these regions, the situation will be significantly different from that for joints with "square" ended lap joints. Therefore, attention will be paid to the difference between joints with and without spew fillets.

6.3 A PROPOSAL FOR THE EXISTENCE OF THE LONGITUDINAL STRESSES

As has be discussed in earlier chapters, the stress state in the adhesive layer is three dimensional rather than one dimensional, especially near the ends of the overlap. Therefore, Poisson's ratio plays an important role in the determination of either stresses or strains in such a situation. As discussed in Chapter 2, the peel stresses are especially due to the deformation in the adherends and to the stiffness of the adhesive. The deformation of the

adherends is controlled by the stiffness of the adherends, the geometrical factors, and applied load (see Chapter 3). As a result, Poisson's ratio of the adhesive has little effect on the peel stresses. It has been shown by Adams *et al* (1973) and in Chapter 4 that Poisson's ratio has significant effects on the stresses across the joint width. Based on these facts, it is natural to propose that the longitudinal stresses are caused by Poisson's ratio of the adhesive because of the peel stresses if the joint is modelled with 2D plane strain. From the constitutive law, it may be argued that the Poisson's ratio affects the longitudinal stresses significantly vie the high peel stresses in the adhesive layer because the longitudinal strains are small for most of the overlap. For joints with spew fillets, however, the situation is slightly different. It has been shown in Chapter 2 that the spew fillets reinforce the highly stressed regions near the ends of the overlap and transfer some load through the ends of the adherends. Therefore, the stress state in the regions near the ends of the adherends is nearly in pure tension at about 45^0 to the applied load as shown before. As a result, the contribution to the longitudinal stresses from the longitudinal strains is much larger than that for square ended joints.

6.4 NUMERICAL EXAMPLES TO ILLUSTRATE THE ABOVE PROPOSAL

To verify the above proposal, numerical examples have been conducted on both single and double lap joints with and without spew fillets. All the analyses here were based on a FE commercial package ANSYS. The joints analysed are shown in Figures 6.1 and 6.2. It may be seen from the figures that different joint geometries were used for joints with and without spew fillets. The reason was that both the joints had been analysed before for different purposes and the meshes used there were adopted here. The FE meshes for joints with spew fillets were finer at the right hand side than at the left hand side because of the interest in the regions at right hand side in those studies. As a result, the stresses at the left hand side are not smooth because of the coarse meshes used. The same boundary conditions were used as in earlier chapters. Analysis was restricted to the cases of linear-elastic materials, which was good enough for the present study.

To investigate the effects of Poisson's ratio on the longitudinal stresses, a fictitious Poisson's ratio of 0.04 has been used here as well as a typical adhesive one of 0.4. Although no such

a Poisson's ratio of 0.04 exists for common engineering materials, the use of such a small Poisson's ratio is merely to verify the above proposal, not intending to give any applicable results. It may be seen that the typical adhesive Poisson's ratio is ten times that of the fictitious one and the effect of Poisson's ratio will be very evident for these two "adhesives". The results are presented below and it should be noted that all the results are plotted at the central line of the adhesive layer. The longitudinal strains will be discussed first followed by longitudinal stresses.

6.4.1 Longitudinal Strains

Figure 6.3 shows the longitudinal strains in the adhesive of a double lap joint with square-ended ends. It is clearly shown that the longitudinal strains hardly change for most of the overlap except near the very ends of the overlap for the two Poisson's ratios, although the Poisson's ratios are so much different. Furthermore, the strains at these regions are more or less equal to that (0.203 %) given by Eq. 6.1. This strongly verifies the above proposal that the strains in the adhesive layer are controlled by the much stiffer adherends rather than the adhesive. This is also so for single lap joints as shown in Figure 6.4. For single lap joints, however, the region in the overlap with constant strains is reduced compared with double lap joints because of the rotation at the ends of the overlap for single lap joints. As discussed in Chapter 2, this rotation enhances all the stresses near the ends of the overlap. For lap joints with spew fillets, however, high longitudinal strains exist at the ends of the adherends, although they also remain almost unchanged inside the overlap as shown in Figures 6.5 and 6.6. The high strains are because of the strain singularity at the unloaded adherend corner. Little difference in the longitudinal strains exists for the two Poisson's ratios in the middle of the overlap. It is noted that the longitudinal strains at the ends of the overlap are higher for the low Poisson's ratio of 0.04 than that for the 0.4 Poisson's ratio. Also, some difference exists near the edges of the spew fillets for the two Poisson's ratios as shown in the figures. The high longitudinal strains result from the load carrying through the ends of the adherends.

6.4.2 Longitudinal Stresses

The longitudinal stresses in the adhesive layer with the two Poisson's ratios are different significantly as shown in Figures 6.7 to 6.10 for both single and double lap joints with and without spew fillets. The longitudinal stresses for the 0.04 Poisson's ratio are close to zero, whilst the longitudinal stresses are very high for the 0.4 Poisson's ratio. Furthermore, the longitudinal stresses in the middle of the joints are roughly equal to the product (5.6 MPa) of the longitudinal strains and Young's modulus (70 MPa) of the adhesive for the two Poisson's ratios, because the peel stresses are nearly zero at these regions. This clearly shows that the longitudinal stresses are mainly caused by Poisson's ratio effect because of the high peel stresses. The contribution from the longitudinal strains in these regions is negligible.

The situation for joints with spew fillets is slightly different from that for joints without spew fillets. It may be seen from Figures 6.9 and 6.10 that high longitudinal stresses exist for both the Poisson's ratios at the ends of the adherends, although the magnitude of the longitudinal stresses for the 0.04 Poisson's ratio is much reduced. This is because the spew fillets transfer some load near the ends of the adherends and the stress state at these regions is nearly in pure tension. The longitudinal stresses are also affected by the stress singularity at the adherend corners. But still, the longitudinal stresses are very small (about 5-6 MPa) in the middle of the overlap for both the Poisson's ratios.

From the above discussion, it may be concluded that the longitudinal strains in the adhesive layer for most of the overlap remain quite constant, being controlled by the much stiffer adherends. As a result of the Poisson's ratio effect, the longitudinal stresses are caused by the peel stresses in the adhesive layer. The contribution from the longitudinal strains is negligible. The situation is slightly different for joints with spew fillets. Even so, the longitudinal stresses for most of the overlap are still controlled by Poisson's ratio.

6.4.3 Other Strains and Stresses

To examine further Poisson's ratio effect, other strains and stresses, especially peel strains and stresses are also analysed. Figures 6.11 to 6.18 show the peel strains and stresses for joints with and without spew fillets for both double and single lap joints. It may be seen

from these figures that the *peel strains* for joints without spew fillets change significantly for the two Poisson's ratios, whilst the *peel stresses* do not change at all. One conclusion from these analyses is that the peel stresses do not depend on the Poisson's ratios. This confirms the discussion in Chapter 2 that the peel stresses only depend on the stiffness of both the adherends and the adhesive, geometric factors and applied load. However, the situation is slightly complicated for joints with spew fillets as seen in these figures. The peel stresses for the 0.04 Poisson's ratio are lower than that for the 0.4 Poisson's ratio at the ends of the adherends, although the peel stresses are identical for most of the overlap. The peel strains for the 0.4 Poisson's ratio are lower than that for 0.04 Poisson's ratio for joints without spew fillets because high longitudinal stresses influence the peel strains through the Poisson's ratio. However, for joints with spew fillets, the peel stresses are higher for the 0.4 Poisson's ratio than for the 0.04 one.

The shear stresses are shown in Figures 6.19 to 6.22. It may be seen that there is almost no change in the shear stresses for the two Poisson's ratios for joints without spew fillets. The reason is that the shear stresses are controlled by the shear stiffness only as discussed in Chapter 2. Because the Poisson's ratio has little effect on the shear stiffness for given elongation stiffness, the shear stiffness for the two Poisson's ratios are very close to each other. As a result, the shear stresses do not change noticeably. For joints with spew fillets, however, there is some difference in the shear stresses for the two Poisson's ratios, which may be affected by the adherend corners.

6.5 CONCLUSIONS

It may be concluded from the above analysis that the longitudinal stresses along the joint overlap are a result of the peel stresses in the adhesive layer through the Poisson's ratio's effect. The contribution to the longitudinal stresses from the longitudinal strains is negligible. For the majority of the overlap, the longitudinal strains remain unchanged, these being controlled by the stiff adherends. The peel stresses do not depend on the Poisson's ratio, which is an important phenomenon in the adhesive layer. The effect of the Poisson's ratio on the shear stresses is also negligible. The situation is rather more complicated for joints with spew fillets. Because the spew fillets transfer some load through the ends of the

adherends, the longitudinal stresses and strains near the ends of the adherends are quite high, even for very low Poisson's ratios.

From the above study, it may also be concluded that the dominant factor controlling the stress state is the high peel stresses. Shear stresses may also play some role in the determination of joint strength. It is well known that adhesives deform much more in shear than in tension. Therefore, failure criteria based on peel stresses will be enough for the determination of joint strength for with "square ended" joints, because joints tend to fail as a result of tension. For joints with spew fillets, because the spew fillets transfer some load through the ends of the adherends, the longitudinal stresses should be taken into account in failure analysis. The easiest way of including the longitudinal stresses is through the maximum principal stresses as demonstrated by Adams *et al* (1973).

Chapter 7

STRESS AND STRAIN ANALYSES OF SINGLE LAP JOINTS WITH RADIUSED ADHEREND CORNERS

7.1 INTRODUCTION

As has been discussed, there exist stress singularities at the re-entrant corners at the ends of overlap. Although analytical methods can predict stresses inside the adhesive layer accurately for most of the overlap, they fail to obtain stresses at the ends of the overlap accurately. Analytical and experimental analyses show that it is at the ends of the overlap where failure starts. As a result, the stresses at the ends of the overlap are critical for joint failure. The stresses at the ends of the overlap are affected by the material properties of both the adherends and the adhesive. It has been shown (Hart-Smith, 1973) that the stiffer the adherends, the lower are the stresses for 'square ended' joints. Also, stresses are reduced if the adhesive is more flexible. The critical stresses may also be affected by the local geometry at the ends of the overlap. In general, adhesively bonded joints have some adhesive squeezed out from the adhesive layer, forming spew fillets at the ends of the overlap. Because these spew fillets are near the critical regions in the joints, it has been shown that the spew fillets affect the local stresses near the ends of the overlap significantly (Adams and Wake, 1984). This effect can only be analysed by FEM. The glue line thickness has been shown to have little effect on the joint strength in the range of 0.1 - 0.4 mm (Adams and Wake, 1084). Another factor affecting the critical stresses at the ends of the overlap is the geometry of the adherend corners. It has been shown that stresses are significantly reduced by rounding the adherend corners (Peppaitt, 1974, Chen, 1985 and Adams and Harris, 1987). Adams and Harris (1987) further demonstrated that the strength of single lap joints with radiused adherends bonded with a toughened adhesive increased substantially compared with joints with sharp adherend corners. Furthermore, the adherend corners are usually not sharp in practice. There is, in general, a small rounding at the adherend corner. This may affect the stress distribution at the adherend corner areas and therefore the joint strength, because stresses in this area are very sensitive to the change in the geometry of the adherend corners. In order to have a better understanding of the effect

of the change in the geometry of the adherend corners on the stresses and therefore on joint strength, this Chapter is a further study on the effect of radiused adherend corners on the stresses and strains of a single lap joint.

7.2 GEOMETRIES AND MATERIAL PROPERTIES OF SINGLE LAP JOINTS IN THIS STUDY

Single lap joints were analysed in this study. 3.2 mm thick aluminium sheets were used as adherends. Joints were made with two adhesives, a brittle MY750 with Hardener HY906 and a rubber-toughened CTBN. The geometry of the joints is shown in Figure 7.1, where the width of the joints is 25.4 mm. The adhesive thickness is 0.25 mm and the overlap length is 25 mm. The adherend length outside the overlap is 75 mm. Four geometries of adherend corners were analysed, sharp, small radius, medium radius and large radius. Material properties are needed before any analysis can be carried out. Material characterisation is discussed in Chapter 8. It is well known that the properties of epoxy resins depend on strain rate, temperature and loading conditions, etc.. The material properties of epoxies under load-control and displacement-control are different. So which properties are used to model single lap joints should be decided. Coppendale (1977) showed that the load condition in a lap joint was more under load-control than under displacement control. This can also be simply verified from the load versus displacement curve in joint tests, because load increases monotonically with the increment in displacements. Therefore, the material properties under load-control was used here for joints bonded with CTBN. Because MY750 with hardener HY906 is brittle, the difference between load and displacement control is small. The material properties of MY750 under displacement control were used here. These are shown in Figures 8.3 and 8.4 in Chapter 8 and are summarised as follows. It should be noted that MY750 with Hardener HY906 is brittle, so it has been treated as a linear elastic material.

MY750 WITH HARDENER HY906

Young's modulus	2.8 GPa
Poisson's ratio	0.4

CTBN

Young's modulus	2.5 GPa
Poisson's ratio	0.37
Yield stress	40 MPa
Flow stress (no hardening)	60 MPa

The aluminium adherend property is shown in Figure 8.2 as below.

Young's modulus	70 GPa
Poisson's ratio	0.33
Yield stress	220 MPa

7.3 ANALYSIS METHODS

In this study, FEM was used for both linear and non-linear analyses. A research programme FELDEP and a commercial package ANSYS were used throughout this study. Because of the large joint width, the joint was modelled as a 2D plane strain problem. To simulate the testing conditions, both ends of the joints were constrained without any motion in the flexural direction and any rotary motion as shown in Figure 7.1. It has been shown that the joint end boundary conditions have little effects on the stress distribution inside the adhesive (Chen, 1985) with large displacements model. Therefore, such boundary conditions can also be used for other load conditions. 8-noded isoparametric elements were chosen for both adherends and adhesives. Because of the limitation in computer power, two steps were involved in analysing the corner areas to obtain stress or strain resolution. The first run was based on a quite coarse mesh for the whole joint, followed by a finer mesh around the adherend corner with the displacements from the first analysis as boundary conditions. In the linear analysis, a large displacement model has been used with both adherends and adhesive being linearly-elastic. In the elastic-plastic analysis, elastic-plastic properties were included for both adherends and adhesive as well as the large displacements. Analysis has

been performed for the four different degrees of adherend rounding described above. In the analyses with a coarse mesh, six uniform elements were used across the adhesive layer and across each of the adherends. In the subsequent refined analyses, ten graded elements were generated across the adhesive layers. To avoid large aspect ratios in the adhesive layer, 50 elements was used along the overlap in the refined analysis. However, such a number of elements along the overlap caused the aspect ratios in the adherends to be high. Fortunately, adherends near the adherend corners did not yield in the current analyses so that the large aspect ratios were still acceptable with the 8-noded isoparametric elements for the adherends. The refined mesh for the stress analysis in the sharp adherend corner region is shown in Figure 7.1A. Similar meshes have been used for other radiused adherend corners. Incremental solutions with a series of load increments were performed for both linearly-elastic and elastic-plastic analyses. In the elastic-plastic analysis, a modified von Mises (Adams and Wake, 1984) yield criterion was included, which takes account of the effect of hydrostatic stress components on the yielding of the adhesive. More load increment steps were used in the elastic-plastic analysis than in the linearly-elastic analysis because of the combination of large displacements and elastic-plastic material.

7.4 RESULTS

7.4.1 Linearly-elastic Analyses with MY750

Analyses with linearly-elastic materials, using large displacements, for both adhesive and adherends are presented first. A load of 20 kN was applied to the joint and the load was applied with 10 increments. Results are presented below.

First, peel, shear, longitudinal and maximum principal stresses plotted at the Gauss points close to the unloaded adherend (0.001 mm from the adherend) for the four types joints are shown in Figures 7.2 to 7.5. It may be seen that almost no difference exists for most of the overlap except near the adherend corners for joints with small radius and sharp adherend corners. This is because the stresses are not defined at the sharp corners and the small rounding is very localised to the adherend corner. The stresses should, in theory, be infinite at the sharp corners (Williams, 1959, Hein and Erdogan, 1971, Adams and Harris, 1987).

Stresses from this analysis, however, were finite because of the mesh used here. To verify the singularity of the stresses, Figure 7.6 shows the logarithmic plot of the stresses against the logarithmic distance from the adherend corner across the adhesive layer. The linear relationship in the figure indicates the singular nature of the distribution of the stresses. However, it should be noted that the stresses in the final element adjacent to the singular point are not reliable because of the normal element rather than the singular element used there. The singular nature of the stresses covers almost the whole adhesive layer as seen from the figure. Another feature of the stresses with the small radiused corner is that a larger area with high stresses exists than with sharp corners in which the stresses are high only in the very small area close to the sharp corner. The stresses around the adherend corner for small radiused adherend corners are finite and much smoother than that around the sharp adherend corner. Furthermore, the positions with the highest stresses move inside the overlap for the small radiused adherend corner. Figures 7.7 and 7.8 show the contour plots of the maximum principal stresses for the sharp and small radiused adherend corners. They clearly show that the stresses around the radiused adherend corner are much smoother than those around the sharp adherend corner. The magnitudes of the stresses for medium and large radiused corners are much reduced and the highest stresses move further inside the overlap. Very smooth stress variations exist for the large degrees of rounding and the area with the highest stresses is much larger than that with small or sharp radius corners. This clearly shows that stress concentration is not severe for the large degrees of rounding. It should be noted that the longitudinal stresses are significant as was discussed in Chapter 6. In fact, the longitudinal stresses for all the radii and sharp adherend corners are much higher than either the peel or the shear stresses plotted at the same positions. In lap joints with square-ended adhesive layer, the longitudinal stresses along the overlap are mainly caused by the Poisson's ratio effect (Chapter 6). In lap joints with spew fillets, this is also so in the middle of the overlap. However, the longitudinal stresses near the ends of the overlap are as important as the peel stresses, because the spew fillets transfer part of the load and this results in large longitudinal stresses near the adherend ends. The rounding of the adherend corners enhances the longitudinal stresses as can be seen from Figure 7.4, which shows that the longitudinal stresses increase dramatically in the region of the rounded adherend corner but remains almost constant in the middle of the overlap. The

stress state in the spew fillet is predominantly in tension at an angle of approximately 45^0 to the applied load. Consequently, the longitudinal stresses play an important role in the failure of joints with spew fillets and radiused adherend corners. The maximum principal stresses at Gauss points close to the unloaded adherend are plotted in Figure 7.5. It may be seen that the distribution of the maximum principal stresses is similar to that of the other stresses, especially the longitudinal stresses, plotted at the same positions. It may be seen that the magnitudes of the maximum principal stresses increase sharply inside the radiused adherend corners, which is a typical feature of the longitudinal stresses plotted at the same positions. This also means that the longitudinal stresses contribute significantly to the maximum principal stresses. Because the maximum principal stresses represent the peel, longitudinal and shear stresses, they may be most responsible for joint failure.

Stresses inside the spew fillets are plotted in Figures 7.9 to 7.12. It may be seen that stresses inside the spew fillets near the fillet edges hardly change for different degrees of rounding. It should be noted that the stresses near the edges of the spew fillet are high, where a weak stress concentration exists. Because this region has high stresses, it should be examined when predicting joint strength, especially for joints bonded with medium and large radius adherends. It is noted that the stresses at the edges of the spew fillet increase sharply and the magnitudes are difficult to determine when the geometry consists of sharp edges. It may be seen that the stresses at the edges of the spew fillet are higher than that near the unloaded adherend corners for medium and large radius adherends. Therefore, for large radius adherends, the spew fillet edges may be important for failure predictions.

Stresses at Gauss points close to the loaded adherend are plotted in Figures 7.13 to 7.16. It may be seen that all the stresses peak in the region opposite to the unloaded adherend corner, although there are no re-entrant corners there. Figure 7.13 shows that there is little difference in the peel stresses between sharp and small radius adherend corners. This is easy to understand because no re-entrant corner exists at this area and the change in adherend geometry is a significant distance away from this region. It may be seen from Figure 7.13 that the peel stresses near the loaded adherend are much lower than that near the unloaded adherend. This means that the area around the unloaded adherend corner is

more important than the loaded adherend for joint strength. Other stresses have similar features. Again, the longitudinal stresses are significant being almost the same magnitudes as the peel stresses. Therefore, they should be taken into account when the failure is to be predicted. The stress distributions across the adhesive layer may also be seen in Figures 7.7 and 7.8, which show the contour plots of the maximum principal stresses around the adherend corners.

To examine further the nature of the maximum principal stresses, their directions are drawn in Figure 7.17 for the small radiused adherend corner. It may be seen that the directions of the maximum principal stresses are approximately at right angles to the interface between the unloaded adherend and the adhesive. In comparison, the directions of the maximum principal stresses around the unloaded adherend corner for a joint with sharp adherend corners are at about 45^0 to the adherend surfaces. In general, adhesives are weakest in tension. At the interface inside the radius adherend corner, the maximum principal stresses act at roughly right angles to the interface. The acting of the stresses is the worst as far as the joint strength is concerned. In a joint with sharp adherend corners, however, the tensile forces acting at the interface is either peel or longitudinal stresses, whose magnitudes are much smaller than the maximum principal stresses. As a result, the acting of stresses for a joint with sharp corners is better than that for a joint with radius corners, although the magnitudes of the former stresses are much larger than the latter. As a result, the joint strength does not improve much in contrast to the reduction in the peek values of stresses for the radius adherend corners (as discussed in Chapter 9).

Finally, the maximum principal stresses across the adhesive layer are shown in Figure 7.18. It may be seen that the magnitudes of the maximum principal stresses increase steadily from the lower adherend to the upper adherend as shown in the figure. It is noted that the stress resolution may be achieved with reasonably fine meshes for small radiused corners. However, for joints with sharp adherend corners, extremely fine meshes are needed to obtain the necessary stress resolution around the adherend corner. From this analysis, it may be concluded that the model with a small radiused adherend corner may be better than the

sharp adherend corners as far as the stress analysis is concerned. However, the amount of rounding needs to be determined.

7.4.2 Elastic-plastic Analyses

Elastic-plastic materials analysis is much more complicated than linearly-elastic materials. As stated by Johnson and Mellor (1973), material constitutive equations are needed before any analysis is attempted. Material characterisation is difficult for epoxies in that the material properties are functions of loading rate, temperature, etc.. The material characterisation is presented in Chapter 8. Figures 8.2 and 8.4 show the material properties of both the adherend and the adhesive, high strength aluminium alloy and a CTBN toughened epoxy. A B-spline curve fitting procedure was used to represent the behaviour of the materials. For the CTBN rubber toughened epoxy, the modified von Mises yield criterion (Raghava and Cadell, 1973) was used to take into account of the hydrostatic stress components, which can be expressed as

$$\{J_1(S-1) + (J_1)^2(S-1)^2 + 12J_2\}/2S = Y_T^2 \qquad (7.1)$$

where S is the ratio of the yield stress in compression to the yield stress in tension, Y_T is the yield stress derived from a uniaxial tensile test on the material, and

$$J_1 = \sigma_x + \sigma_y + \sigma_z$$

$$J_2 = 1/2((\sigma_x - J_1/3)^2 + (\sigma_y - J_1/3)^2 + (\sigma_z - J_1/3)^2 + (\tau_{xy})^2 + (\tau_{xz})^2 + (\tau_{yz})^2).$$

where σ_i (i=x,y,z) and τ_j (j=xy, yz, zx) are stress components. For the high strength aluminium alloy, the von Mises yield function

$$f(\{\sigma\}) = \sqrt{(3J_2)} - Y_T = 0 \qquad (7.2)$$

was used, where J_2 is defined as above.

Because the materials are elastic-plastic for both the adhesive and adherends and large displacements are involved, 30 load steps were used for the analysis. A load of 20 kN was

applied throughout the analysis. Again, the analysis involves two steps: first a coarse mesh analysis followed by a refined mesh analysis. The results are presented below.

First, plastic energy density plotted at the unloaded adherend is shown in Figure 7.19. A similar trend of the plastic energy density exists as that of the stresses in linearly-elastic analysis. A high plastic energy density was apparent around the corner; this should, in theory, be infinite for a sharp corner as discussed by Adams and Harris (1987). The plastic energy density with the small radius corner was finite and the position of the peak value moved inside the overlap. As for the stresses in the linearly-elastic analysis, the area with a large plastic energy density in the small radiused corners was much larger than that in the sharp corner. For joints with medium and large radius corners, the magnitudes of the plastic energy density were much reduced and the positions of the peak values moved further inside the overlap. Again, the larger the rounding, the larger the area in which the plastic energy density reached its peak values and the further the position moved inside the overlap.

The plastic energy density inside the spew fillets is shown in Figure 7.20. It can be seen that the majority of the spew fillets did not yield much with applied load. However, yielding happened at the edges of the spew fillet where there existed a stress concentration in the stress analysis for linearly-elastic materials. This shows that the regions around the unloaded adherend corners and the fillet edges are important areas to examine for failure analysis. However, because of the difficulty of determining the geometry at the edges of the spew fillets, no further analysis was performed with varied geometries of the spew fillets.

Strains have also been studied to analyse the failure mechanics. Because the strain distribution is very similar to that of the plastic energy density, no plot with regards to the strain magnitudes is made here. However, the directions of the maximum principal strains are presented here, which gives more information on the failure modes. The directions of the maximum principal strains in the adhesive layer of a joint with a small radiused corner are shown in Figure 7.21. It may be seen that, like the directions of the maximum principal stresses in linearly-elastic analyses, the directions of the maximum principal strains were

approximately at right angles to the interface between the adherend and the adhesive for small radiused adherend corners. It can also be seen that the magnitudes of the maximum principal strains close to the unloaded adherend were much larger than that at other places in the adhesive layer. The magnitudes of the other principal strains in the same lane were also significant, but they were in compression. This means that the shear strains at these points were very significant compared with elongational strains. As discussed in the linearly-elastic analysis, the interface is the weakest of the whole joint, because the stresses and strains are the highest near the interface. The action of the maximum principal strains is most responsible for the joint failure. The directions of the maximum principal strains with sharp adherend corners were almost the same as those with small radiused adherend corners and were roughly at right angles to the interface between the adhesive and adherends. It should be noted that the maximum principal strains did not actually act at right angles to the interface between the adherend and adhesive for joints bonded with sharp adherend corners. Such a loading was preferred to that with small radius corners although the magnitude of the peak value with sharp adherend corners was much higher than that with small radius corners. However, considering the small area in which the strain concentration existed for the adherends with sharp corners, the strain concentration at the very small area was not very important in the determination of joint failure for ductile adhesives. It is a small finite area around the unloaded adherend corner that is important for the failure of joints bonded with ductile adhesives.

Finally, the shear and peel strains across the adhesive layer are shown in Figure 7.22, in which the strains were calculated with a coarse and fine meshes. It may be seen from the Figure that the shear strains are much larger than the elongation strains close to the unloaded adherend. The strains remain reasonably constant for the majority of the adhesive layer. However, the shear strains peak up sharply close to the unloaded adherend and are much larger than the longitudinal strains. The change in longitudinal strains is not as sharp as shear strains. Another feature is that fine meshes are needed for elastic-plastic analyses, which is in contrast to the linearly-elastic material analyses. As discussed above, reasonably fine meshes are accurate enough for the stress resolution. Therefore, due care is needed to use fine meshes when elastic-plastic analyses are attempted.

7.5 CONCLUSIONS

Some conclusions may be drawn from the above analyses.

(i). The stresses or strains in the adhesive layer of a joint with radiused adherend corners are finite and are easy to obtain stress resolution. In real joints, adherends generally have small rounded corners. Consequently, the model with small radius corners may be used to represent real adherends. However, the magnitude of the rounding of the adherend needs to be determined.

(ii). Rounding the adherend corners reduces the magnitudes of the stresses or strains around the adherend corners. The larger the rounding, the larger the reduction in the magnitudes of the stresses. Furthermore, the peak values of the stresses or strains move inside the overlap for joints with radiused adherend corners: the larger the rounding, the further inside the overlap the peak values move.

(iii). Rounding of the adherend corners worsens the stressing conditions around the adherend corners as far as the joint strength is concerned, although the peak values of stresses and strains are much reduced. Rounding the adherend corners results in a large area of the interface between the adherend and the adhesive which endures large stresses or strains acting at roughly right angles to the interface between the adherend and the adhesive. Such loading condition is the worst for adhesives as far as adhesive strength is concerned.

(iv). Rounding the adherend corners is restricted in that the stresses or strains at the edges of the spew fillets do not change much for different degrees of rounding. For large degree of rounding, the edges of the spew fillets may become the critical points for joint failure.

(v). The stress or strain concentrations are very much localised to the unloaded adherend corners, whilst stresses or strains away from the corners are quite smooth. This means that the strength does not change much for joints with sharp and small radius adherend corners.

(vi). Finally, the longitudinal stresses (or strains) along the overlap, which are generally ignored by closed form solutions, are more significant than the peel stresses (or strains)

around the radiused adherend corners. They should be taken into account in failure studies. The maximum principal stresses are the most responsible for joint failure because they take into account of all the stress components. Shear strains for elastic-plastic analyses are much larger than either peel or longitudinal strains around the radius adherend corners.

Chapter 8

MECHANICAL EXPERIMENTS

8.1 INTRODUCTION

It has been discussed that the theoretical methods have been well developed in the stress and strain analysis of lap joints. However, all the theoretical analyses depend on the basic material properties of both adherends and adhesives, and these are still under debate because of the uncertainty of the material properties *in situ*. Even though the stresses and strains may be calculated accurately, failure tests are also essential to determine joint strength and to verify the theoretical predictions. In the initial joint failure testing, not only can the ultimate strength of a joint be measured, but also the failure modes may be determined. Failure modes are very important not only in the understanding of joint failure, but also in the choices of failure criteria, based on which joint strength can be accurately predicted theoretically. These failure criteria can then be used to predict joint strength of other configurations.

The determination of the mechanical properties of adhesives is still in its infancy. Debate is concentrated on the consistency of material properties in bulk and *in situ*. Bulk tests are free of any stress concentrations and therefore the test data from these tests are true material properties. Adhesives are, however, rarely used in bulk but are almost always in the thin-film form. As a result, the question as to whether the material properties are the same in bulk and *in situ* arises. Tests *in situ* have been extensively performed. Basically, there are two aspects concerning the joint tests, elastic material properties such as Young's modulus and Poisson's ratio, and the yield and failure strength. There are numerous test procedures *in situ* which have been listed in various official bodies such as ASTM. Unfortunately, these test procedures have not been well documented and therefore different tests have different material properties as discussed by Adams and Wake (1984) and Kinloch (1988). The main reason is that most of the test procedures involve stress concentrations or large uneven stresses even though the test appears to have a uniform stress field. Some adhesive properties such as Young's modulus or Poisson's ratio, may be

determined by tests *in situ*. Young's modulus and Poisson's ratios have, in some studies (Adams and Wake, 1984, Hughes *et al*, 1985, Jangblad, *et al* 1988, etc.), been shown to be invariant in bulk and *in situ*. However, the yield and failure strength deduced from these tests is the joint strength rather than the adhesive strength, because stress and strain concentrations are inherent in the tests *in situ* and the joint strength is the function of adherends and the geometry of the joint. As a result, such test data should be interpreted appropriately and cautiously.

Because the bulk test is free of any stress or strain concentration, it is preferred in the determination of adhesive strength. However, such data on strength are also difficult to use in practice because stress concentrations exist inherently in joints. The behaviour of adhesives in joints with stress concentrations needs to be determined. Consequently, the applications of the adhesive strength from bulk test to joint strength prediction still needs more research. Therefore, it may be concluded that no satisfactory test methods exist from which the test data can be used to predict initial joint strength.

In engineering applications, it is usual practice to use a convenient failure criterion to predict the joint strength using the basic material properties determined in bulk tests. Such a criterion runs into difficulty when stress concentrations exist inherently in joints. However, because of its usefulness in practice, the next Chapter describes a method to correlate the adhesive strength in bulk to that in joints in order to predict joint strength based on material properties in bulk tests. As a result, material properties determined in bulk test was used in the present work. There were a large amount of data on adhesive properties in this laboratory cumulated for many years. Because the present work was to study the failure of lap joints, bulk tests on the material properties used in this study were quoted from other people's work in this laboratory.

Tests on lap joints were extensively performed with both brittle and ductile adhesives. Two aspects were tested, initial ultimate strength and failure modes. Tests on the strength and failure modes were a main part of the present work, which is very important in the understanding of joint failure and in the verification of failure criteria. Based on the failure strength and modes from these tests, the failure mechanics of lap joints was

discussed. Particular attention was given to the effect of the rounding of the adherend corners on the joint strength. Adherend corners in practice are generally rounded, which may affect joint strength. Also, rounding the adherend corners may help the understanding of failure mechanics.

8.2 MATERIAL CHARACTERISATION

8.2.1 Adherends

All the adherends used here were aluminium alloys. Figure 8.1 shows the dimension of the test specimens machined to the British Standard BS 18 from a large sheet. The specimen thickness was equal to the sheet (and joint) thickness of 3.2 mm. The test was carried on a Nene screw-driven test machine. Forces were recorded with a 30KN load cell, whilst extensions were measured with an extensometer. The stress and strain relationship was derived from the forces and extensions with the given geometry. The extensometer was hand-operated and the machine was stopped at a series of loads to obtain the readings of the extensions of the gauge length. When the strain reached about 2.6% (2.3% plastic strain), the extensometer was out of range and the test was stopped. As can be seen from Figure 8.2, the stress and strain curve is nearly a straight line after yielding. For modelling plastic deformation, a straight line was drawn beyond the test data, which was believed to be accurate enough to represent the stress hardening part of the aluminium for the current purpose.

Figure 8.2 shows the stress-strain curve of the aluminium used. The Young's modulus is close to 68 GPa. To verify this test, a dynamic test was also carried out to measure the Young's modulus. Dynamic tests to measure Young's modulus and Poisson's ratio have been widely used and shown to be accurate (Adams and Cawley, 1985). This dynamic test gave a slightly higher value of Young's modulus of 72.3 GPa. A value of 70 GPa was used in the analysis. A value of 0.33 was used for Poisson's ratio (Gere and Timoshenko, 1984). For the elastic-plastic analyses, a cubic B-spline was used to represent the adherend stress-strain curve in the range of interest.

8.2.2 Adhesives

Two adhesives were used in the present work, Ciba-Geigy MY750 (diglycidyl ether of bisphenol A) with hardeners HY906 (anyhdride), HY956 (hydroxyalkylated polyamine) and HY4076, and CTBN (carboxyl-terminated butadiene-acrylonitrile). The preparation of MY750, with hardeners HY906, HY956 and HY4076, and CTBN is described in Appendix 3 together with bonding process. Except MY750 with hardener HY4076 whose property was not known, the material properties of the adhesives used had been previously obtained in this laboratory by Harris (1983), Chen (1985) and Mallick (1990), so no effort was made to repeat these tests. Figures 8.3 shows the uniaxial tensile property of MY750 with hardener HY906 tested under displacement control at room temperature. Figure 8.4 shows the stress-strain curve of CTBN tested under load control at room temperature. It may be seen from these figures that MY750 with hardeners HY906 and HY956 are brittle, while CTBN is a ductile adhesive. From manufacturer's product information, MY750 with hardener HY4076 is also brittle but less brittle than MY750 with hardeners HY906 and HY956.

8.3 JOINT TESTS

8.3.1 Some tests on failure modes

8.3.1.1 Fatigue tests

It is well known that the failure of lap joints bonded with structural adhesives, in quasi-static tests, is in a sudden manner. In order to find the failure modes of single lap joints, fatigue tests were performed, in which cracks propagated slowly. Six single lap joints were prepared and tested on a fatigue testing machine under the loading of 80% tension / 0% compression of the failure load. The single lap joints were made of aluminium adherends whose thickness was 1.6 mm and MY750 with hardener HY4076 with an adhesive layer of 0.125 mm. The overlap was 12.7 mm and the joint width was 25.4 mm. The joints were prepared according to standard procedure as described in Appendices 2 and 3. Because the aim of this test was to determine failure modes, no data regards to the actual load cycles were recorded. Four joints were tested on the department ??? machine before the machine

became defective. However, all of the four joints had the same pattern of failure mode, which is discussed below.

The failure mode is shown in Figure 8.5, in which all the cracks initiated at the unloaded adherend corners. After the initiation, the cracks propagated along or close to the adherend surface and, at the same time, along the adherend ends as shown in the Figure. However, even under fatigue tests, crack initiation was very difficult to determine across the joint width. No observation has been made in relation to the propagation across the joint width. After some cycles, complete failure was observed at the end of the unloaded adherend across the joint width. The cracks then propagated along the overlap slowly close to the upper adherend as shown in the figure. The tests were stopped before the joints were completely broken.

It may be concluded from the fatigue tests that failure always initiates at the unloaded adherend corners, where the stresses are the highest. After the initiation, the cracks propagate close to the unloaded adherends along the overlap and at the same time, along the vertical interfaces between the adhesive and the adherend ends as shown in the figure. Then complete cracks are apparent at the vertical interface between the adhesive and the ends of adherends before the cracks propagate further into the overlap.

8.3.1.2 Quasi-static tests with double lap joints

Although failure of single lap joints was generally in a sudden manner, tests with double lap joints could sometimes be stopped after a crack initiated but before it propagated to catastrophic failure. The reason for the crack arresting may be that the other adhesive layer may not fail at the same time and therefore it can support the load without catastrophic failure. For this reason, double lap joints were chosen here to test failure modes. Twelve double lap joints were prepared with aluminium adherends and MY750 with hardener HY956. The outer adherends were 1.6 mm thick and the thickness of the central adherends were close to 3.2 mm (consisting of two 1.6 mm aluminium sheets bonded together). The adhesive layer was 0.125 mm. The overlap was 12.7 mm long and the joints width was 25.4 mm. Human hearing was used to detect the initiation of cracks, because the crack initiation

was generally accompanied by an audible sound. It was possible then to stop the machine before the cracks became unstable. The test was done on a Nene, screw-driven test machine with a strain rate of 1 mm/min.

Once the machine was stopped, the joints were examined with a magnifier. It seemed that the cracks did not run at the adherend corners if examined at the edges of the joints, but were at a significant distance away from the corners as shown in Figure 8.6. It was also observed that the cracks were complicated across the joint width, so sectioning was used to examine the failure locus. All the joints were then machined into halves along the central line of the joints. It still seemed that cracks did not run at the corners even when examined on the middle surfaces of the joints for some joints. Because the sectioning process cut a large amount of material away, no further sectioning was attempted. Instead, the joints were pulled to failure on the tensile machine. Then they were examined again under an optical microscope and an interesting feature was observed. It was almost certain that the cracks ran across the adherend corners somewhere across the joint width as shown in Figure 8.6. It seemed that, at these points, the cracks initiated and propagated from these points along the ends of the adherends as shown in the Figure. No further work was done on the examination of the failure surfaces. However, with a preliminary study of the failure surfaces with the aid of the three dimensional stress analysis in Chapter 5, it was proposed that cracks initiated at the adherend corners somewhere near but not at the joint edges. Because of the large stresses in these regions and the brittle nature of the adhesive used, the cracks propagated rapidly across the joint width. The fast crack propagation might run into the adhesive layer rather than along the adherend corners. As a result, some adhesive was left on the adherend corners at the joint edges.

Failure modes along the overlap are shown in Figure 8.7, which is in line with other workers' observations, and in Figure 8.8 across the joint width. However, examination of the failure surfaces across the width indicated that the interior part propagated in advance of that at the edges. This strengthened the proposal above that cracks initiated at the adherend corners in the interior part of the joints across the joint width. This proposal was further supported by the three dimensional stress analysis in Chapter 5. Chapter 5 has

shown that the stresses in the interior near the edges of the joints are the highest. It should be noted that the failure modes in the two adhesive layers in a double lap joint were different as shown in Figure 8.7. The reason may be as follows. In a double lap joint, large peel exist at one end of the overlap but compression at the other end of the overlap. Generally speaking, the two adhesive layers do not fail at the same time. Once one adhesive layer fails at the peel end of the overlap, the cracks propagate towards the central adherend at an angle of roughly 45^0 to the applied load and then propagate towards the other end of the overlap close to the central adherend surface. The stiffness of the joint will change and the load will be re-distributed. The loading condition of the unbroken half of the double lap will be similar to a single lap joint. For this half of the joint, the failure locus was typically the one of a single lap joint as shown in the figure. The early failed half of the joint had a failure locus as shown in the Figure.

8.3.2 Tests on both failure loads and modes

Corresponding to the stress analysis in Chapter 7, tests were performed on the same joints whose dimension is shown in Figure 7.1. Two aspects were recorded, failure loads and failure modes. The adherend corners had four geometries, sharp (90^0) and different radii, small (0.25 mm), medium (1.6 mm) and large (3.2 mm). The adherend corners were machined to different radii so as to have smooth adherend surfaces. Then, surface preparation was carried out according to the procedure outlined in Appendix 2. Two adhesives were used, MY750 with hardener HY906 and CTBN. It should be noted that the adherend thickness is twice that in the previous tests and so is the adhesive layer. The adherends were tested as described earlier and the adhesives' properties were quoted from other people's work in this laboratory. The tests were carried out on a Zwick computer-controlled testing machine.

8.3.2.1 Brittle adhesive MY750

First, the results with the brittle adhesive MY750 are presented. Four batches with each batch having six joints were made with adherends geometries defined in previous section. Because of the brittle nature of the MY750 adhesive, some small cracks were introduced in

the spew fillets in some joints when the joints were taken out from the mould. This may affect the strength of joints. However, it will be shown that the effect of the initial cracks was small. The thickness of the joints was measured before testing. The thickness of the adhesive layers varied slightly even within one batch and typical thickness within one batch is listed in Table 8.1. Adams *et al* (1978) have shown that the effect of the adhesive thickness on joint strength is small in the range of 0.1-0.4 mm for joints bonded with MY750. Therefore, the thickness listed in Table 8.1 would be expected to have little effect on the strength of the joints. The joints were tested on a Zwick testing machine at room temperature (20^0 C) with a cross-head speed of 1 mm/min. The load and the cross-head displacements were recorded during the tests, and a typical load versus cross-head displacement curve is shown in Figure 8.9. The joints were carefully examined during the testing process, and failure loci were also studied when the joints were tested to failure.

(a) Load-displacement curves

Figure 8.9 shows that the load versus cross-head displacement curve is closely linear for all joints tested. Such a failure process means that the failure was in a brittle nature and, consequently, brittle failure criteria should be used.

(b) Failure process

During the process of testing, the joints were watched closely. Some interesting phenomena were observed. At the initial stage of loading, the load increased steadily with the increase in the cross-head displacements. However, at a load of between 80-90% of the failure load, a sound, corresponding to the initiation of a small crack or the small stable propagation of cracks for specimen having small initial cracks, was heard for some of the specimens. After this, the joints could still support loads but more sound was evident before final failure. This clearly shows that crack initiation or small stable propagation was evident before final failure, although the period was very short. It may be concluded that the failure process was very complicated, and small crack propagation took place before the final failure. This information is very important for failure prediction in that the crack initiation and the final joint failure are two stages in the failure process even though the process for the small

cracks to propagate into unstable ones is very short. Because the crack initiation is very difficult to detect and the usual joint tests measure the final joint strength, simplified failure criteria are needed to give fairly accurate failure prediction for the final joint strength. This will be discussed in detail in Chapter 9.

(c) Failure mode

Because there were small cracks in the spew fillets, caused either by air bubbles or by taking specimens out from the mould, in some specimens before testing began, the failure loci were complex and different in the spew fillets for different joints. However, there were some distinct features in the failure modes of the specimens tested. Basically, there were three failure modes observed in the experiments for joints bonded with different degrees of rounding of the adherend corners. For sharp adherend corners, the failure mode is as shown in Figure 8.10a. Two features were observed for this failure mode. First, either adherend had some adhesive left on it after failure with the centre of the overlap being the point where the two cracks met as shown in the figure. The other feature is that some cracks ran across the unloaded adherend corners into the spew fillets at both ends of the overlap for some joints as shown as A in Figure 8.10a. However, for some joints, the crack at one end of the overlap ran to the adhesive fillet edge with the whole spew fillets being left to the end of the unloaded adherend as shown as B in Figure 8.10a.

For small radiused adherend corners, the failure locus is shown in Figure 8.10b. It is different from those observed in joints with sharp adherend corners in that the whole adhesive inside the overlap was left on one of the adherends. But again, the cracks ran across the unloaded adherend corners at both ends of the overlap. Another feature concerning this failure mode is that there was a small crack starting from the unloaded adherend corner to the other adherend surface, which intersected with the crack close to the upper adherend surface as shown in the figure. This was also observed in joints bonded with ductile adhesives as discussed in next section. A possible explanation for this failure locus is that the initial crack ran from the unloaded adherend corner to the other adherend surface at an angle of about 45^0 to the applied load. Then, it was arrested. Before this crack propagated, a new crack started at the other end of the overlap and this new crack

propagated to the upper adherend and through the overlap, resulting in final failure as shown in the figure.

The failure mode for large rounding is shown in Figure 8.10c. This failure mode is different from that in Figure 8.10b in that there is no first crack apparent as shown in Figure 8.10c. Another feature is that the crack ran along the curved adherend corner on the upper surface of the adherend as shown in the Figure. At the other end of the overlap, most of the cracks ran across or near the adherend corners. However, some cracks ran through the adhesive fillets to the adhesive fillet edges. A possible explanation for this failure mode is that cracks started at the adherend corners at right hand side of the overlap. Then, either the other end of the overlap failed or the crack at the right hand side of the overlap ran through the whole overlap to the other end of the overlap.

8.3.2.2 Ductile adhesive CTBN

A ductile adhesive, CTBN, was then used, which was more representative of modern toughened adhesives. The preparation of CTBN is presented in Appendix 3. Again, four batches each having six joints were made with one or two of all the degrees of rounding in the same batch and tested on the Zwick testing machine. This was to make sure that the bonding process did not introduce any variation in the joint strength. The strain rate was 5 mm/min and they were tested at room temperature (20^0 C). Unlike the brittle adhesive MY750, the load versus cross-head displacement curve was non-linear for large loads and a typical curve is shown in Figure 8.11. It can be seen that the curve was basically linear with load up to 80% of the breaking load. Then, a large amount of yielding took place in the adherends.

First, the failure mode is discussed. All the failure modes are similar as shown in Figure 8.12 for all the joints tested. However, more evidence needs to be found in order to determine at which end the cracks started first. From the study of failure loci under an optical microscope, it may be argued that failure started at the unloaded adherend corners of the upper adherend as shown at A in Figure 8.12. This is supported by the fact that smooth failure surfaces existed at this end in which the crack ran across the unloaded

adherend corner (A in Figure 8.12), but very rough at the other end of the overlap (B in Figure 8.12). This was particularly true for joints with large radiused adherend corners. However, there is some difference in the failure loci between joints with sharp or small adherend corners and with large degrees of rounding of the adherend corners. The failure process for sharp or small radiused adherend corners was complicated, and involved more than one crack as shown in Figure 8.12a. It is shown in Figure 8.12a that there was a small crack running across the unloaded adherend corner to the lower adherend surface at the right hand side of the overlap. This crack intersected with the main failure locus near the adherend corner. Further examination of the failed joints indicated that the fillet of the joint at the same end as the "first" crack yielded much more extensively along the failure locus than the other end of the overlap. This shows that the crack propagated stably at this end in the spew fillet, which resulted a large amount of yielding and corresponding stress-whitening. Also, the shape of these "first" cracks across the joint width was similar to the stress distribution across the width as discussed in Chapter 5 and is shown in Figure 8.13. As may be seen from Figure 8.13, the cracks did not extend to the edges of the joints, where the stresses or strains were lower than those inside the width. Based on this information, the failure process may be interpreted as follows.

(a). Joints with large radius corners

Joints with large radius adherend corners failed in the way as shown in Figure 8.12. Stresses or strains in the region of the rounded corner regions were the highest but quite uniform. These regions were large as shown in Chapter 7. The directions of the maximum principal stresses and strains were approximately at right angle to the adherend surfaces in the radiused region. The interfaces between the adhesive and adherends were the weakest link in this structure because the stresses are highest at the interfaces. As a result, cracks were likely to initiate and propagate in these regions. Once cracks started near the interface, the crack sizes were relatively larger compared with joints with sharp adherend corners because the stresses or strains were smooth in the radiused region for the large radiused adherend corners. However, the joints could still support load because of the ductile adhesive used. The load would, however, be re-distributed and the material surrounding the cracks would

carry more load resulting in extensive yielding. At some stage, the other end of the overlap also failed. This crack propagated towards the upper adherend surface and into the overlap resulting catastrophic failure as shown in the figure. The roughness of the adhesive surface at the left hand side of the overlap, B, was caused by the fast growth of the crack as shown in figure 8.12.

(b). Sharp and small radius corners

Joints with sharp or small radiused adherend corners failed in a slightly different manner from those with large radiused adherend corners. For the sharp or small radiused adherend corners, a large amount of yielding occurred in a localised area near the ends of the unloaded adherends. Because of the strain concentration in this area, failure might initiate at the corners at a load of lower than the final failure load at the right hand side of the overlap as shown in the figure. This "first" crack propagated stably towards the other adherend surface at an angle of roughly 90^0 to the maximum principal strains in that region. The load would then be redistributed and the strain concentration would be relieved. Because the adhesive used here was ductile and the strain concentration was localised, small cracks would not cause catastrophic failure and might be arrested. When the adhesive yielded, and especially when the crack initiated, the stiffness of the adhesive would be decreased dramatically and the adhesive inside the overlap would, in consequence, support more load and yield. When the crack propagated to the lower adherend surface, further propagation would require a large amount of energy. Instead, new cracks might start at the other end of the overlap at the unloaded adherend corner (B in Figure 8.12). The new crack first propagated towards the upper adherend roughly at right angles to the maximum principal strains then along the interface between the adhesive and adherends (surface S in the figure) after it reached the upper adherend as shown in the figure. This crack caused the final failure. It may be seen that such a process absorbed a large amount of energy, so that joints bonded with ductile adhesives were generally much stronger than those bonded with brittle adhesives.

8.3.2.3 Breaking loads

(a). Brittle adhesive MY750

Failure loads have been recorded for all of the tests and the results listed in Table 9.1. It clearly shows that rounding the adherend corners has some effect on the strength of the joints. It can be seen from the Table that the strength of the joints with large radiused adherend corners increased by about 40% compared with those with sharp adherend corners. Even a small radius of the adherend corner made the strength of the joints rise about 16%. The strength of the joints with medium radius lay between the small and large radius results. From the analyses in Chapter 7, it can be seen that the magnitudes of the stresses around the adherend corners change dramatically with the radii of the adherend corners, whilst the stresses near the edges of the spew fillets remain almost unchanged. This shows that the cracks could not have started at the spew fillet edges as shown as E in Figure 8.12a. Had this been the case, there would not have been difference in the joint strength. The difference in the magnitudes of the maximum principal stresses near the adherend corners explains why rounding the adherend corners increased the joint strength, because the stresses at the adherend corners were much reduced for such joints with radiused adherend corners.

(b). Ductile adhesive CTBN

The test results are listed in Table 9.3. Surprisingly, joints with sharp adherend corners were the strongest of all the joints tested. This conflicts with the feeling that rounding the corners reduces the strain concentration at the adherend corners and therefore the strength should not be lower than that of the sharp adherend corners. However, detailed examination of the failure surfaces will help understand the mechanics concerning the difference in the joint strength. It may be seen that joints with large radiused adherends were stronger than those with medium radiused adherends, although the difference was quite small. This is because the stresses or strains in such joints were smooth near the adherend corners. Once a crack was formed, it would have a reasonably large size. This large crack would develop into catastrophic failure. Therefore, the strength of joints with large radius adherend

corners was higher than that for medium radiused adherend corners. The problem exists in understanding the higher strength of joints with sharp adherend corners. Obviously, stress or strain concentration in joints with sharp adherend corners was much more severe than that in joints with radiused adherend corners. However, the area with strain concentration was much smaller than that near the large radiused adherend corners. Because of the ductility of the adhesive used and the small area with strain concentration, strain concentration might initiate small cracks, but the cracks might not cause catastrophic failure. In fracture tests, it has been shown that the crack-tip deformation plays an important role in the determination of fracture energies for rubber toughened epoxies (Hunston *et al*, 1989, Hunston *et al*, 1990). Also, in doing fracture tests on both bulk and joints bonded with CTBN, it has shown that small stable crack propagation and/or crack arresting are evident before the crack develops into a unstable one (Davy *et al*, 1989, Shaw, 1986, etc). In lap joints with sharp corners, although the initial plastic area might be smaller than that with radiused adherend corners, small cracks inside the adhesive layer might initiate at lower load for joints with sharp adherend corners than for joints with radiused adherend corners. These small cracks might be arrested without growing into catastrophic failure unless further load was applied. The existence of the crack would dramatically change the strain state near the ends of the adherend. Once the cracks had initiated, more load would be carried by the spew fillets and the adhesive around the small cracks. This would cause a large amount of yielding in the adhesive layer and in the spew fillets. In joints with radiused adherend corners, however, the maximum principal stress or strain acted nearly at right angle to the interface between the adhesive and the adherends and the area with such stresses or strains was much larger than that with sharp adherend corners. Thus, much larger cracks would be formed in joints with rounded adherend, although the load inducing these cracks might be higher than that causing small cracks in joints with sharp adherend corners. Because of the large size cracks in the adhesive in joints with rounded corners, the cracks would propagate much faster than the small cracks in joints with sharp corners, thus causing catastrophic failure. As a result, joints with radiused adherend corners have lower strength than that with sharp adherend corners. An

important point here is that the final failure load is different from that causing initial cracks for joints bonded with ductile adhesives.

8.4 CONCLUSION

From the above discussion, some conclusions may be drawn. First, material characterisation is very difficult, especially for the determination of the failure stresses or strains. Adhesive properties depend on strain rate, temperature and loading conditions. Test data *in situ* should be appropriately interpreted.

Failure modes are complicated in lap joints. Failure modes are different in fatigue tests than in quasi-static tests. However, they also have common features--the areas around the unloaded adherend corners are most critical. Joints bonded with brittle and ductile adhesives have similar failure modes. Finally, the failure locus across the joint width is also complicated.

In general, the failure process involves two steps: cracks around the unloaded adherend corners initiate and are then arrested; new cracks at the other ends of the overlap may start and these cracks propagate, forming the final failure. This process is similar for joints with both brittle or ductile adhesives. The joint strength tested is the final joint strength.

The shape of the unloaded adherend corners is not as critical for the joint strength as the theoretical analyses for unbroken joints suggest, although they have some effects on the joint strength. For joints bonded with brittle adhesives, the effect of radiused adherend corners is larger than that with ductile adhesives. The joint strength with a large radiused adherend corner increases about by 40% compared with that with sharp adherend corners. The effect of the rounding of the adherend corners is reversed for joints with ductile adhesives. Joints with sharp adherend corners are the strongest of all the joints tested, whilst joints with medium radii are the weakest. Small and large radius adherend corners have almost the same strength. This clearly shows that the failure mechanics of joints bonded with brittle and ductile adhesives is different.

Chapter 9

STRENGTH PREDICTION OF SINGLE LAP JOINTS

9.1 INTRODUCTION

It has been shown that the analysis of stresses or strains can be accurately made with the aid of FE programs. Although the stress or strain analyses are useful, it is more important to be able to predict joint strength. Before the strength prediction is attempted, the failure process and mechanics need to be studied. Generally speaking, there are two types of failure, termed brittle and ductile failure. In brittle failure, the deformation of the specimen under test is very small before sudden catastrophic failure. Examples of such materials are glass and ceramics. Ductile failure, on the other hand, involves a large amount of plastic deformation and necking before final failure. Some metals are typical of such materials. Experiments in Chapter 8 showed that adhesive lap joints failed in a brittle manner whatever adhesives were used. However, examining the failed surfaces, it was shown that a large amount of plastic deformation occurred in the adhesive layer of joints bonded with ductile adhesives. Therefore, ductile failure also needs to be studied, even though the failure was apparently brittle. Before predictions can be made, failure criteria are required to correlate the stresses or strains in a complex structure to that in a simple standard test specimen, where the failure stresses or strains can easily be found. Also, the failure mechanics and, in particular, the failure mode are very important in the determination of failure criteria. Because the stress or strain state in the adhesive layer has successfully been performed and the failure mode has been carefully examined, this chapter is devoted to the determination of suitable failure criteria based on which the joint strength can be accurately predicted. The predictions of strength based on the stress and strain analysis is, however, extremely difficult. The main reason is that stresses or strains at the adherend corners of joints are generally singular. Because of this, the failure criteria based on continuum mechanics are not applicable here. Fracture mechanics can, however, fill this knowledge gap. Elastic (brittle failure) and elasto-plastic (ductile failure) fracture mechanics has specially been developed to handle defects in a material, in which the stresses or strains at fracture are not defined. Below, both criteria based on continuum

mechanics and on fracture mechanics are reviewed first and a criterion combining these two approaches is proposed to predict the strength of the joints tested in Chapter 8. Finally, the predicted strengths of the joints are compared with the experimental results to assess the validity of the present failure criterion.

9.2 FAILURE CRITERIA CURRENTLY USED FOR LAP JOINTS

9.2.1 Criteria based on continuum mechanics

(1). *Maximum principal stresses*

Initially, maximum principal stress was proposed for very brittle materials whose failure mode is at right angles to the direction of maximum principal stress. This criterion ignores all the other principal stresses, even though they are not zero. Establishing the failure modes in lap joints bonded with brittle adhesives, Adams *et al* (1978) have extensively used this criterion to predict joint strength with success. However, because of the singularity of stresses at the re-entrant corners of joints, the stresses depend on the mesh size used and how close to the singular points the stresses are taken. Values of stresses calculated at Gauss points near the singularity or extrapolation of Gauss points values to the singularity were, in fact, used. Therefore care must be taken when using criterion. Although the criterion is sensitive to the mesh size used, the physical insight into the failure process is very clear. It is the maximum principal stress which is most responsible for the failure of joints bonded with brittle adhesives.

(2). *von Mises criterion*

Von Mises proposed a yield criterion, which states that a material yields under multi-axial stresses when its distortion energy reaches a critical value, that is

$$\sigma_{VM}^2 = (\sigma_1-\sigma_2)^2 + (\sigma_2-\sigma_3)^2 + (\sigma_3-\sigma_1)^2 = \text{constant}, \qquad (9.1)$$

where σ_i (i=1,2,3) are the principal stresses. Such a criterion has been used by Ikegami *et al* (1989) to study the strength of scarf joints between glass fibre composites and metals. It should be noted that this criterion is more applicable to material yielding than strength.

(3). *Shear stress*

Shear stress has be extensively used to predict lap joint strength with a limiting maximum shear stress equated to that of the bulk adhesive. Greenwood (1969) used the maximum shear stresses calculated by Goland and Reissner's analysis to predict joint strength. Grant *et al* (1976, 1983) have also applied this criterion to stepped lap joints. The engineering Sciences Data Unit (ESDU, 1979) implemented this criterion into a commercial package. More recently, John *et al* (1991) used shear stresses together with a critical distance to predict double lap joint strength. This approach ignores the normal stresses existing in lap joints and therefore it over-estimates joint strength.

(4). *Maximum principal strain*

When ductile adhesives are used, criteria based on stresses are not appropriate because joints can still endure large loads after adhesive yielding. For ductile adhesives, Adams and Harris (1984) used maximum principal strain as the failure criterion for predicting joint strength. This criterion can also predict the failure mode. Again, this criterion is sensitive to the mesh size used as discussed in the maximum principal stress approach.

(5). *Maximum shear strain*

Hart-Smith (1976) proposed that the maximum shear strains might be used as a failure criterion when plastic deformation was apparent. Another analysis goes beyond Hart-Smith's, which allows both shear and peel contributions to plasticity by Harwell (1986). ESDU (1979) also implemented this criterion in their commercial program.

(6). *Criteria based on energy*

Strain energy is the area under the stress-strain curve. Therefore, both stress and strain criteria can be related to strain energy. However, it should be noted that criteria based on strain energy take account of all the stress and strain components. As a result, it should be more suitable as a failure criterion than either stresses or strains. Plastic energy density has also been used. It is similar to the total strain energy criterion because it only takes the plastic part of the deformation into account.

It should be realized that all the above criteria are applicable to continuous structures only. They run into difficulty when defects occur or more than one material is present. For structures with defects or with more than one materials with re-entrant corners, stresses or strains are not well defined at the singular points. As a result, new criteria or modified versions of the above criteria should be used.

(7). *Global yielding*

In the analysis of lap joints, Crocombe (1989) found that, for very ductile adhesives, the whole overlap yielded before failure. He then proposed a new failure criterion based on the yielding of adhesive in the whole overlap. Once a path of yielding was found in the overlap with a given load, the joint was thought to be failed. Such a criterion is useful for very ductile adhesives in that once the whole adhesive layer yields, the adhesive layer cannot support any larger load. Some of the present work verifies this criterion. However, it should be noted that the adhesives need to be very ductile for the whole adhesive layer to yield before final failure. Unfortunately, joints tend to fail before the whole adhesive layer yields. Also, this criterion is only applicable to lap joints.

9.2.2 Criteria based on defects or more than one materials with re-entrant corners

Continuum mechanics assumes that the structure and its material are continuous. Defects or two materials with re-entrant corners obviously violate such an assumption. Consequently, continuum mechanics gives no solutions at these singular points resulting in stress or strain singularities. Cracks are the most common defects in structures, for which Fracture Mechanics (FM) has been developed. In fracture mechanics, it is well accepted that stresses calculated by using continuum mechanics are singular (infinite) at the crack tip. The reason that the singularity exists may be explained as follows. Fig. 9.1 shows the stresses given by continuum mechanics around the tip of a sharp crack in an infinitely large plate. Physically, the y-stress at the crack tip A must be finite, say σ_y (instead of infinite as theory predicts). However, the y-stresses away from the tip of the crack into the crack in the area shown as B are zero because of the free surfaces. Consequently, a discontinuity of σ_y in the y-stresses is apparent at point A unless σ_y is zero there. Such a stress distribution

cannot be accommodated in continuum mechanics which requires all the stresses to be continuous. As a result, the stresses at the crack tip are not defined (being infinite). With current theories on mechanics, such a singularity always exists when the crack angle is less than 180^0. Result was developed by Williams (1959) for stress singularities for a wedged notch. This argument is also applicable to the stress singularity in two materials bonded together with a re-entrant corner. In bi-materials with a re-entrant corner, the stress discontinuity still exists, although the free surfaces do not exist.

For ductile materials, a large amount of material yielding occurs and the crack may propagate stably before final failure. Linear fracture mechanics does not work any more for such materials. The HRR solution developed by Hutchinson (1968) and by Rice and Rosengren (1968) has, however, been used extensively in ductile fracture. Another important parameter governing the failure is the so-called crack tip opening displacement (Dugdale, 1960). However, strain singularity still exists for ductile materials, even though the stress singularity has disappeared.

(1) Linear fracture mechanics

For brittle adhesives, the linearly elastic fracture mechanics (LEFM) has successfully been used to predict lap joint strength with or without a pre-crack (Wang *et al*, 1978, DeVries *et al*, 1974, Chen, 1985, Groth, 1987, etc.). Fracture tests have, for brittle adhesives, been performed both on bulk materials of adhesives and *in situ* (Kinloch and Shaw, 1981, Cuckson, 1988, etc.). It has been shown that little difference exists in the fracture toughness in bulk and *in situ* for brittle adhesives. As a result, fracture mechanics can be used to predict joint strength or residual joint strength.

(2). Plastic fracture mechanics

Fracture mechanics is extremely difficult to apply to joint strength predictions bonded with ductile adhesives. For ductile adhesives, the fracture energy is not independent of the joint geometry (Kinloch and Shaw, 1981, Hunston *et al*, 1982). This is mainly because the adherends restrict the development of the yield zone in the adhesive layer so that fracture toughness is a function of joint geometry. Furthermore, because most of the cracks lie close

to the interface between the adherends and adhesives, Chen (1985) has showed that the evaluation of the parameter J is not independent of interface length enclosed in the evaluation of J for joints with re-entrant corners. Therefore, the parameter J cannot be used as a strength criterion for joints without a pre-crack. Moreover, failure modes are extremely complicated in the area of stress or strain concentrations as shown in Chapter 8. Therefore, if Fracture Mechanics is to be used for ductile adhesives, the process will be prohibitive: first it needs to be determined when and where a crack with a reasonable size initiates. Then, this crack has to propagate stably and be arrested. Next, a new crack at another place may initiate and propagate into an unstable one, causing catastrophic failure. This process is very difficult to simulate because the crack sizes and positions are very difficult to determine. Furthermore, such a process will involves a large amount of computing time with very fine mesh and the mesh shifting and releasing will be very difficult to perform.

It may be seen from the above discussions that fracture mechanics is very difficult to be applied to the initial strength prediction of lap joints. For brittle adhesives, very fine meshes are needed to obtain the stress resolution and sufficient curve fitting is also essential.

9.3. A NEW FAILURE CRITERION FOR THE STRENGTH PREDICTION OF LAP JOINTS

In this section, a new criterion combining continuum and fracture mechanics is proposed. It may be used as a first approximation to joint strength predictions. It will be demonstrated that it is reasonably accurate, easy to use, and insensitive to the mesh size used. It is particularly useful for engineering applications because a modest mesh is sufficient to predict the strength of a lap joint.

From an engineering point of view, joint strength should be predictable once the material properties and the stress or strain state are known. It has been shown in Chapter 8 that the stress or strain concentration at the re-entrant corners is not significantly important in the determination of joint strength, although the stresses or strains are reduced significantly

with small radius adherend corners. In fact, experiments showed, for a ductile adhesive, that the joints with sharp adherend corners were slightly higher than the joints with different degrees of rounding of the adherend corners. It seems that the stresses or strains in a finite area around the stress concentration point govern the failure of lap joints. Davy *et al* (1989) showed that cracks propagated stably (about 0.2 mm in their CT specimen) before they became so large that catastrophic failure occurred. This suggests that the failure process has two stages: first, cracks initiate, then the cracks propagate until the applied forces are so large that the cracks develop into unstable ones.

Kinloch and Shaw (1981) suggested a criterion based on a critical stress at a critical distance away from the crack tip. This approach is equivalent to the linear fracture mechanics approach as commented by Crocombe (1989). However, it requires very accurate calculation of the stresses around the crack tip. Based on this idea and taking into account the fact that stresses around the crack tip are most responsible for the joint failure, it is therefore proposed that failure is governed by the "averaged" stresses or strains within a critical distance from stress singular points. The critical distance may be such chosen that the averaged stress or strain equates to the failure stress or strain in tensile tests. This criterion has the advantage that the averaged stress or strain does not require a very fine mesh-it is reasonably insensitive to the mesh size used. Also, because it is based on averaged stresses or strains over a *finite* area, it takes account of the failure process mentioned above. However, one question arises with this criterion which is: does the integral of either the stresses or strains over a finite distance from the crack tip converge? It will be shown below that the integral does converge, although the stresses or strains are singular at the re-entrant corners. The critical distance may be so determined that the integral of the stresses, strains or strain energies over the distance divided by the distance is equal to that in uniaxial tensile tests. However, as a first approximation to the prediction of the strength of lap joints, the adhesive thickness may be used as the critical distance if the thickness is small. Therefore, the criterion may be simplified to the one generally used in practice. The averaged stresses or strains across the adhesive layer may be used as a failure criterion. The limiting stresses or strains are simply those obtained in bulk tests. Such a proposal is also in line with the criterion, proposed by Pavier (1989), that the relative displacements of the

adherends may be used as a failure criterion. To demonstrate this failure criterion, joints bonded with brittle (MY750) and ductile (CTBN) adhesives have been studied and the results are presented below.

9.3.1 Weighted average maximum stress criterion

It is well known that the stresses are singular at the unloaded adherend corner (Williams, 1959). Experiments have shown that failure starts at the unloaded adherend corner. As a result, the stresses around the corners need to be studied in detail if joint strength it to be predicted. It should be noted that joints bonded with brittle adhesives, such as MY750, fail in a brittle manner, i.e., once a crack starts, the whole joint fails following a short period of crack propagation. The stress analyses in Chapter 7 have shown that the stress concentration is very *localised* near the unloaded adherend corner. Consequently, the failure process involves little stable crack propagation but is dominated by the crack start process. Bearing this in mind, it may be said that the joint failure for brittle adhesives is dominated by the stress concentration. Unlike joints bonded with ductile adhesives, the area with high stresses is much reduced for joints bonded with brittle adhesives. As a result, the distance over which stresses are averaged is much reduced compared with joints bonded with ductile adhesives. This requires a reasonably fine mesh to obtain stress resolution. For the current configuration of the joint, the thickness was initially used as the distance over which the maximum principal stresses were averaged. The predicted joint strength for the sharp adherend corners with the limiting value of 84 MPa (From Harris, 1983) is listed in Table 9.1. It may be seen that the predicted joint strength is very high compared with the experimental result. As a result, the distance from the singularity over which the maximum principal stresses need to be determined. This involves the correlation of the stresses around the unloaded adherend corners with that in uniaxial tensile tests, and the distance from the unloaded adherend corner can be determined, over which the integral of the maximum principal stresses divided by the distance is equal to that of uniaxial tensile tests. The distance was found to be 0.04 mm from the singular point. By using this distance, the strength was predicted to be 8.02 kN for the joints with sharp adherend corners with the limiting value of maximum principal stresses being 84 MPa (Harris, 1983). Comparison of

the new predicted joint strength with experiments is also listed in Table 9.1. It may be seen that reasonable prediction was achieved by using this method. It should be noted that two meshes were used for the new prediction, and the results were insensitive to the mesh sizes used. However, Harris (1983) found, in his experiments with strain gauges on the specimens, that the averaged tensile fracture stress was 47 MPa. He attributed the low fracture stresses to be the strain gauge effects on the specimens. However, it may be argued that this low fracture stress may be preferred as a limiting value because there is always stress concentration in joints. For this reason, prediction were also made with the limiting value of 47 MPa for joints with sharp adherend corners. The averaged maximum principal stresses across the whole adhesive layer were used here. Again, three meshes with three, six and ten elements across the adhesive layer were used to obtain the stresses. It was found that the averaged maximum principal stresses across the adhesive layer were almost constant as listed in Table 9.2. Table 9.2 also lists the maximum values of the maximum principal stresses for the three meshes. It may be seen that the maximum values for the three meshes changed significantly, while the averaged maximum principal stresses were almost constant. It may be concluded that the maximum values of the maximum principal stresses may not be used to predict joint strength because they depend so much on the mesh sizes. The averaged values of the maximum principal stresses across the adhesive layer may be used as a failure criterion because they are insensitive to the mesh sizes. However, the predicted joint strength by using the averaged maximum principal stresses across the adhesive layer yielded very high strength if the limiting value of 84 MPa was used. If the 47 MPa fracture stress was used, accurate prediction were achieved as listed in Table 9.1.

Predictions for the joints bonded with small radius adherends were also listed in Table 9.1. For joints with small radius adherends, finite stresses were obtained as discussed in Chapter 7. For an applied of 20 kN, the highest maximum principal stress was calculated to be 158.06 MPa. The averaged maximum principal stress across the adhesive layer was 121.39 MPa. If the limiting value, 84.0 MPa, of the maximum principal stresses was used, the predicted joint strengths would be 10.6 kN and 13.0 kN based on the maximum and averaged values, respectively. However, the experimental joint strength was only 7.98 kN. It is clear that the predictions based on the limiting value of 84.0 MPa were much higher than

the experimental results. However, if the limiting value of 47.0 MPa was used, the predicted joint strengths would be 7.29 kN and 5.93 kN, respectively, based on the averaged and peak values. It may be seen that very accurate prediction was achieved by the averaged value across the adhesive layer with the limiting value of 47 MPa.

For joints bonded with medium radius adherends, the maximum values are used. The highest maximum principal stress was 100.3 MPa near the unloaded adherend corner with an applied load of 20 kN. If the limiting value of 84 MPa was used, the predicted joint strength would be 16.8 kN. Clearly, the predicted strength is much higher than the experimental result. However, the predicted joint strength would be 9.40 kN if the limiting value of 47 MPa was used. The prediction of the joint strength based on the limiting value of 47 MPa improved significantly as listed in Table 9.1.

The predicted joint strength for the large radius adherends based on the limiting value of 84 MPa was 23.0 kN, while the experimental result was 9.60 kN. This was done by using peak values of the maximum principal stresses because the stresses were smooth near the adherend corners. Clearly, the error was too much. However, if the limiting value of 47 MPa was used, the predicted joint strength would be 12.9 kN. This prediction was much better than that based on the limiting value of 84 MPa as seen in Table 9.1. The higher predicted joint strength of 12.9 kN may be because there were small cracks in the adhesive in some of the test specimens. These small cracks decreased the joint strength.

The strength of joints whose adherends have small radius corners is slightly higher than that with sharp adherend corners. This is because of the reduction in the stress concentration at the unloaded adherend corners. However, the increase in joint strength does not correlate to the decrease in the maximum principal stresses with the rounded adherend corners. This may be explained as follows. Although the stress concentration is responsible for the joint failure, the stress concentration does not apply to a single point. The stress concentration inside a very small area around the unloaded adherend corner causes failure. The maximum stresses in joints bonded with small rounded adherends differ from that for joints bonded with sharp adherend corners only in an area very close to the sharp adherend corner. The averaged maximum principal stresses inside a small area do not

differ much from that in joints bonded with adherends with sharp corners. Furthermore, the stressing condition for joints bonded with small adherend corners is worse than that in joints bonded with sharp adherend corners. As a result, the strength of joints bonded with small rounded adherends improves slightly compared with joints bonded with sharp adherend corners.

9.3.2 Average plastic energy density criterion

It has been shown by Adams and Harris (1987) that the plastic energy density at the re-entrant corners in a lap joint, has a distribution of the form

$$W_p \propto r^{-n} \tag{9.2}$$

where n is approximately 0.9. The plastic energy density is defined as the strain energy that stresses do work over plastic strains divided by the whole volume of the structure. The integration over a finite distance of t from the singularity, becomes

$$W_T \propto \lim_{x \to 0} \int_x^{x+t} r^{-n}\, dr = \frac{1}{1-n}\, t^{1-n} \tag{9.3}$$

where 1-n is always greater than zero and therefore t^{1-n} and W_T are finite. W_T is the total plastic energy over the distance of t from the singular point and therefore the average plastic energy density is

$$W_{av} \propto t^{-n}. \tag{9.4}$$

The failure criterion is then

$$W_{av} \leq W_{bulk} \tag{9.5}$$

Because W_T is the integral over the distance of t from the singularity, it is not sensitive to the mesh size used and a reasonably coarse mesh is enough to calculate the plastic energy density. It should be noted that n cannot be unity, otherwise the integral is infinite. This excludes the use of total energy density and therefore the plastic energy density is used here.

In lap joints, because the adhesive thickness is normally small (say, 0.1-0.4 mm), the thickness may be used as t as a first approximation to the strength predictions. In FE analysis, plastic energy density is available at Gauss points, and numerical integration can be easily performed. If uniform elements are used across the adhesive layer, the average plastic energy density is simply the average of the plastic energy density at these Gauss points across the adhesive layer.

Analyses have been made on joints with four types of adherends as discussed before, and CTBN adhesive. The geometry and material properties are shown in Figure 8.1. For large and medium degrees of rounding, no severe stress or strain concentration exists. Thus, continuum mechanics can be used here to predict the strength of the joints. Results are listed in Table 9.3, in which a limiting plastic energy density of 7.3 X 10^6 Jm^{-3} has been used according Adams and Harris (1987). It can be seen that very accurate predictions have been achieved for the large and medium radii. This is expected because no severe stress or strain concentration exists. This also indirectly verifies that the material properties in the bulk form are the same as *in situ*. Continuum mechanics can also predict the failure mode accurately as described in Chapter 8. A very interesting point here is that the global yielding criterion proposed by Crocombe (1990) is also applicable to the large rounding. A full path of plastic yielding was found in the adhesive layer and the FE analysis failed to reach convergence with a load a little higher than the predicted one. The reason is that the whole adhesive layer has yielded and cannot support any higher load. Such a criterion is commonly used in the prediction of collapse loads with ductile materials. However, it should be noted that such a phenomenon does not happen to all the other joints.

For the joints with a small radius and sharp adherend corners, continuum mechanics gave very low strength if peak values of the plastic energy density were used. Instead, the criterion proposed above is used here for the joints with sharp adherend corners. To test the sensitivity of the mesh size used, three, six and ten layers have been used to model the adhesive layer in a single lap joint. It has been found that the average plastic energy density is almost constant for the three meshes as shown in Table 9.4. However, it has also been observed that the maximum plastic energy density changes significantly for the three

different models also shown in Table 9.4. It may be seen from this table that the maximum values of the plastic energy density cannot be used as the failure criterion, because it depends so much on the mesh sizes. However, the averaged plastic energy density is not sensitive to mesh sizes used and therefore, it is appropriate to be used as a failure criterion. The predictions are listed in Table 9.3. It can be seen that the predictions are within 10% accuracy with the experiments. However, it should be noted the predictions are higher than the experimental results. This is because the strain singularity does not occur in the whole layer, only being so close to the adherend corners. However, the criterion is accurate enough for engineering applications, because the adhesive thickness is usually small. Care need to be taken to ensure that the values taken in the calculation of the plastic energy density is at the ends of the overlap.

Prediction for small radius adherend corners is also listed in Table 9.3. The prediction was made with the averaged plastic energy density over the adhesive layer near the adherend transition point into curved shape. Larger error existed in the prediction of joint strength for small radius adherend corners than that with sharp adherend corners. This may be explained as follows. As discussed in Chapter 8, the radius adherend corners of the small rounding support a large amount of stresses in a small area. The loading condition is worse than that in joints with sharp adherend corners. This decreases the strength of the joint. Because the change in geometry is small, the variation in strength is also small as listed in Table 9.3.

It may be concluded that the present failure criterion is very accurate for joints bonded with ductile adhesives. It is not sensitive to the mesh size used and the physical meaning is very clear. The average criterion is thought to be more reasonable than the pointwise criteria, because it does not require very accurate determinations of stresses or strains. It is very useful in engineering applications in that it only requires the material properties and geometry of the joint and a modest mesh is accurate enough.

9.4 CONCLUSIONS

It has been shown that the failure process is very complicated, which makes the understanding of failure and the predictions of joint strength extremely difficult.

Because of the stress and strain singularity at the ends of the joints, Fracture Mechanics might appear to be the only tool which can accommodate the singularity. However, it is well known that much more work, both theoretical and experimental, needs to be done before it can be used to predict joint strength, particularly for joints with ductile adhesives.

For large radii adherend corners, the criteria based on continuum mechanics can be used to predict joint strength, because there is no stress singularity.

For joints with sharp and small adherend corners, a new criterion combining continuum and fracture mechanics has been proposed and demonstrated to be accurate for joint strength prediction with ductile adhesives. Such a criterion is especially useful in engineering applications.

Chapter 10

GENERAL DISCUSSIONS AND CONCLUSIONS

Based on the previous Chapters, some general discussions and conclusions may be drawn. Generally speaking, there are two main aspects in the mechanical modelling of adhesively-bonded joints--the understanding of the mechanics of adhesive bonding and the quantitative predictions of joint strength. These two aspects are normally aided by stress analysis in the bonds. In this thesis, a particular kind of joint, the lap joint, has been studied. Below, three aspects will be discussed concerning the mechanics, stress analysis, and strength prediction of lap joints.

10.1 MECHANICS OF LAP JOINTS

It has been shown that stresses inside a lap joint are very complicated. There are large direct, peel and shear stresses in the adhesive layer. The direct stresses in the adhesive layer of 'square ended' joints come from Poisson's ratio effect due to peel stresses. However, for joints with spew fillets, the transfer of load at the adherend ends contributes to the direct stresses.

Large peel stresses exist in both single and double lap joints. The peel stresses in single lap joints are because of the bending moments at the ends of the overlap. The bending moments cause peel stresses through the bending of the adherends. As a result, the magnitudes of the peel stresses depend on the bending of the adherends. The peel stresses in double lap joints are from the internal bending moments caused by the shear stresses in the adhesive. However, the shearing of the central adherends contributes significantly to the peel stresses in double lap joints. Any factors reducing the bending deformation and shearing of the adherends will decrease the peel stresses in the lap joints.

Shear stresses in the adhesive layer of a lap joint are discussed. The large, uneven shear stresses are because of the uneven stretching of the adherends (Volkersen, 1938).

Stress distributions across the joint width have also been studied in this thesis. It has been found that the stresses are highest near the edges of the joint width as shown in Chapter 5.

This may be because of the anti-clastic effect and Poisson's ratio effect. In the interior, the stresses are much more uniform.

10.2 STRESS ANALYSIS

Basically, there are two kinds of method in the stress analysis for lap joints, closed-form algebraic and numerical. For single lap joints, the adherend deformation outside the overlap can be well handled by plate bending theory. As a result, the solution process can be divided into two steps. In the first step, the bending moments and the shear forces may be determined by plate theory with some assumption for the overlap, because there is discontinuity at the ends of the overlap and the adhesive layer (Goland and Reissner, 1944). Chapter 3 presents a new assumption on the overlap region. Here, it is assumed that the overlap does not deform at all under load. The assumption works well for reasonably long overlap. It can also deal with dissimilar adherends. For double lap joints, however, there is no method of obtaining the shear stresses in the central adherends at the ends of the overlap, although there is almost no bending moment at the ends of the overlap. The shear stresses in the central adherends contribute significantly to the peel stresses in the adhesive layer. Chapter 4 showed that the contribution to the peel stresses from the shearing of the central adherends was almost 50%. New research is needed to determine the shearing of the adherends in order to obtain peel stresses in the adhesive layer accurately. Chapter 4 presented an approximate method for determining the shearing of the adherends. This method may now be used for determining the shear stresses in the central adherends for double lap joints.

Numerical methods, mainly FEM, are much more versatile than the analytical methods thanks to the development in computing technologies. Numerical methods will certainly dominate the stress analysis field for the foreseeable future. Numerical methods can yield solutions to any problems once a model has been set up. However, it requires large computing resources. Until the time when a numerical solution is routine work comes, some combination of numerical and analytical methods may be useful. This is the purpose of Chapter 4, in which FEM was used to analyse the overlap region with the bending moments given by the analytical method.

10.3 STRENGTH PREDICTIONS

The greatest difficulty in the analysis of adhesively bonded joints lies in the quantitative prediction of joint strength. This may be because stresses or strains are singular at the re-entrant corners in adhesively bonded joints and the adhesive layer is very thin compared with the adherends. The interaction between the adhesive and the adherends makes the situation more complicated. In engineering applications, it is common practice to predict the strength of a structure once its materials, geometry and loading are known. This is almost impossible for adhesively bonded joints. In adhesive bonding, the best that can be done is to predict the strength of joints with similar configurations as a basic configuration, in which experimental and theoretical analyses have been studied. Even when experimental and analytical studies are known for a basic joint, it is not always possible to predict the strength of joints with other configurations, because the loading conditions are very complicated in lap joints. This is particularly true for joints bonded with ductile adhesives. As a result, the ability to predict joint strength is very limited. For joints bonded with brittle adhesives, Chapter 9 presented an approximate method for predicting joint strength. Chapter 9 also presented an approximate method for predicting joint strength for joints bonded with ductile adhesives. More studies are needed to verify this method.

Failure processes and modes are also complicated. Some studies have been carried out in this thesis concerning this aspect. Basically speaking, there are three stages in the failure for joints, crack initiation, stable crack propagation, and final catastrophic failure. This is true for joints bonded with both brittle and ductile adhesives, although there is a large difference in the periods of the three stages. For joints bonded with brittle adhesives, crack propagation involves a short period before it grows into catastrophic failure. However, there is large adhesive yielding and small crack propagation before the final failure for joints bonded with ductile adhesives. Another significant feature for joints bonded with ductile adhesives is that there may be more than one crack existing in the adhesive layer before the failure. This makes strength prediction much more difficult. Failure modes have also been studied in this thesis. It has been found that cracks run roughly at right angles to either the maximum principal stresses for joints with brittle adhesives or the maximum principal

strains for joints with ductile adhesives in the areas around the overlap end. This clearly shows that either the maximum principal stresses or strains are responsible for the joint failure.

10.4 SUGGESTIONS FOR FUTURE WORK

As has been discussed, there are many unknowns in the field of adhesively bonded joints. As a result, extensive research is needed in adhesive characterisation, joint modelling and strength, and life predictions of adhesive joints. However, from this study, some future work can be suggested.

(1). In closed form solutions, an accurate determination of the bending moments at the ends of the overlap is essential. The method given in Chapter 3 needs to be extended to include elastic-plastic behaviour of the adherends, because adherends tend to yield before the adhesive fails. The inclusion of elastic-plastic behaviour of the adherends may adopt the same assumption as in Chapter 3.

(2). The shearing of the central adherends in double lap joints plays an important role in the determination of peel stresses in the adhesive. The shear stresses in the central adherends need to be calculated accurately. Some development in the determination of the shear stresses in central adherends is therefore needed.

(3). The three dimensional stress analysis in Chapter 5 was based on a coarse mesh. To calculate accurately the three dimensional stresses, finer meshes are needed to obtain better stress resolution.

(4). Although FE analysis is very versatile and powerful, some development is still needed. To obtain the stresses at the re-entrant corners of joints, singular elements are needed in the vicinity of the corners. Because different combinations of adhesives and adherends produce different stress singularities, this development will be difficult. Another difficulty in the FE modelling of adhesive joints is the inability to determine the geometry of joints accurately. This is partly because adhesives squeeze out in the process of bonding. Finally,

the interface between adhesives and adherends needs more study into the interface properties and how to model it. This may strongly affect the joint strength.

(5). Most new developments will undoubtedly lie in the predictions of joint strength. This requires all the aspects concerning adhesive joints. From a modelling point of view, not only are criteria for initial joint strength prediction very important, but also the ability to follow the joint failure process is needed. This will be particularly difficult for joints bonded with ductile adhesives. Also, the ability to include defects in the adhesive layer is important.

Appendix 1

FINITE ELEMENT METHOD

Finite Element Method is a standardised numerical method which divide a whole structure into discrete *elements* interconnected at *nodes*. A *basic variable*, usually displacements, is mathematically represented by the nodal values. In the elements, some assumptions are made so that the variable can be expressed with the nodal values. Therefore, the whole structure is represented with the nodal values. Variational principles are then used to find these nodal values by minimising energy while ensuring force and displacement continuity between adjacent elements approximately.

In the present work, the plane strain is assumed. If $\{q\}$ is a vector of the nodal displacements and $\{\epsilon\}$ the strains throughout the element then

$$\{\epsilon\} = [B]\{q\} \tag{A1.1}$$

where the [B] matrix is the strain-displacement relationship and is consisted of shape functions. The shape functions define the displacement pattern in the element and relate displacements at any point within the element to the nodal displacements. The shape functions generally ensure the continuity of displacements at the element boundary with adjacent elements. Obviously, the displacement compatibility is automatically satisfied inside the element.

The next basic requirement in the continuum mechanics is the satisfaction of the stress equilibrium within the whole structure. Inside the element, stresses are related to strains through the elastic modulus matrix [D]

$$\{\epsilon\} = [D]\{\sigma\} \tag{A1.2}$$

Then, to satisfy the stress equilibrium, the total potential energy may be used and expressed as the functional P

$$P = \frac{1}{2} \{q\}^T[K]\{q\} + \{q\}^T\{f\}$$

where {f} is a vector of nodal forces and may be related to applied forces {F} (initial and body forces are assumed not to exist) through

$$\{f\} = \int_V [B]^T \{F\}\, dv \tag{A1.3}$$

and [K] is the stiffness matrix given by

$$[K] = \int_V [B]^T [D][B]\, dv \tag{A1.4}$$

Then the functional P may be minimized with respect to the nodal displacements and we have

$$\{f\} = [K]\{q\} \tag{A1.5}$$

This is the basic equation of the finite element method. It may be seen that the stress equilibrium is best approximated with the given displacement assumptions. Therefore, the accuracy of FEM based on displacements is governed by the displacement assumption (shape functions). In other words, the shape functions control the accuracy of such elements.

The above procedure can be used either to obtain the elemental stiffness matrix or the global stiffness matrix. The global stiffness matrix [K] may be assembled from the elemental contributions and so the load vector {f}. The displacements, for the complete structure, are then given by

$$\{q\} = [K]^{-1}\{f\} \tag{A1.6}$$

Once displacements are known, the stresses and strains can be calculated from eqns (A1.1) and (A1.2).

It should be realised that such a model to represent the whole structure is stiffer than the actual structure in that only a finite number of degrees of freedom are used rather than the infinite degrees of freedom of the structure. Therefore, stresses calculated with this method are smaller than the real values. However, the meaning of "smaller" is only applicable to the whole structure. Stresses at some individual points may be larger than actual situation.

Appendix 2

SURFACE PREPARATION OF ALUMINIUM ALLOY ADHERENDS FOR BONDING

The following standard surface preparation was followed throughout this work:

(i) Degreasing with trichlorethylene.

(ii) Degreasing in an alkaline degreaser (3% by weight of stripalene 532 in deionised water) for 3 minutes at 60^0 C.

(iii) Etching in a chromic-sulphutic acid solution (15% by volume of concentrated sulphuric acid, 7.5% by weight of potassium dichromate, made up with deionised water) for 20-30 minutes at 60^0 to 65^0 C.

(iv) Rinsing in cold deionised water.

(v) Washing in deionised water at less than 65^0 C for 10 minutes.

(vi) Drying in a warm air stream not exceeding 75^0 C.

It should be noted that once the specimens have been etched, the bonding must be made within 24 hours.

Appendix 3

THE PROCEDURES OF MAKING AND CURING OF ADHESIVES (MY750 AND CTBN)

1. The following standard procedure was used for the making and curing of MY750:

A. The making of MY750

(i) Pour hardener HY906 into resin MY750 with the ratio of 85 to 100 by weight.

(ii) Degas

(iii) Pour accelerator DY062 into the MY750/HY906 mixture with the ratio of 2 to 185 by weight.

B. The procedure of bonding

(i) Pre-heat moulds to 80^0 C.

(ii) Make bonding.

(iii) Cure at 80^0 C for 6 hours under pressure.

(iv) Cure at 125^0 C for 5 hours under pressure.

2. The following standard procedure was used for the making and curing of CTBN:

A. The making of CTBN

(i) Mix MY750 and CTBN with the ratio of 100 to 15 by weight.

(ii) Heat to 60^0 to 65^0 C in a water bath.

(iii) Stir for 10 minutes.

(iv) Stir with electric stirrer for 5 minutes in water bath at 60^0 to 65^0 C.

(v) Leave in water bath for 15 minutes.

(vi) Heat to 90^0 C.

(vii) Degas and allow to cool to 25^0 to 30^0 C.

(viii) Add hardener piperdine 5 parts by weight and mix carefully.

B. The bonding procedure

(i) Warm resin to 60^0 C and preheat moulds to 120^0 C.

(ii) Making bonding.

(iii) Cure at 120^0 C for 16 hours.

REFERENCES

Adams, R. D., Atkins, R. W., Harris, J. A. and Kinloch, A. J., *Stress Analysis and Failure Properties of Carbon-Fibre-Reinforced-Plastic/Steel Double-Lap Joints*, J. Adhesion, Vol. 20, pp29-53, 1986.

Adams, R. D. and Cawley, *Vibration Techniques in Nondestructive Testing*, Nondestructive testing, Vol. 8, 1985.

Adams, R. D., Chambers, S. H., del Strother, P. J. A., and Peppiatt, N. A., *Rubber Model for Adhesive Lap Joints, J. Strain Analysis*, 8, pp. 52-57, 1973.

Adams, R. D., Coppendale, J. and Peppiatt, N. A., *Failure Analysis of Aluminium-Aluminium Bonded Joints*, Adhesion 2, Allen, K. W. Ed., Appl. Sci. Publ., London, p. 105, 1978.

Adams, R. D. and Harris, J. A., *Strength prediction of Bonded Single Lap Joints by Non-linear Finite Element ethods*, Int. J. Adhesion and Adhesives, Vol. 4, No. 2, April, 1984.

Adams, R. D. and Harris, J. A., *The Influence of Local Geometry on the Strength of Adhesive Joints*, Int. J. Adhesion and Adhesives, Vol. 7, No. 2, April, 1987.

Adams, R. D., and Peppiatt, N., A., *Effect of Poisson's Ratio Strain in Adherends on Stresses of an Idealised Lap Joint*, J. Strain Analysis, 8, pp134-139, 1973.

Adams, R. D., and Peppiatt, N., A., *Stress Analysis of Adhesively-Bonded Lap Joints*, J. Strain Analysis, 9, pp. 185-196, 1974.

Adams, R. D. and Wake, W.C., *Structural Adhesive Joints in Engineering*, Elsevier Applied Science Publishers, 1984.

Allman, D. J., *A Theory for the Elastic Stresses in Adhesive Bonded Lap Joints*, R.A.E. Tech. Rep. 76024, 1977.

Allman, D. J., Quarterly J. Mechanics and Appl. Maths., 30, 415, 1977.

Amijima, S., Fujii, T. and Yoshida, A., *Two Dimensional Stress Analysis on Adhesive Bonded Joints*, Proceedings of Japanese Congr. Mater. Res. 20th, Kyoto, Jpn, Sep. 1976, pp275-281.

ANSYS, *Engineering Analysis System, User's Manual I and II*, Swanson Analysis Systems Inc., 1989.

ANSYS, *Engineering Analysis System, Theoretical Manual*, Swanson Analysis Systems Inc., 1989.

Atluri, S. N., Gallagher, R. H. and Zienkiewicz, O. C., *Hibrid and Mixed Finite Element Methods*, John Wiley & Sons, 1982).

Benson, N. K., Influence of stress distribution on joint strength, Adhesion-Fundamentals and Practice, UK Ministry Technology, MacLaren, London, p. 191, 1969.

Brooker, M.J., *The Stress Distribution in Adhesively Bonded Lap Joints*, M.Sc. Thesis, Imperial College of Science and Technology, 1980.

Chen, D, and Cheng, S., An Analysis of Adhesive Bonded Single Lap Joints, ASME J., ppl. Mech., 50, 1983.

Chen, Z., *GMESH - A Novel Finite Element Mesh Generating Program*, Internal Report, Dept. of Mech. Eng., University of Bristol, 1982.

Chen, Z., *The Failure and Fracture Analysis of Adhesive Bonds*, Ph.D. Thesis, University of Bristol, 1985.

Collar, A., R. and Simpson, A., *Matrices and Engineering Dynamics*, Ellis-Horwood, Chichester, 1987.

Coppendale, J., *The Stress and Failure Analysis of Structural Adhesive Joints*, Ph.D Thesis, University of Bristol, 1977.

Crocombe, A. D., *The Non-linear Stress and Failure Analysis of Adhesive Tests*, Ph.D. Thesis, University of Bristol, 1981.

Crocombe, A. D., *Global Yielding as a Failure Criterion for Bonded Joints*, Int. J. Adhesion and Adhesives, Vol. 9, No. 3, July, 1989.

Crocombe, A. D. and Adams, R., D., *The Influence of the Spew Fillet and other Parameters on the Stress Distribution in the Single Lap Joint*, J. Adhesion 13, 1981.

Cuckson, A., K., Measurement of the Fracture Energy of Aluminium Bonded by Epoxy Resins, Ph.D Thesis, University of Bradford, 1988.

Davy, G., Hashemi, S. and Kinloch, A. J., *The Fracture of a Rubber-modified Epoxy Polymer Containing Through-thickness and Surface Cracks*, Int. J. Adhesion and Adhesives, Vol. 9, No. 2, April, 1989.

Dillard, D. A., *Some Developments in Testing Adhesive and Adhesive Joints*, 7th Annual Program Review/Workshop, Donaldson Brown Centre, Blacksburg, Virginia, 1989.

Dugdale, D. S., *Yielding of Steel Sheets Containing Slots*, J. Mech. Phys. Solids, Vol. 8, 1960.

Engineering Sciences Data Item Number 79016, *Inelastic shear stresses and Strains in the Adhesives Bonding Lap Joints Loaded in Tension or Shear (computer program)*, Engineering Sciences Data Unit, 1979.

Engineering Sciences Data Item Number 80039, *Elastic Adhesive stresses in Multistep Lap Joints Loaded in Tension (computer program)*, Engineering Sciences Data Unit, 1979.

Gere, J. M. and Timoshenko, S. P., *Mechanics of Materials*, Second SI Edition, PWS Engineering, 1985.

Goland, M. and Reissner, E., *The Stresses in Cemented Joints*, J. Appl. Mech, Trans. ASME 66, A17, 1944.

Grant, P. and Taig, I., C., *Strength and Stress analysis of Bonded Joints*, BAC Report, No. SOR(P) 109, 1976.

Grant, P., Sanders, R. C. and Waed, A. P., *Developments in Bonded Joint Analyses*, BAC report No. SOR(P) 137, 1983.

Greenwood, L., *The Strength of a Lap Joint*, In Aspects of Adhesion - 5, Univ. London Press, pp40-50, 1969.

Groth, H. L., *Analysis of Adhesive Joints*, Ph.D. Thesis, Royal Inst. Tech., Stockholm, Sweden, 1987.

Hahn, K., F., *Photo stress investigation of bonded lap joints*, Part II: Analysis of experimental data, McDonnell-Douglas Co. Research Report SM 4000-1, Long Beach, California, 1960.

Harborne, R. A. and Howard, I. C., *Ply Drop-off in Carbon Fibre Laminates*, Final MoD Contract Report, University of Sheffield, 1989.

Harris, J. A., *Non-linear Analysis and Testing of Adhesive Joints Under Impact and Quasi-static Loading*, Ph.D. Thesis, University of Bristol, 1983.

Harris, J. A. and Adams, *Strength Prediction of Bonded Single Lap Joints by Non-linear Finite Element Methods*, Int. J. Adhesion and Adhesives, Vol. 4, No. 2, April, 1984.

Hart-Smith, L. J., *Adhesive-bonded Single Lap Joints*, CR-112236, NASA, Langley Res. Centre, 1973.

Hart-Smith, L. J., Developments in Adhesives-2, Kinloch, A. J., Ed., Appl. Sci. Publ., London, p.1, 1981.

Harwell Report AERE G 4115, *A Computer Program for the non-linear Stress Analysis of Adhesively Bonded Single Lap Joints*, 1986.

Hein, V. L. and Erdogan, F., *Stress Singularities in a Two-material Wedge*, Int. J. of Frac. Mech. Vol. 7, 1971.

Hughes, Althof, Krieger, *Mechanical Properties of Adhesives*, in Adhesive Bonding of Aluminium Alloys, Marcel Dekker, New York, 1985, pp. 141-175.

Hutchinson, J. W., J. Mechanics and Physics of Solids, 16, 1968.

Hunston, D. L., Kinloch, A., J., and Shaw, S. J., and Wang, S. S., *Characterisation of the Fracture Behaviour of Adhesive Joints*, Adhesive Joints, Formation, Characteristics and Testing, Ed. K. L. Mittal, Plenum Press, 1982, pp789-807.

Hunston, D. L., Kinloch, A. J. and Wang, S. S., Journal of Adhesion, 28, p103, 1989.

Hunston, D. L., Mizumachi, H. and McDonough, W., *Micromechanics of Fracture in Rubber-Toughened Epoxies*, Adhesion'90, University of Cambridge, 1990.

Ikegami, K., Takeshita, T., Matsuo, K. and Sugibayashi, T., *Strength of Adhesively Bonded Scarf Joints Between Glass Fibre Reinforced Plastics and Metals*, Structural Adhesives in Engineering II'89, 1989, pp157-159.

Irwin, G. R. and Roland, de Wit, *A Summary of Fracture Mechanics Concepts*, J. Testing and Evaluation, Vol. 11, No. 1, 1983.

Jangblad, D., Gradin, P., and Stenstrom, T., *Determination and Verification of Elastic Parameters for Adhesives*, Adhesively Bonded Joints: Testing, Analysis, and Design, ASTM STP 981, W. S. Johnson, Ed., American Soc. Testing Materials, Philadelphia, 1988, pp. 54-68.

John, S., J., Kinloch, A., J., Matthews, F., L., and Albelda-Vitorial, J., *The Durability of Composite Joints Using Cold-setting Adhesives*, 1991.

Johnson, W. and Mellor, P. B., *Engineering Plasticity*, Van Nostrand Rheinhold Co., 1973.

Kinloch, A. J., *Adhesion and Adhesives, Science and Technology*, Chapman and Hall, 1987.

Kinloch, A. J., *Test Methods for Adhesive Joints*, Conference Proceedings, ASE88, 1988, pp. 117-127.

Kinloch, A. J. and Shaw, S. J., *A Fracture Mechanics Approach to the Failure of Structural Joints*, Developments in Adhesives-2, Chapter 3, pp83-124, Applied Science Publishers, 1981.

Kutscha, D, *Mechanics of Adhesive Bonded Lap Type Joints-Survey and Review*, US Forest Products Lab. Report MLTDR-64-298, US Dept. of Agric., Madison, Wisconsin, 1964.

Lubkin, J.L. and Reissner, E., *Stress Distributions and Design Data for Adhesive Lap Joints Between Circular Tubes*, Trans. ASME, 78, pp.1213-1221, 1956.

Mallick, V., *Stress Analysis of Metal/CFRP Adhesive Joints Subject to the Effects of Thermal Stress*, Ph.D. Thesis, University of Bristol, 1989.

Matthews, F., L. *et al*, *A Review in the Strength of Joints in Fibre Reinforced plastics*, Composites 13, 1, Jan., 1982

McLaren, A. S. and MacInnes, I., *The influence of the stress distribution in an adhesive lap joint of bending and adhering sheets*, British J. Appl. Phy., 9, pp.72-77, 1958.

Mises, R. von, *Mechanik der Festen Korper in Plastisch Deformablem Zustant*, Gottingen Nachr. Maths. Phys., k.1, p582, 1928.

Moult,A., C., Msc Thesis, University of Surrey, 1986.

Peppiatt, N. A., *Stress Analysis of Adhesive Joints*, Ph.D. Thesis, University of Bristol, 1974.

Pian, T. H. H., *Derivation of Element Stiffness Matrices by Assumed Stress Distributions*, AIAA J., 2, pp1613-1620, 1964.

Pian, T. H. H., Chen, D., P., *A New Formulation of ybrid/mixed Finite Elements*, Comp. Struct. 16, 1983.

Pivier, M., J., unpublished results, university of Bristol, 1989.

Post, D., *Moiré Interferometry*, SEM Handbook on Experimental Mechanics, A. S. Kobayashi, Ed., Prentice-Hall, Englewood Cliffs, N. J., 1987.

Post, D., Czarnrk, R., Wood, J. D., and Joh, D., *Deformations and Strains in Thick Adherend Lap Joint*, Adhesively Bonded Joints: Testing, Analysis, and Design, ASTM STP 981, W. S. Johnson, Ed., American Soc. Testing Materials, Philadelphia, 1988, pp. 107-118.

Przemieniecki, J. S., *Theory of Matrix Structural Analysis*, McGraw-Hill, 1968.

Raghava, R. S.,Cadell, R. M., and Yeh, G., S., Y., J. Mat. Sci., 8, 225, 1973.

Raghava, R. S. and Cadell, R. M., *The Macroscopic Yield Behaviour of Polymers*, J. Mat. Sci., Vol. 8, 1973.

Renton, W. J. and Vinson, J. R., *The Efficient Design of Adhesive Bonded Joints*, J. Adhesion 7(3), p175, 1975.

Rice, J. R. and Rosengren, G. F., J. Mechnics and Physics of Solids, 16, 1968.

Robinson, J., *Understanding Finite Element Stress Analysis*, Robinson and Associates, 1980.

Sehmi, N., S., Ph.D. thesis, University of Bristol, 1987.

Shaw, S., J., *The Fracture of Epoxy Resins and the Effect of Rubber Inclusions*, Ph.D. thesis, City University, London, 1984.

Sneddon, I., Adhesion, Ed. ELEY, D., Chapter 9, Oxford University Press, 1961.

Volkersen, O., *Die Nietkraftverteilung in Zugbeanspruchten Nietverbindungen Mit Konstanten Laschenquerschnitten*, Luftfarhtforschung, 15, pp.41-47, 1938.

Volkersen, O., *Recherches sur la theorie des assemblages colles*, Construction Metallique, 4, pp. 3-13, 1965.

Wake, W., C., *Adhesion and the Formulation of Adhesives*, 2nd ed., Appl. Sci. Publ., London, 1982.

Wang, S. S., Mandell, J. F. and McGarry, F. J., *An Analysis of the Crack Tip Stress Field in DCB Adhesive Fracture Specimens*, Int. J. Fracture, Vol. 14, No. 1, Feb., 1978, pp.39-58.

Washizu, K., *Variational Methods in Elasticity and Plasticity*, Pergamon Press, 1982.

Williams, M. L., *The stresses Around a Fault or Crack in Dissimilar Media*, Bull. Seismal Soc. of America, 1959.

Zhao, X., *The Poisson's ratio effect on longitudinal stresses*, Unpublished results, 1990.

Zhao, X. and Adams, R.D., *Adhesive Joint Strength Predictions for Real Boundary Conditions*, Structural Adhesives in Engineering II '89.

Zhao, X., Adams, R., D., and Pavier, M., J., *A New Approach to Determinating the Bending Moment Factors in Single Lap Joints*, Fourth international. Conference, Adhesion 90, University of Cambridge, 1990.

Zhao, X and Simpson, A., *Kron's Procedure for a Freely Vibrating Spinning Structure*, Q. Jl Mech. appl. Math., Vol. 41, Pt. 4, pp597-618, 1988.

Zienkiewicz, O.C. and Taylor, R.L., *The Finite Element Method*, Fourth Edition, McGraw-Hill Book Company, 1988.

Specimen No.	Thickness (mm)
1	0.25
2	0.19
3	0.24
4	0.24
5	0.25
6	0.23

Required thickness: 0.25 mm

Table 8.1 Typical thickness of the adhesive within one batch

Corners	Predictions (kN) (limiting value 84 MPa)			Predictions (kN) (limiting value 47 MPa)		Experiments (kN)
	0.04 mm	Averaged	Maximum values	Averaged	Maximum values	
Sharp	8.02	11.0	——	6.15	——	6.85 (6.12 %)
Small rounding	——	13.0	10.6	7.29	5.93	7.98 (7.93 %)
Medium rounding	——	——	16.8	——	9.40	8.22 (12.8 %)
Large rounding	——	——	23.0	——	12.9	9.60 (15.0 %)

Table 9.1 Comparison of joint strength of predictions and experiments with MY750

Meshes	Max. prin. stresses MPa (peak values)	Max. prin. stresses MPa (averaged values)
Three elements across adhesive layer	78.60	52.33
Six elements across adhesive layer	89.34	52.27
Ten elements across adhesive layer	96.63	52.12

Applied load: 6.85 kN

Table 9.2 Comparison of peak and averaged max. prin. stresses

Rounding	Predictions	Experiments
Sharp	29.3	27.8 (6.32 %)
Small radius	28.7	26.1 (3.95 %)
Medium radius	23.8	24.3 (5.56 %)
Large radius	25.22	25.4 (3.02 %)

Table 9.3 Comparison of strength predictions and experiments with CTBN

Meshes	Max. values of plastic ene. density	Averaged values of plastic ene. density
Three elements	8.132	2.447
Six elements	11.52	2.741
Ten elements	13.78	2.720

Table 9.4 Plastic. energy density of three meshes with 20 kN load

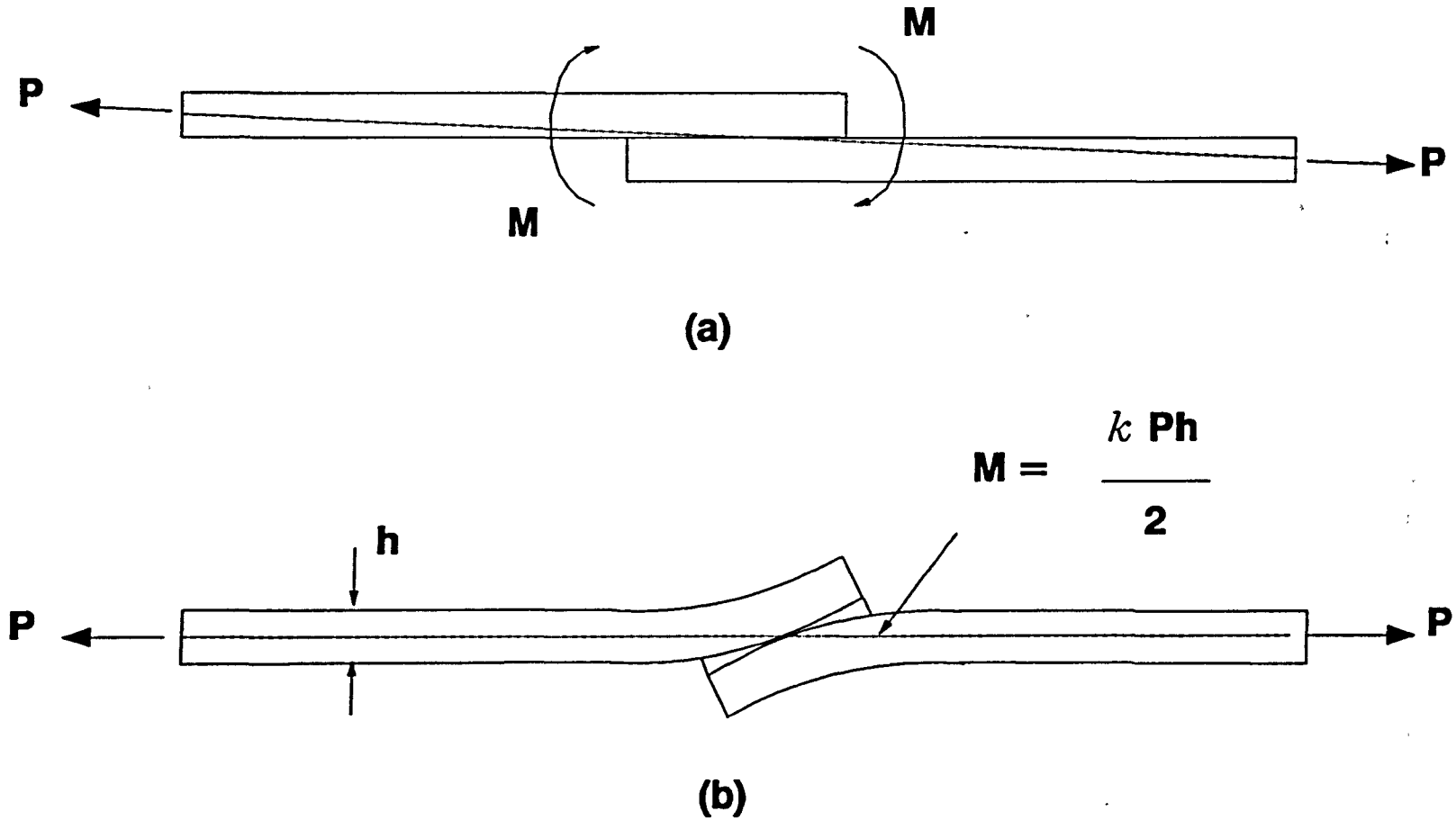

Fig. 2.1 A single lap joint with rotation of the overlap

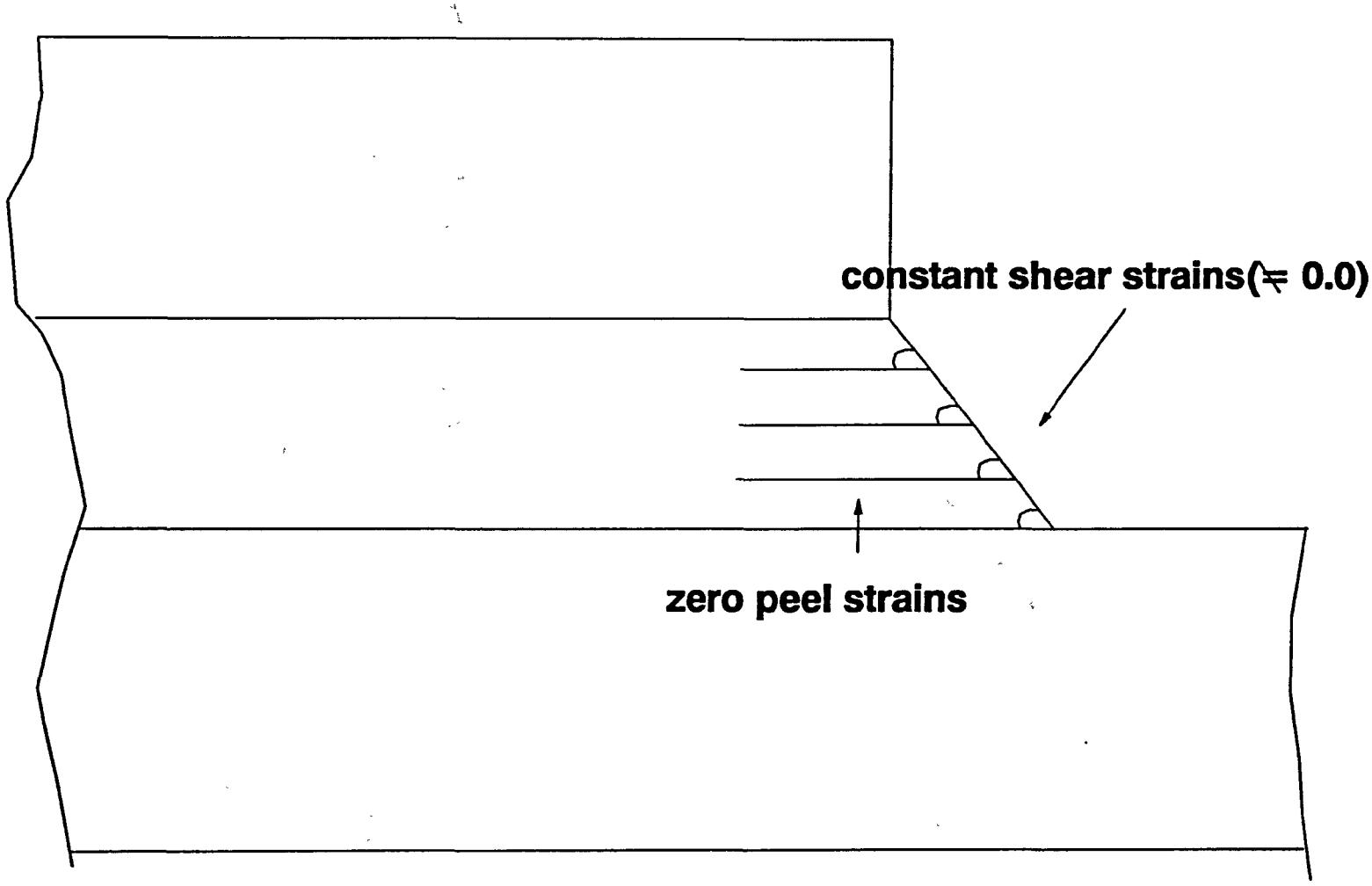

Fig. 2.2 Figure showing that shear stresses cannot be zero

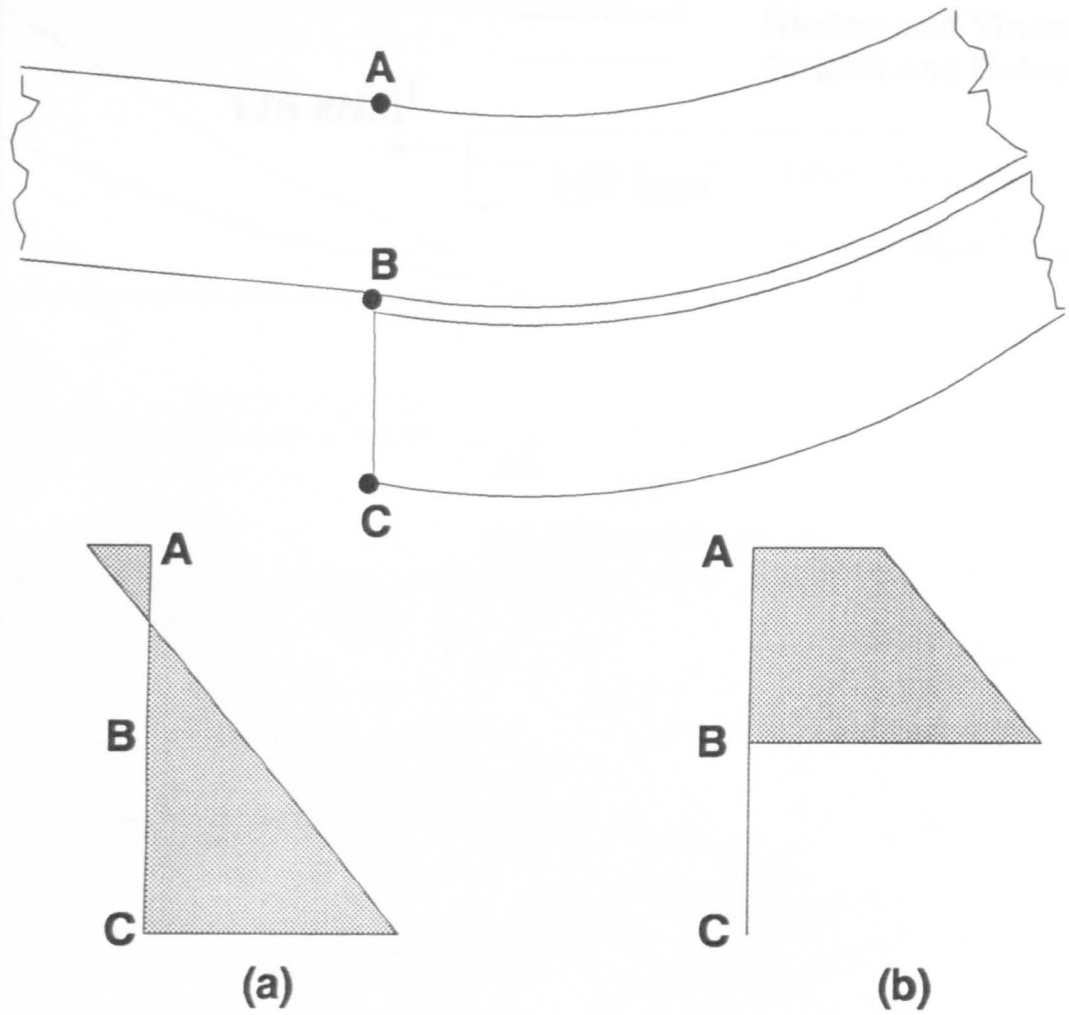

Fig. 2.3 Comparison of longitudinal stresses assumed by (a) Goland & Reissner and (b) Hart-Smith

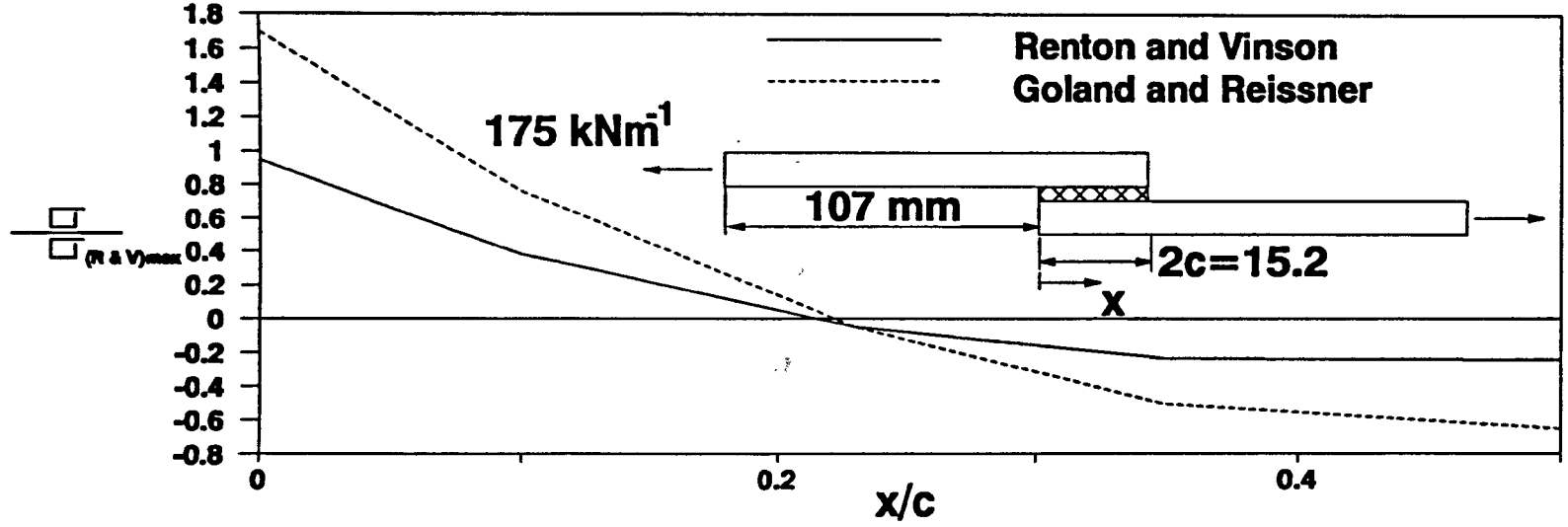

(a) Peel stresses

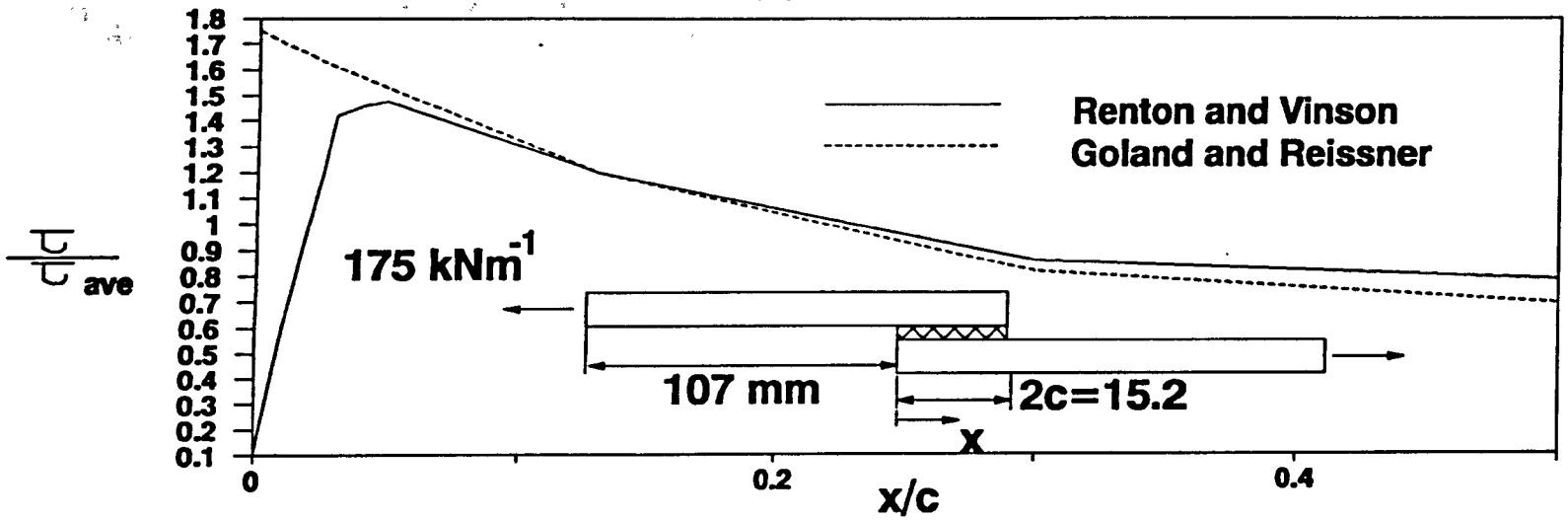

(b) Shear stresses

Fig. 2.4 Comparison of Renton & Vinson's ans Goland & Reissner's analyses

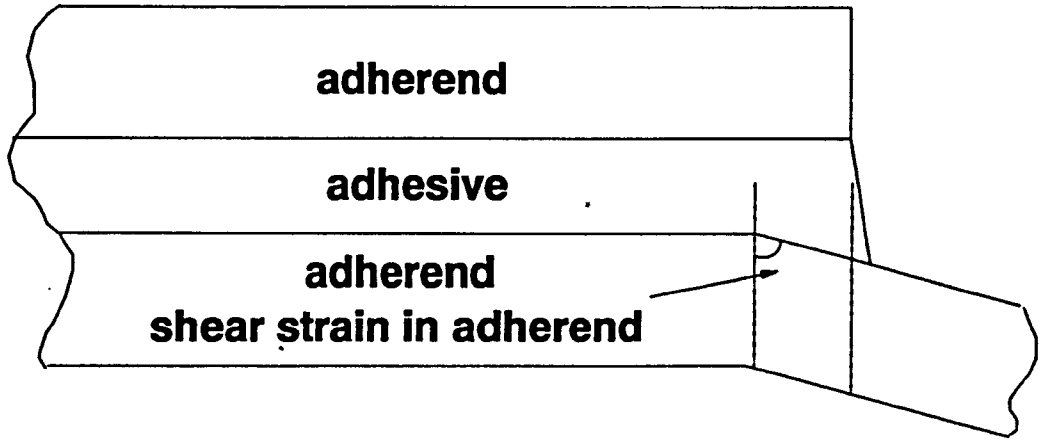

Fig. 2.5. Effect of adherend shearing on the stresses in adhesive

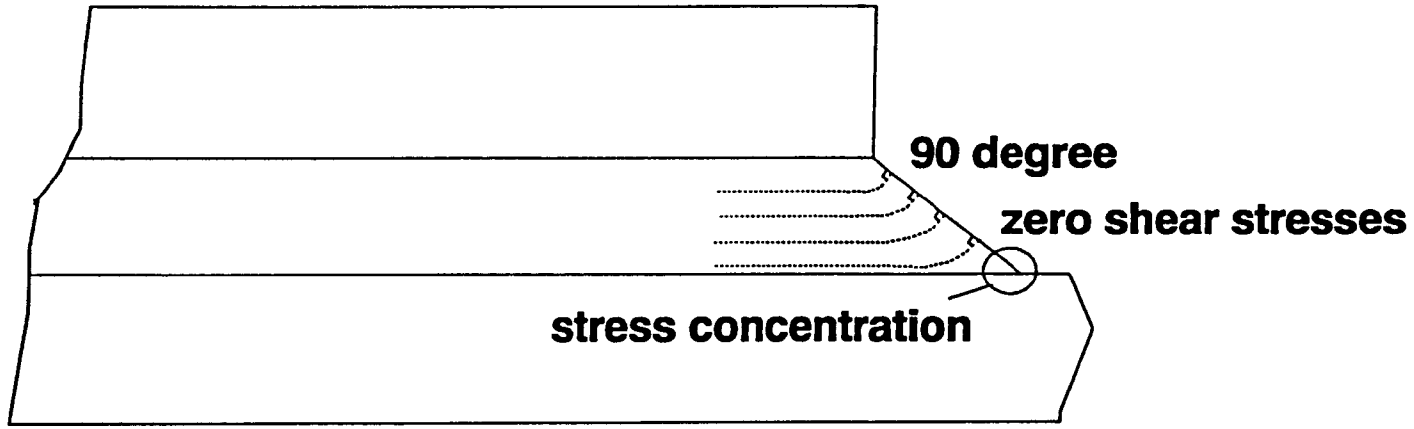

Fig. 2.6 zero-shear stresses at the edges of adhesive

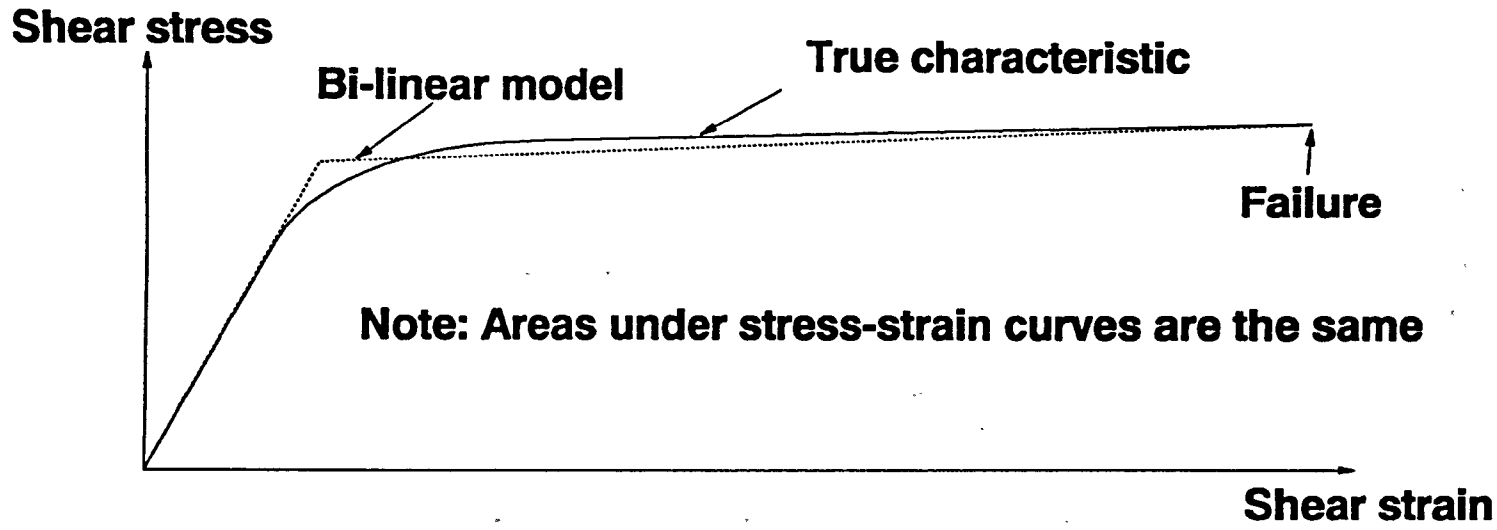

Fig. 2.7 Adhesive shear stress-strain curves and math. models

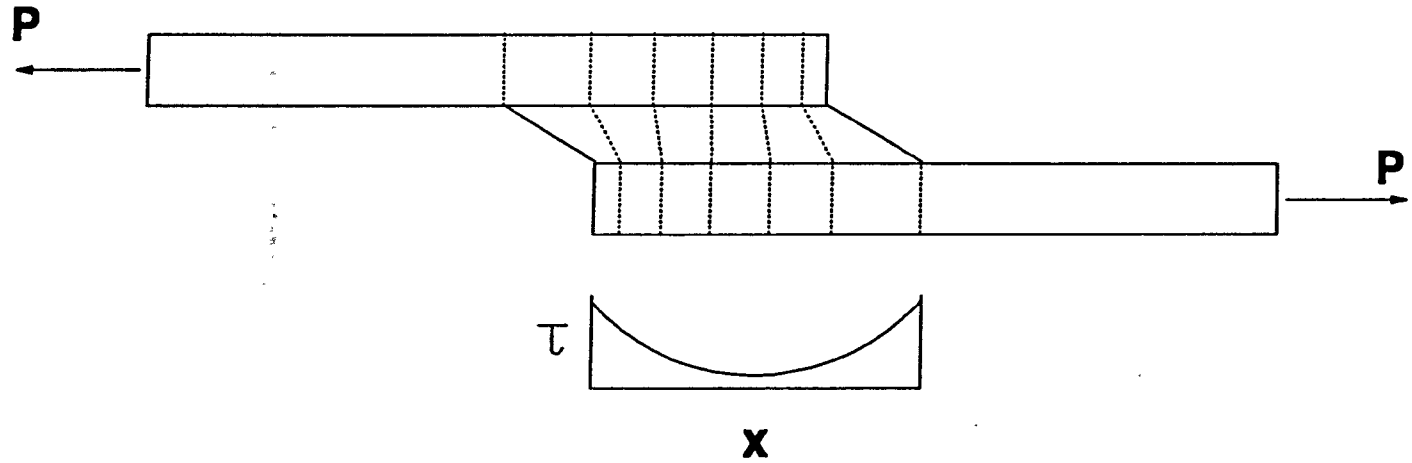

Fig. 2.8 Exaggerated deformation in single-lap joint

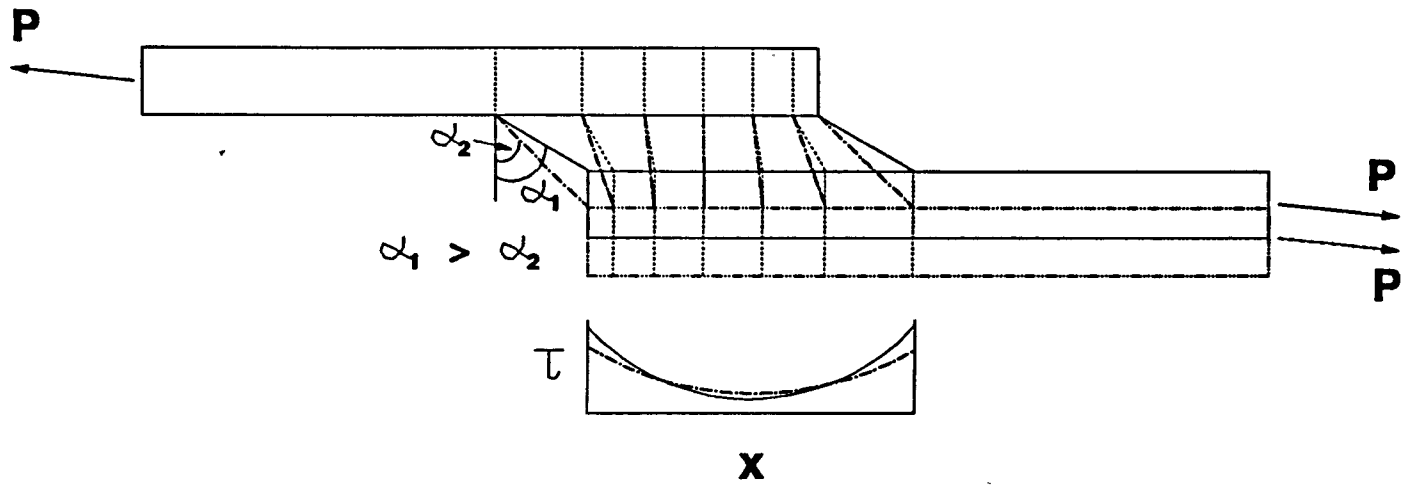

Fig. 2.9 Comparison of different adhesive thicknesses

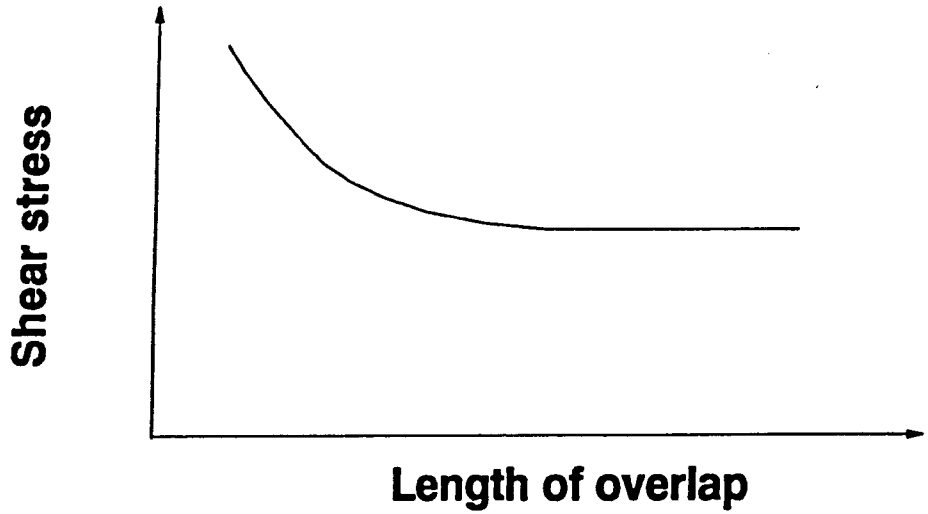

Fig. 2.10 Variations in shear stresses with the length of overlap

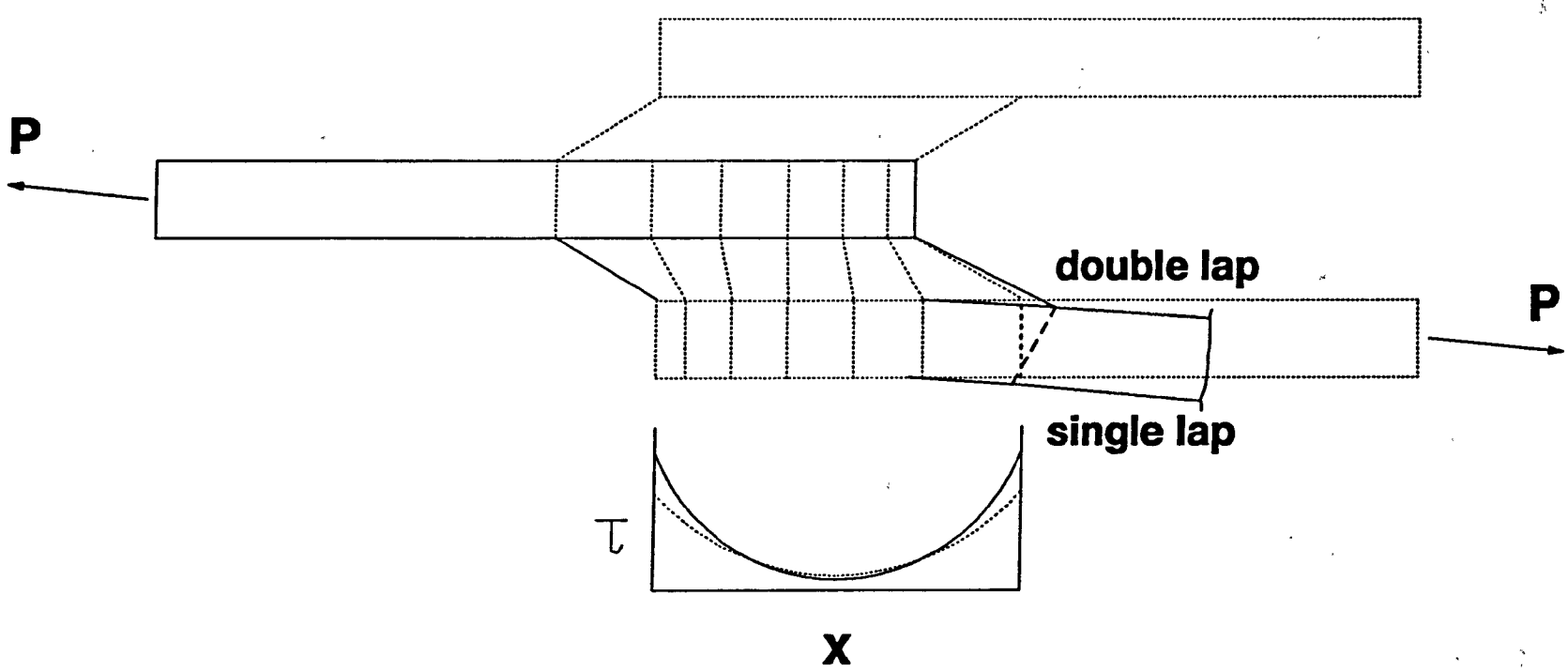

Fig. 2.11 Shear stresses in single and double lap joints

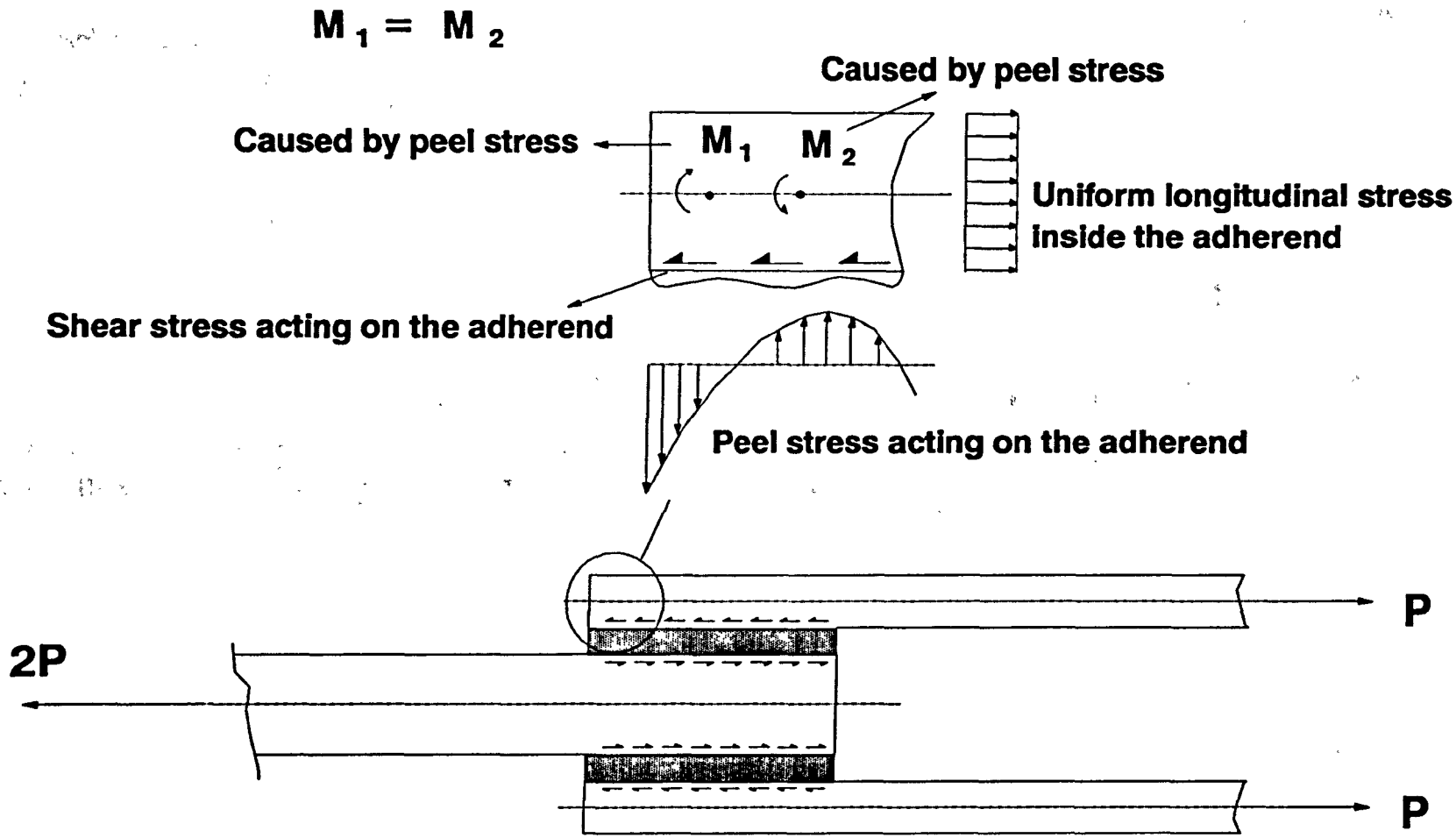

Fig. 2.12 Bending moments in a double lap joint

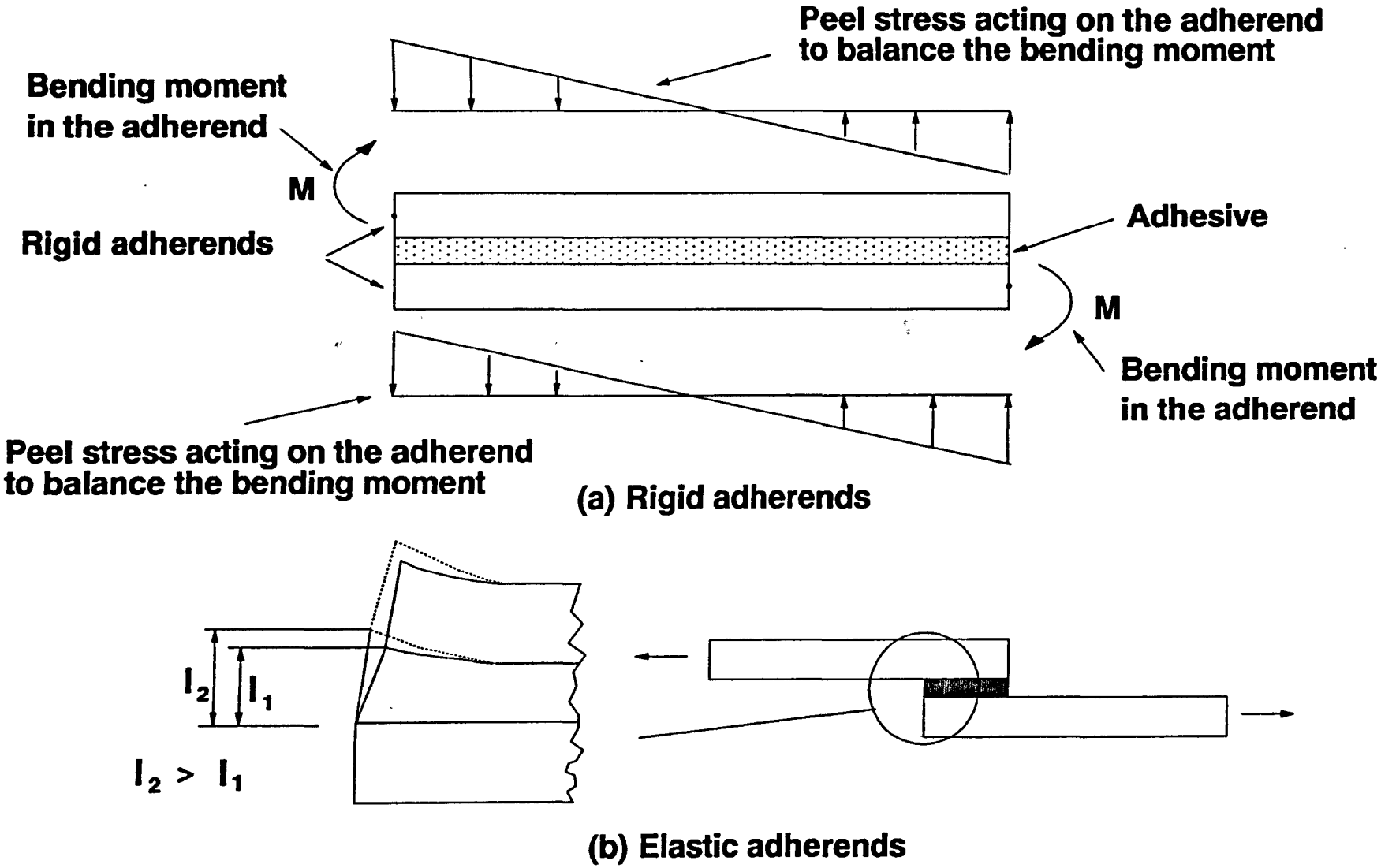

Fig. 2.13 Effect of adherend bending stiffness on the peel stress

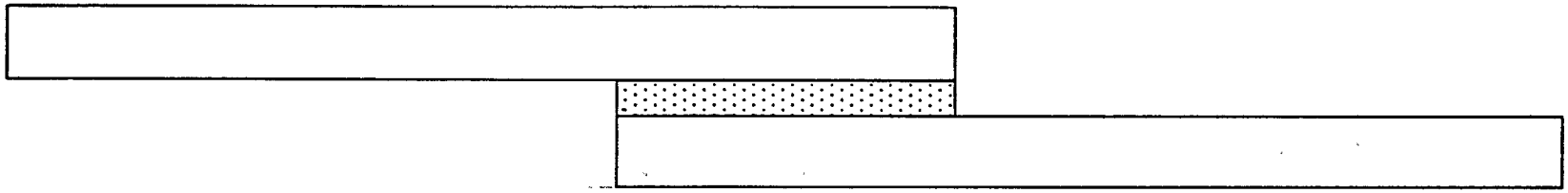

Fig. 2.14a "Square Ended" Joint

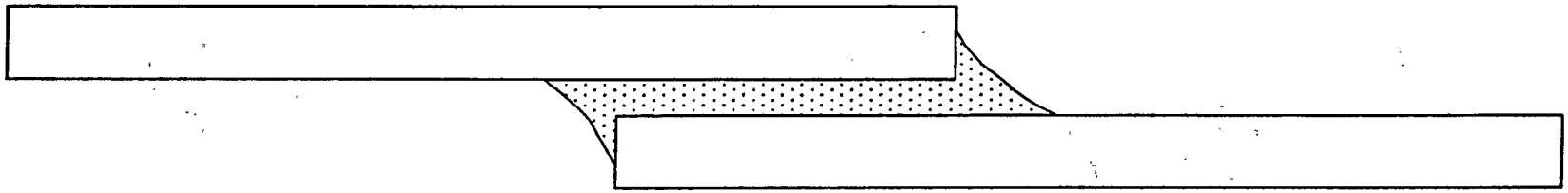

Fig. 2.14b Joint with Spew Fillets

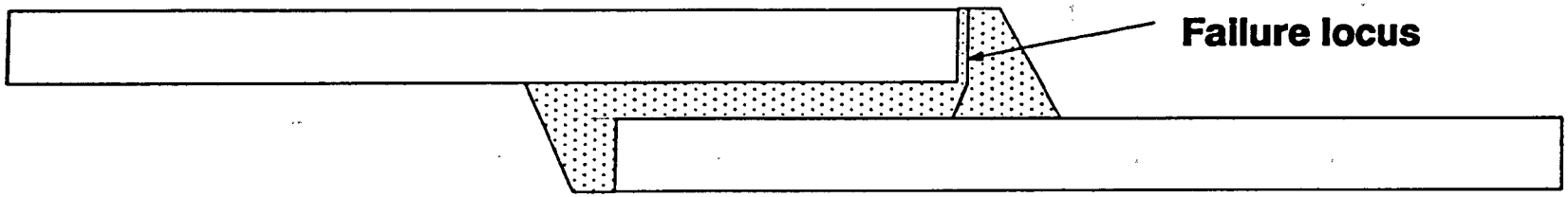

Fig. 2.14c Joint with Large Spew Fillets

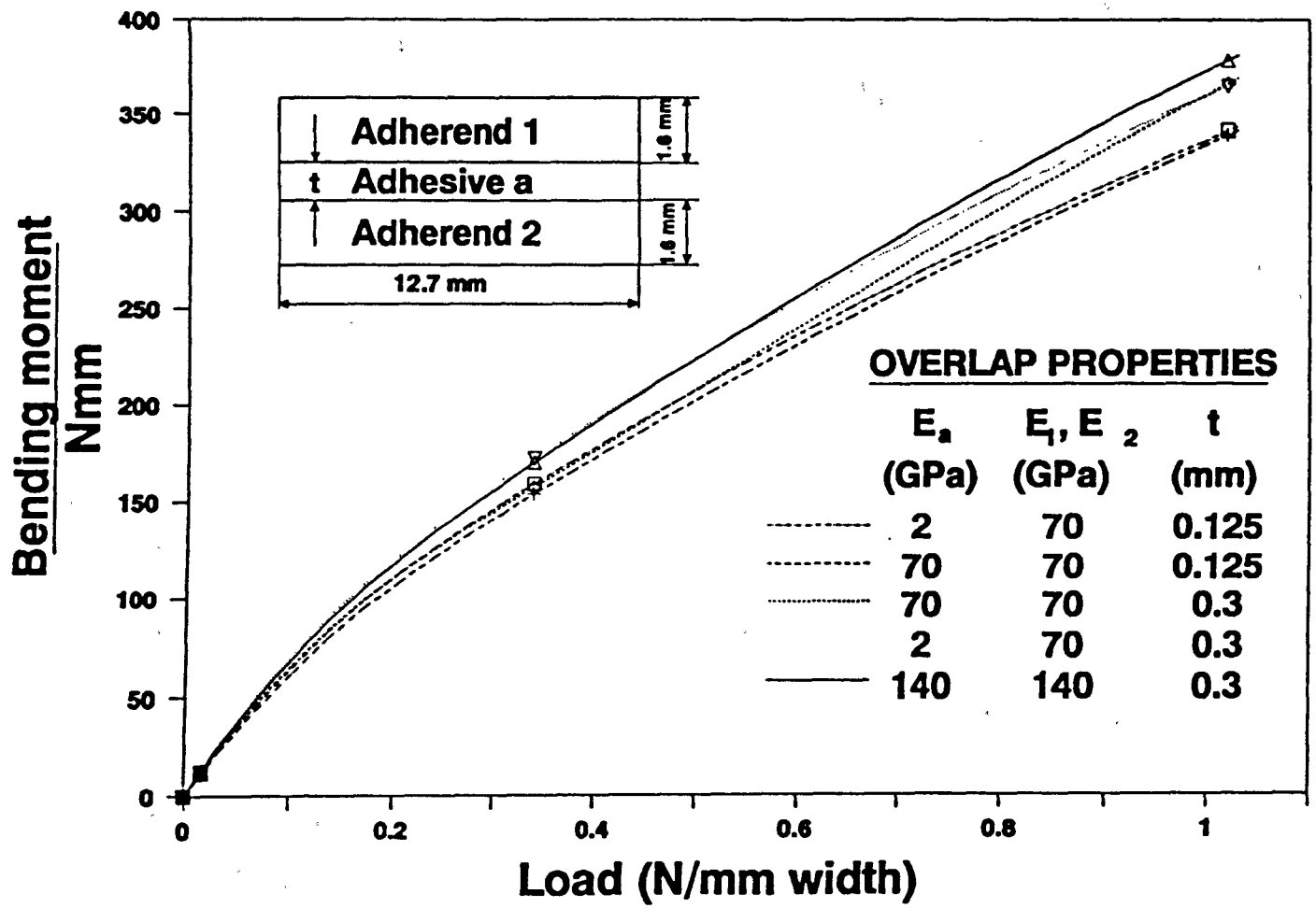

Fig. 3.1 Bending Moments for Different Properties of Overlap with FEM

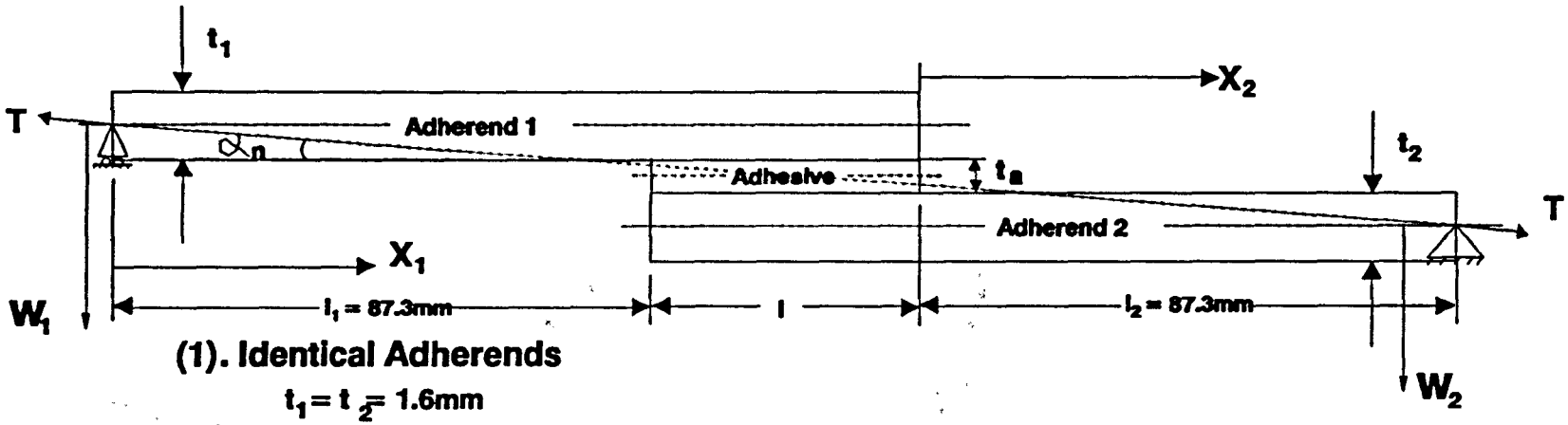

(1). Identical Adherends

$t_1 = t_2 = 1.6mm$

$t_a = 0.125mm$

$E_1 = E_2 = 70GPa$ (aluminium)

$E_a = 2.8GPa$

(2). Adherends with Different Stiffness

$t_1 = t_2 = 1.6mm$

$t_a = 0.125mm$

$E_1 = 207GPa, E_2 = 70GPa$ (e.g. steel/aluminium)

$E_a = 2.8GPa$

(3). Adherends with same Material Properties but Different Thickness

$t_1 = 5t_2 = 8mm$

$t_a = 0.125mm$

$E_1 = E_2 = 70GPa$

$E_a = 2.8GPa$

Fig. 3.2 Geometry and Material Properties of Joints (not to scale)

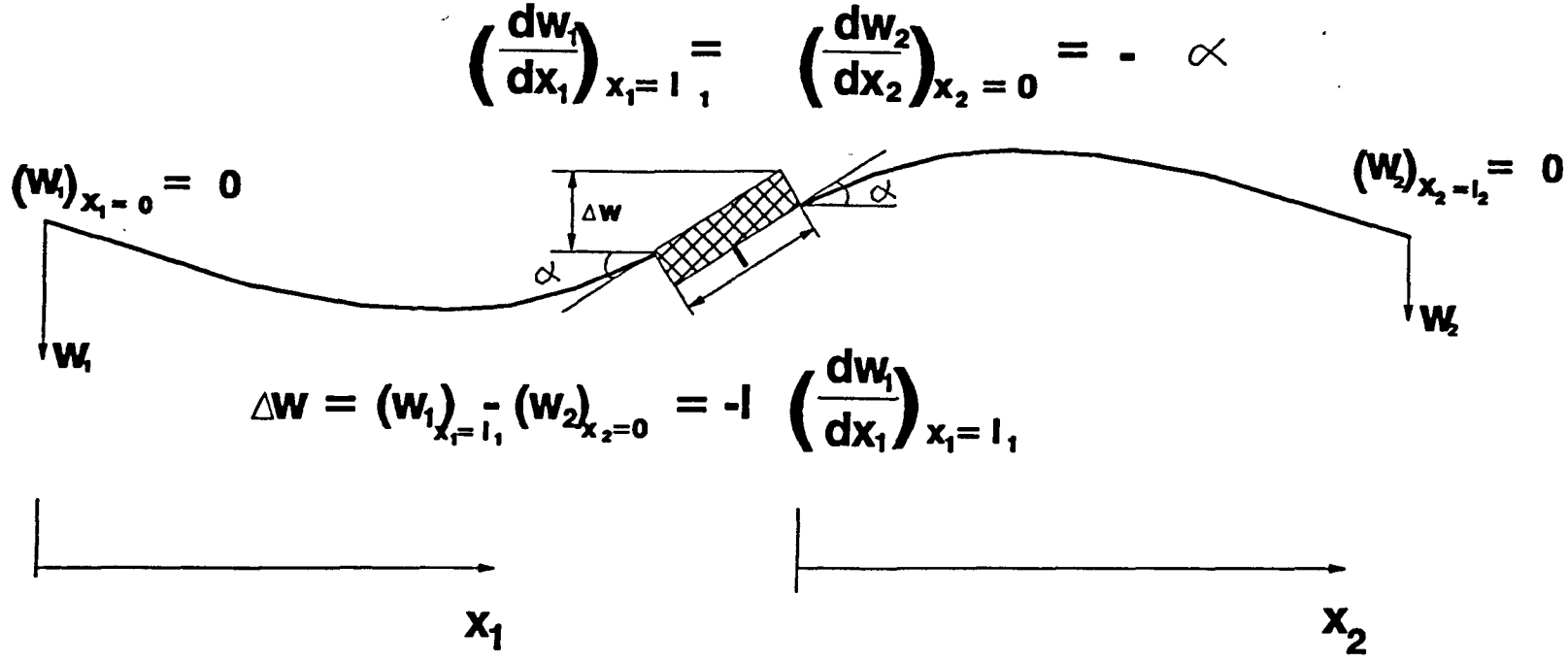

Fig. 3.3 Sketches of Boundary Conditions for the Analysis

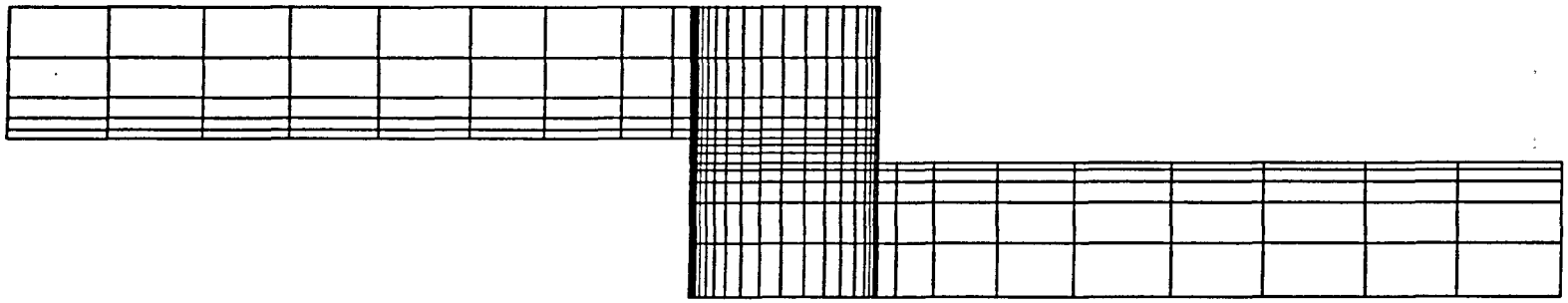

Fig. 3.4 A Typical Mesh for the Finite Element Analysis (not to scale)

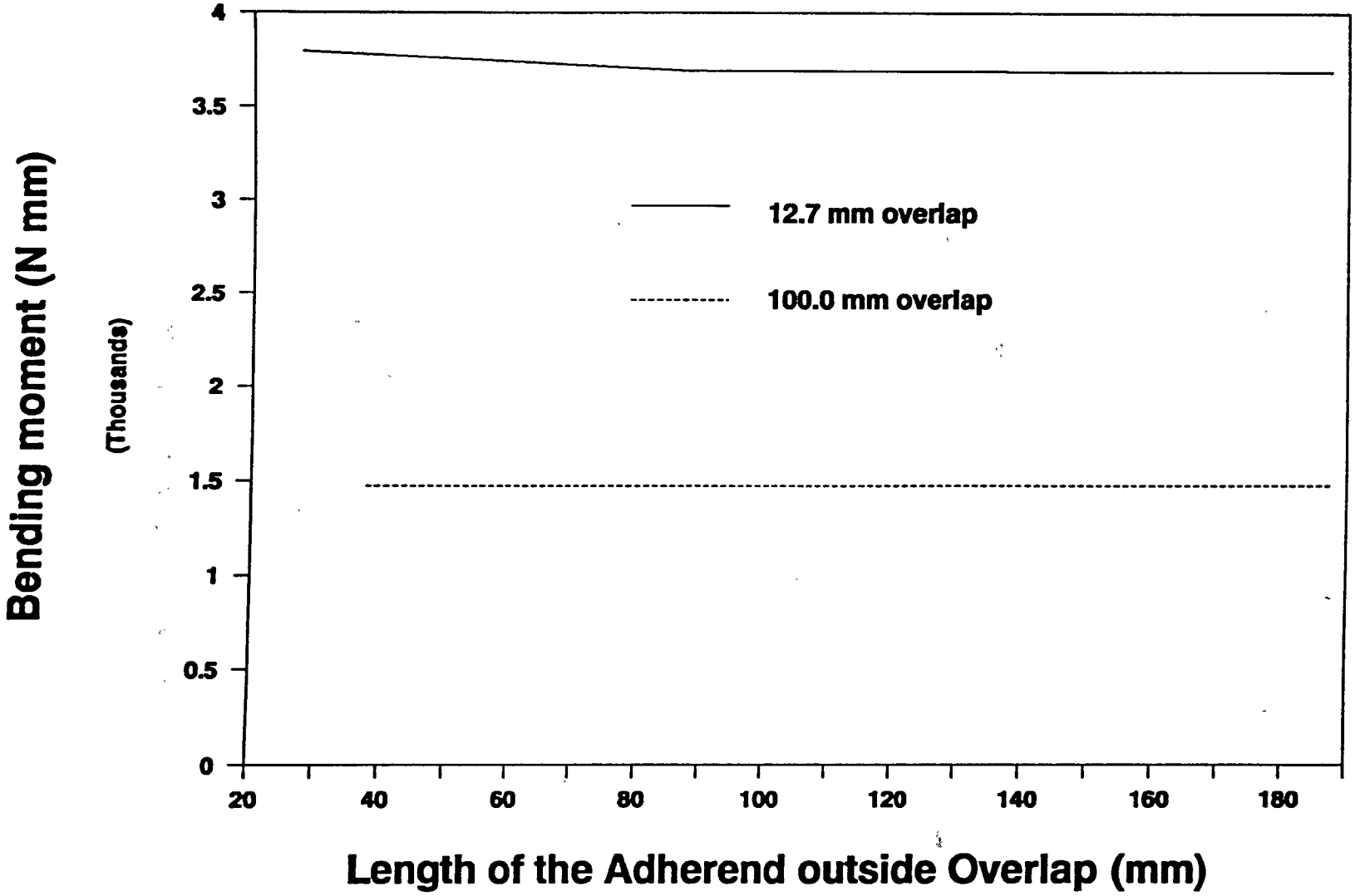

Fig. 3.5 Bending Moments with Different Lengths of Adherends

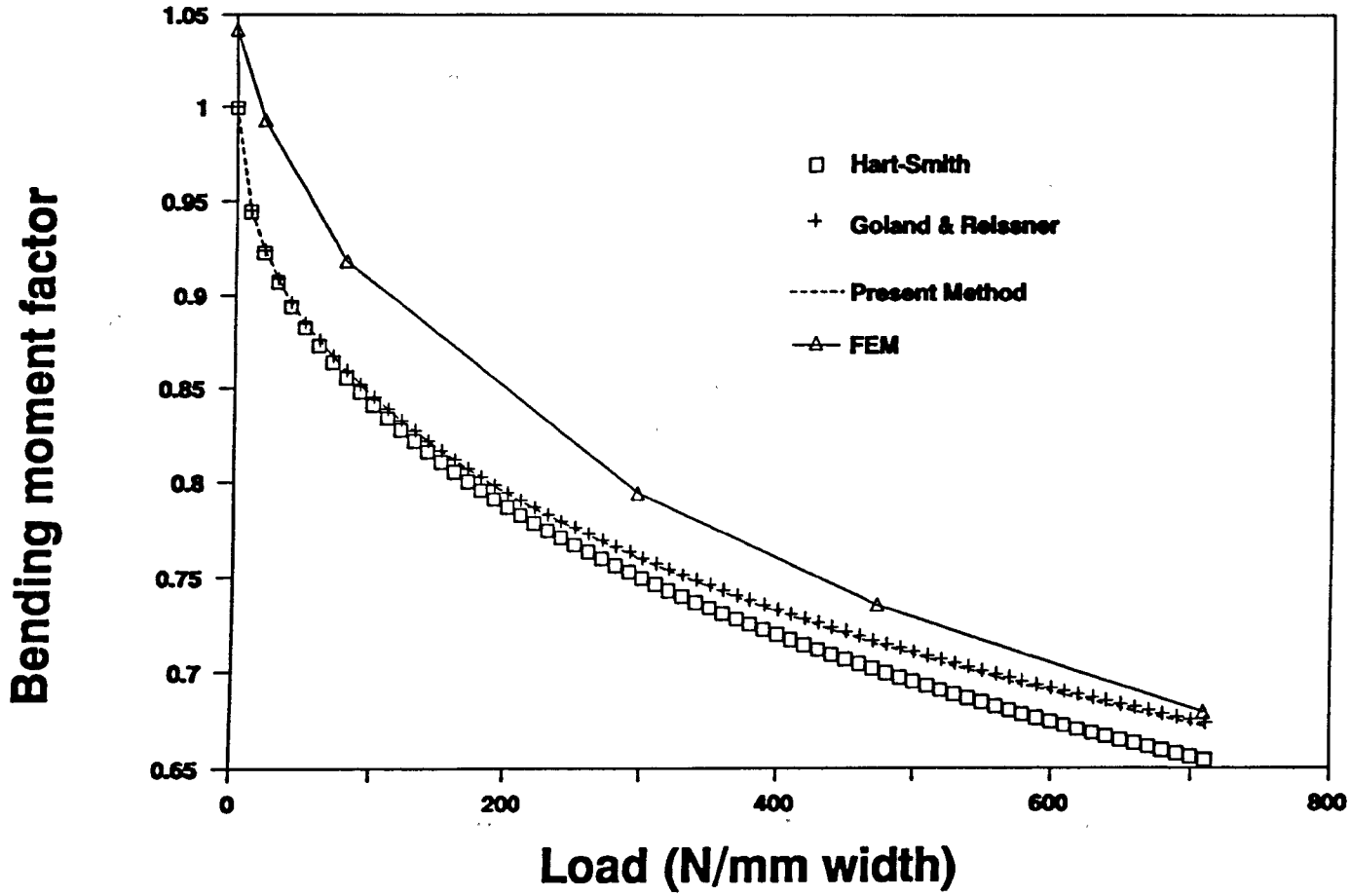

Fig. 3.6 Bending Moment Factors with 6 mm Overlap

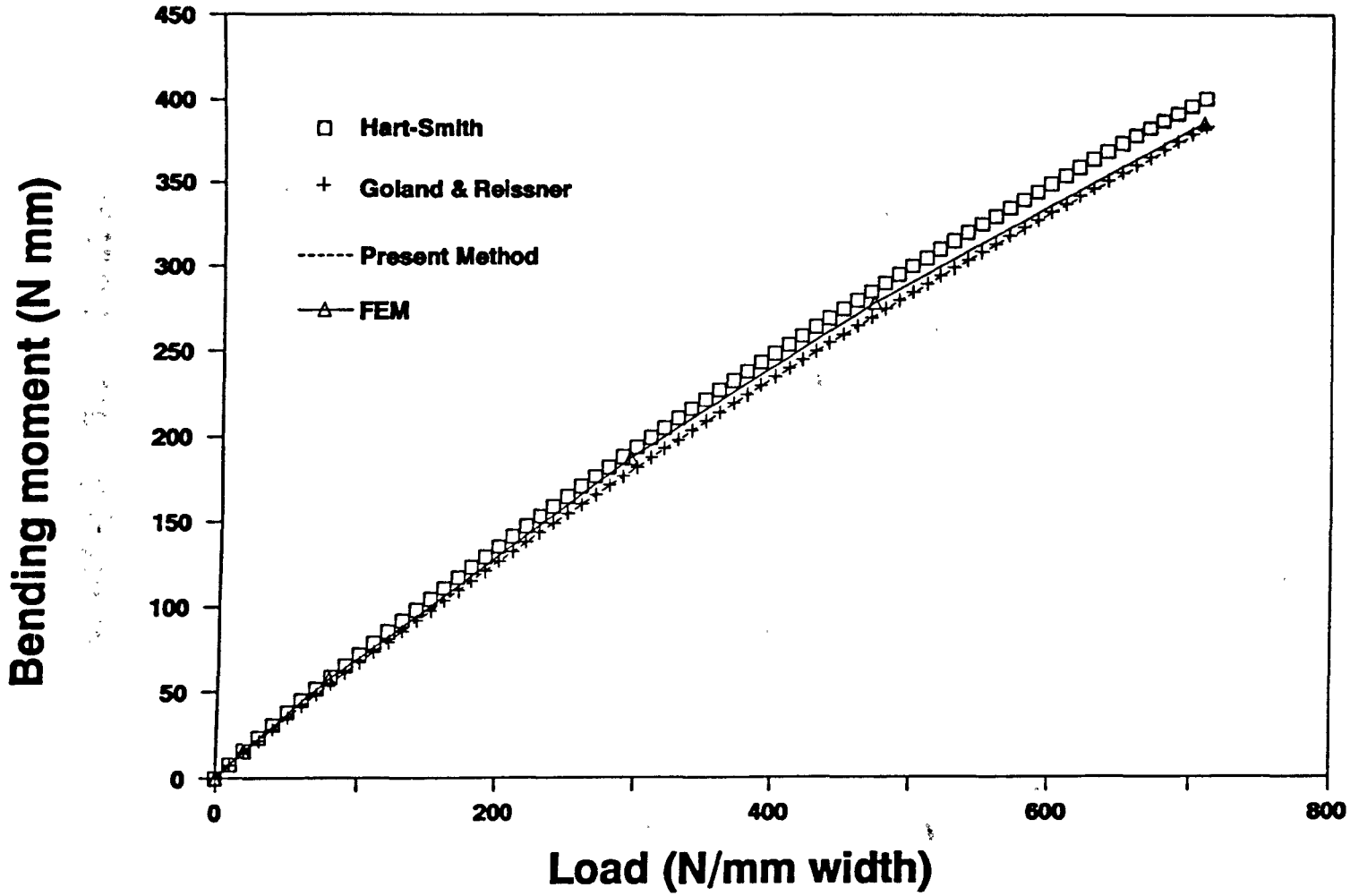

Fig. 3.7 Bending Moments with 6 mm Overlap

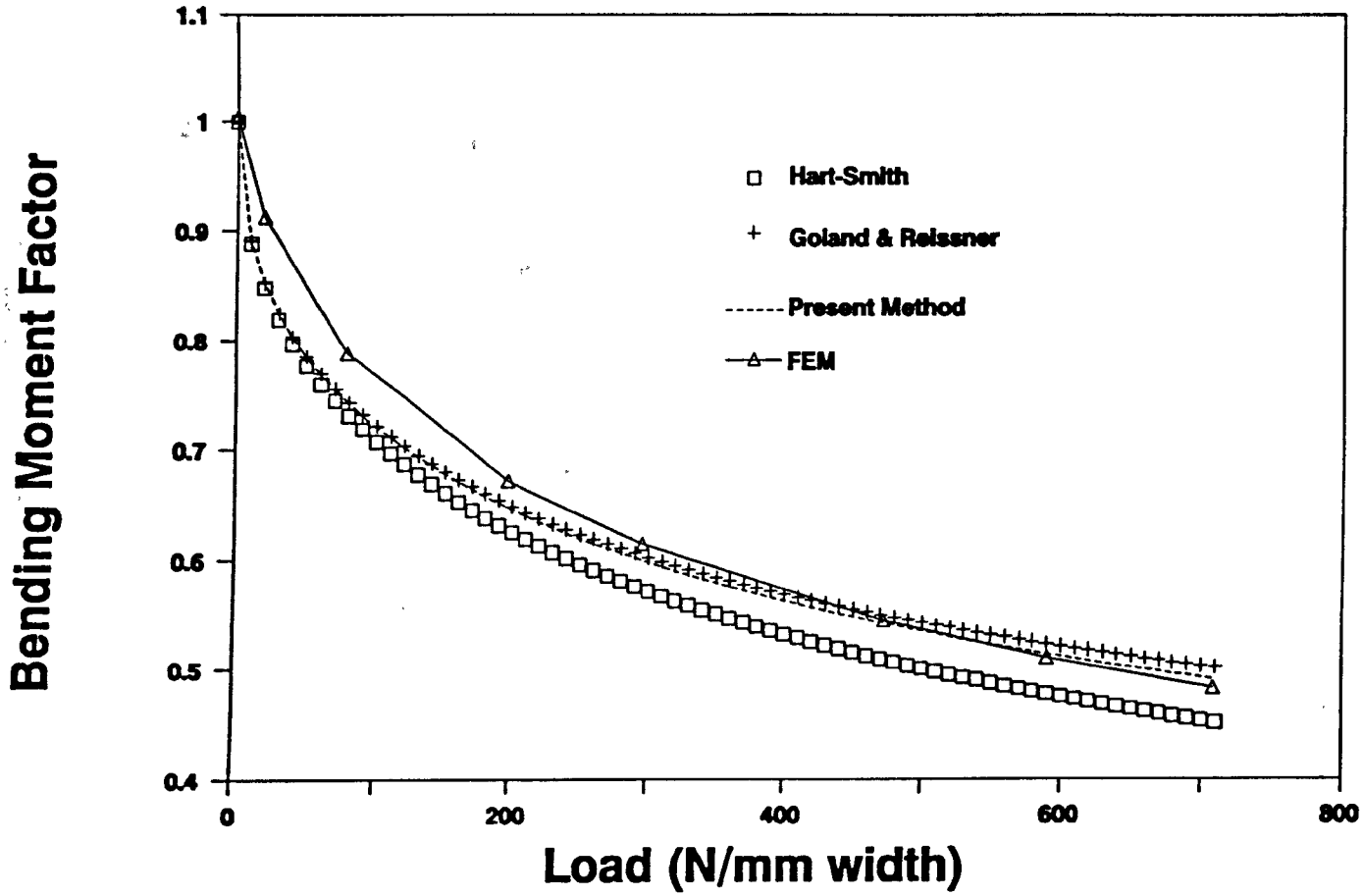

Fig. 3.8 Bending Moment Factors with 12.7 mm Overlap

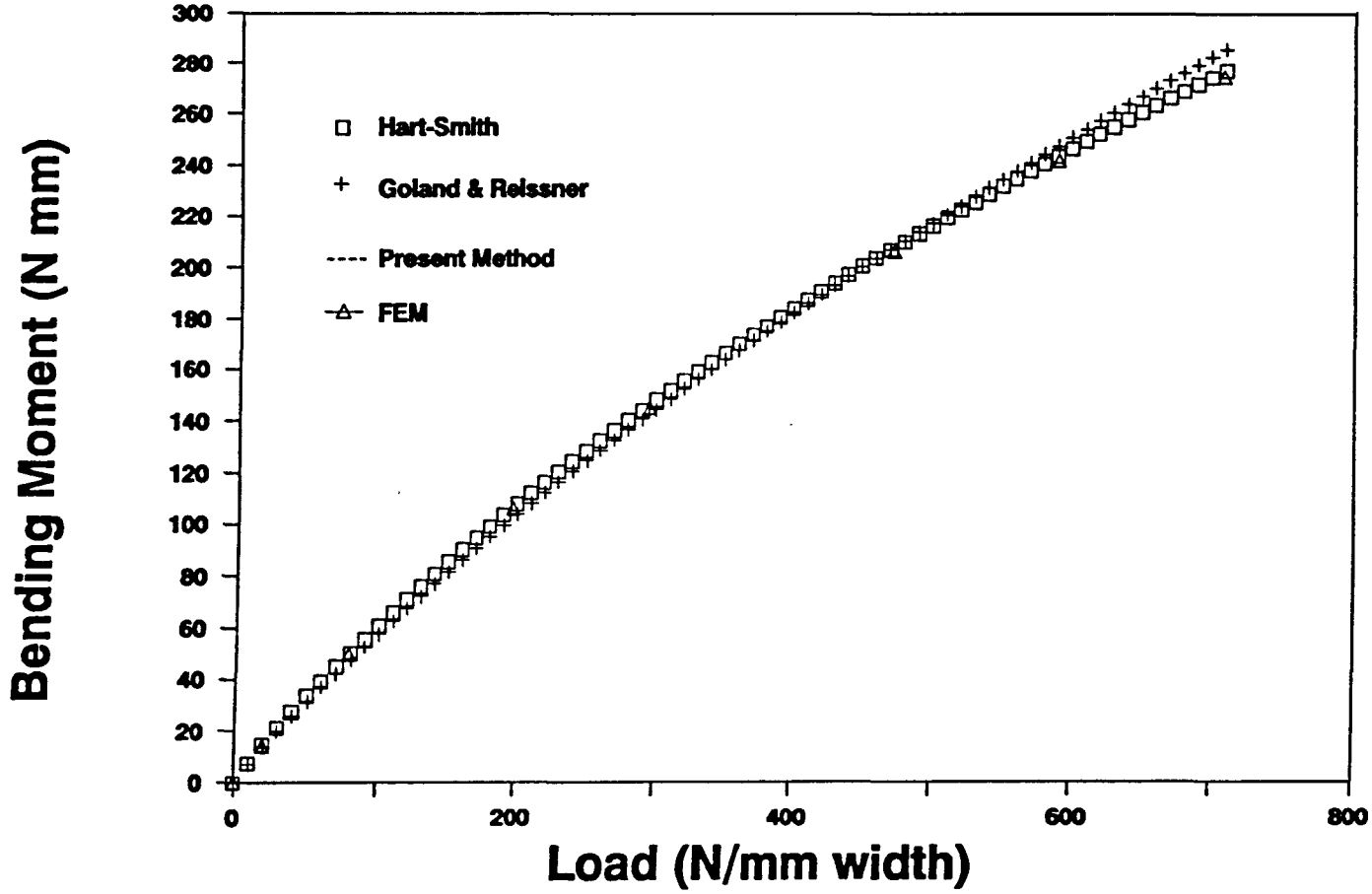

Fig. 3.9 Bending Moment with 12.7 mm Overlap

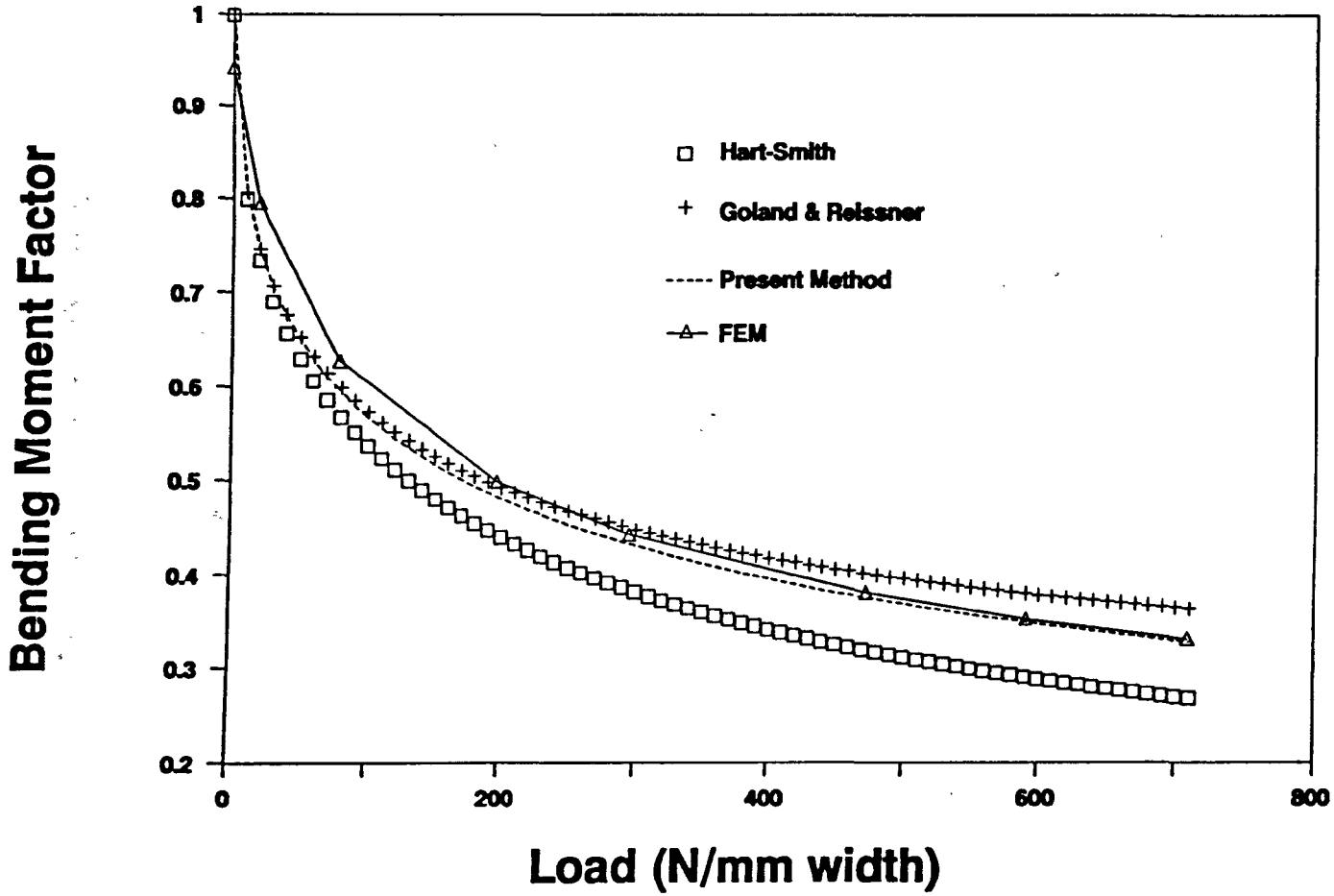

Fig. 3.10 Bending Moment Factors with 25 mm Overlap

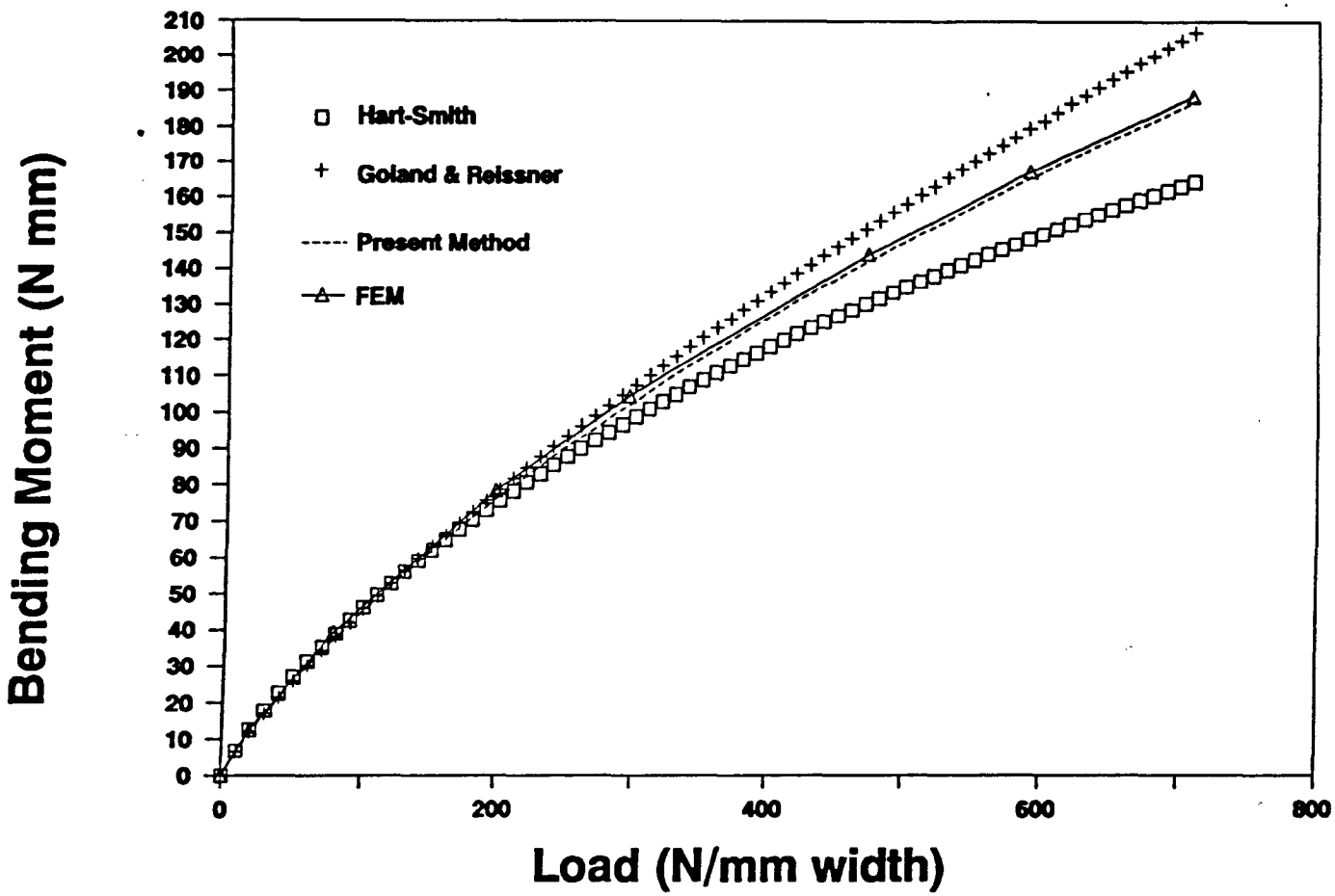

Fig. 3.11 Bending Moment with 25 mm Overlap

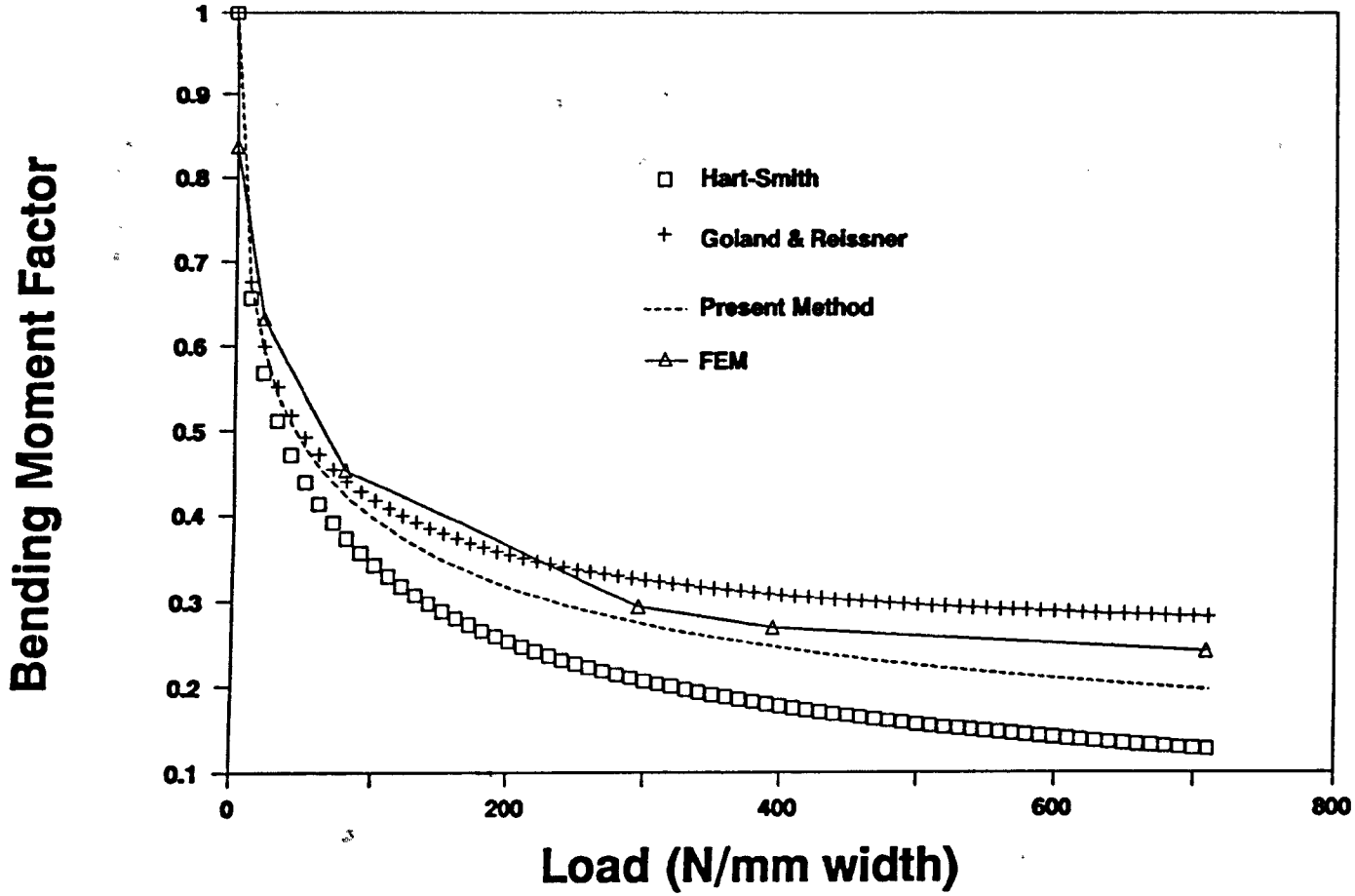

Fig. 3.12 Bending Moment Factors with 50 mm Overlap

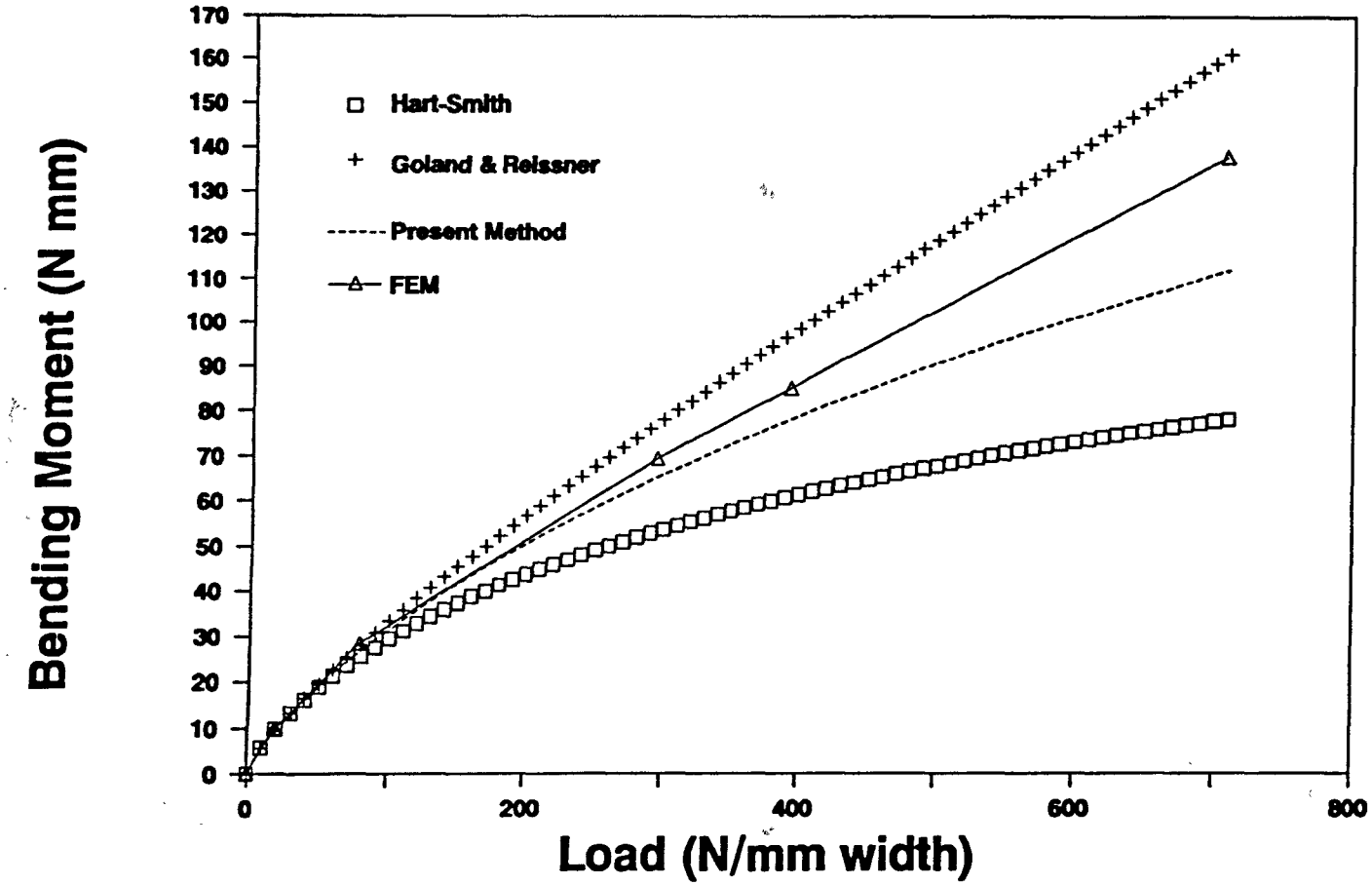

Fig. 3.13 Bending Moment with 50 mm Overlap

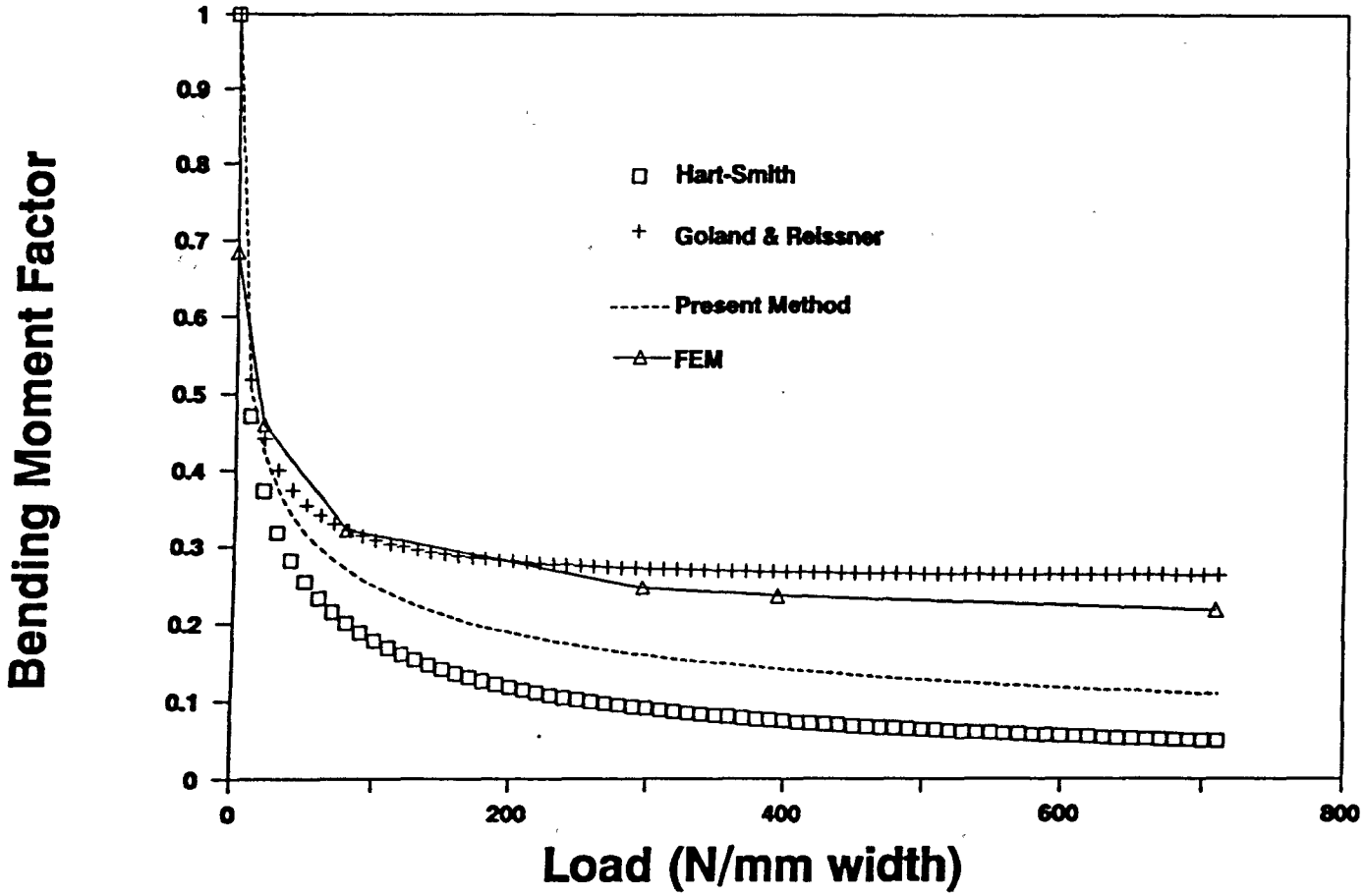

Fig. 3.14 Bending Moment Factors with 100 mm Overlap

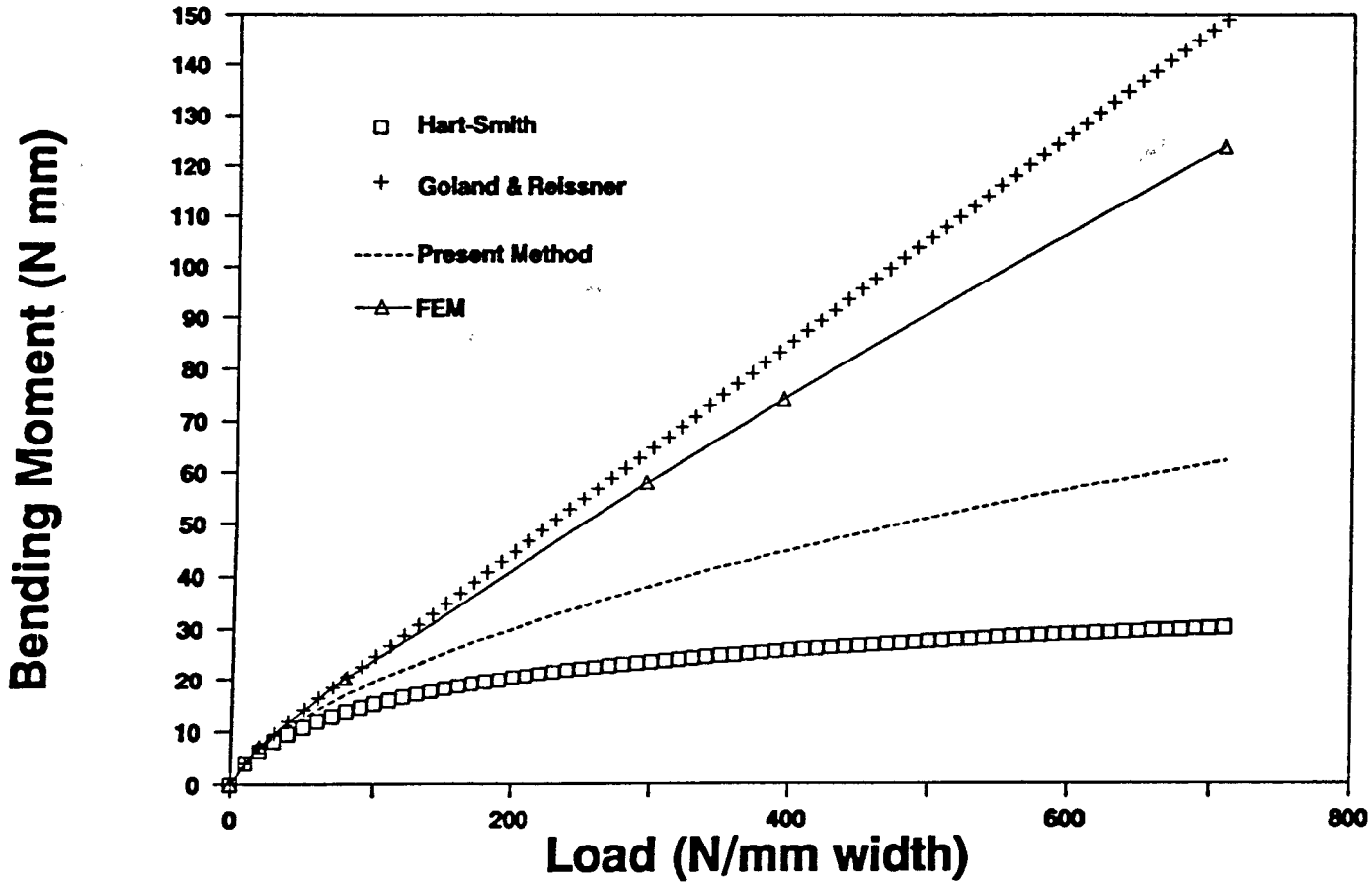

Fig. 3.15 Bending Moment with 100 mm Overlap

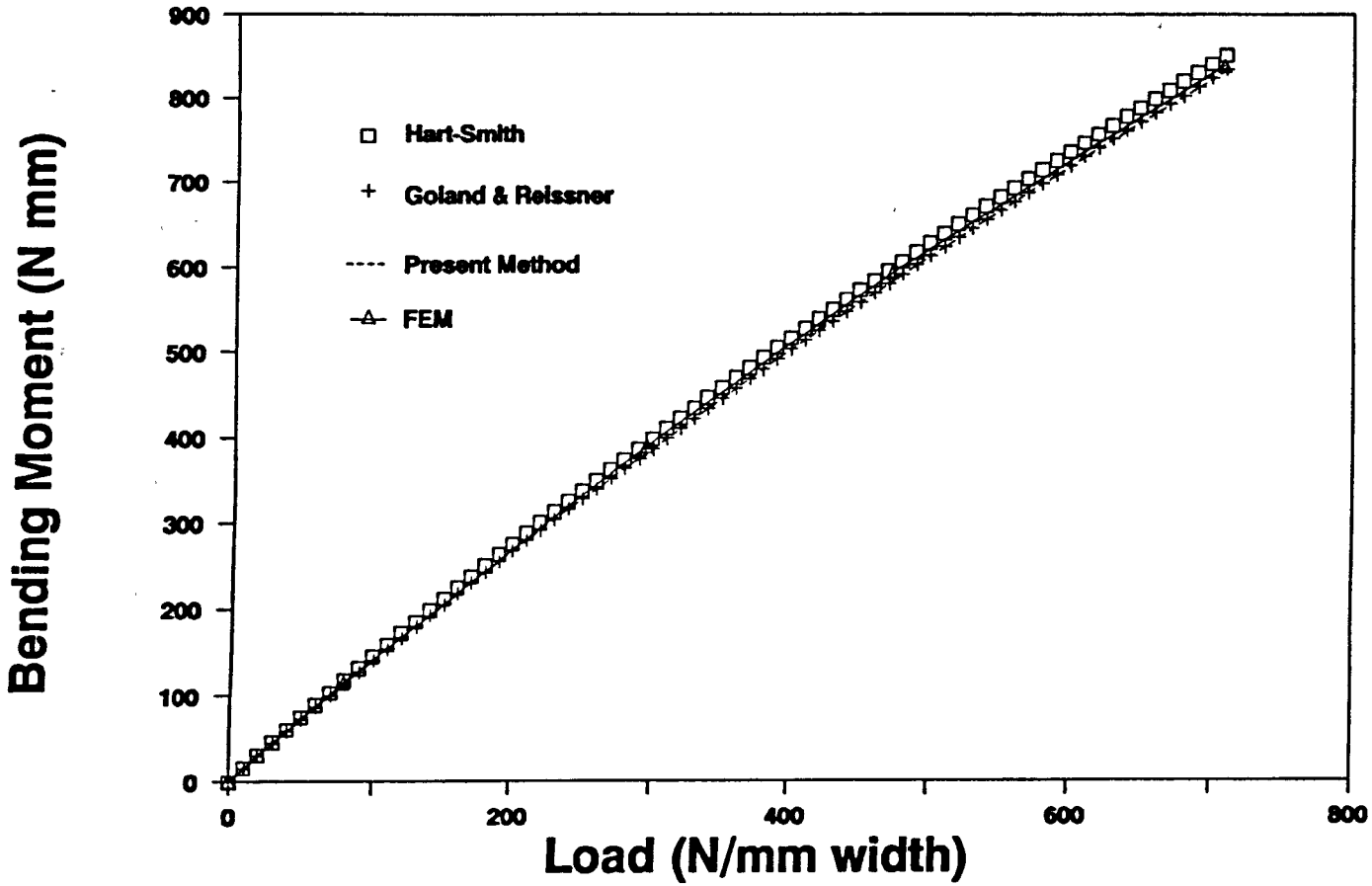

Fig. 3.16 Bending Moments for 12.7 mm Overlap and 3.2 mm Adherends

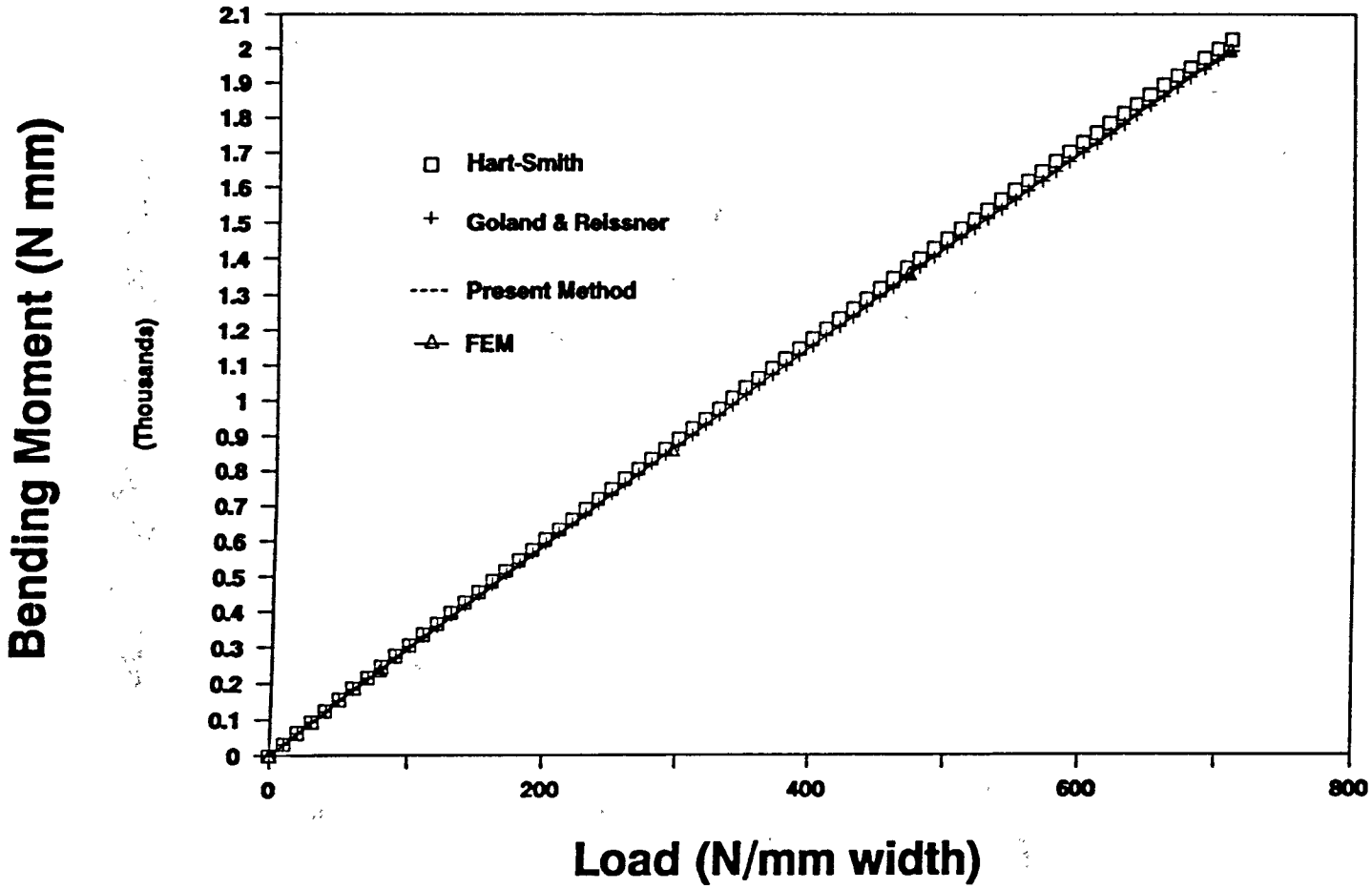

Fig. 3.17 Bending Moments for 12.7mm Overlap and 6.35mm Adherends

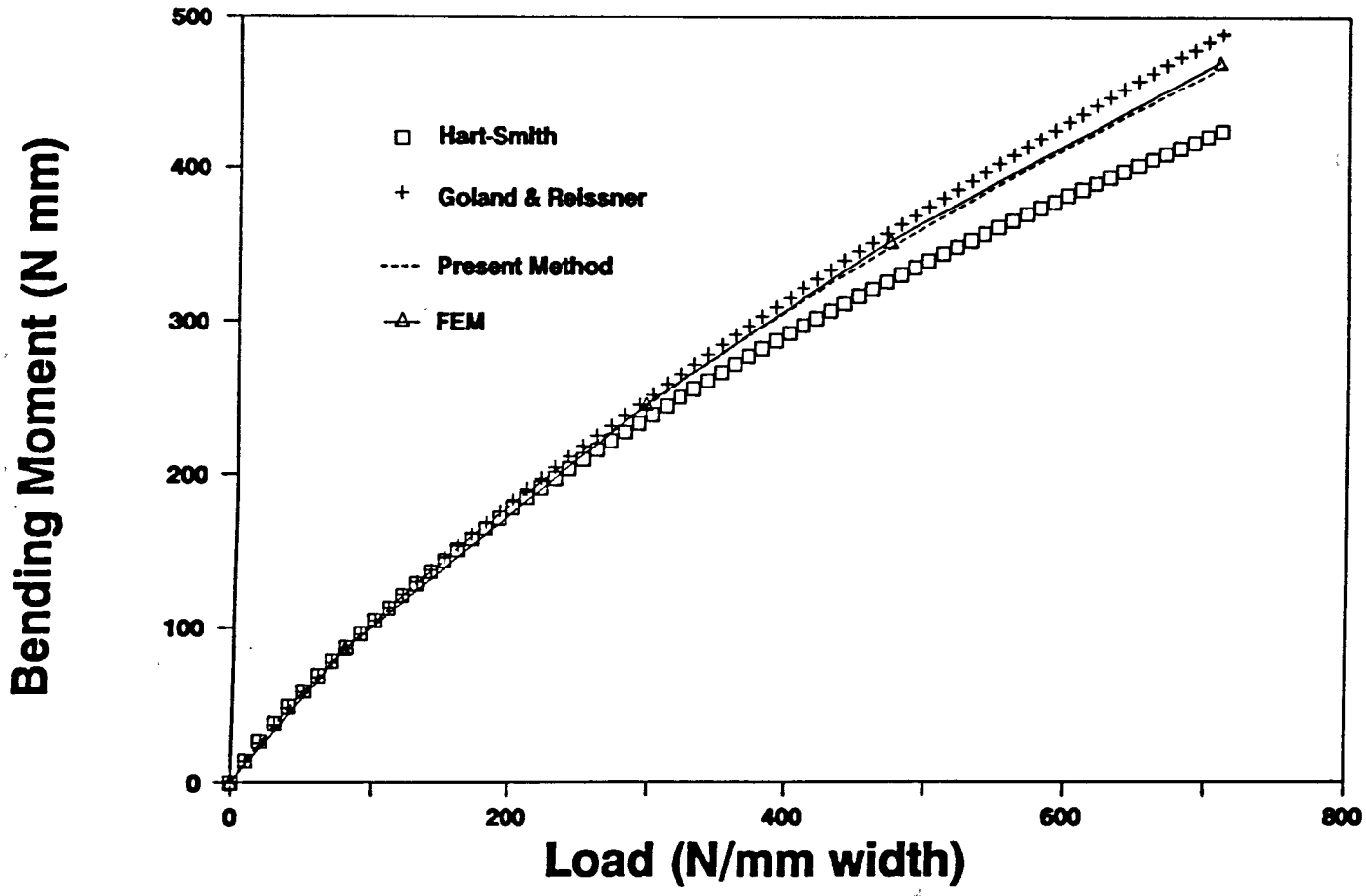

Fig. 3.18 Bending Moments for 50 mm Overlap and 3.2 mm Adherends

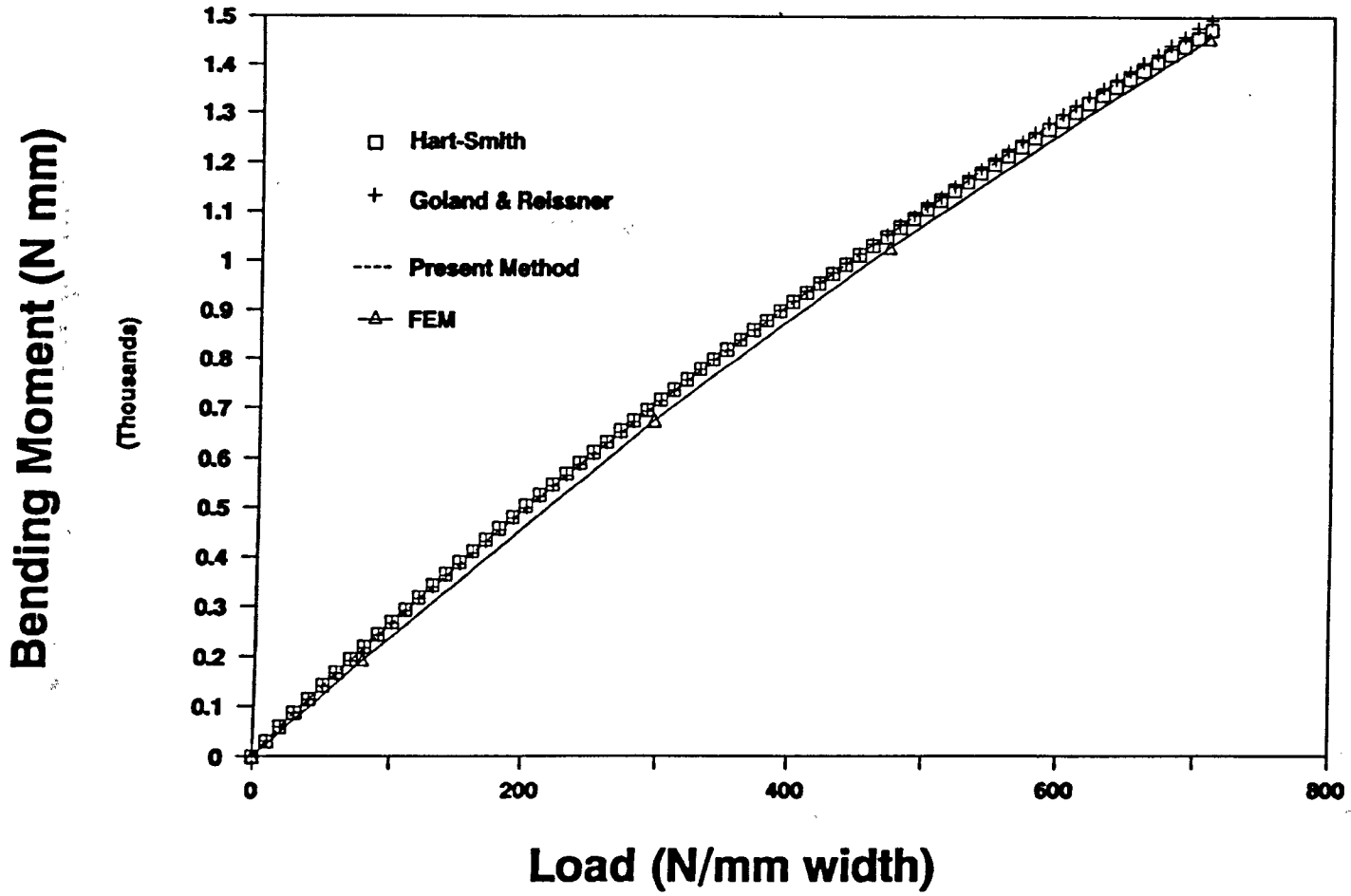

Fig. 3.19 Bending Moments for 50 mm Overlap and 6.35 mm Adherends

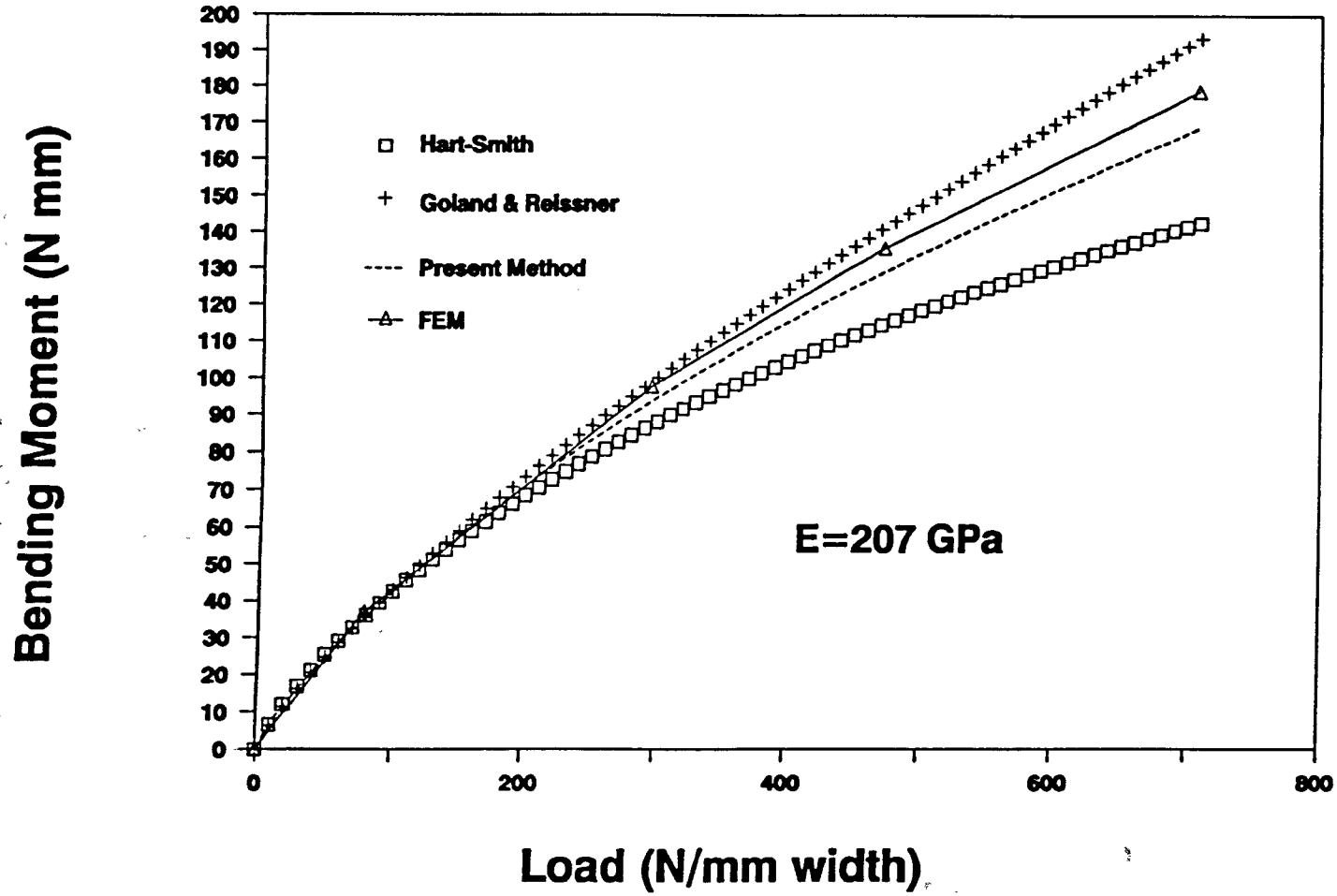

Fig. 3.20 Bending Moments for 50mm Overlap & 6.35mm Adherends

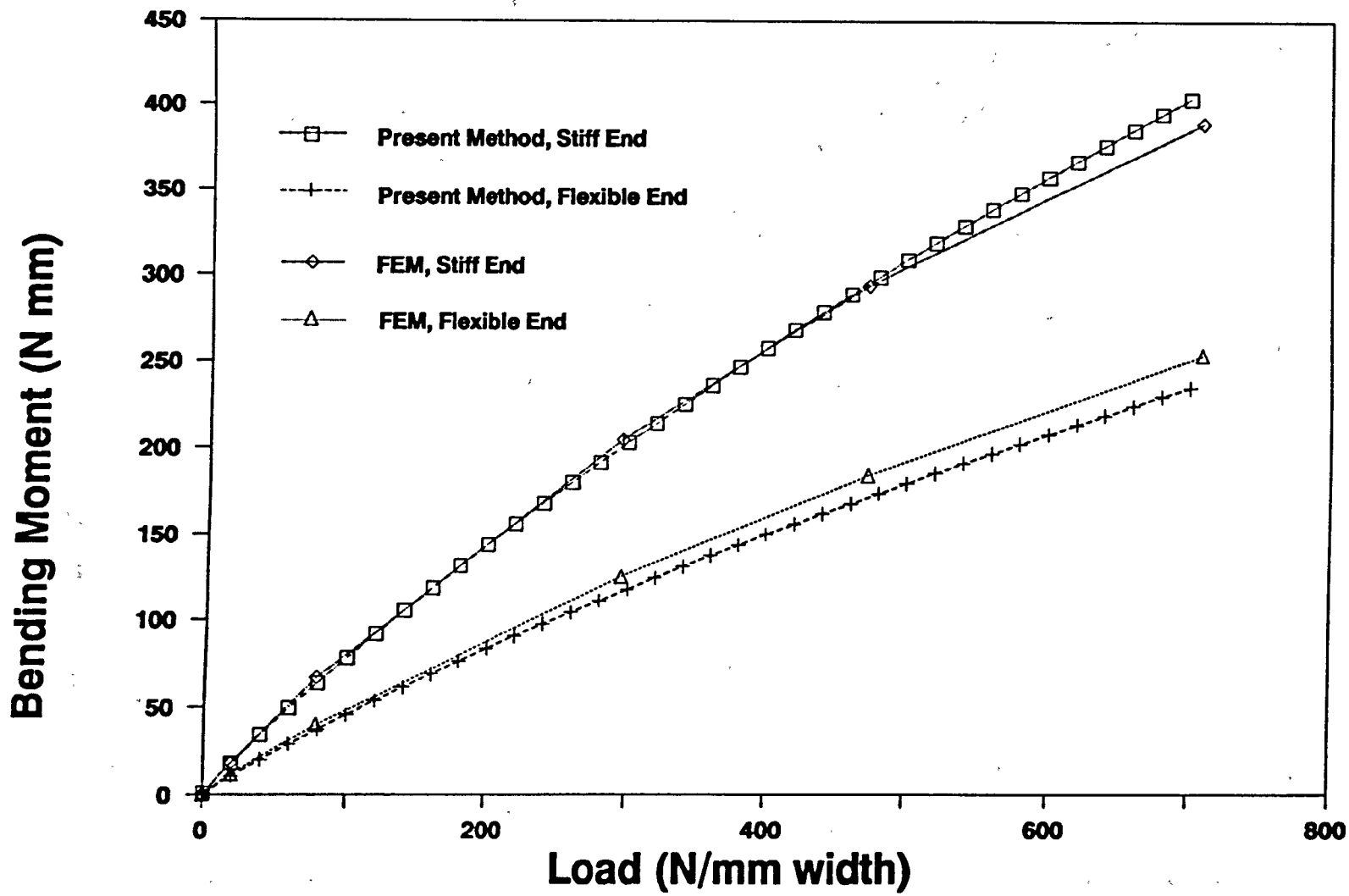

Fig.3.21 Bending Moments for 12.7mm Overlap for Stiff-flexible Adherends

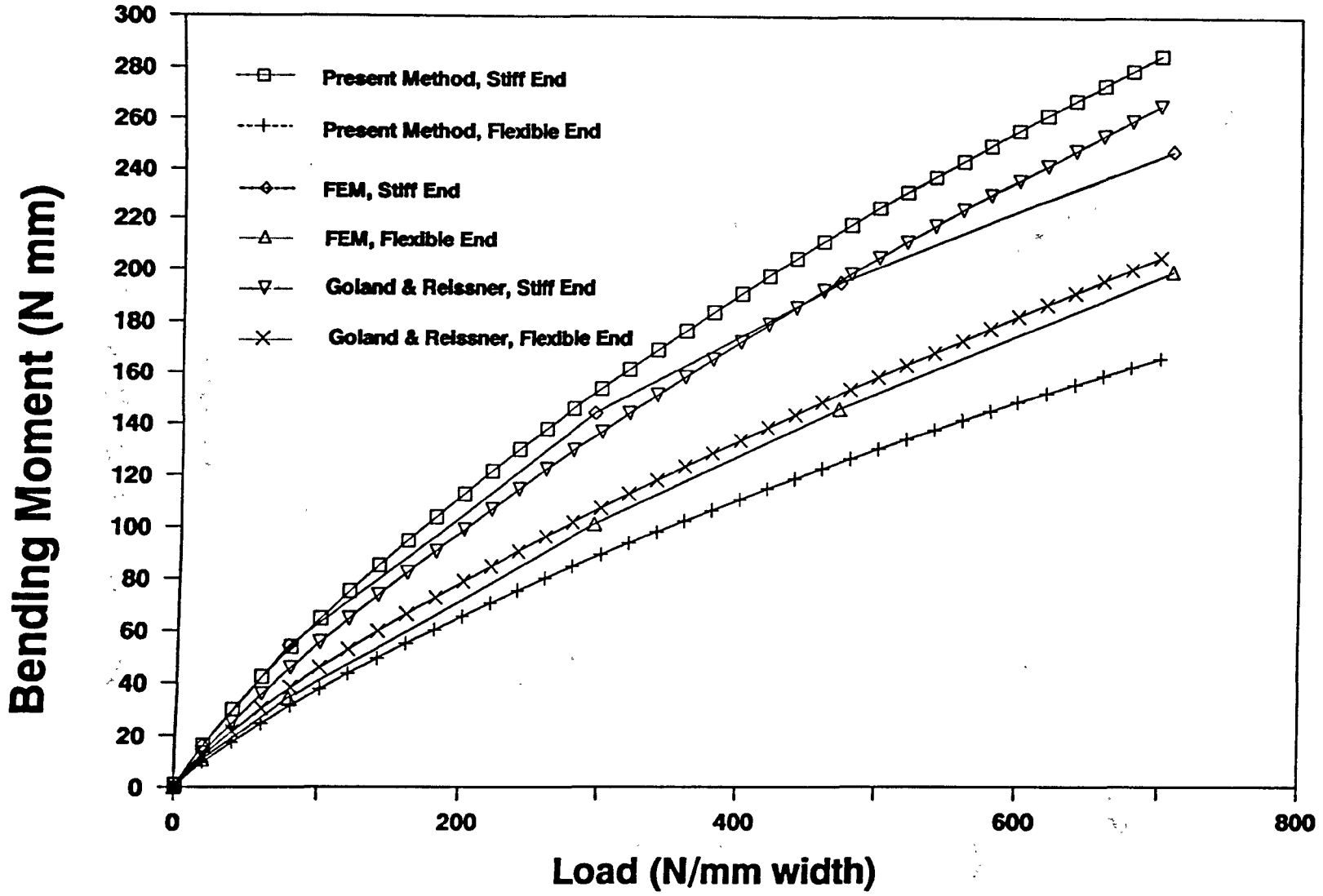

Fig. 3.22 Bending Moments for 25 mm Overlap for Stiff-flexible Adherends

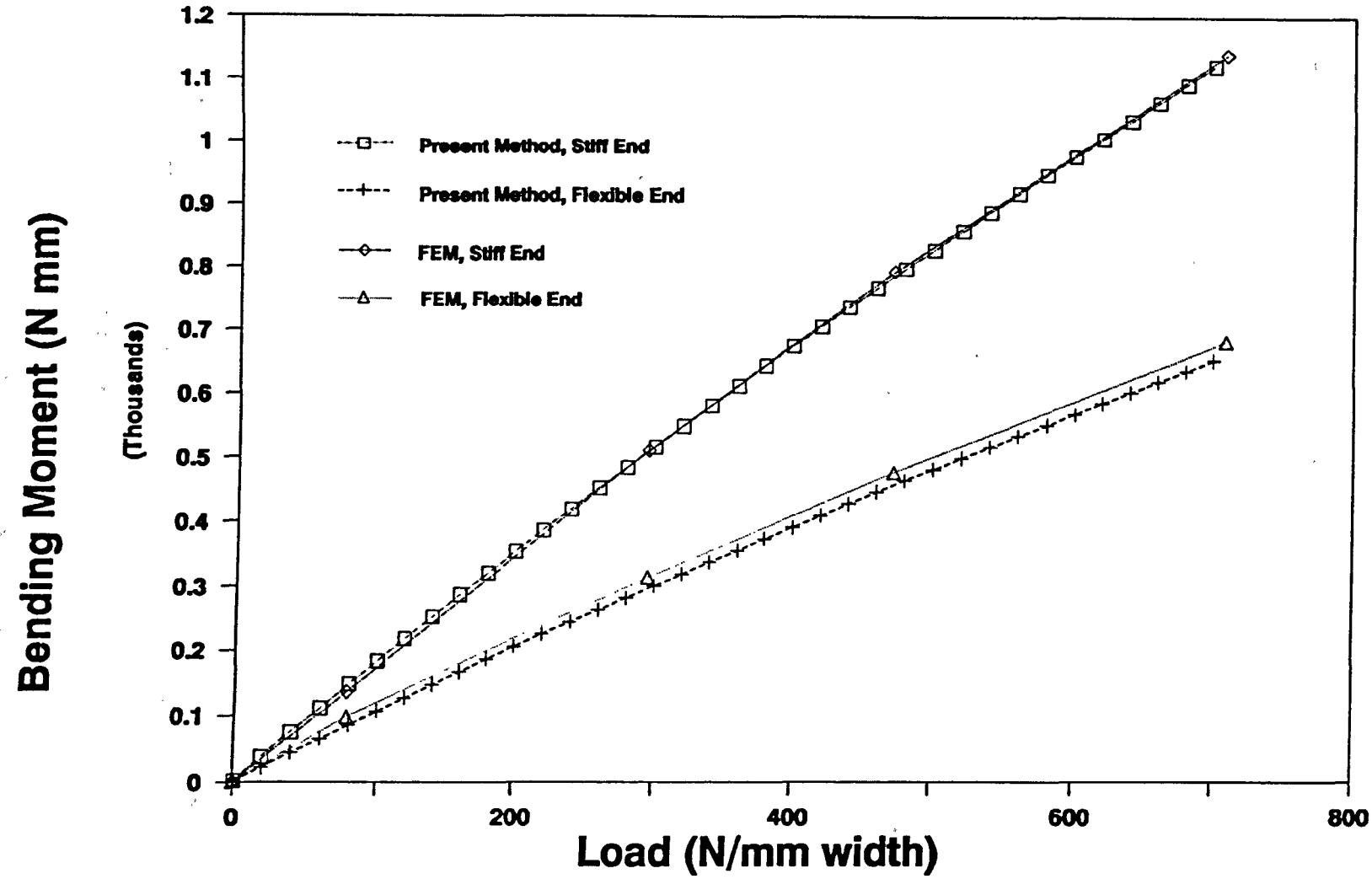

Fig. 3.23 Bending Moments for 12.7 mm Overlap with Stiff-flexible 3.2 mm Adherends

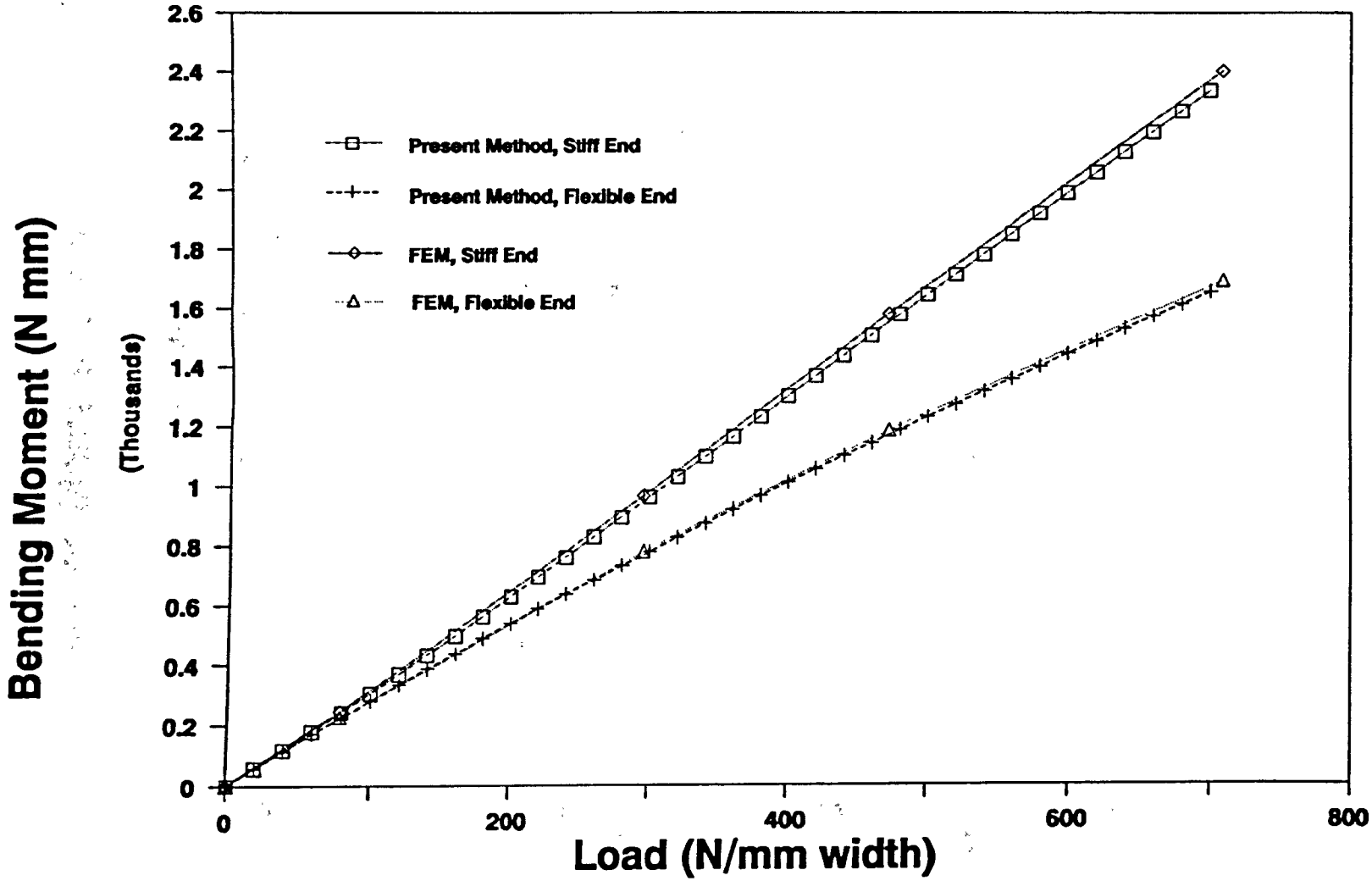

Fig. 3.24 Bending Moments for 12.7mm Overlap with Stiff-flexible 6.35 mm Adherends

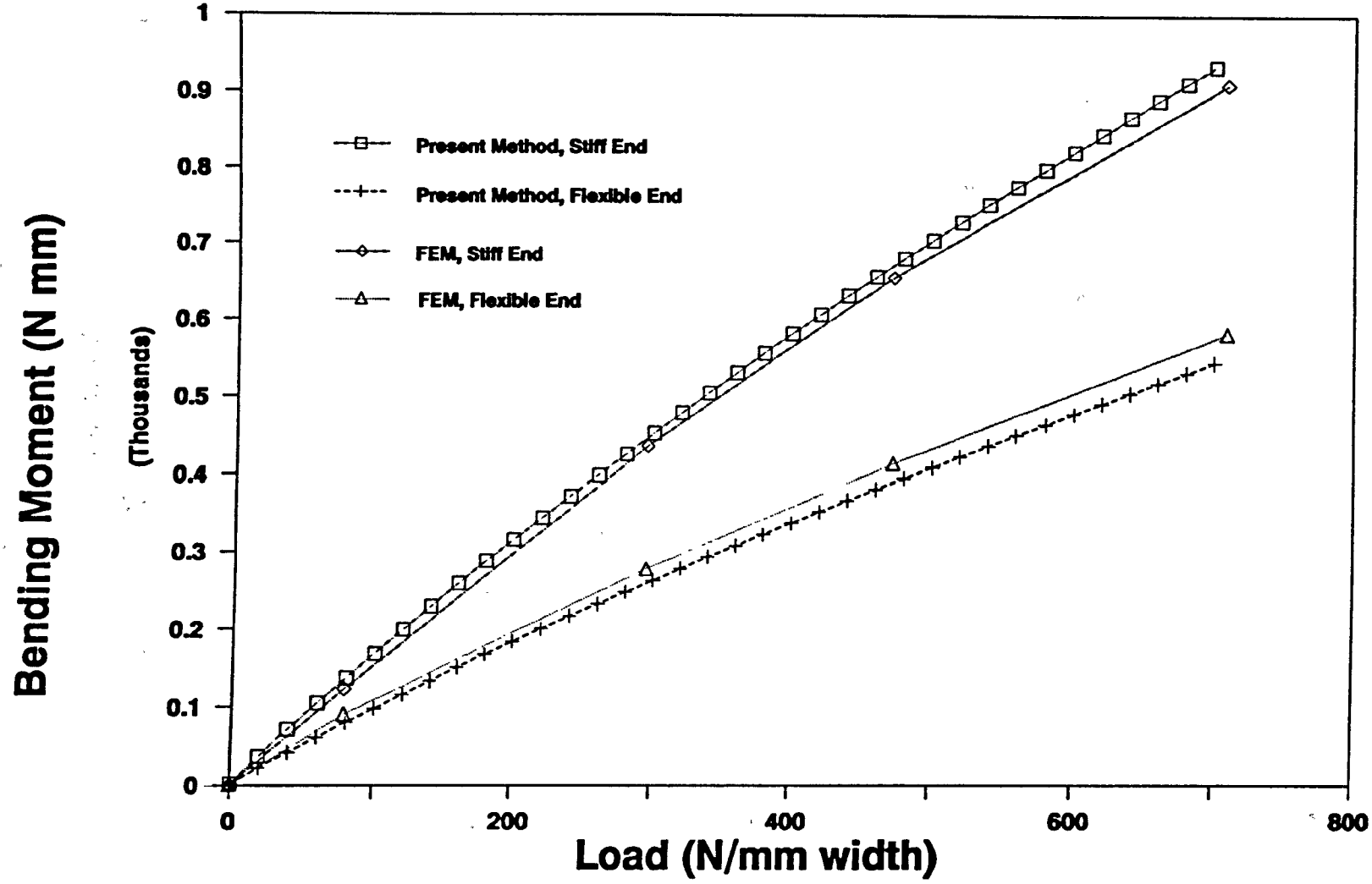

Fig. 3.25 Bending Moments for 25 mm Overlap with Stiff-flexible 3.2 mm Adherends

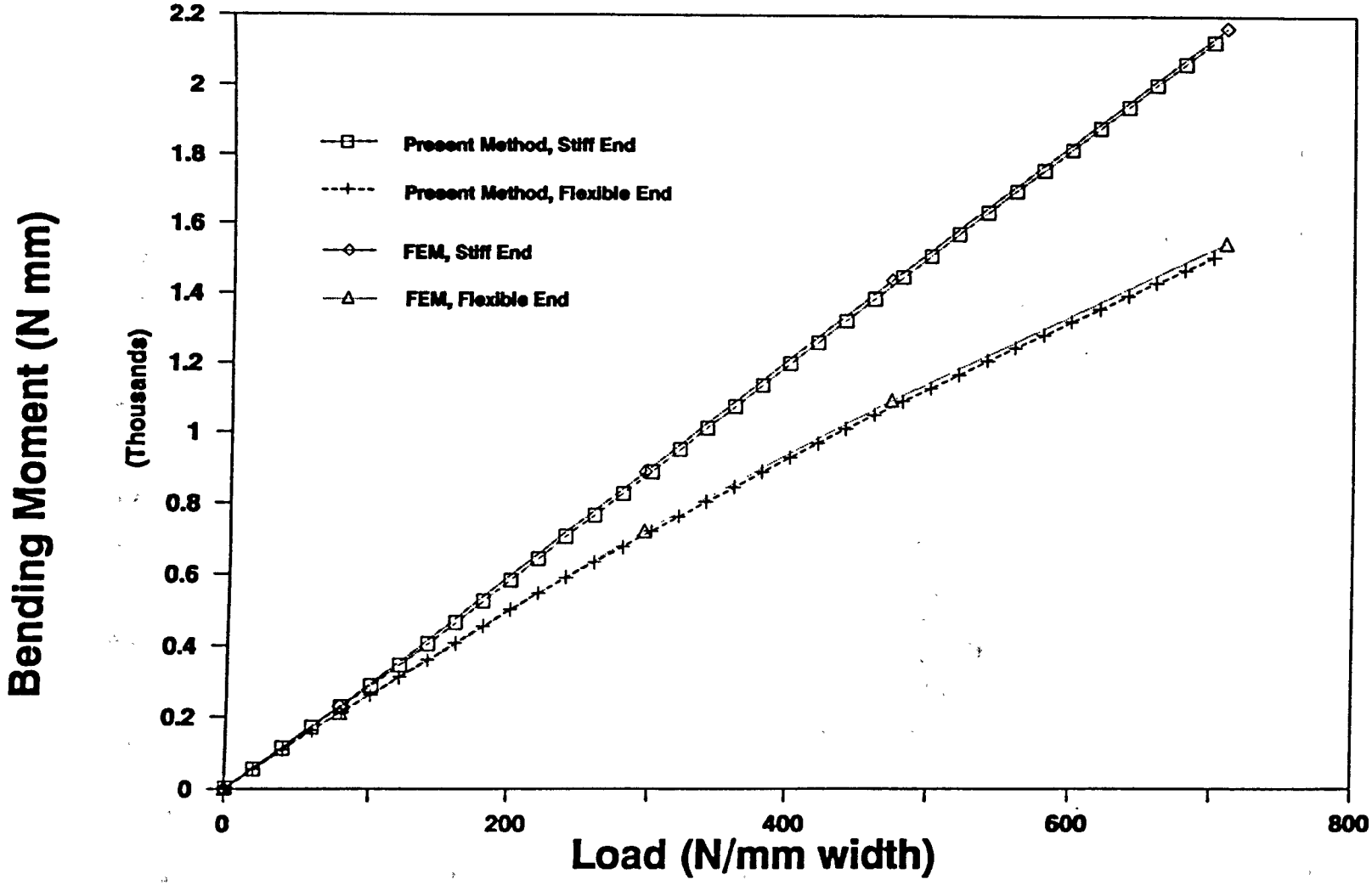

Fig. 3.26 Bending Moments for 25 mm Overlap with Stiff-flexible 6.35 mm Adherends

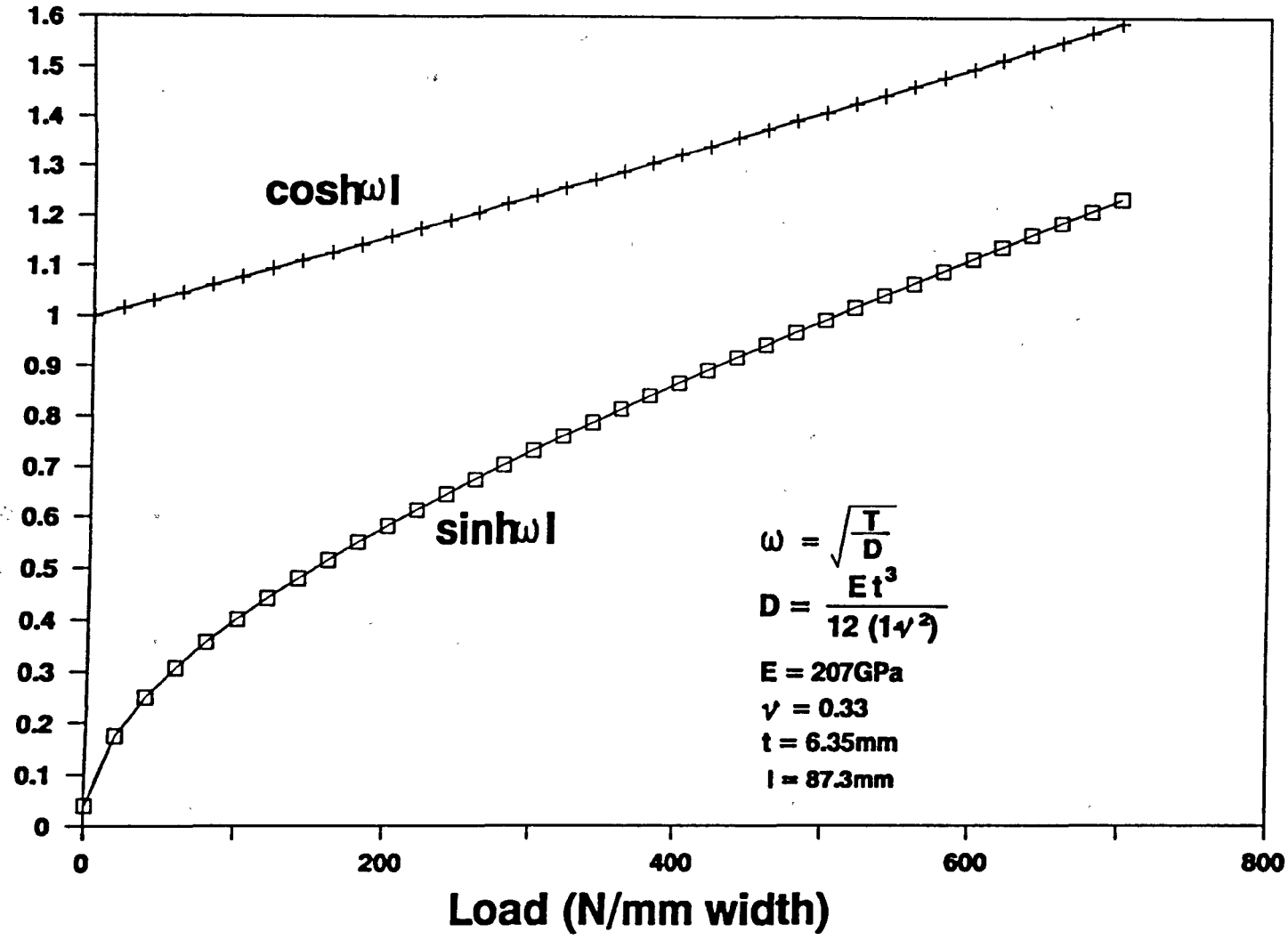

Fig. 3.27 Comparison Between Functions sinhωl and coshωl

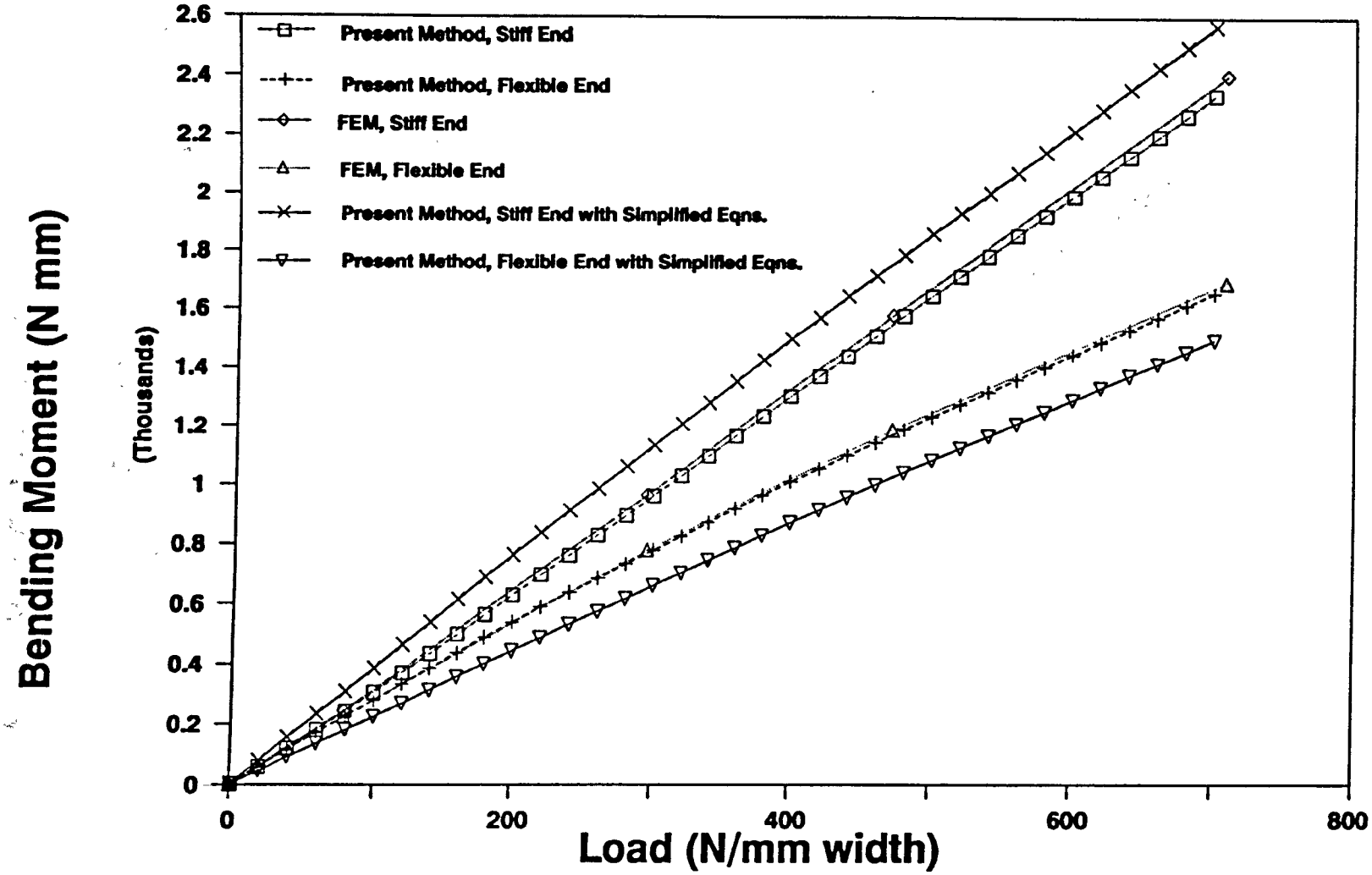

Fig. 3.28 Bending Moment with 12.7 mm Overlap for Stiff-Flexible 6.35 mm Adherends Using and Without Using Simplified Eqs.

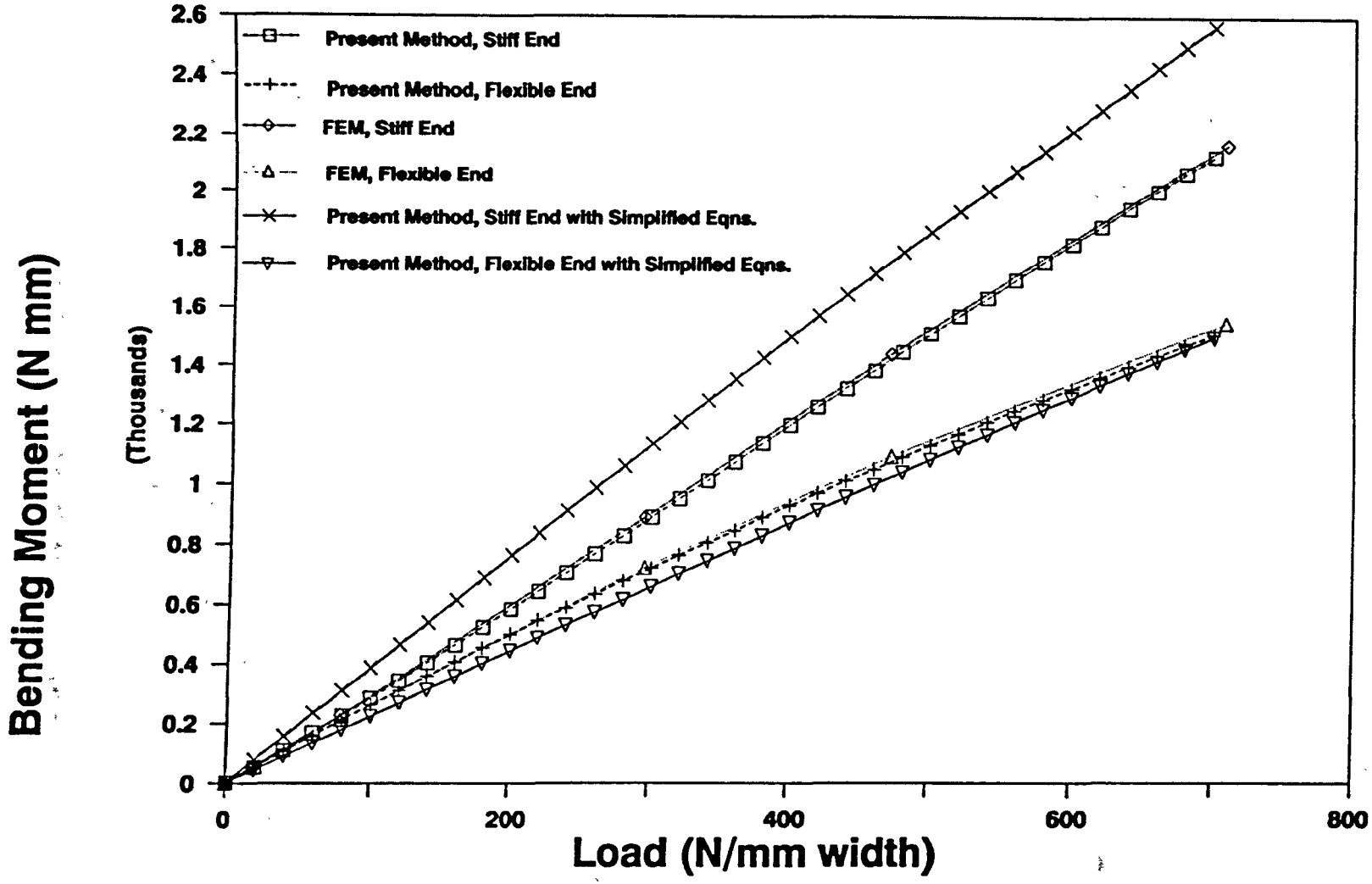

Fig. 3.29 Bending Moment with 25 mm Overlap for Stiff-Flexible 6.35 mm Adherends Using and Without Using Simplified Eqs.

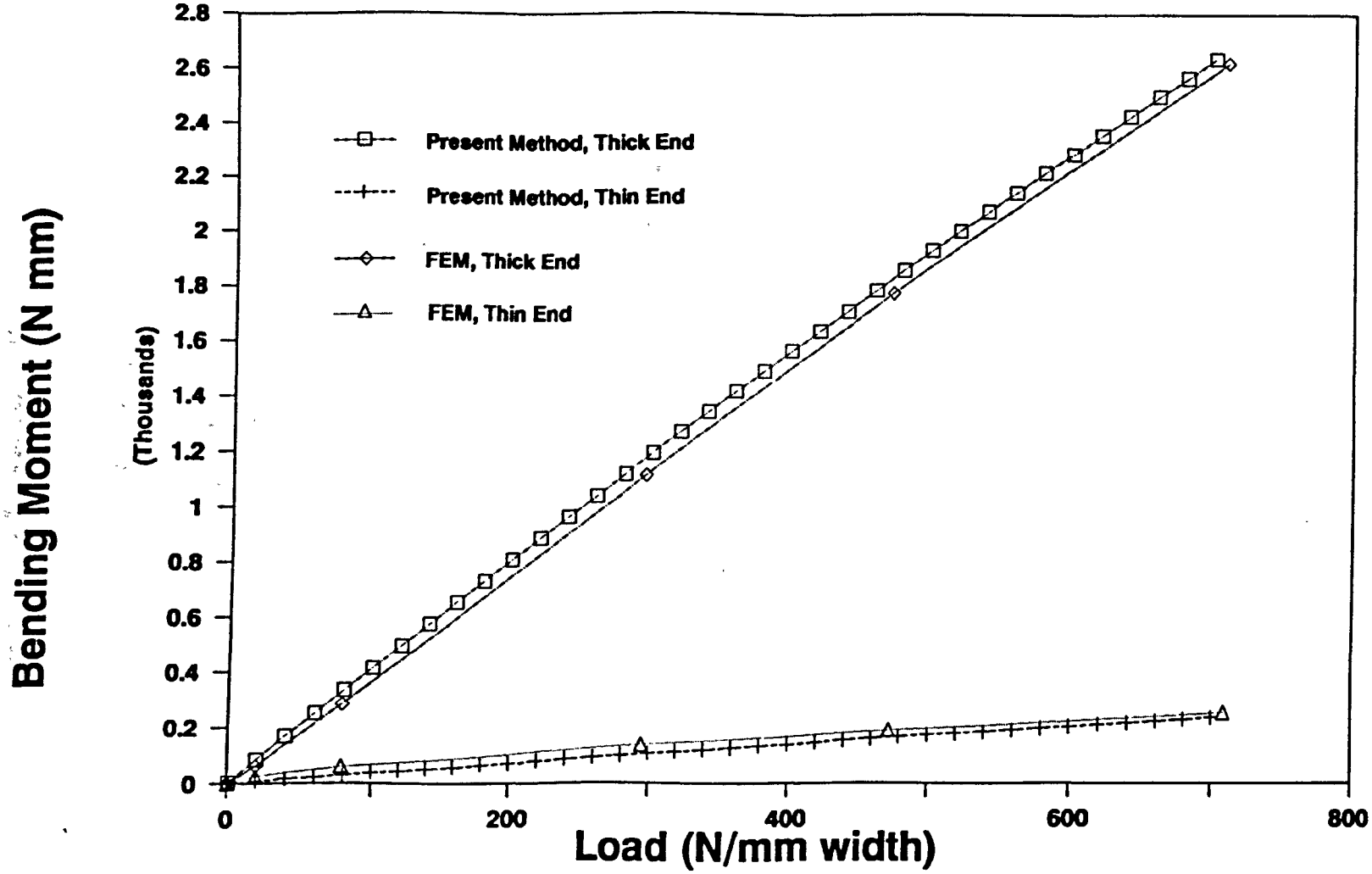

Fig. 3.30 Bending Moment with 12.7 mm Overlap forThick-thin Adherends

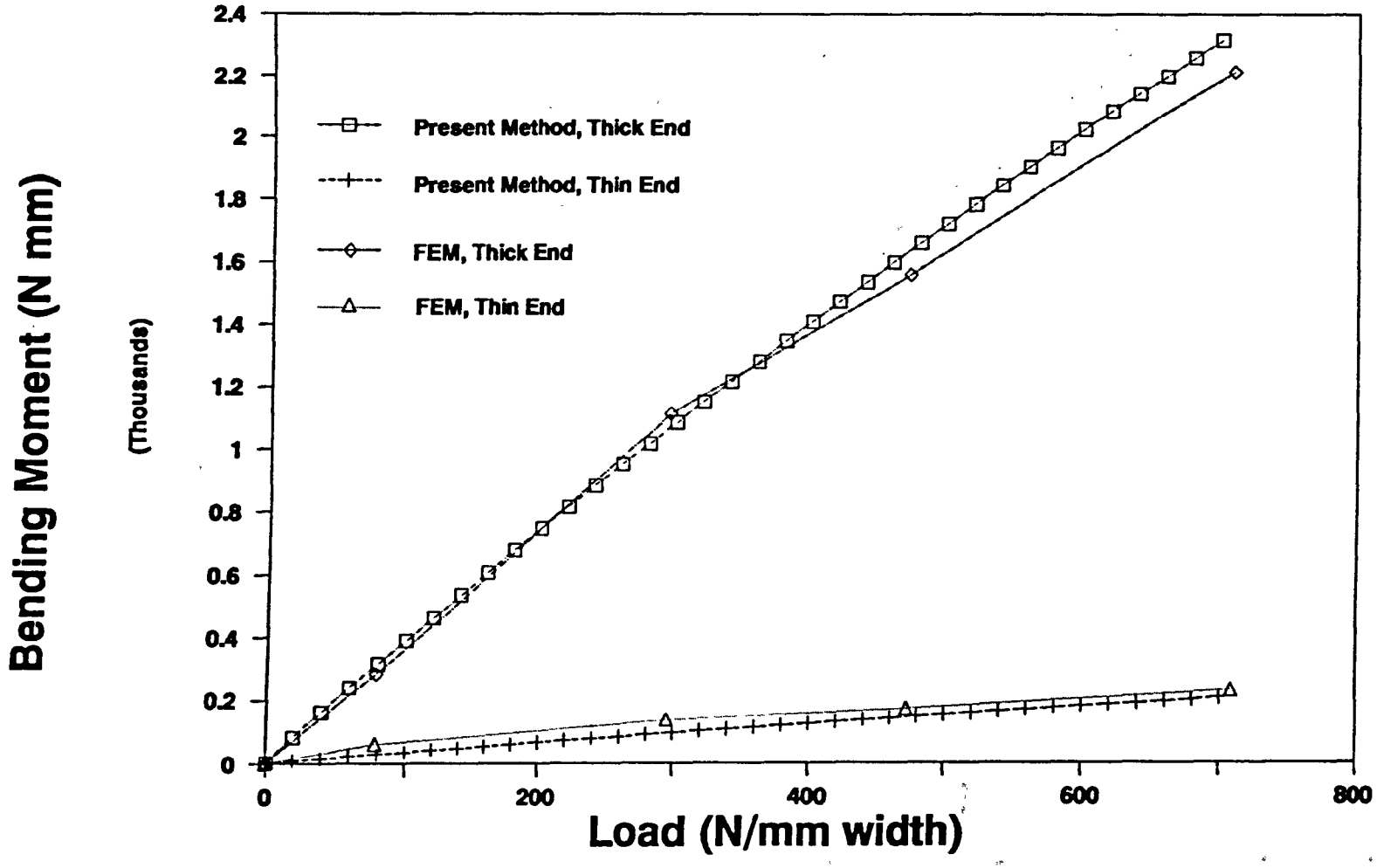

Fig. 3.31 Bending Moment with 25 mm Overlap for Thick-thin Adherends

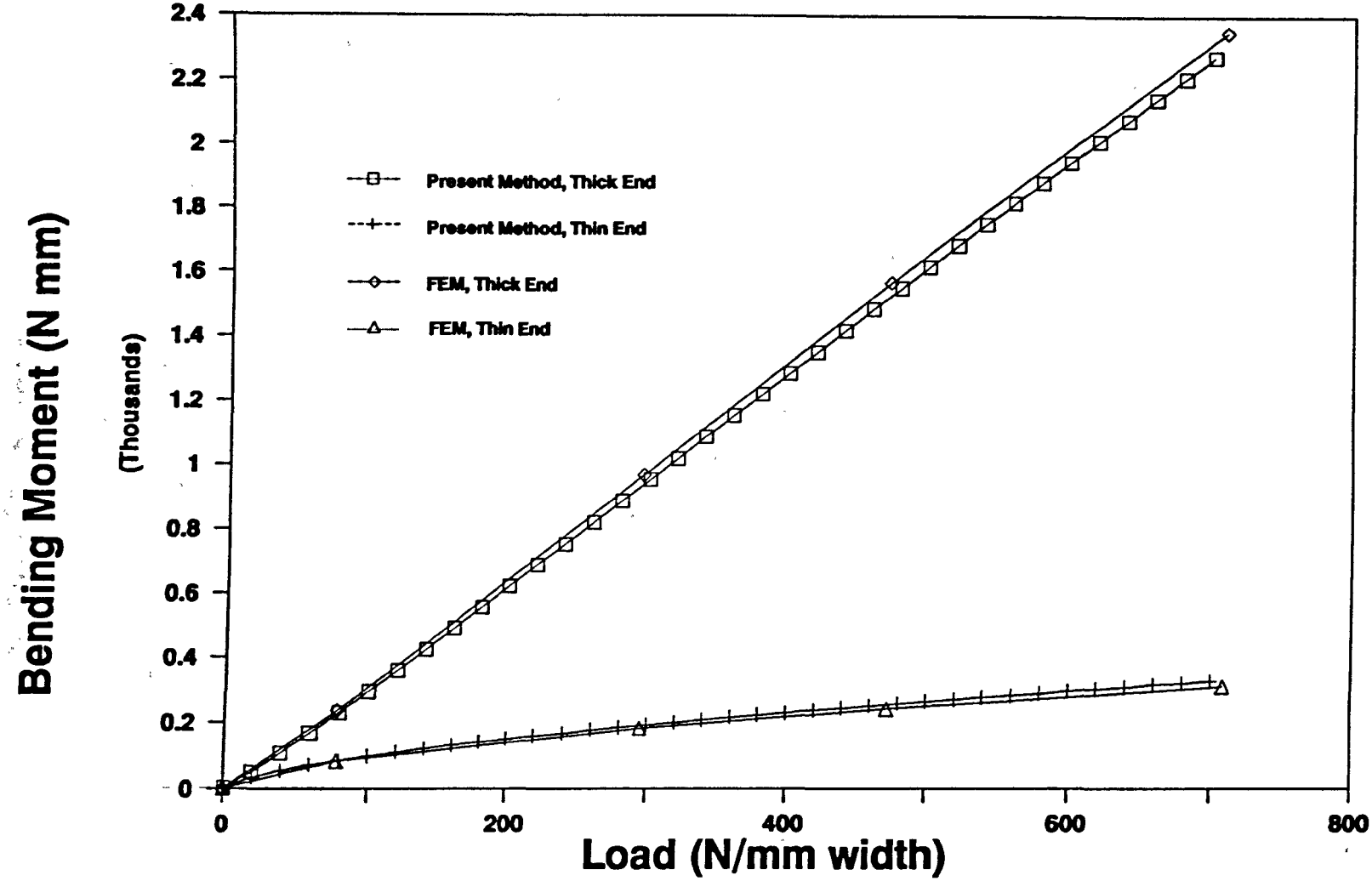

Fig. 3.32 Bending Moment for a Thick-Thin Adherends Joint with 25 mm Overlap and Young's Modulus being 207 GPa

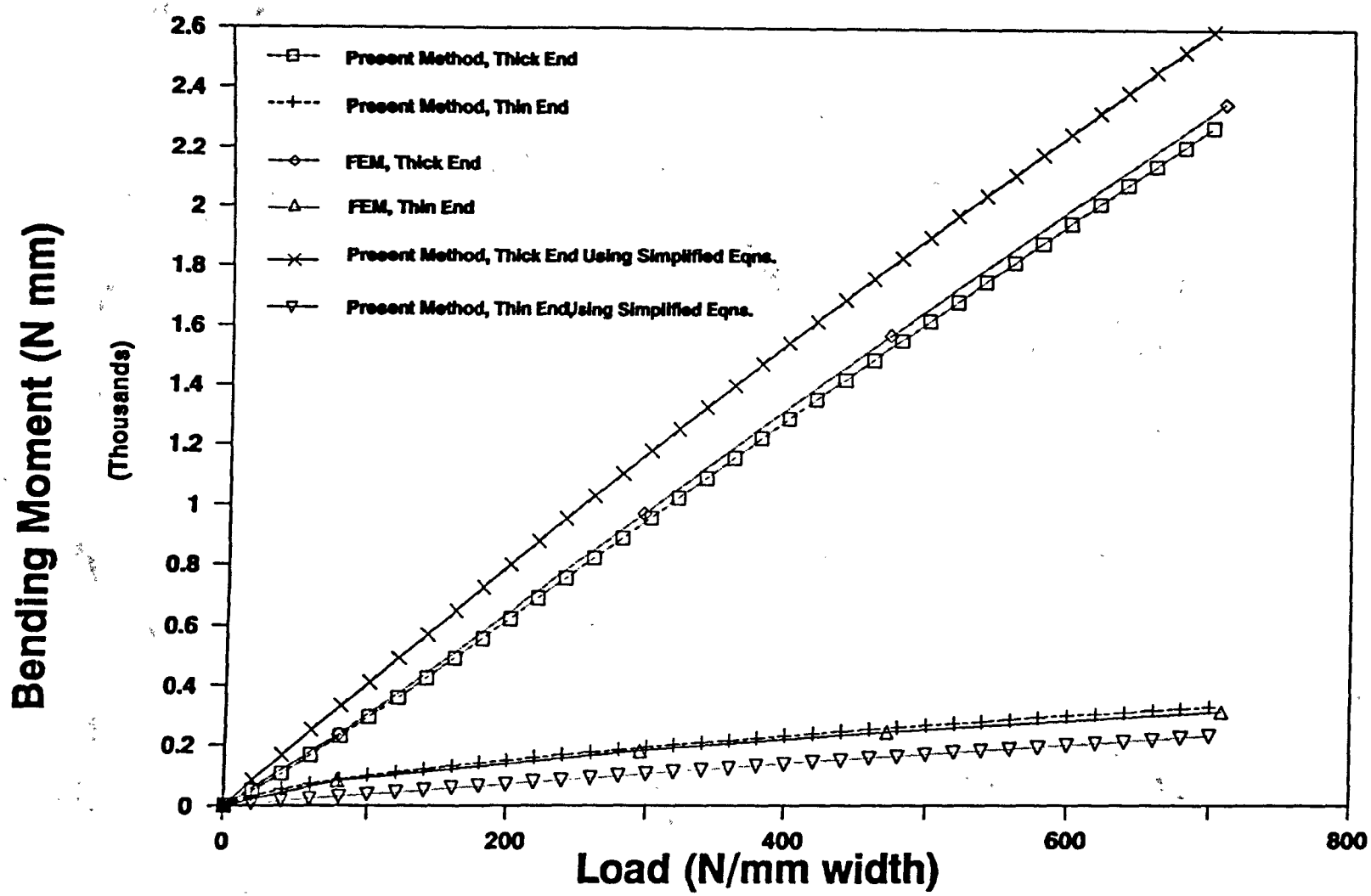

Fig. 3.33 Bending Moment with 25 mm Overlap for a Thick-Thin Adherends Joint with 25 mm Overlap and Young's Modulus 207GPa

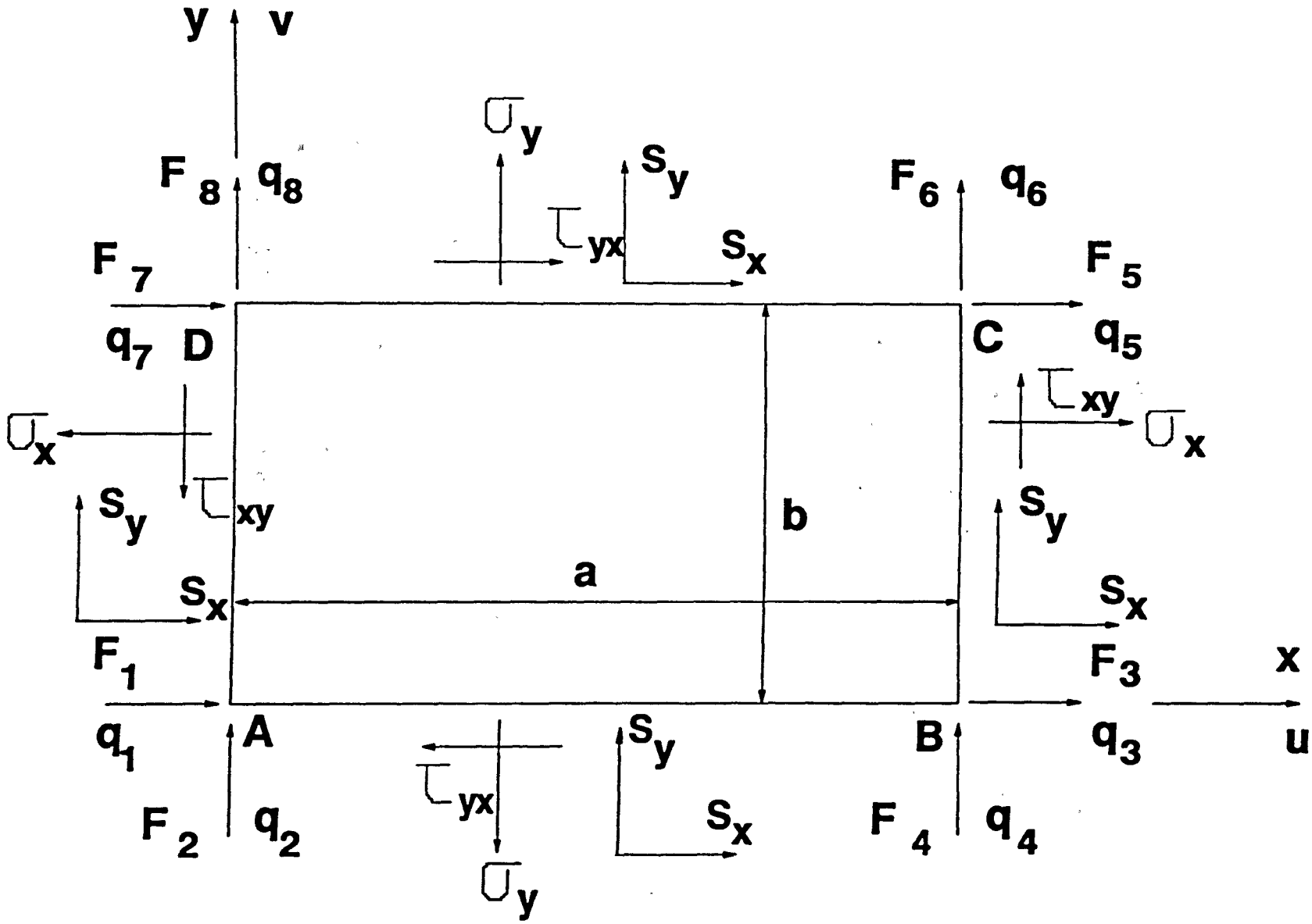

Fig. 4.1 Generalised forces and displacements of a rectangular element

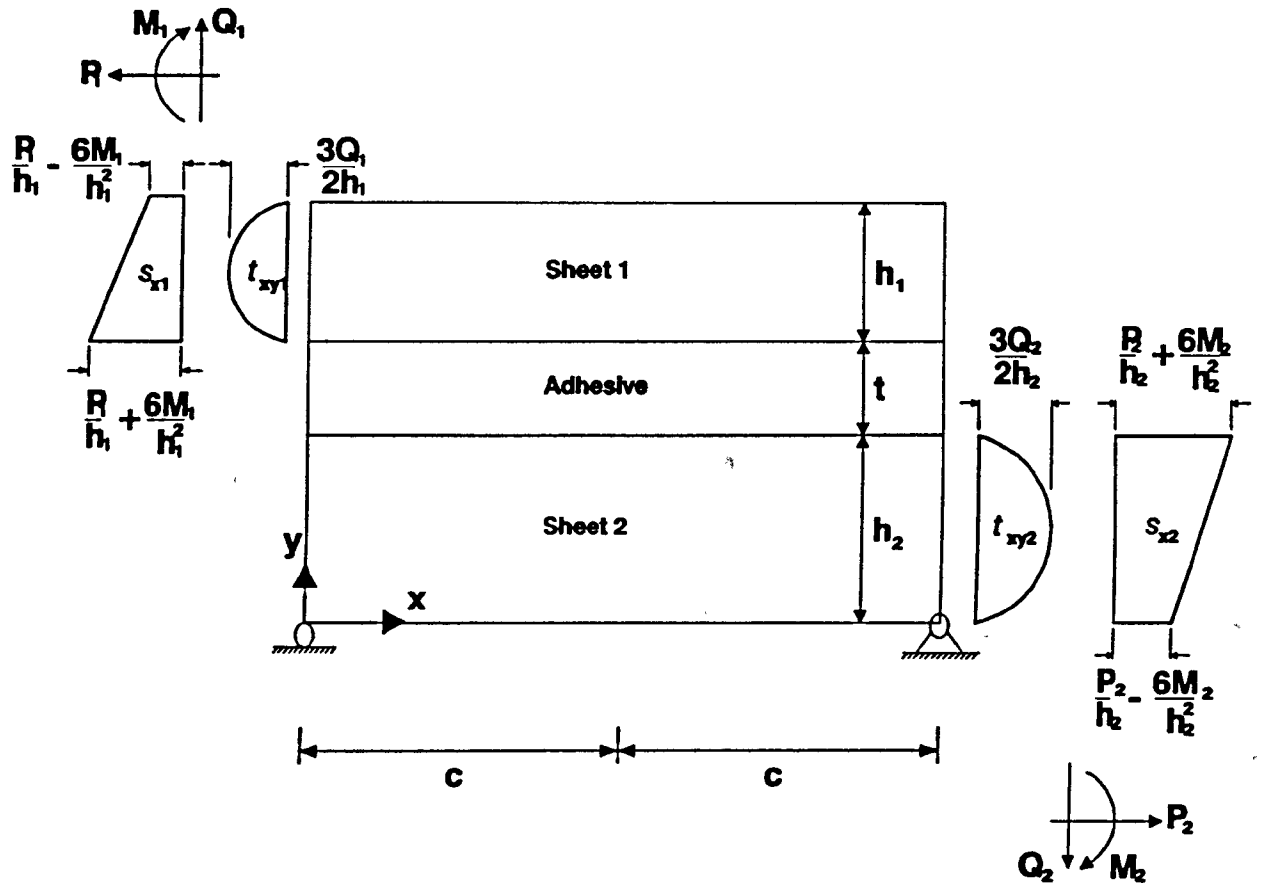

Fig. 4.2 Boundary conditions for the overlap region of a single lap joint

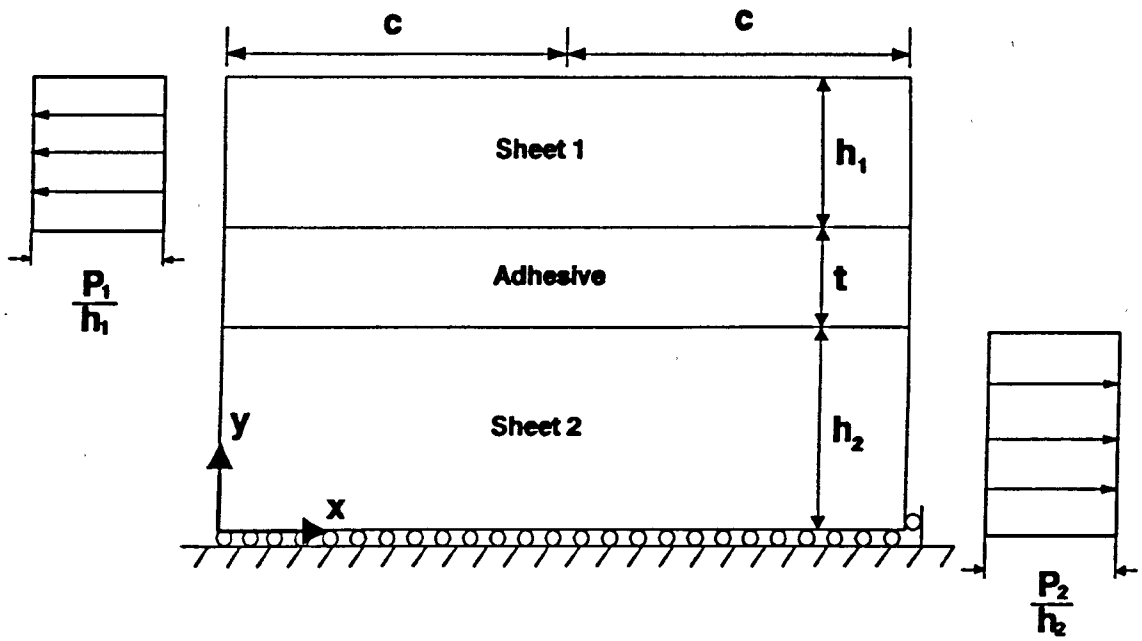

Fig. 4.3 Boundary conditions for the overlap region of a double lap joint

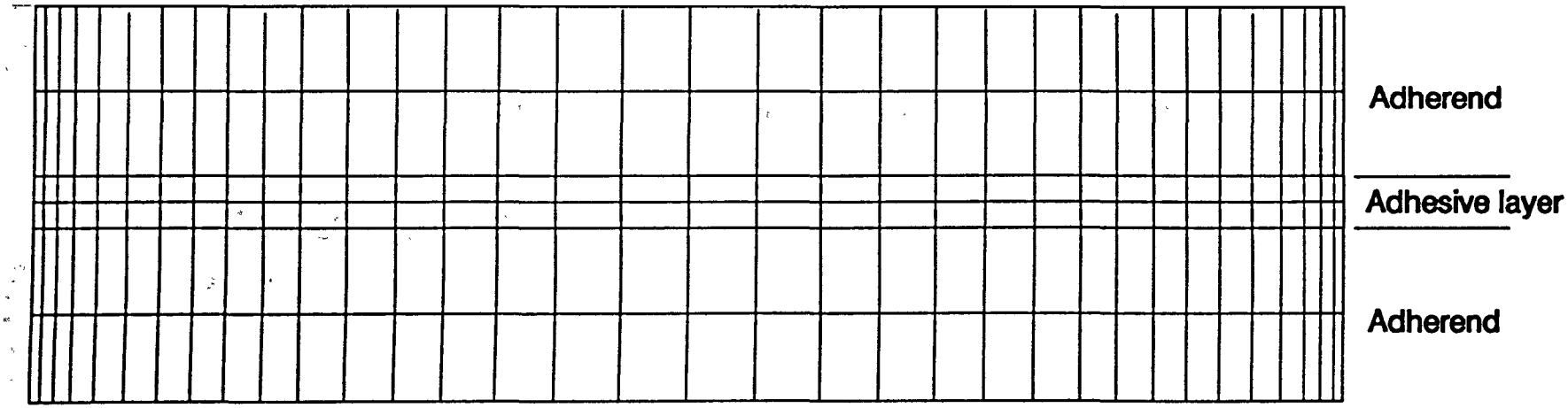

Fig. 4.4 Mesh used for the present Hybrid element (not to scale)

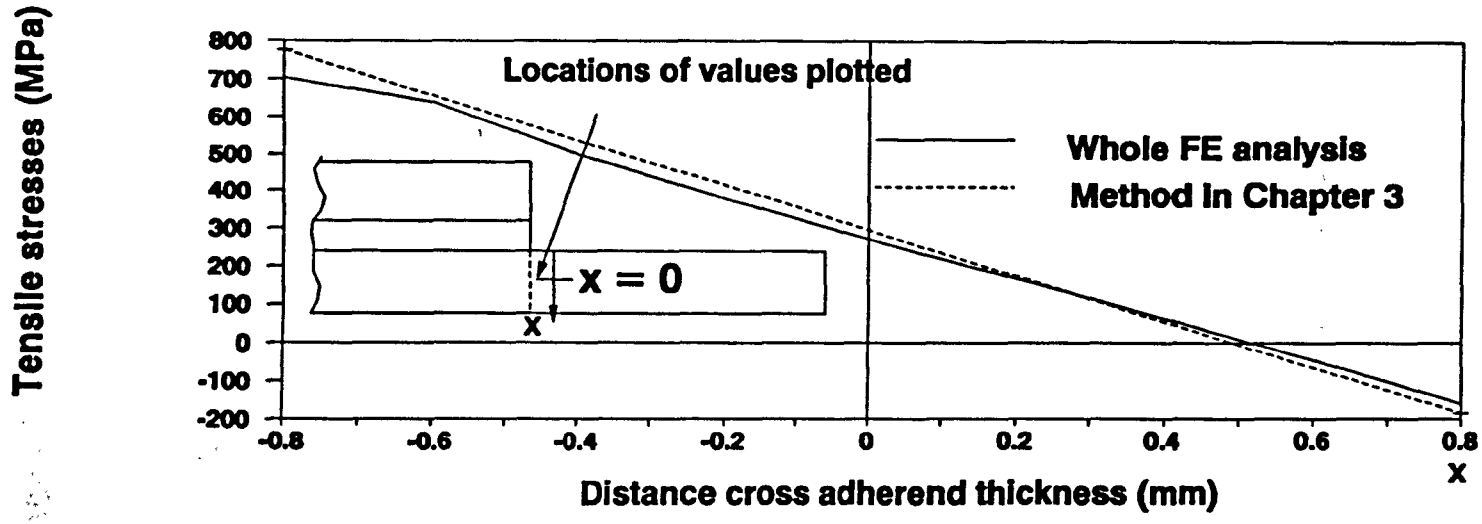

Fig. 4.5a Longitudinal stresses across adherend thickness

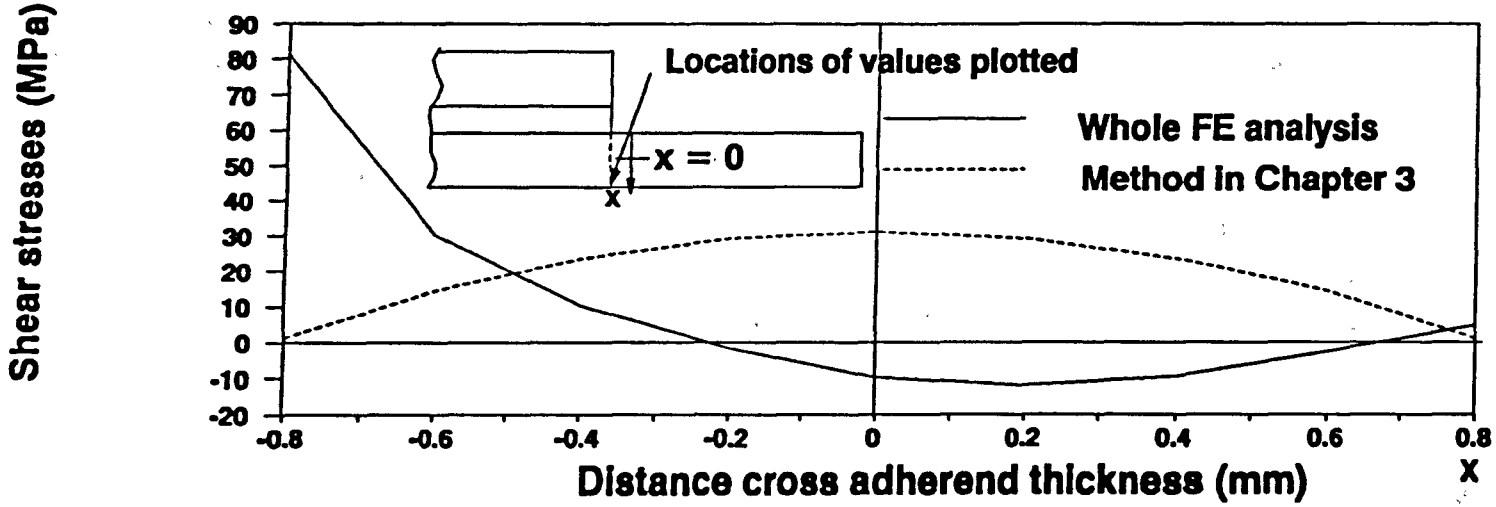

Fig. 4.5b Shear stresses across adherend thickness

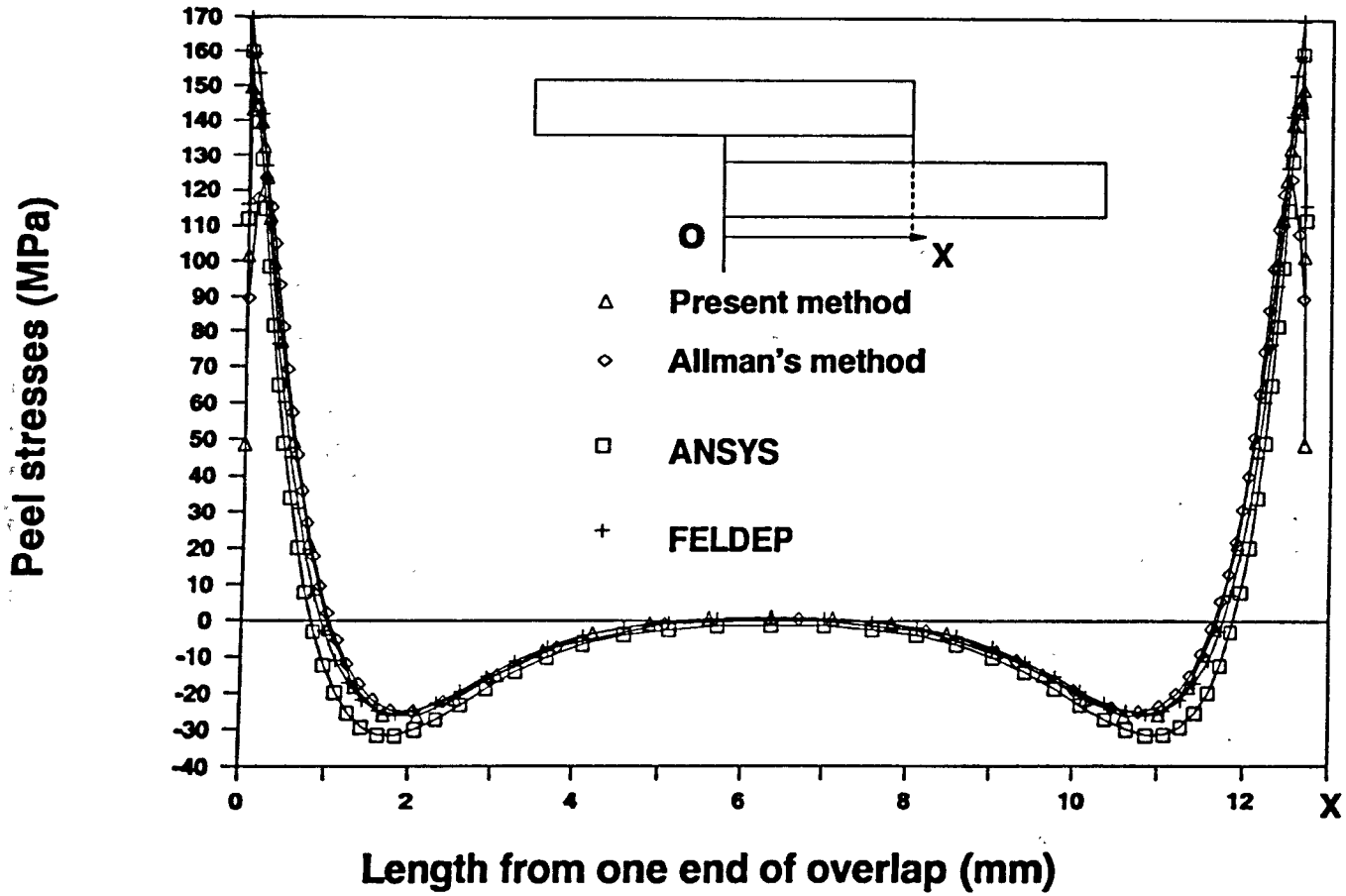

Fig. 4.6 Comparison of peel stresses from different analyses

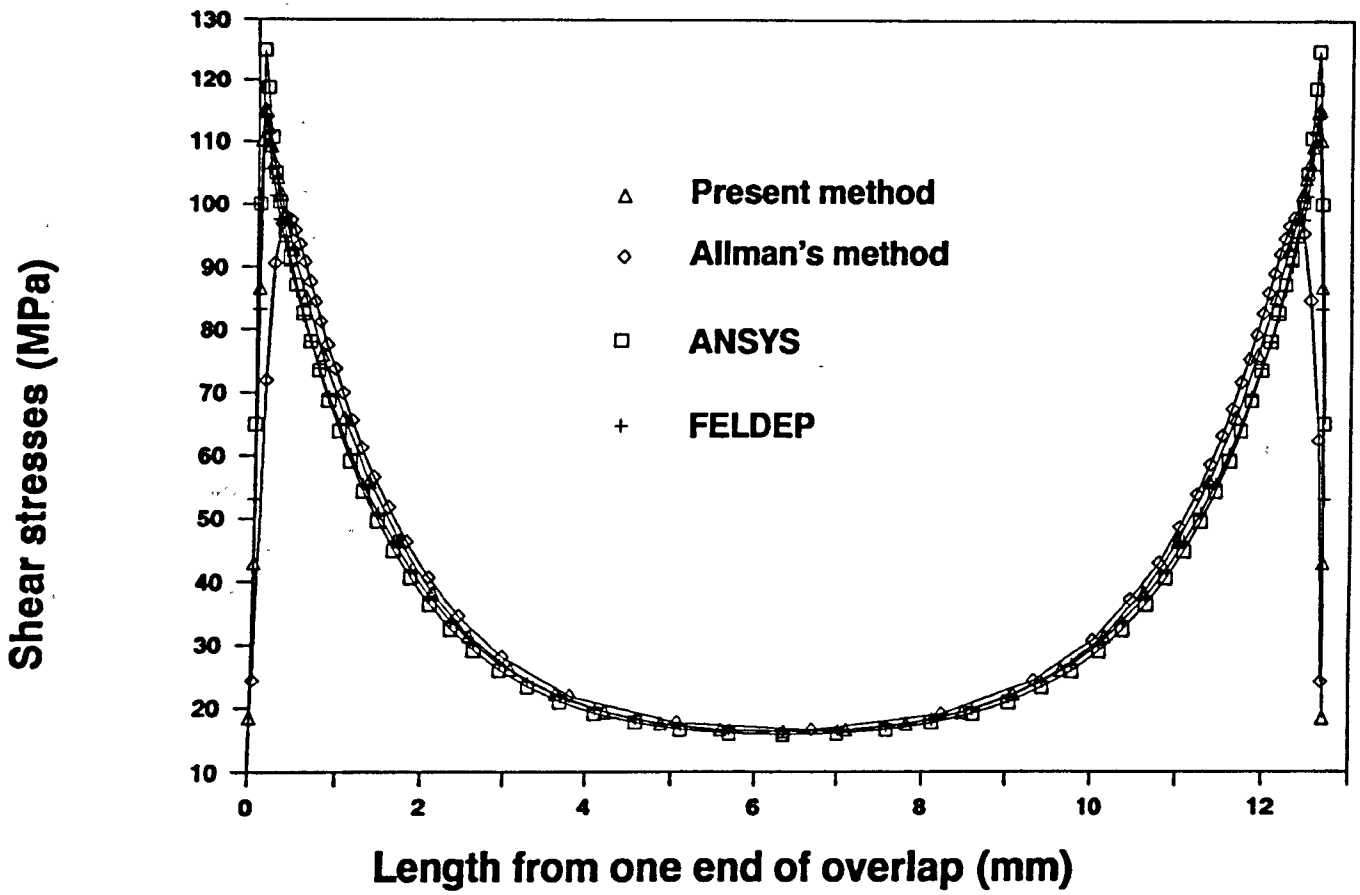

Fig. 4.7 Comparison of shear stresses from different analyses (averaged)

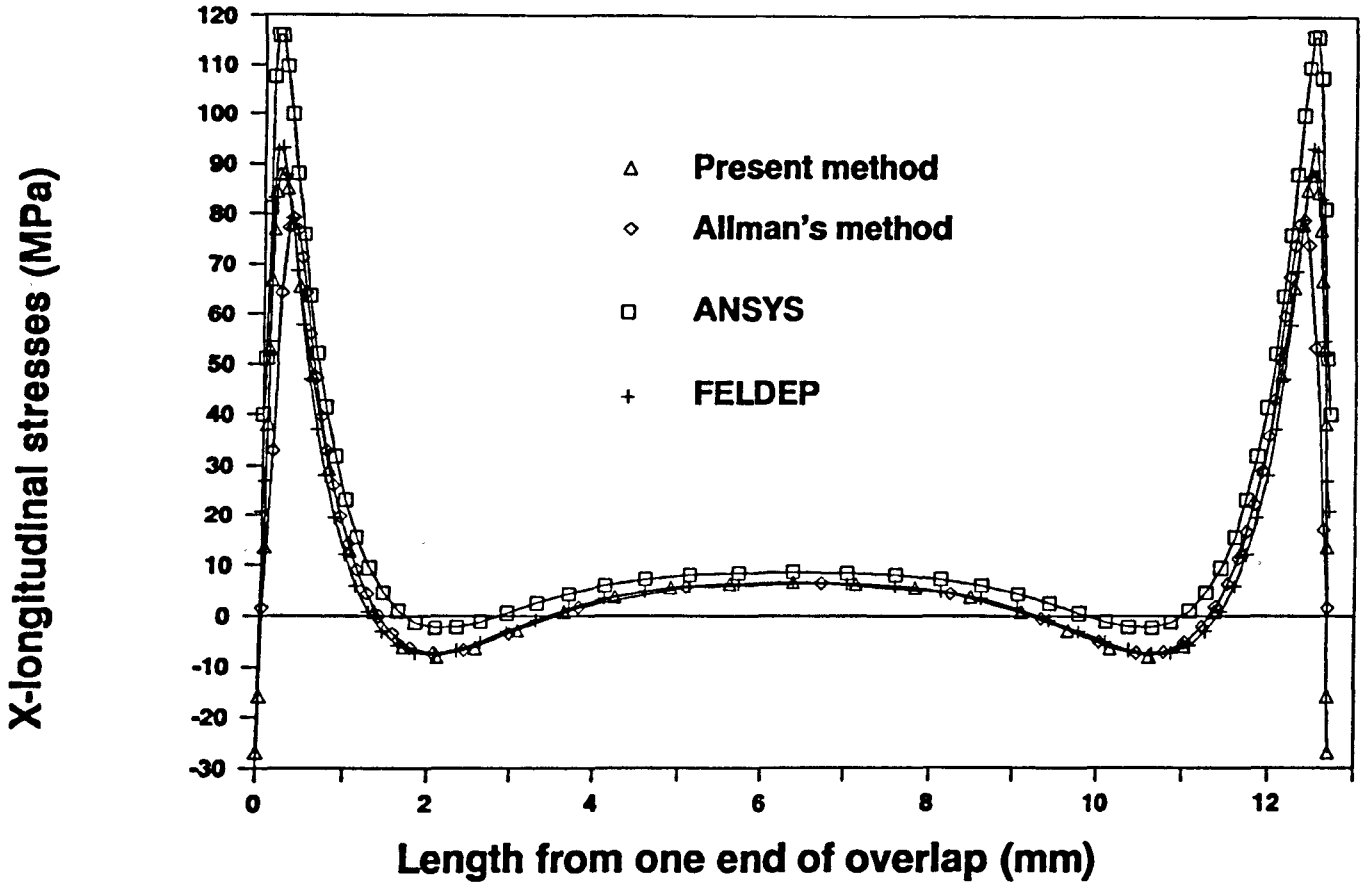

Fig.4.8 Comparison of longitudinal stresses(averaged) from different analyses

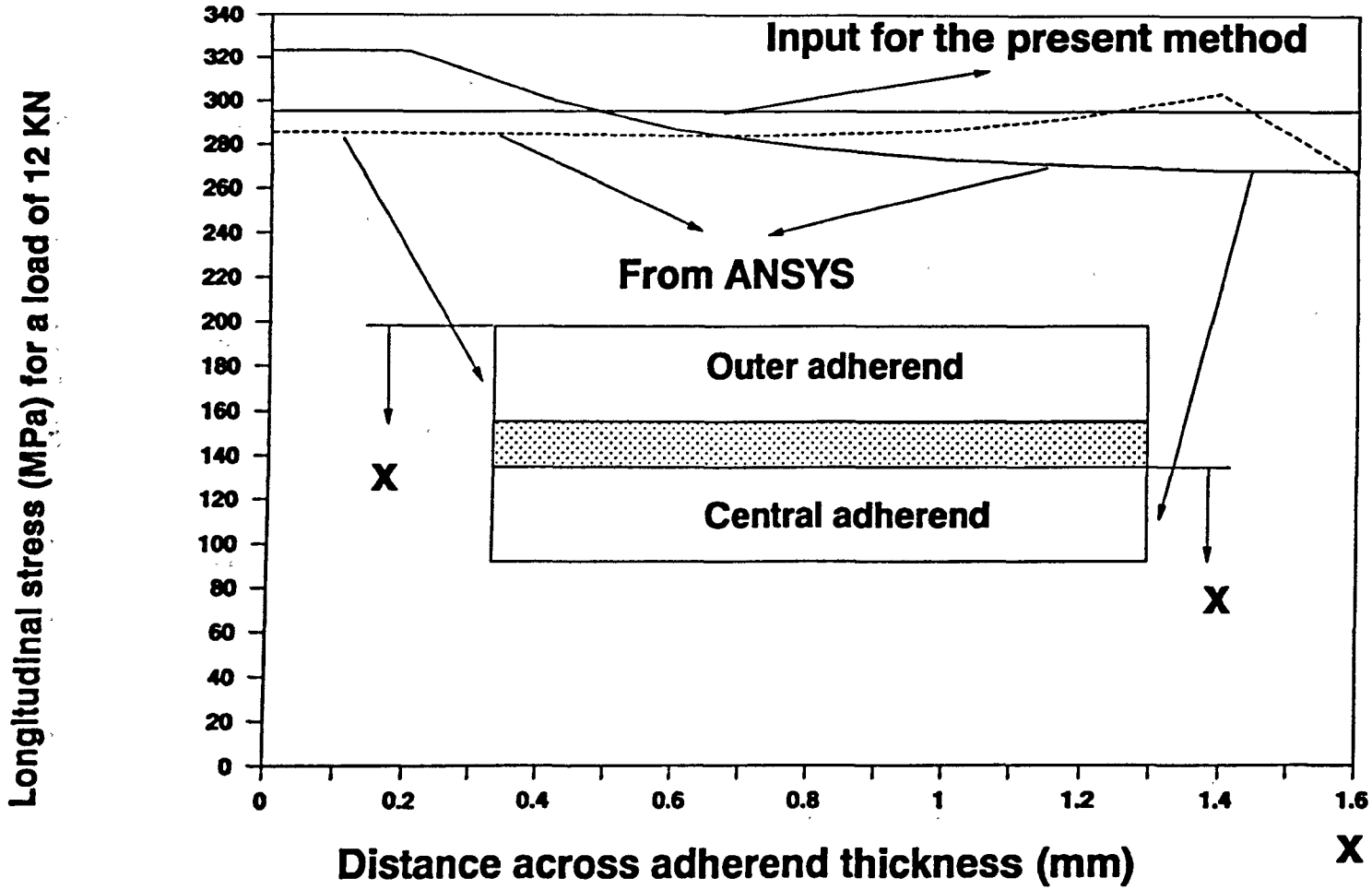

Fig. 4.9 Longitudinal stress boundary conditions for a double lap joint

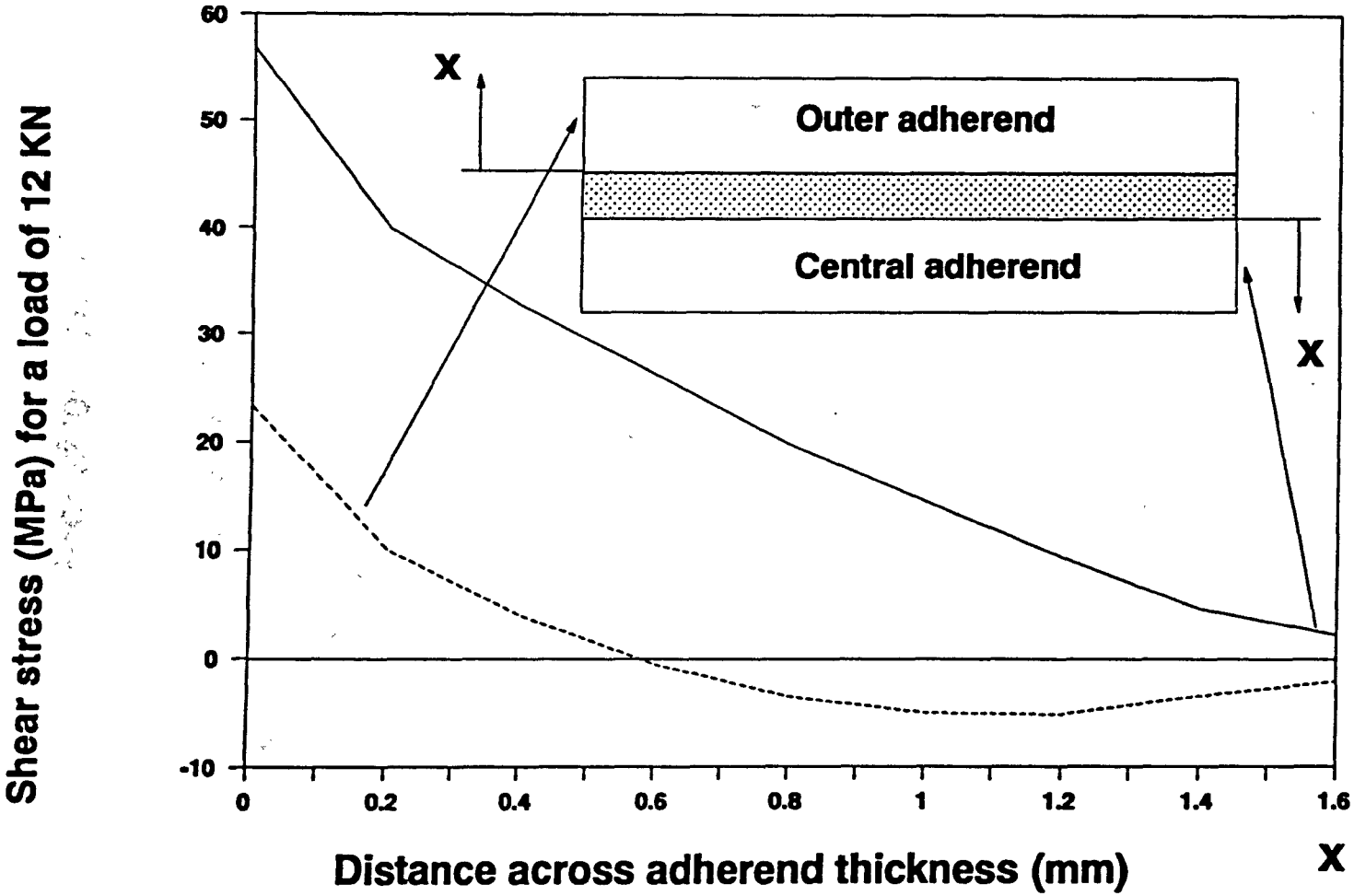

Fig. 4.10 Shear boundary conditions for a double lap joint

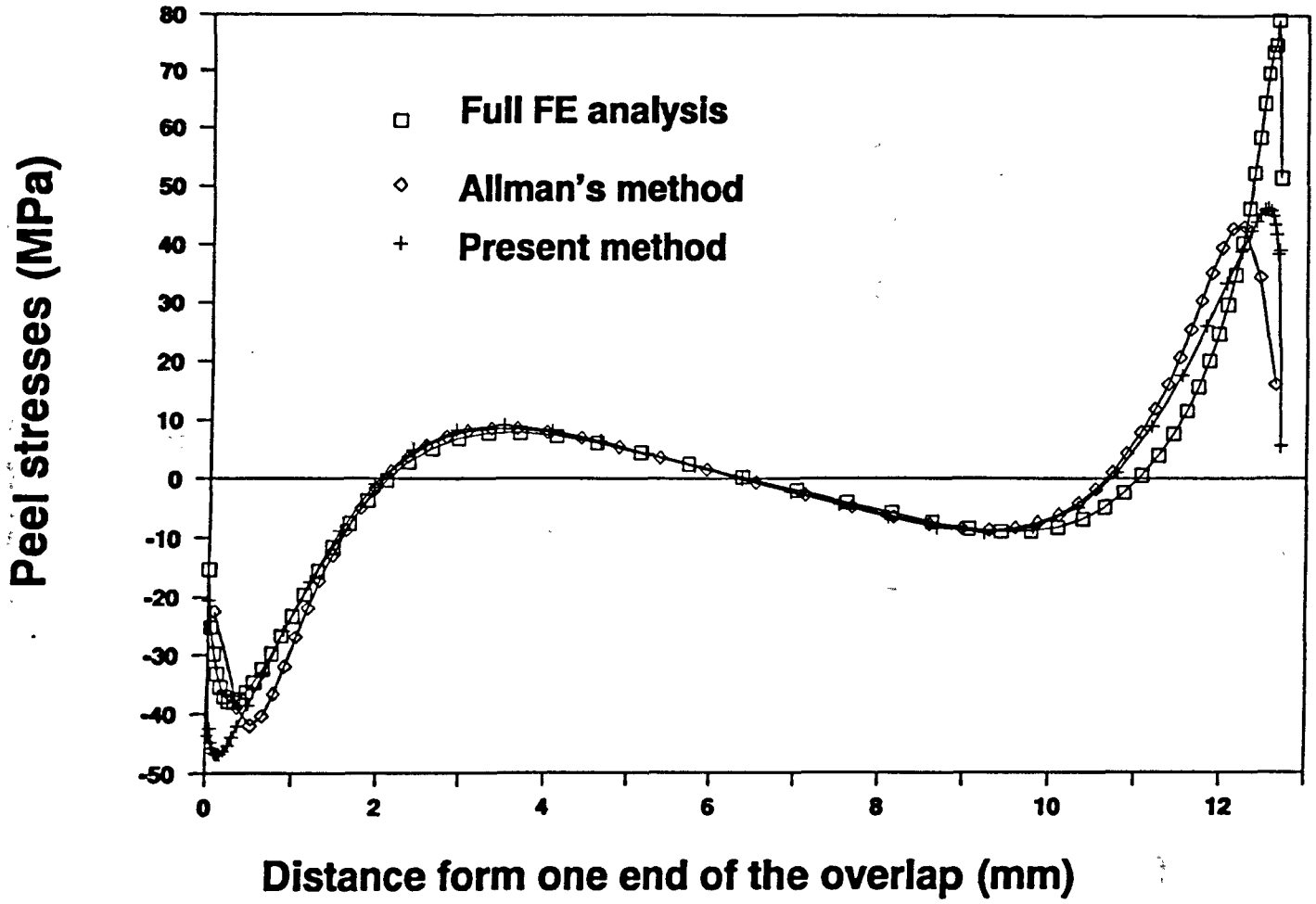

Fig. 4.11 Peel stresses in a double lap joint with a load of 12 KN

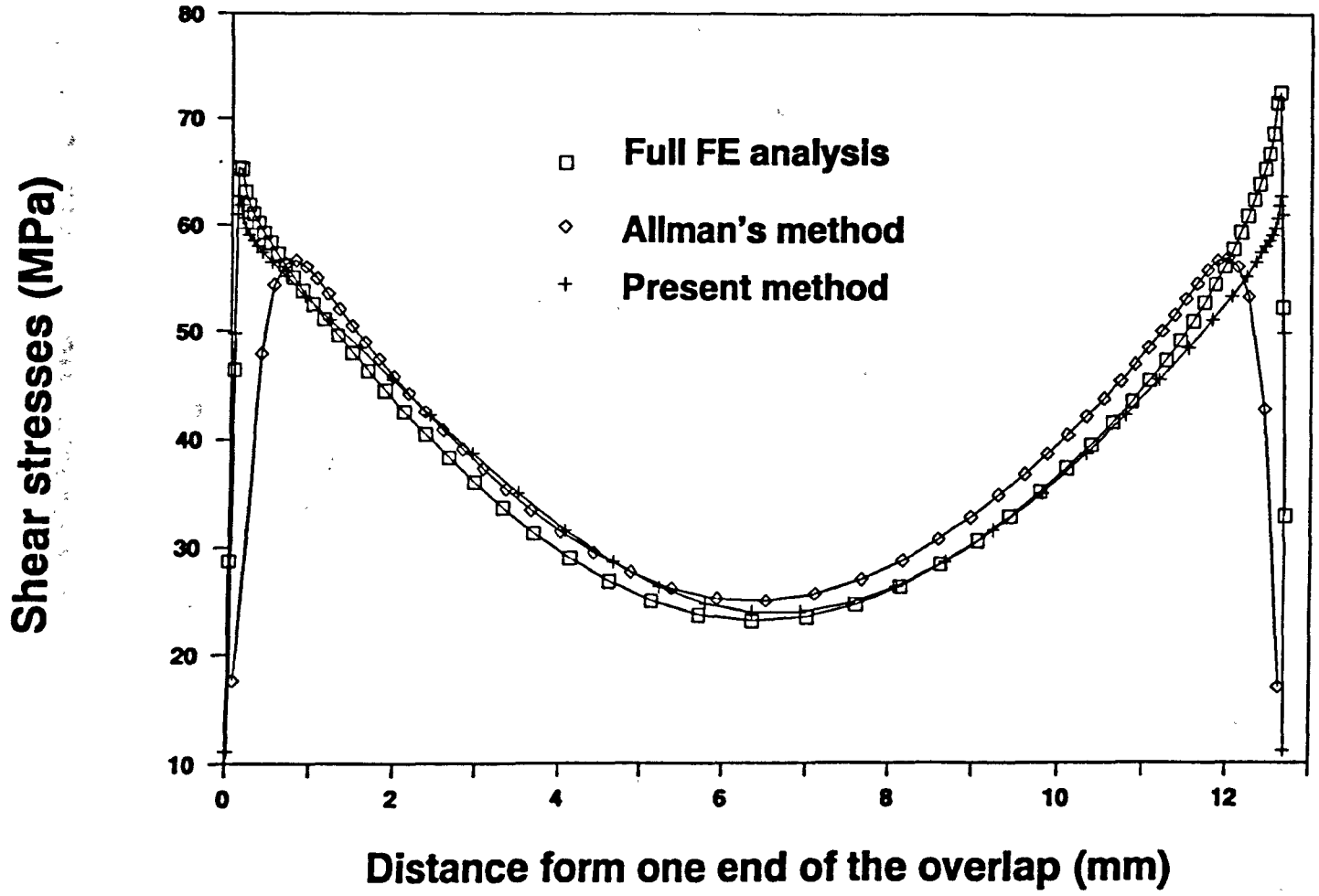

Fig. 4.12 Shear stresses in a double lap joint with a load of 12 KN

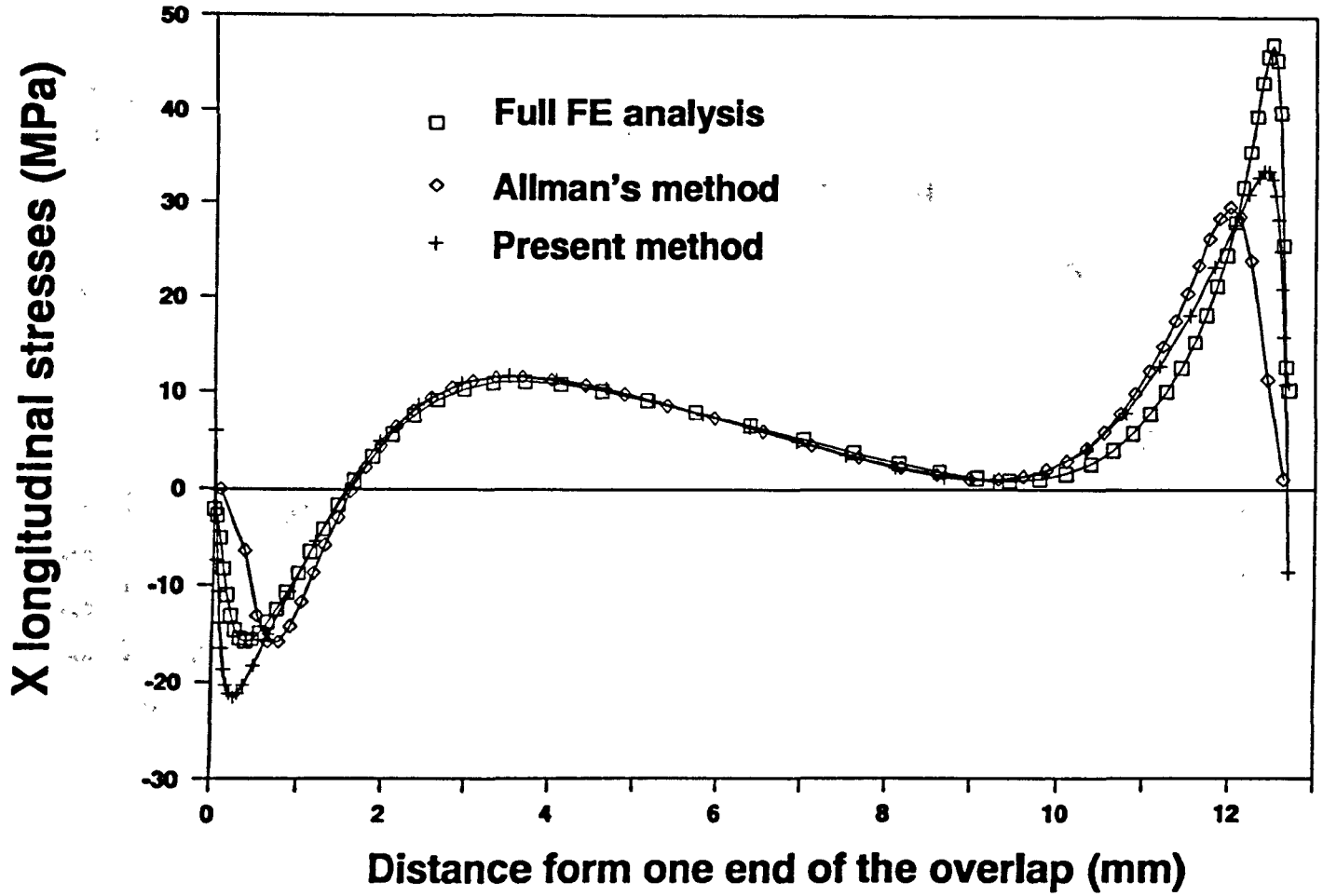

Fig. 4.13 Longitudinal stresses in a double lap joint with a load of 12 KN

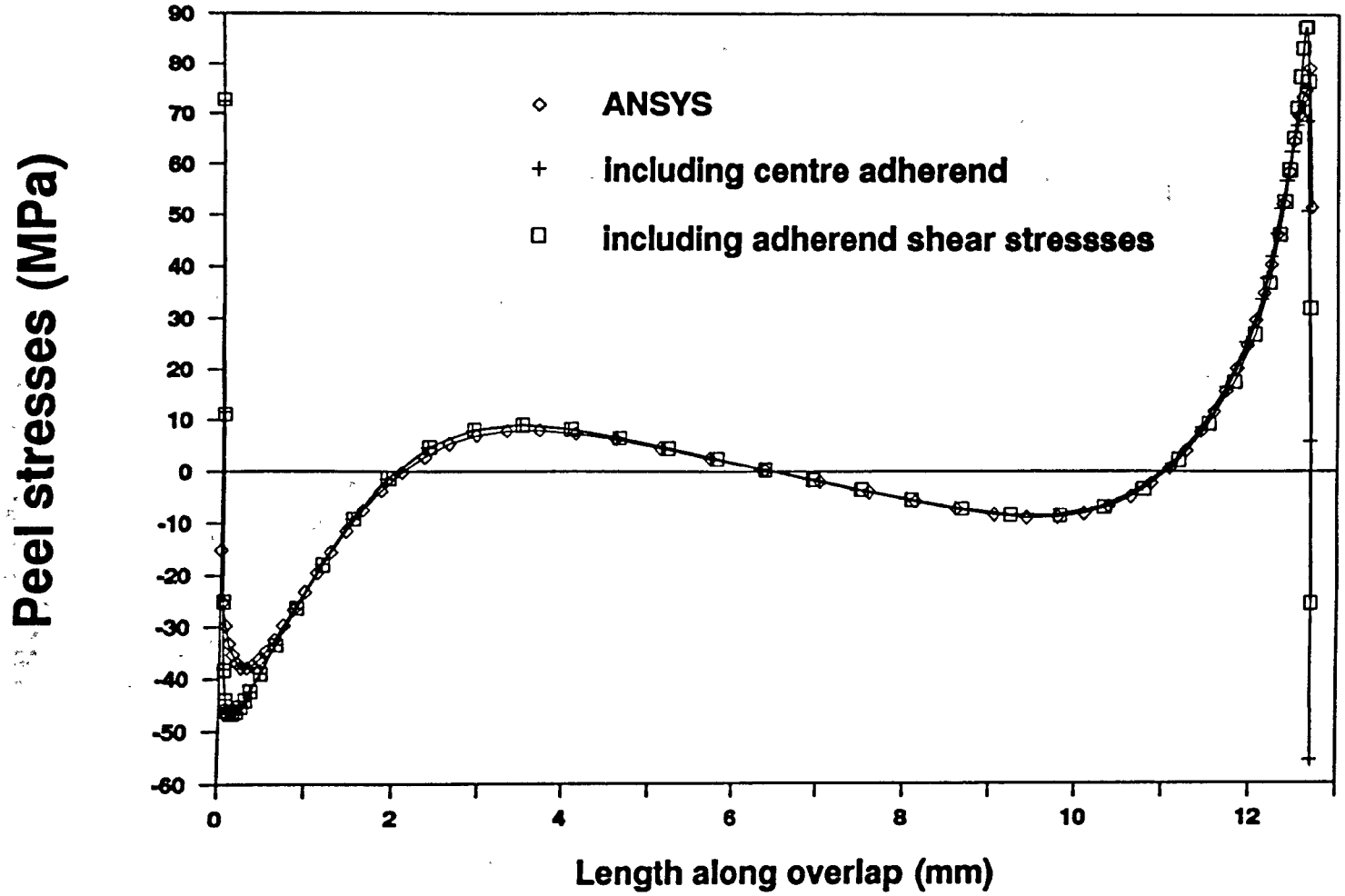

Fig. 4.14 Peel stresses with improved analyses

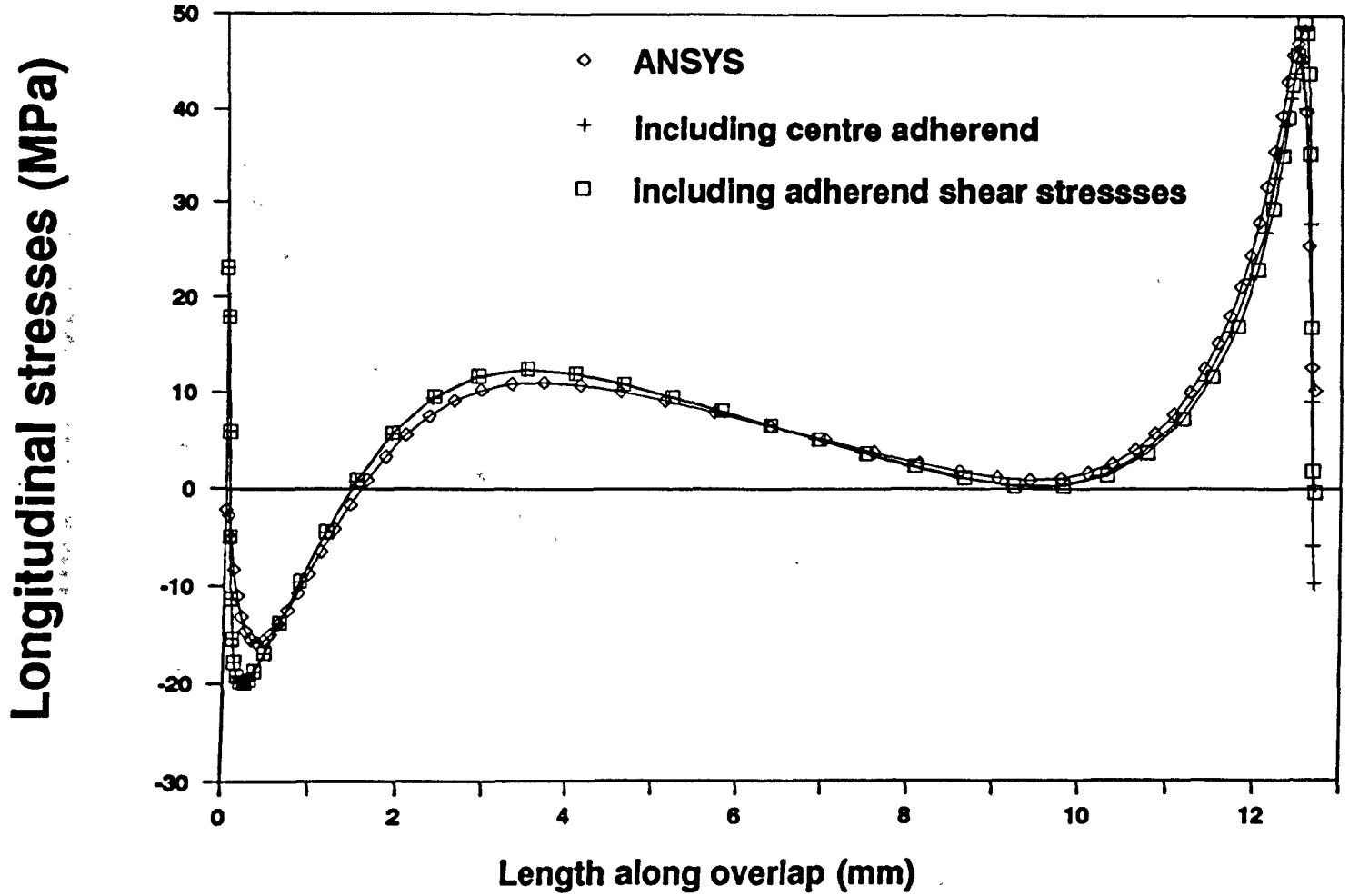

Fig. 4.15 Longitudinal stresses with improved analyses

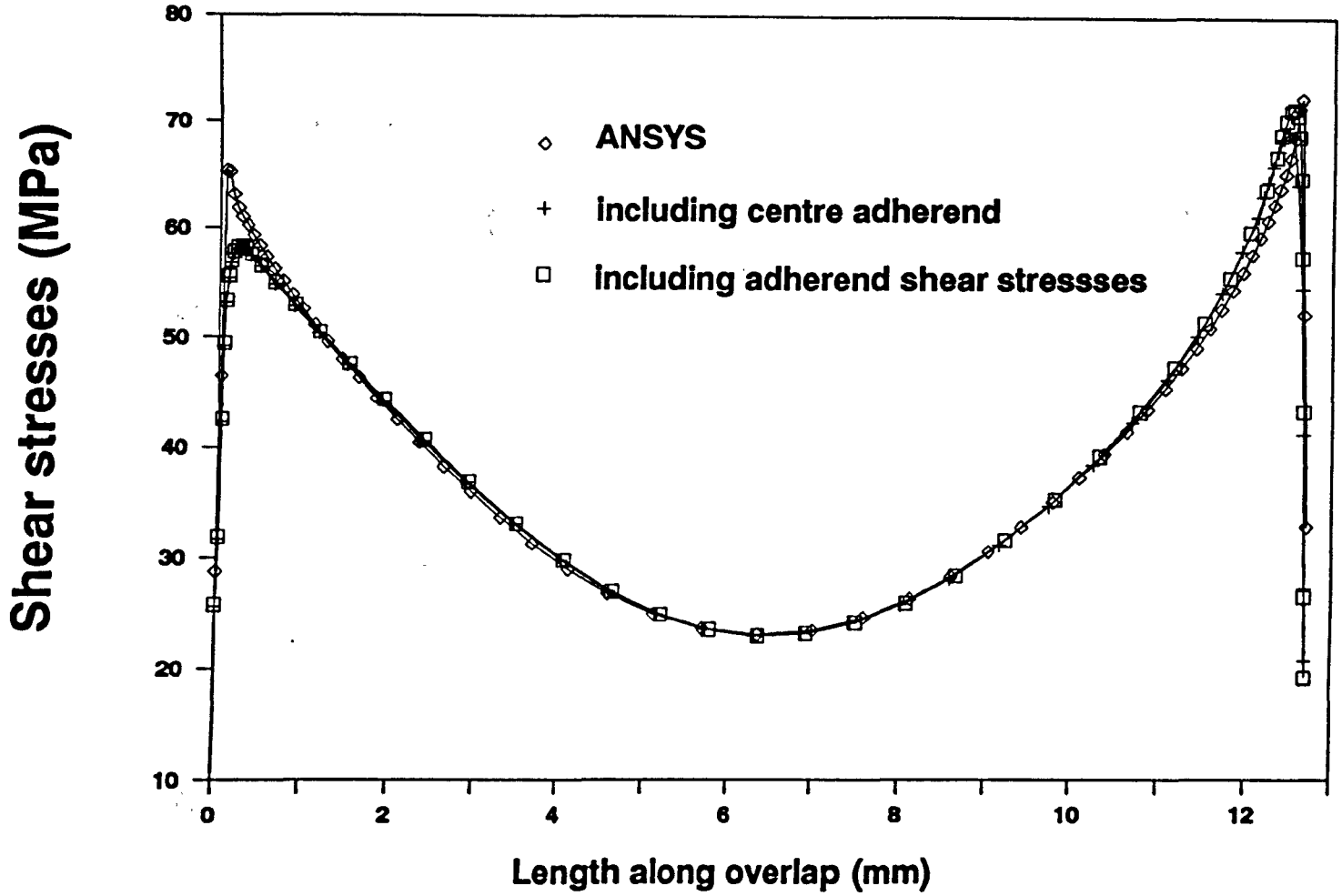

Fig. 4.16 Shear stresses with improved analyses

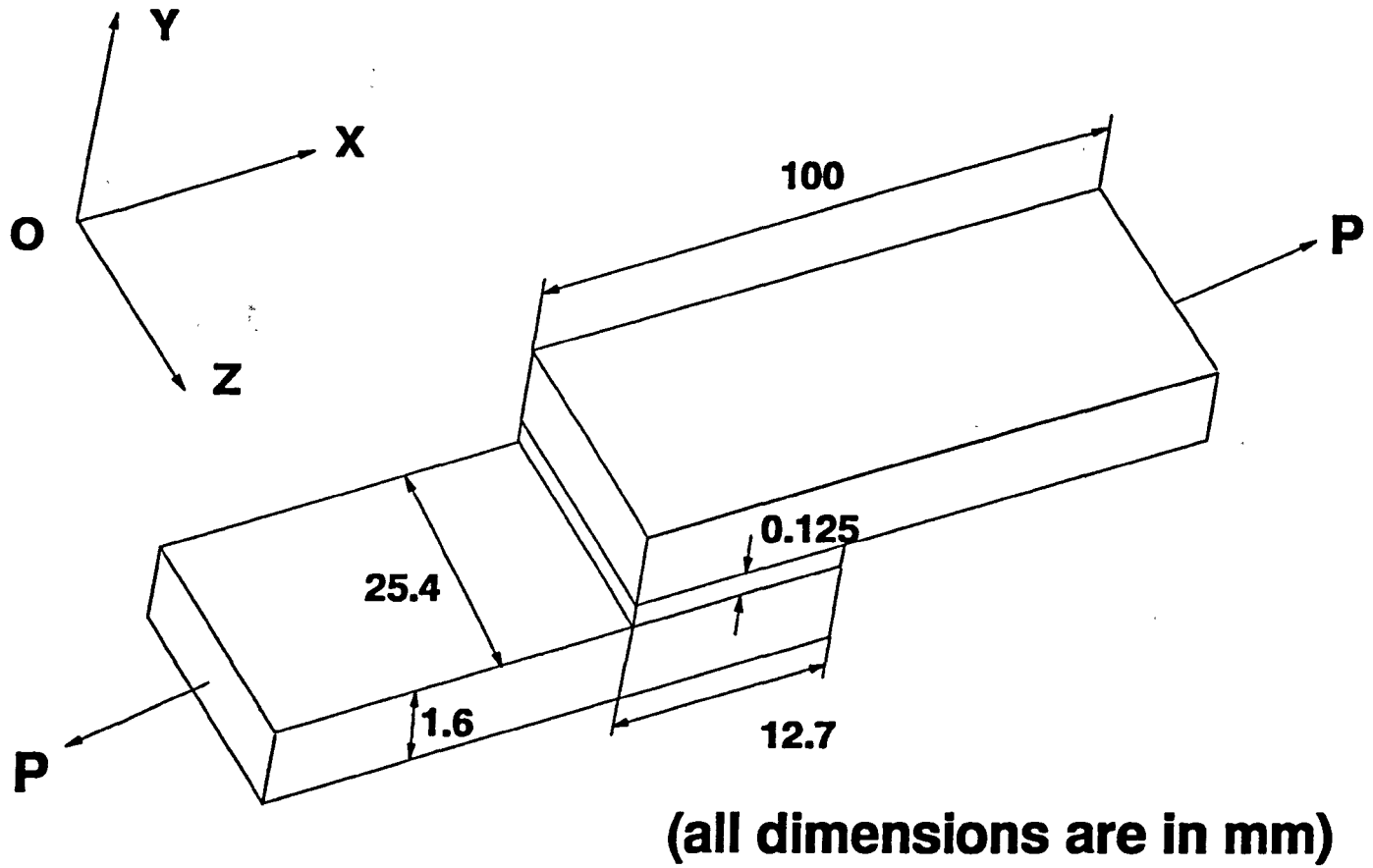

Fig. 5.1 Geometry of a single lap joint

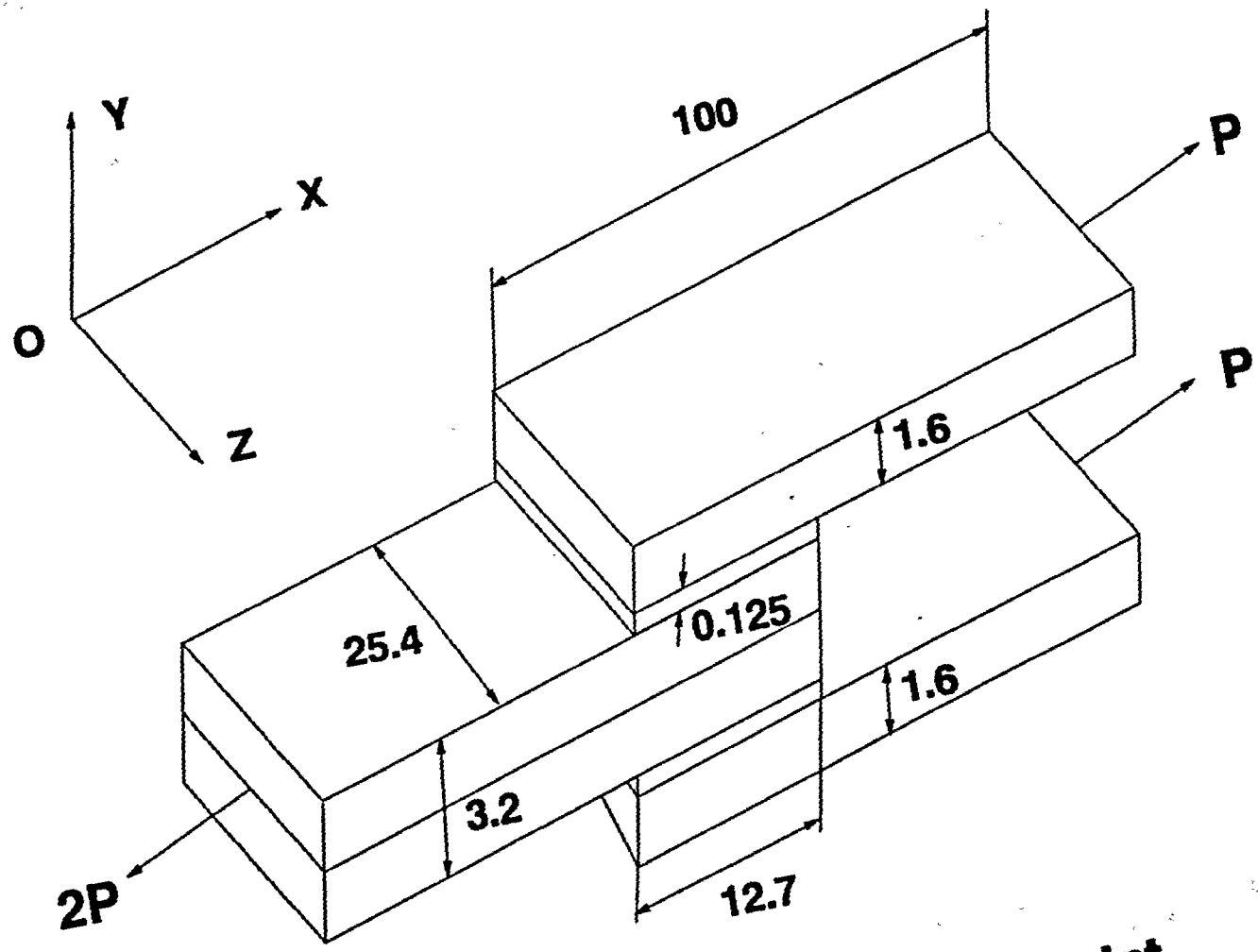

Fig. 5.2 Geometry of a double lap joint

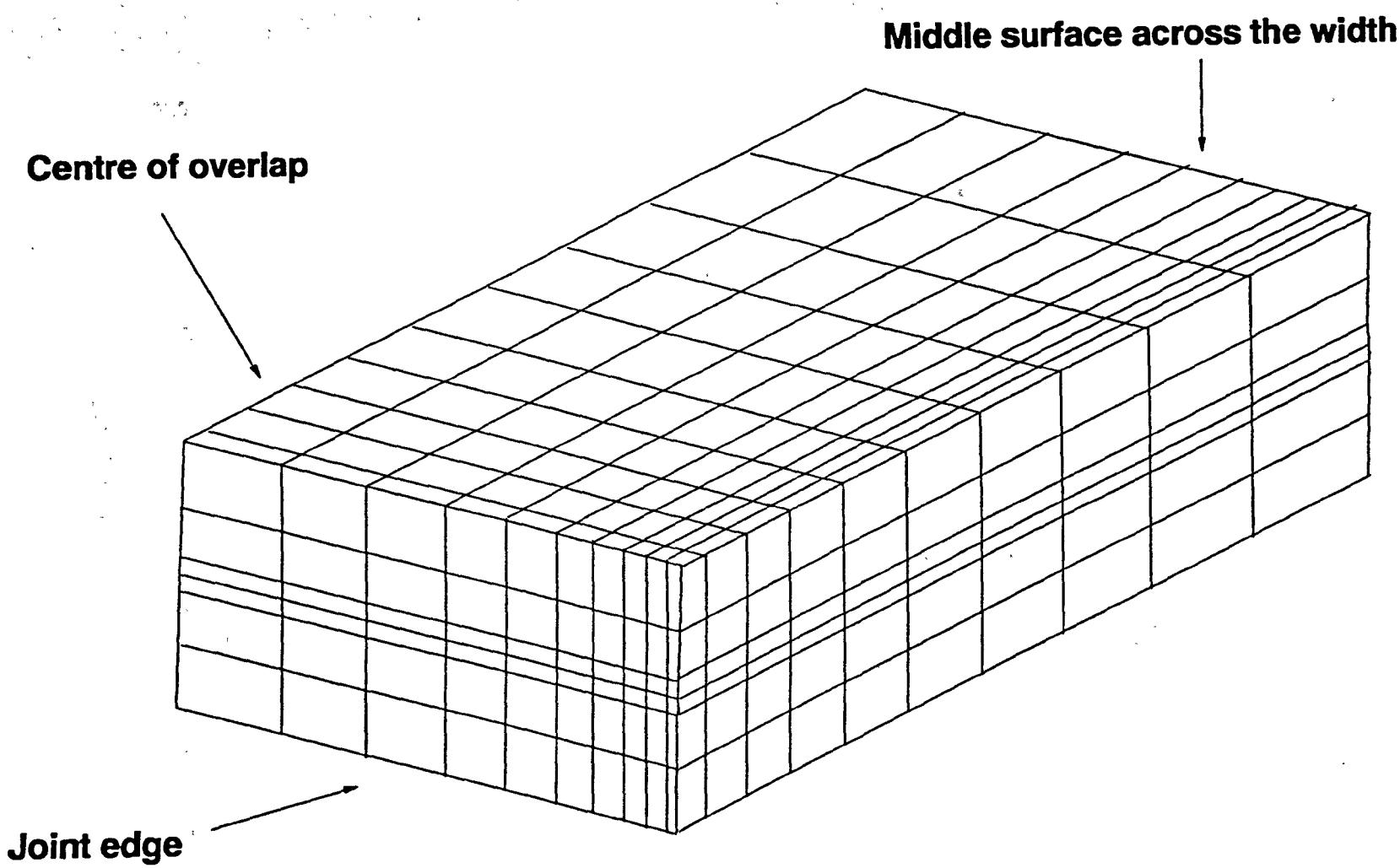

Fig. 5.3 A typical mesh of 3D analysis of a lap joint

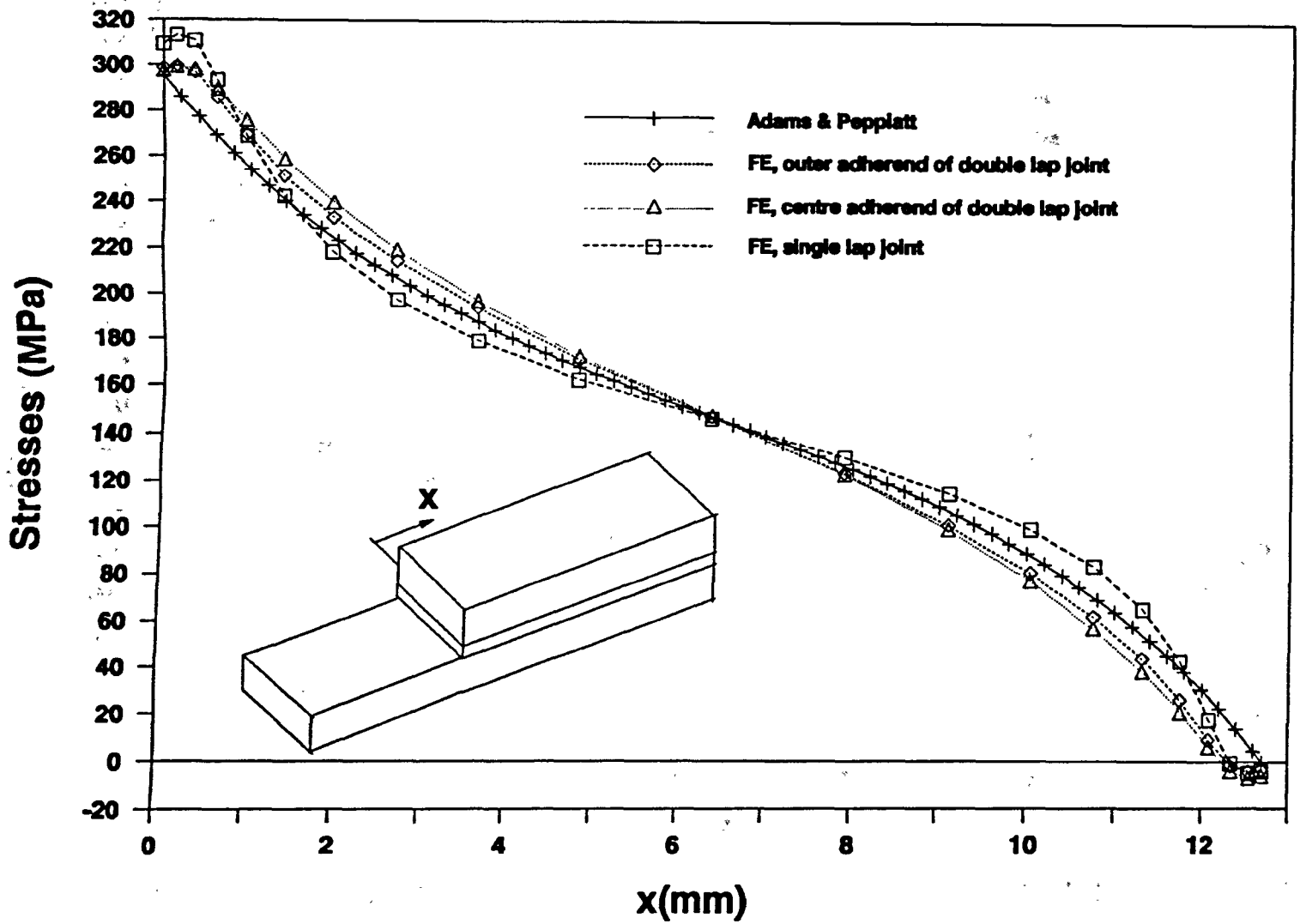

Fig. 5.4 Tensile stresses along overlap in adherends plotted against x

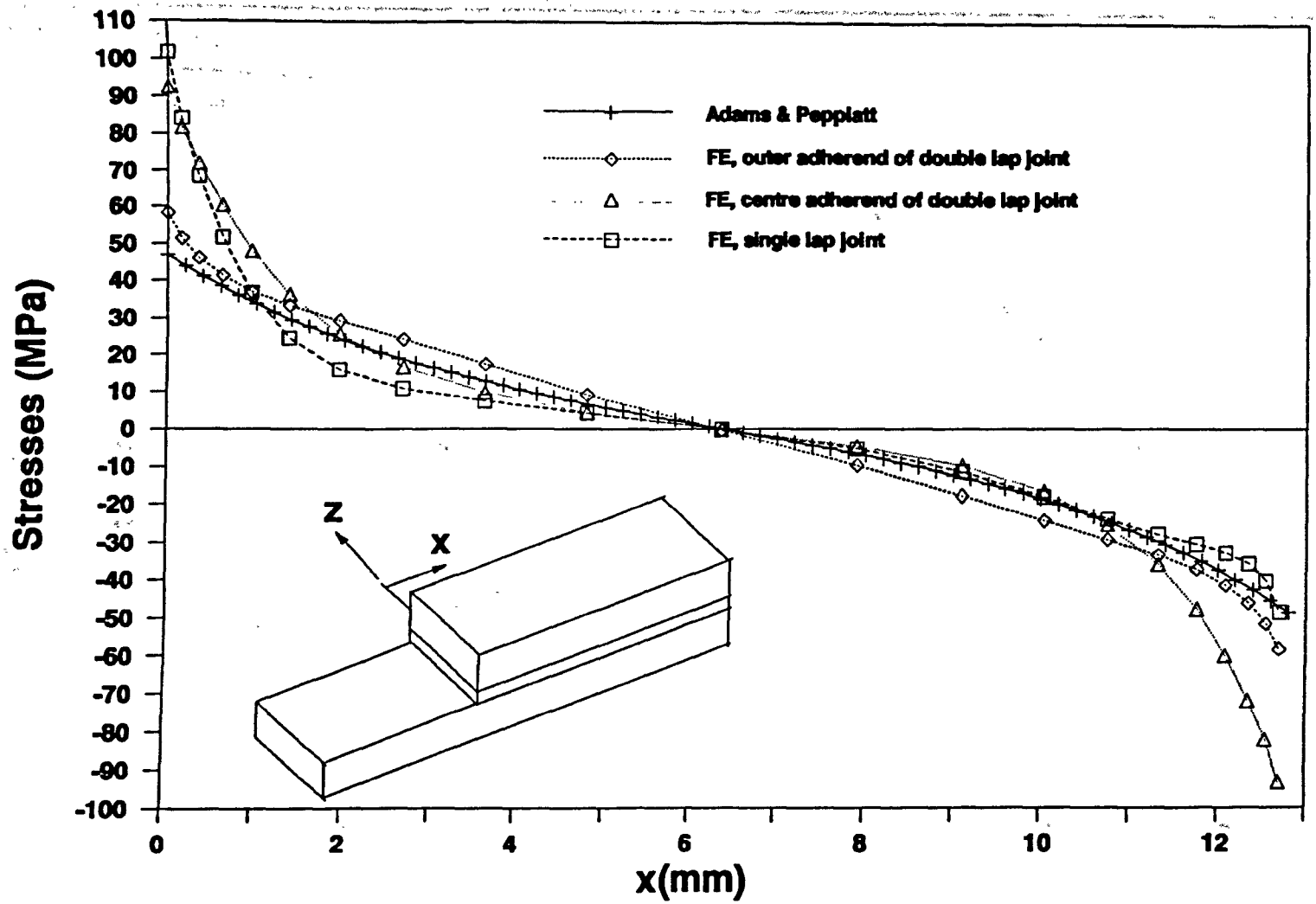

Fig. 5.5 Tensile stresses in the adherend at right angles to load plotted against x at the centre of width

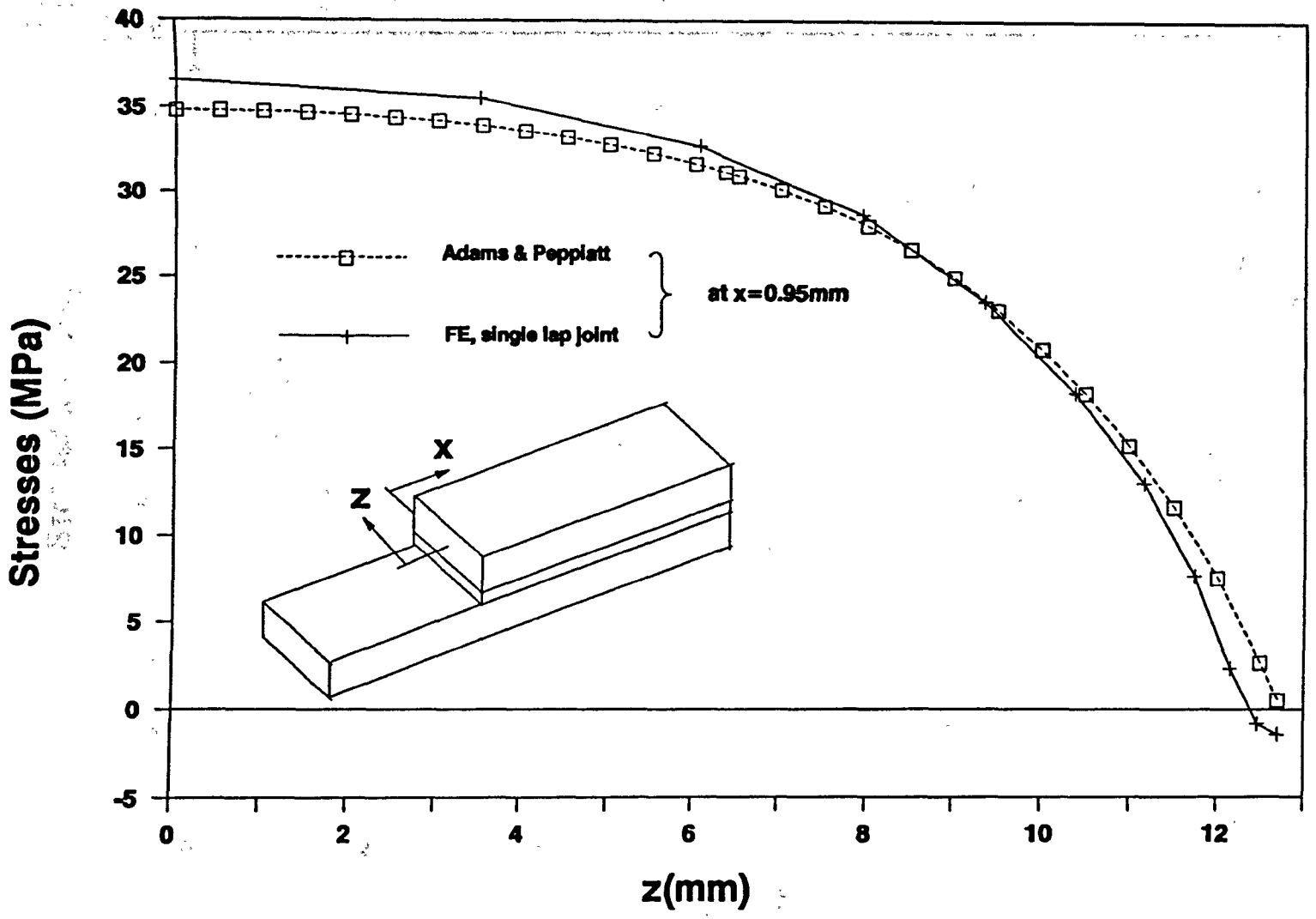

Fig. 5.6 Tensile stress in the adherend at right angles to load plotted across the joint width

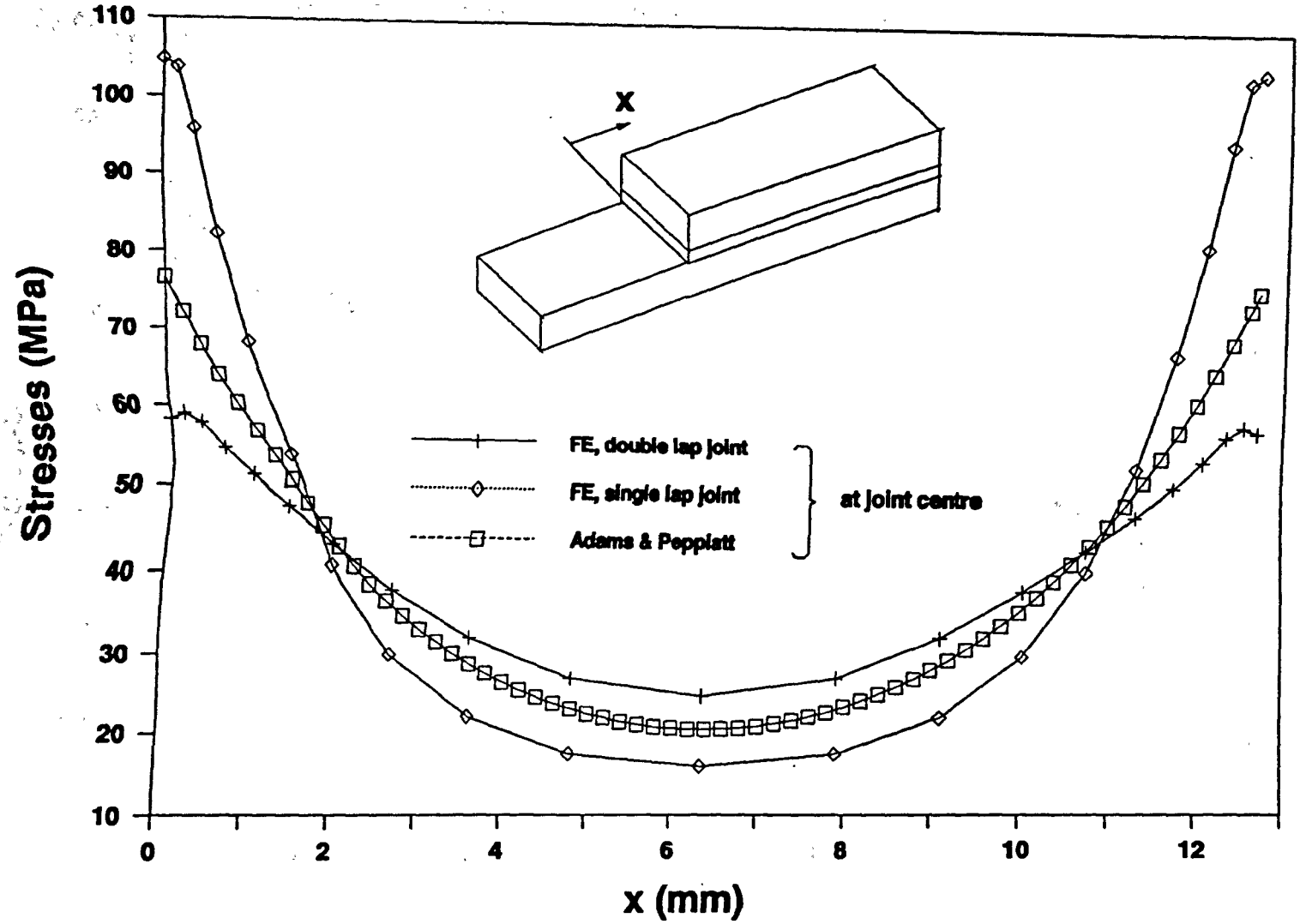

Fig. 5.7 Shear stresses in the adhesive along the overlap at the centre of the joint

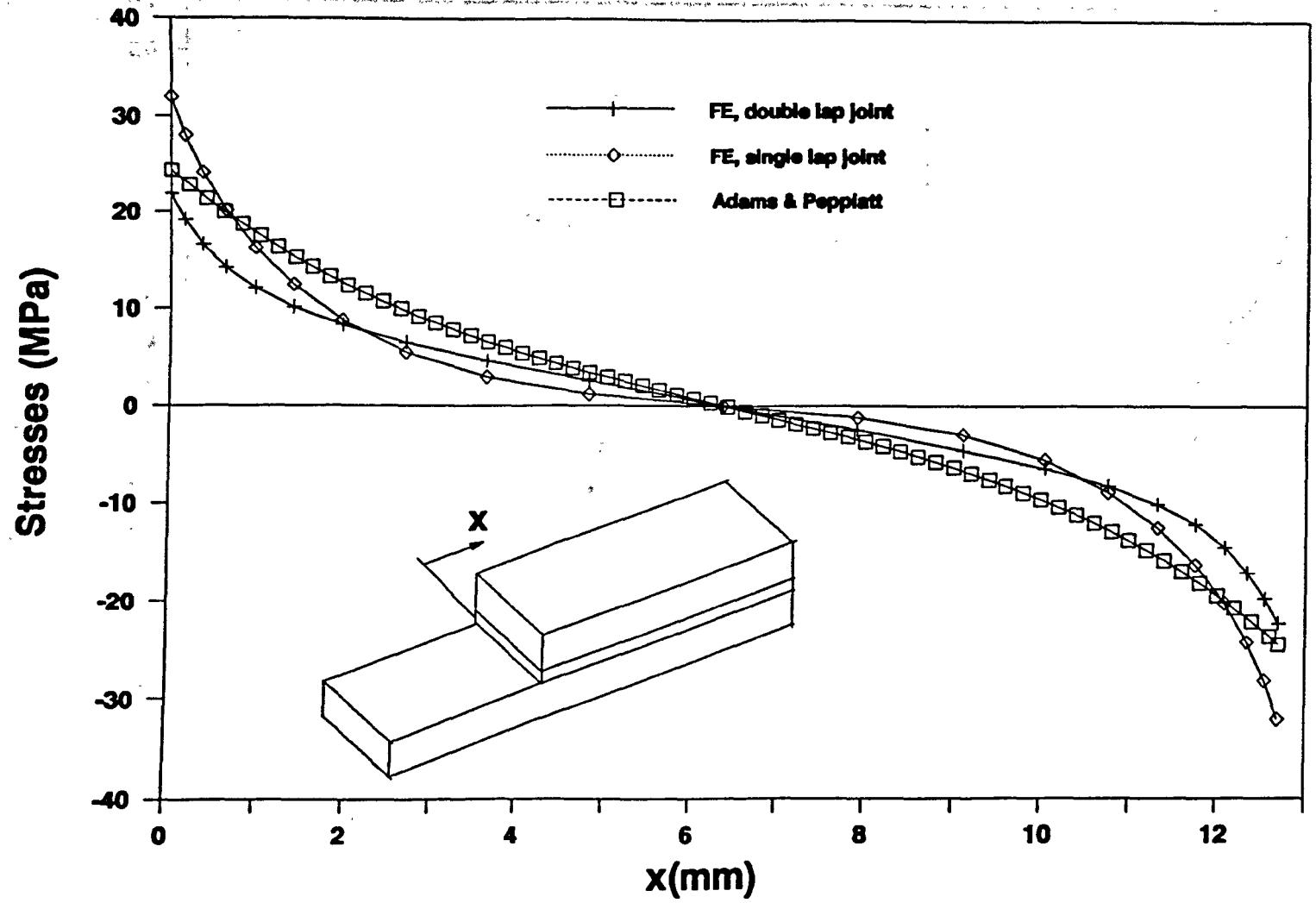

Fig. 5.8 Shear stresses in the adhesive at right angles to the load plotted against x at the edges of the width

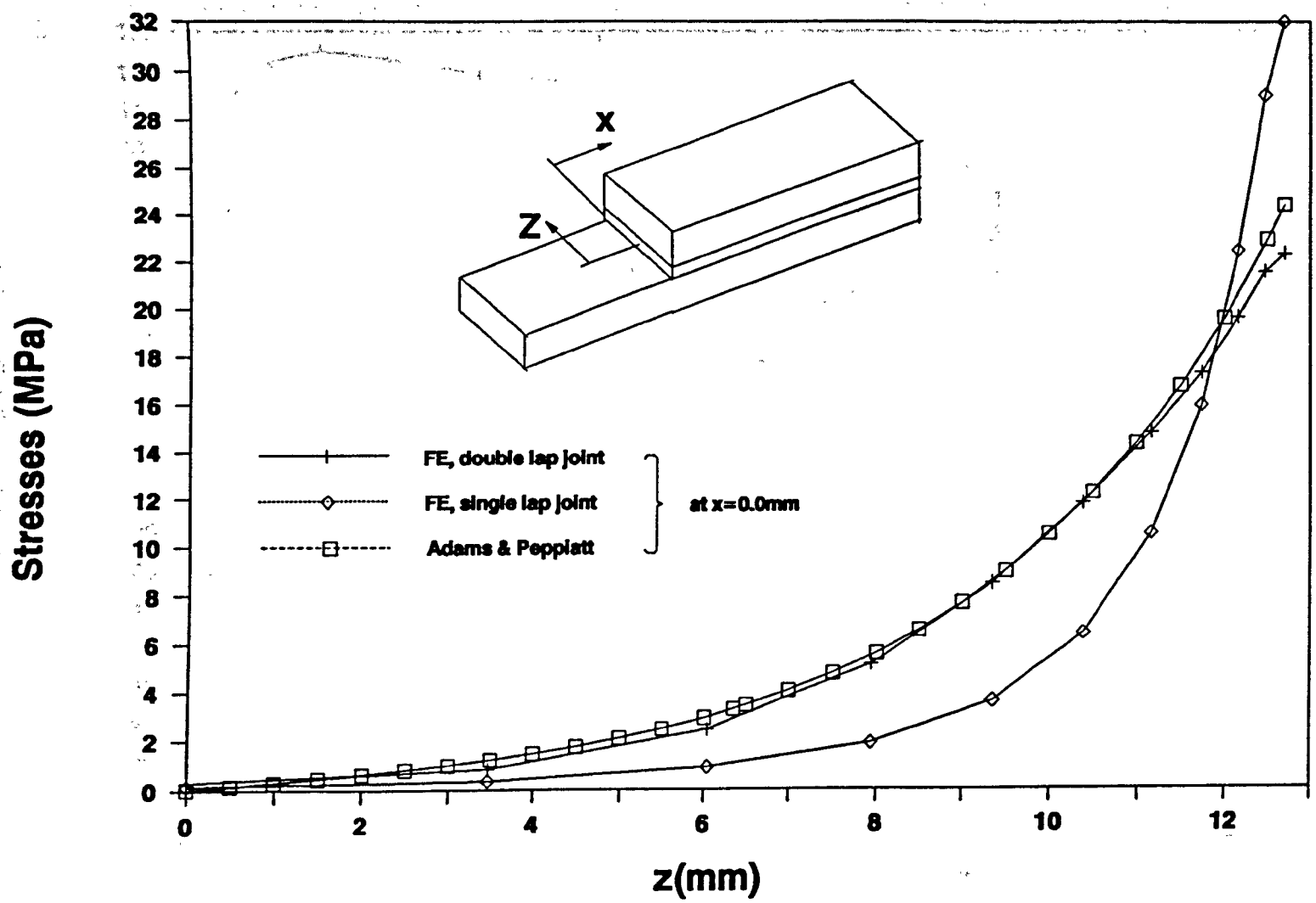

Fig. 5.9 Shear stresses in the adhesive at right angles to the load plotted across the width

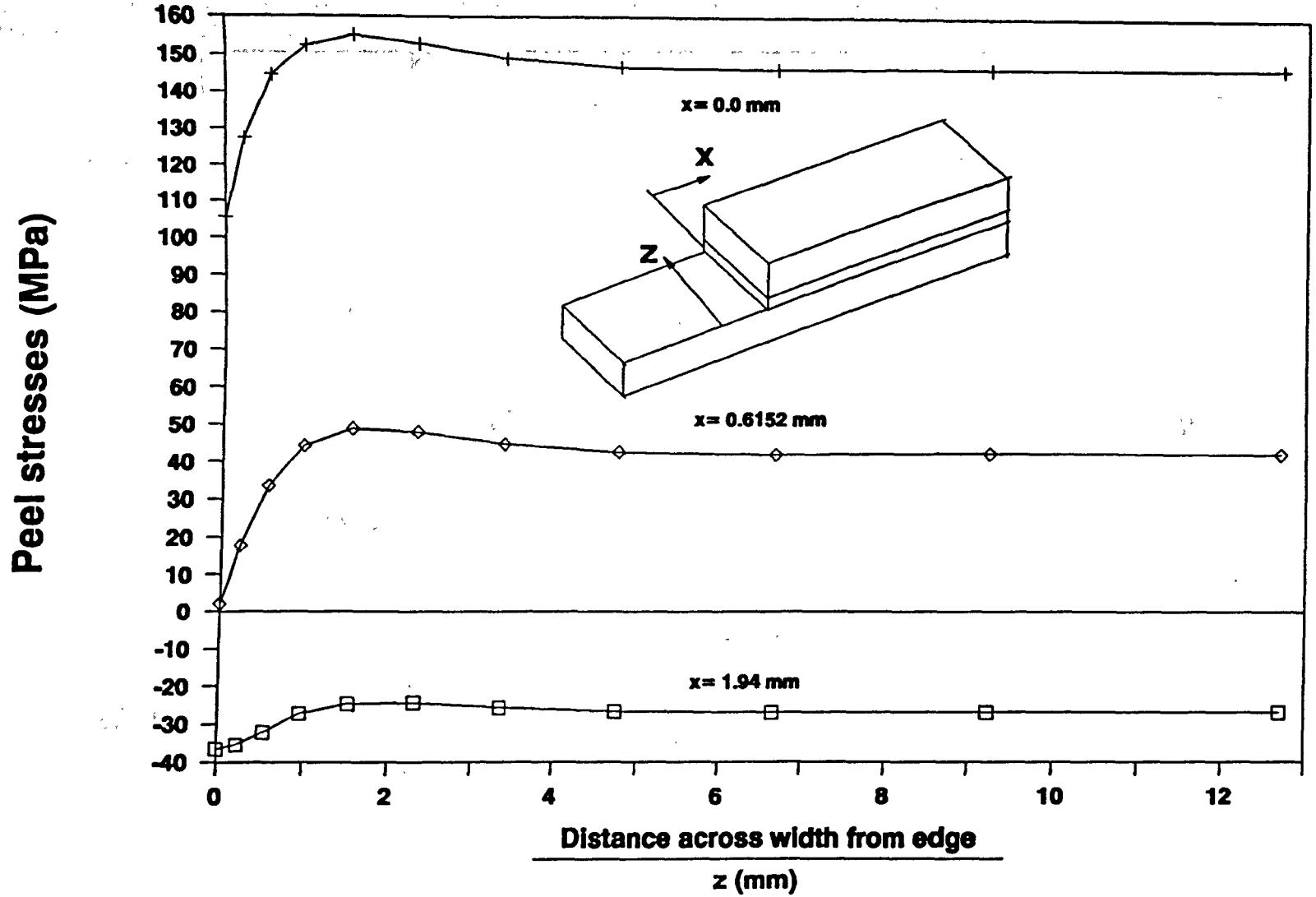

Fig. 5.10 Peel stresses across the width at different positions along overlap

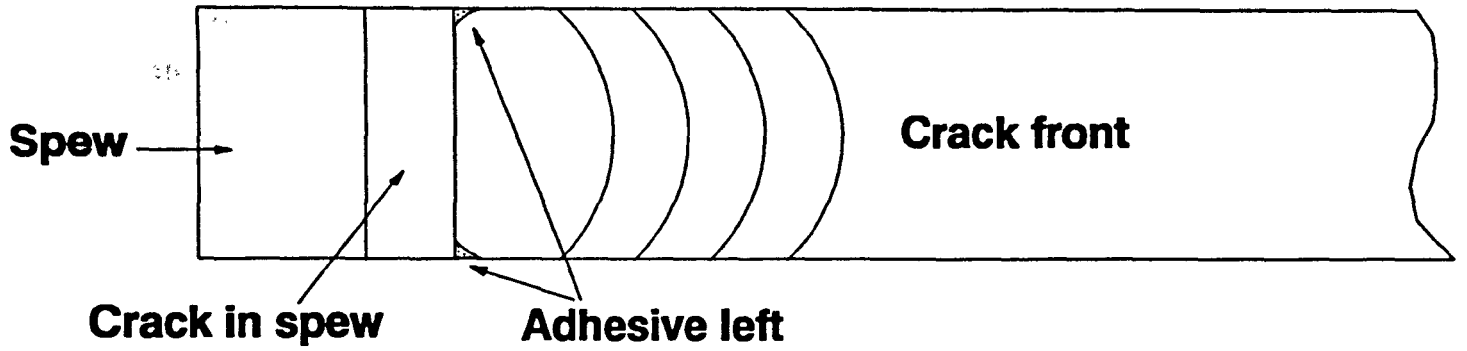

Fig. 5.11 Crack front in a typical lap joint

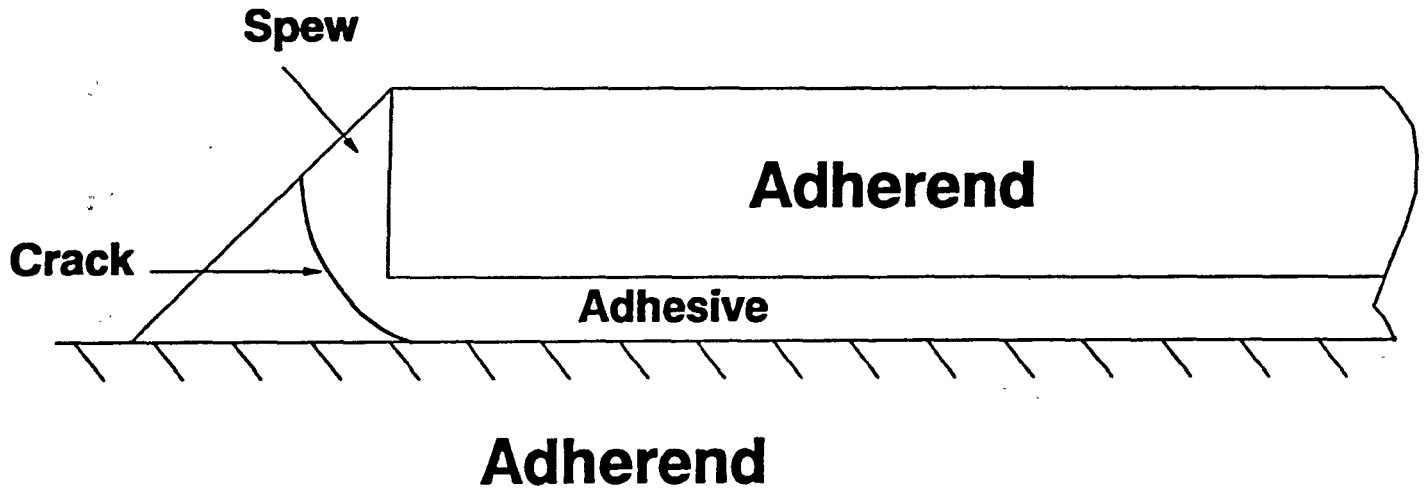

Fig. 5.12 Crack shape at one edge of a lap joint

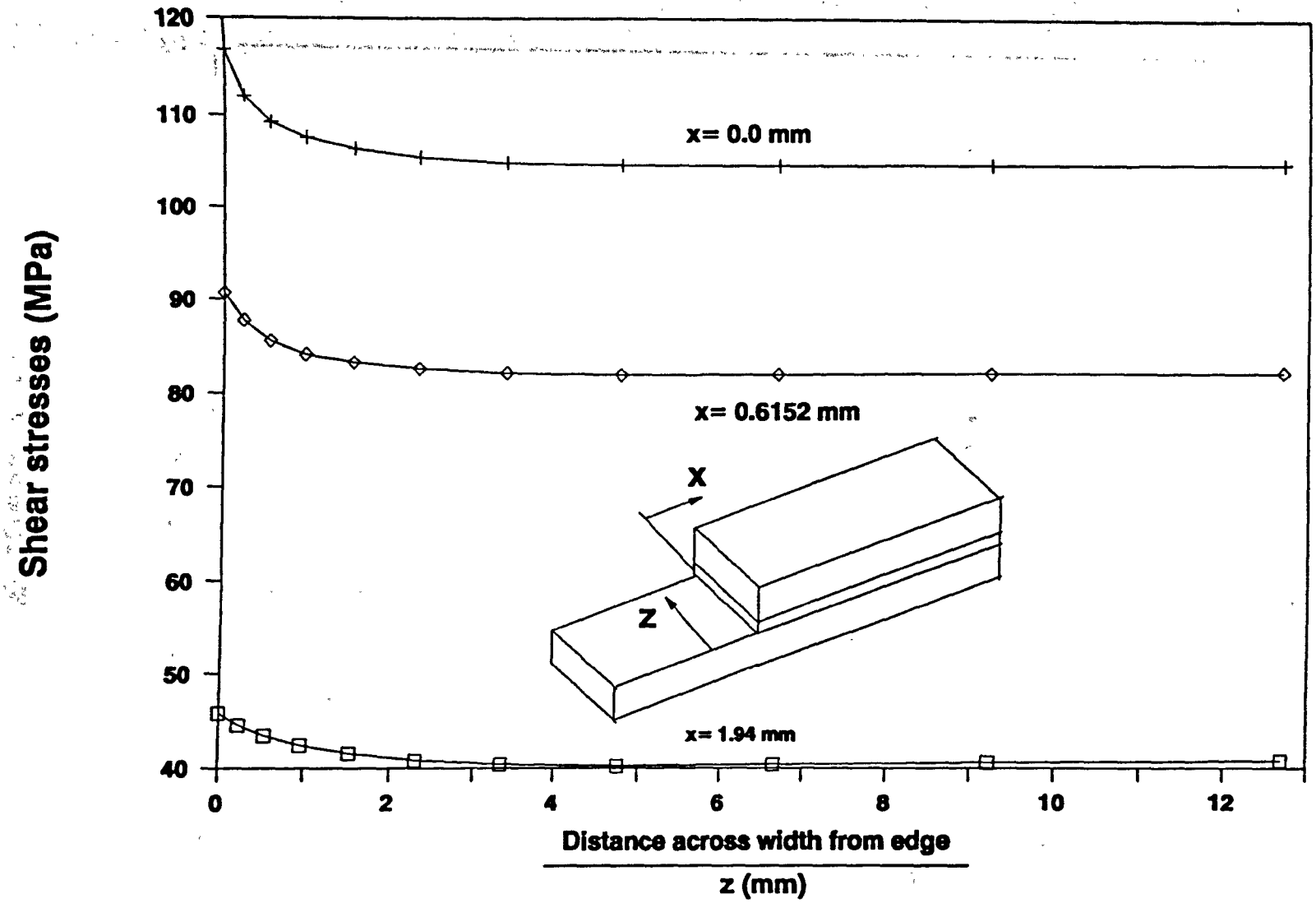

Fig. 5.13 Shear stresses across the width at different positions along the overlap

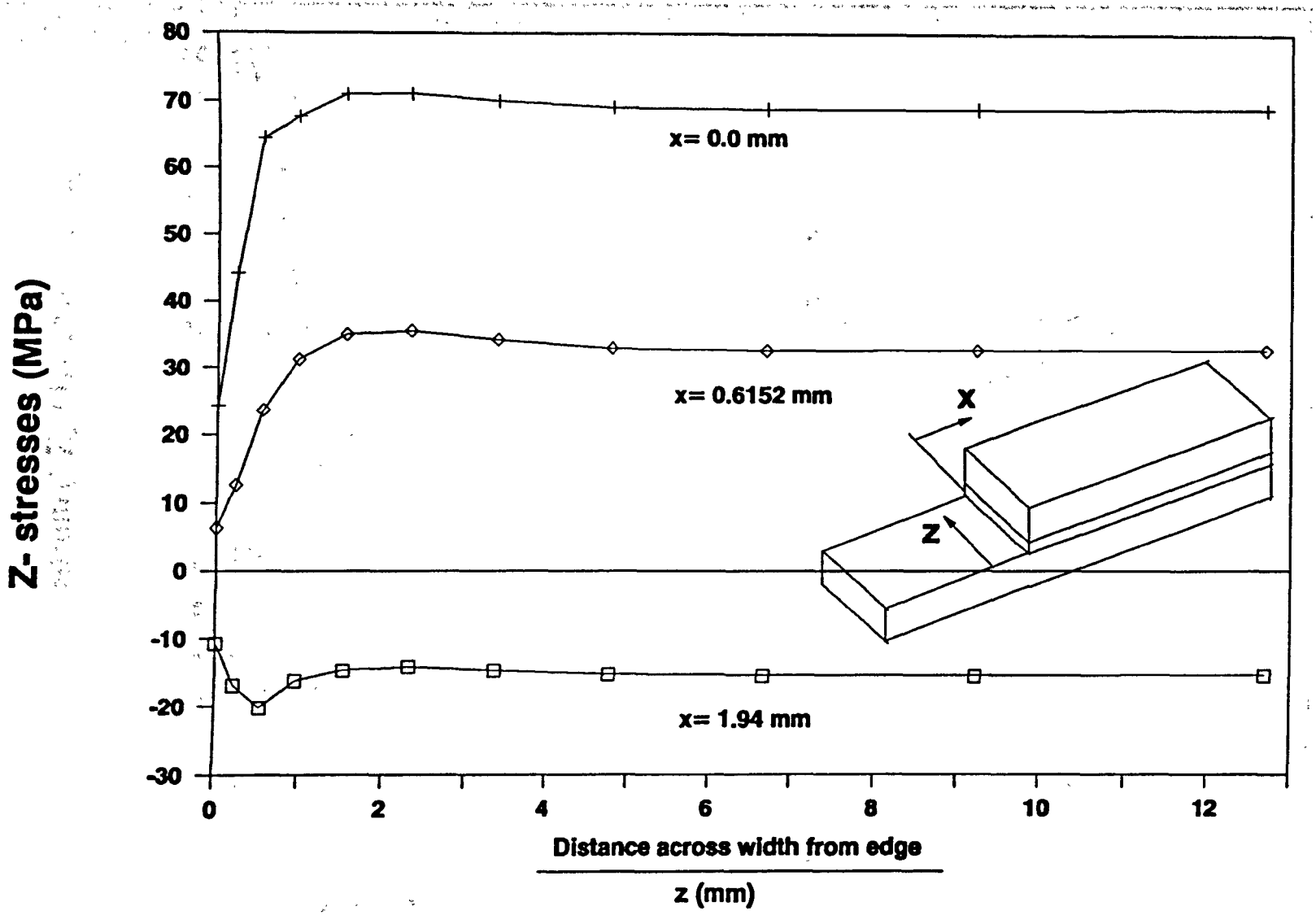

Fig. 5.14 Z- stresses across the width at different positions along the overlap

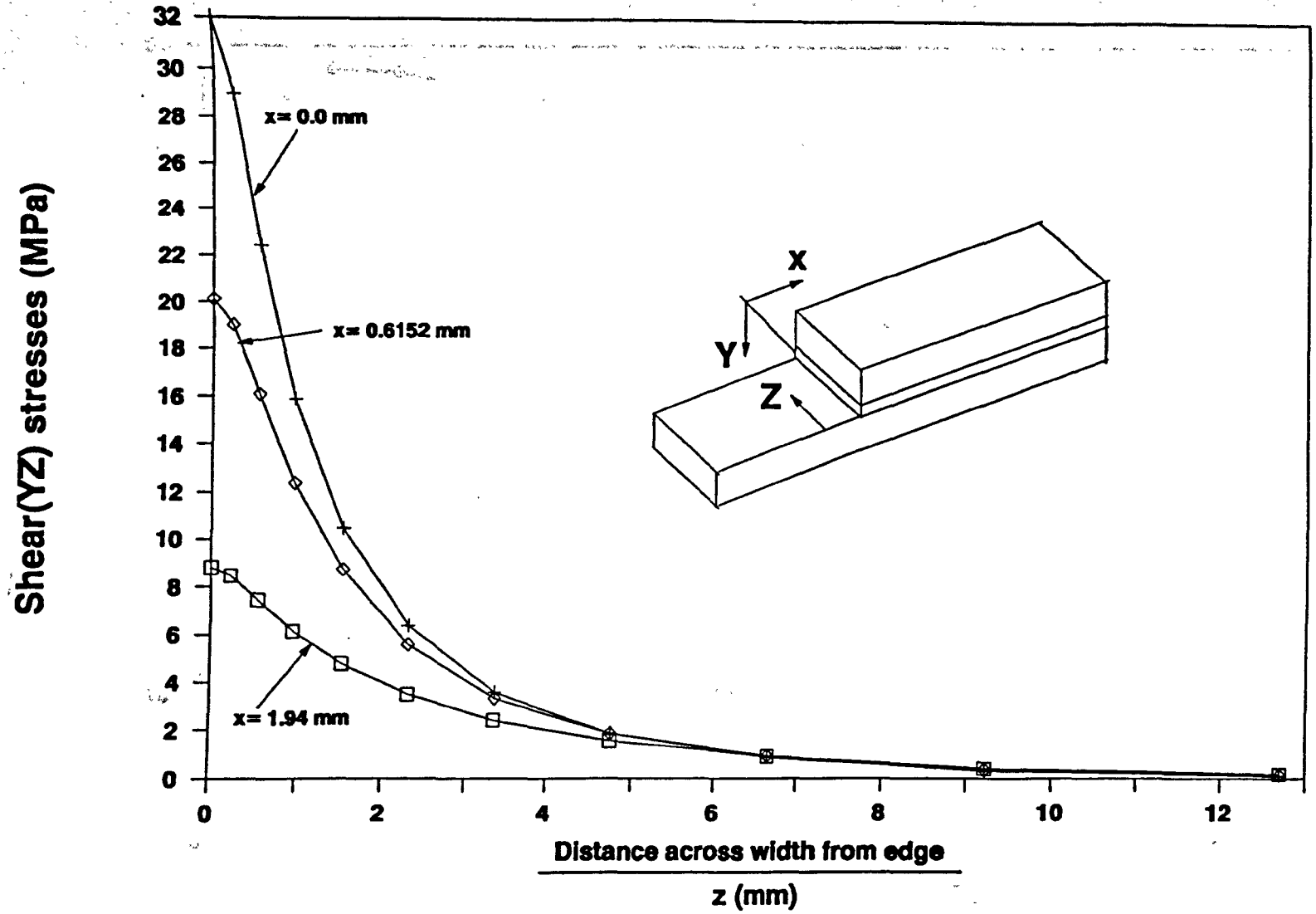

Fig. 5.15 Shear(YZ)- stresses across the width at different positions along the overlap

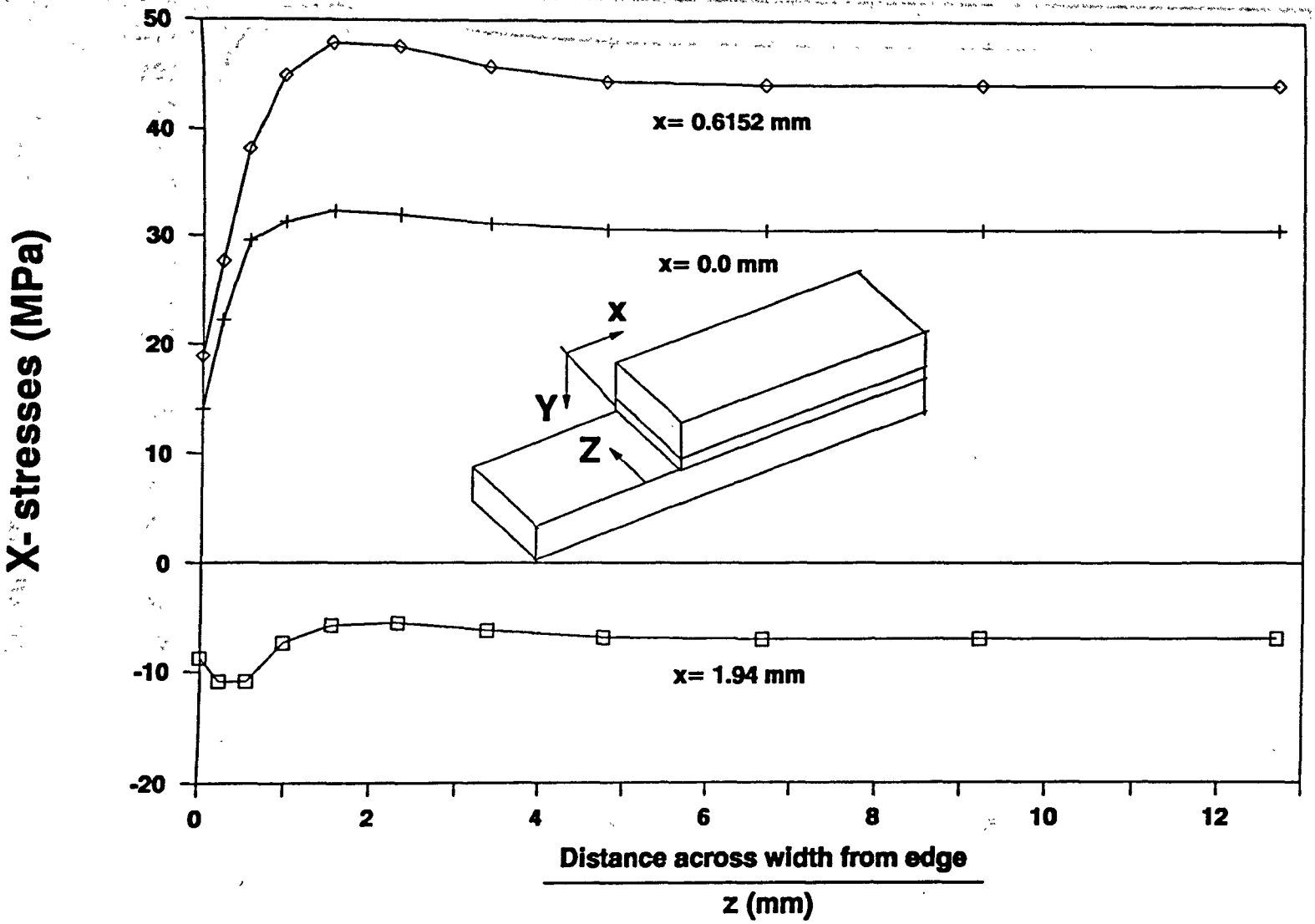

Fig. 5.16 X-stresses across the width at different positions along the overlap

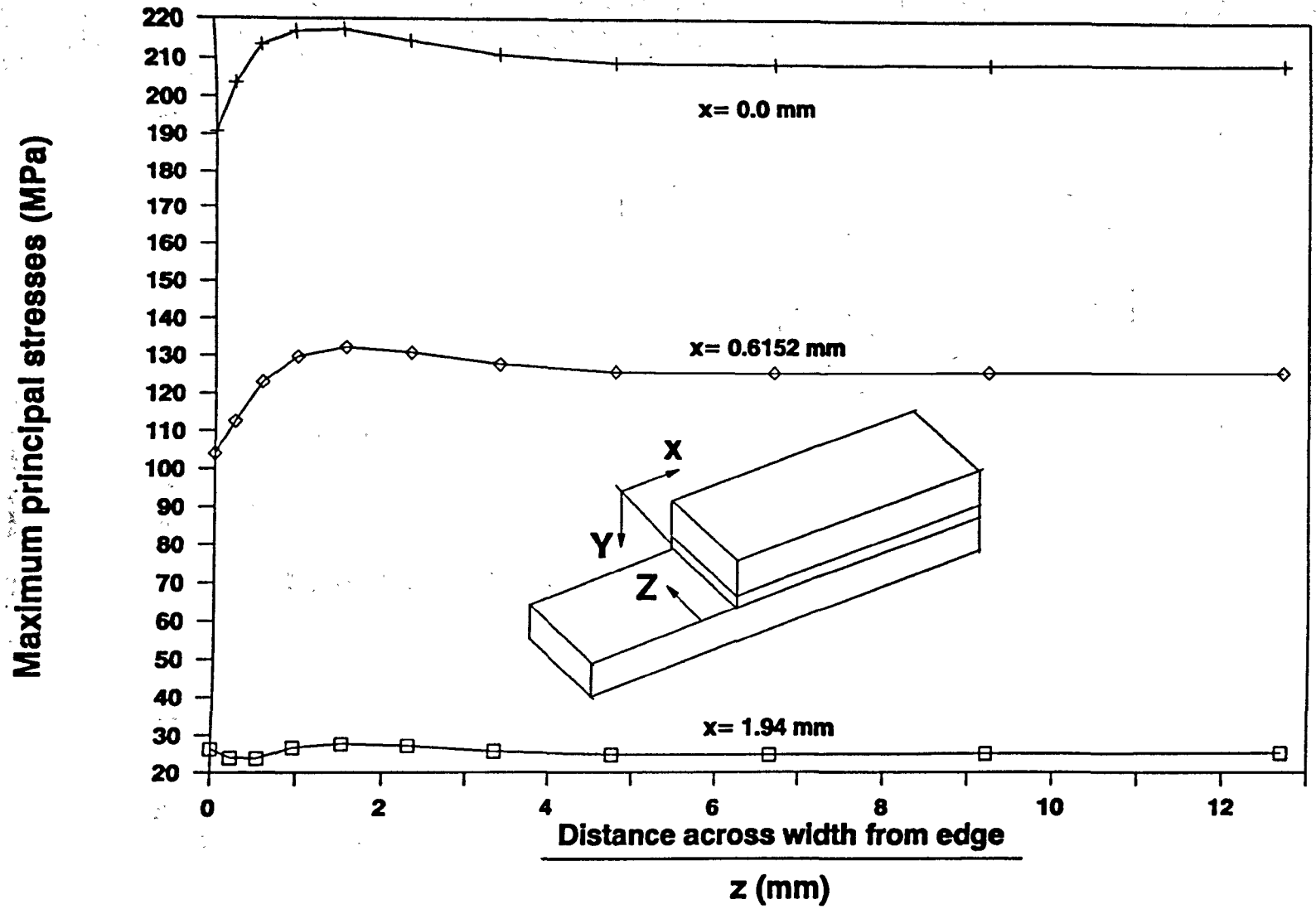

Fig. 5.17 Maximum principal stresses across the width at different positions along the overlap

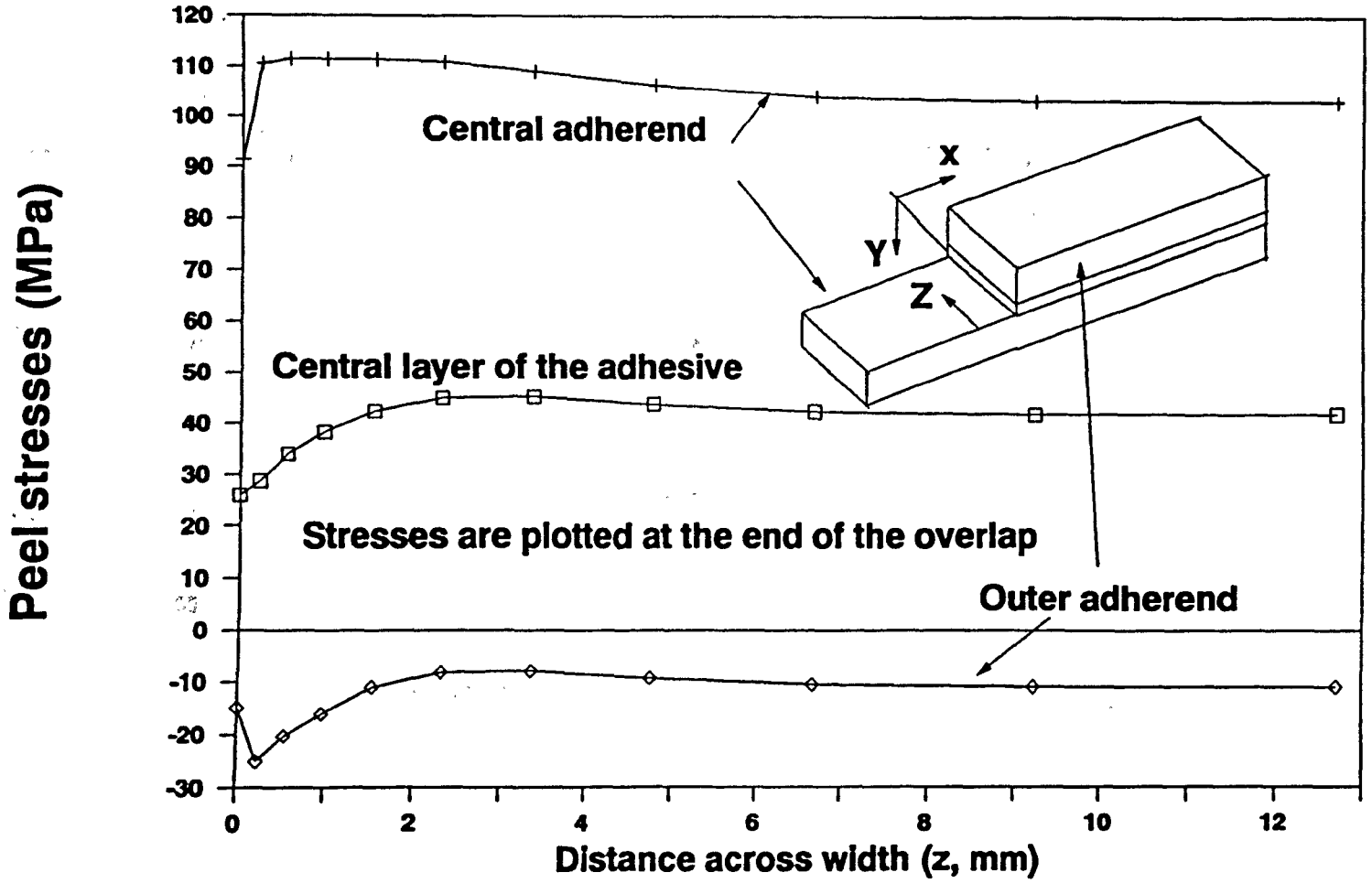

Fig. 5.18 Peel stresses at the end of the overlap for a double lap joint

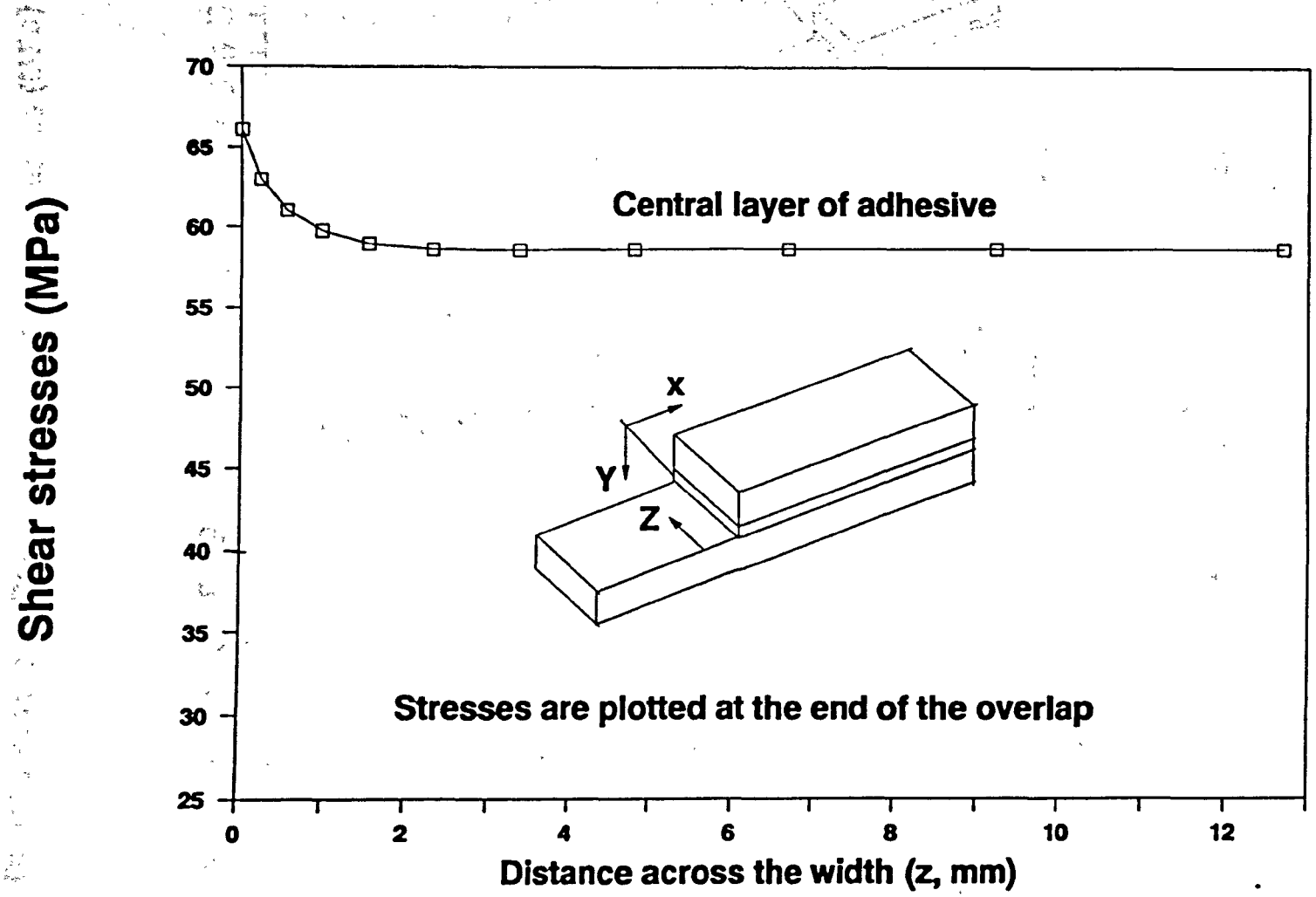

Fig. 5.19 Longitudinal shear stresses in the adhesive for a double lap joint

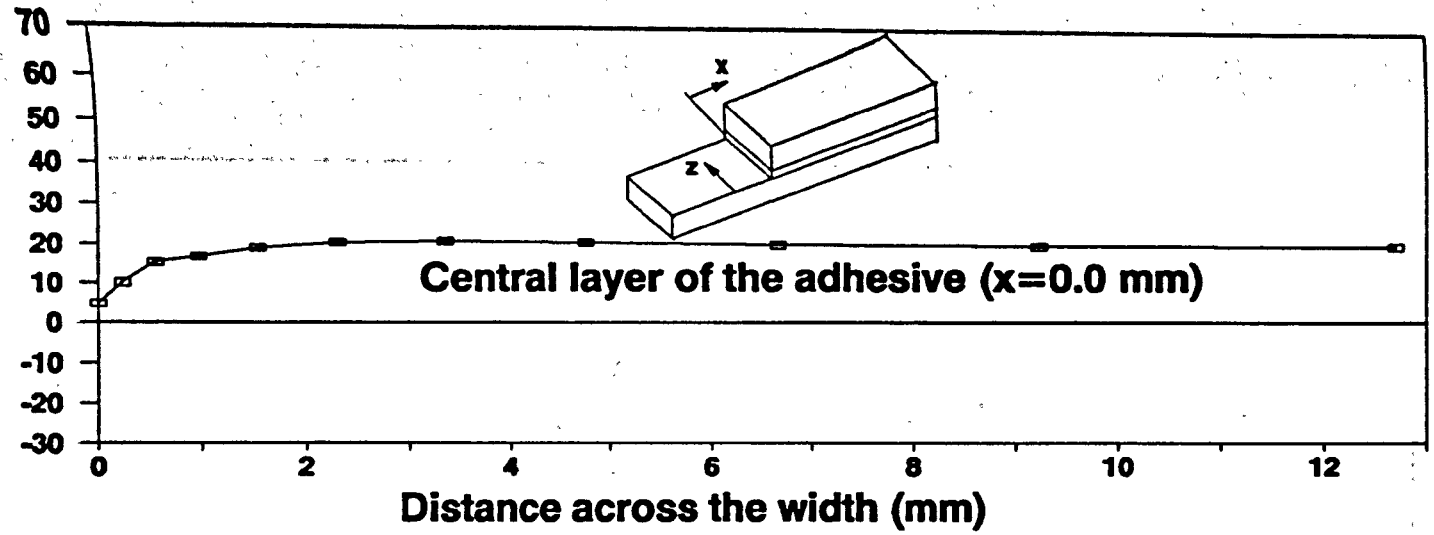

Fig. 5.20. Z Direct stresses for a double lap joint

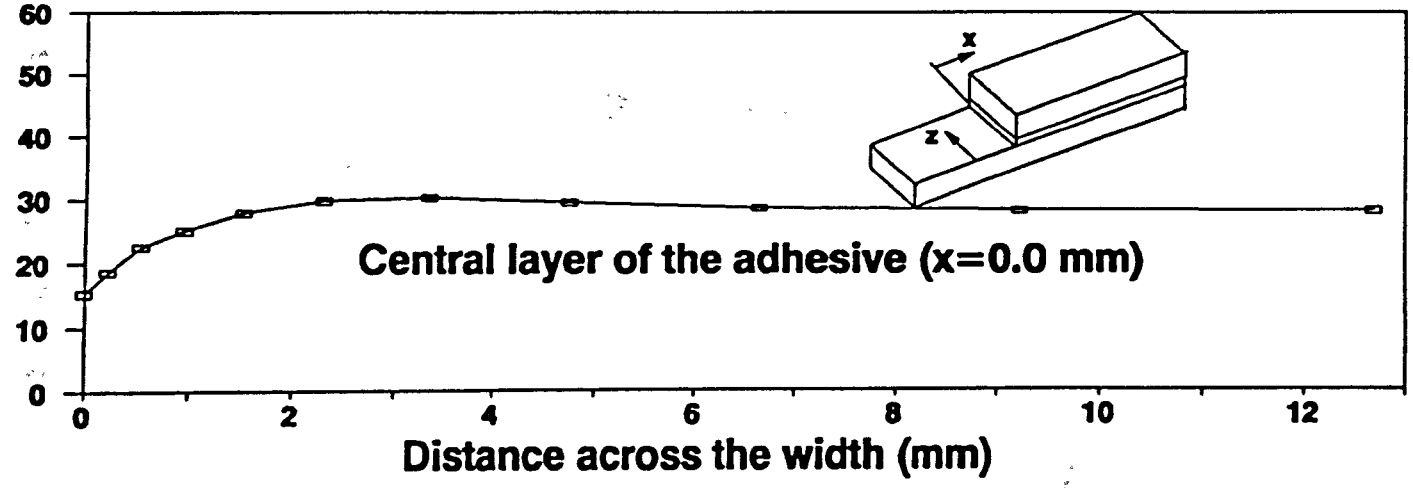

Fig. 5.21 X Direct stresses for a double lap joint

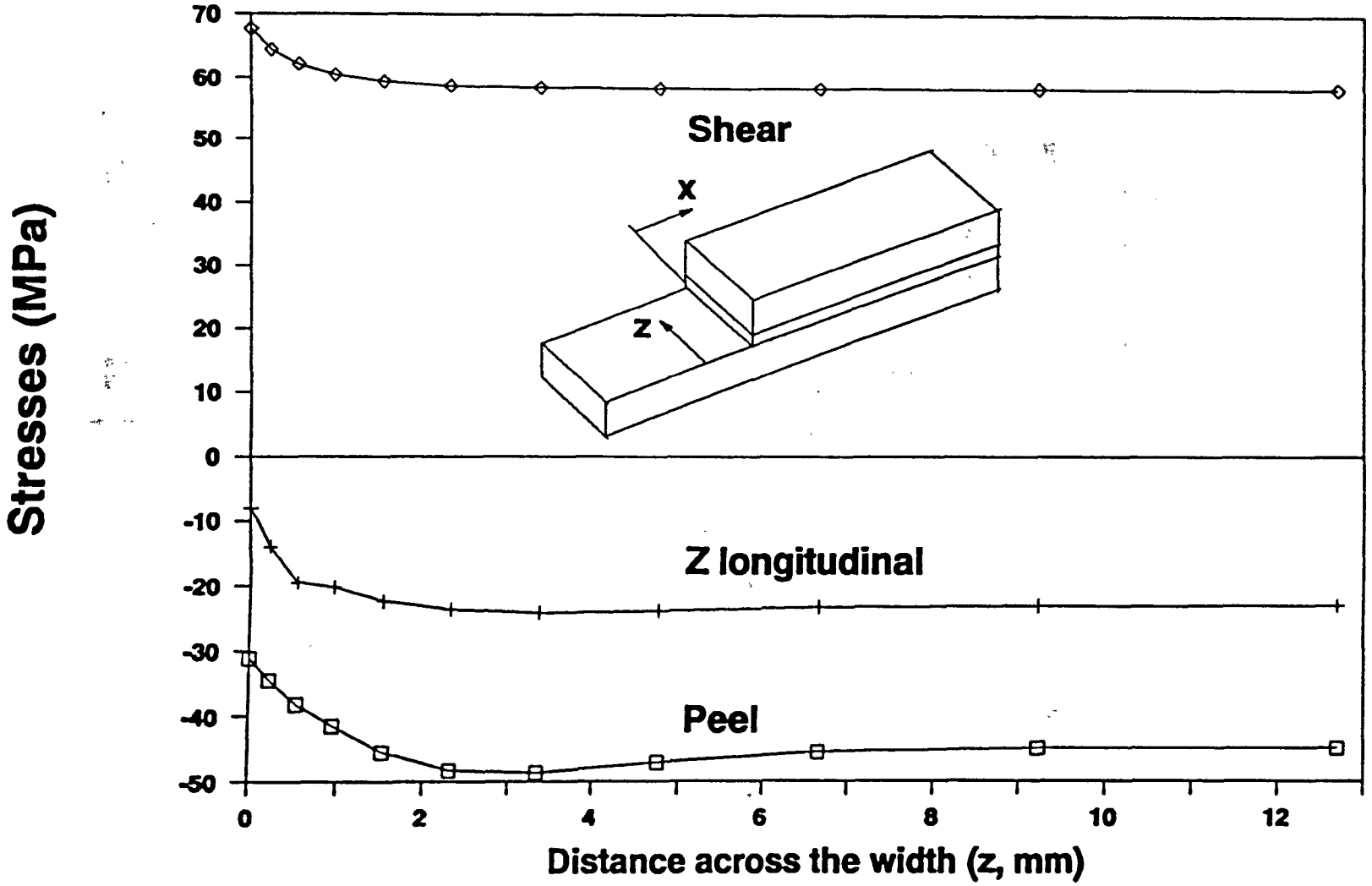

Fig. 5.22 Stresses at compression end of a double lap joint

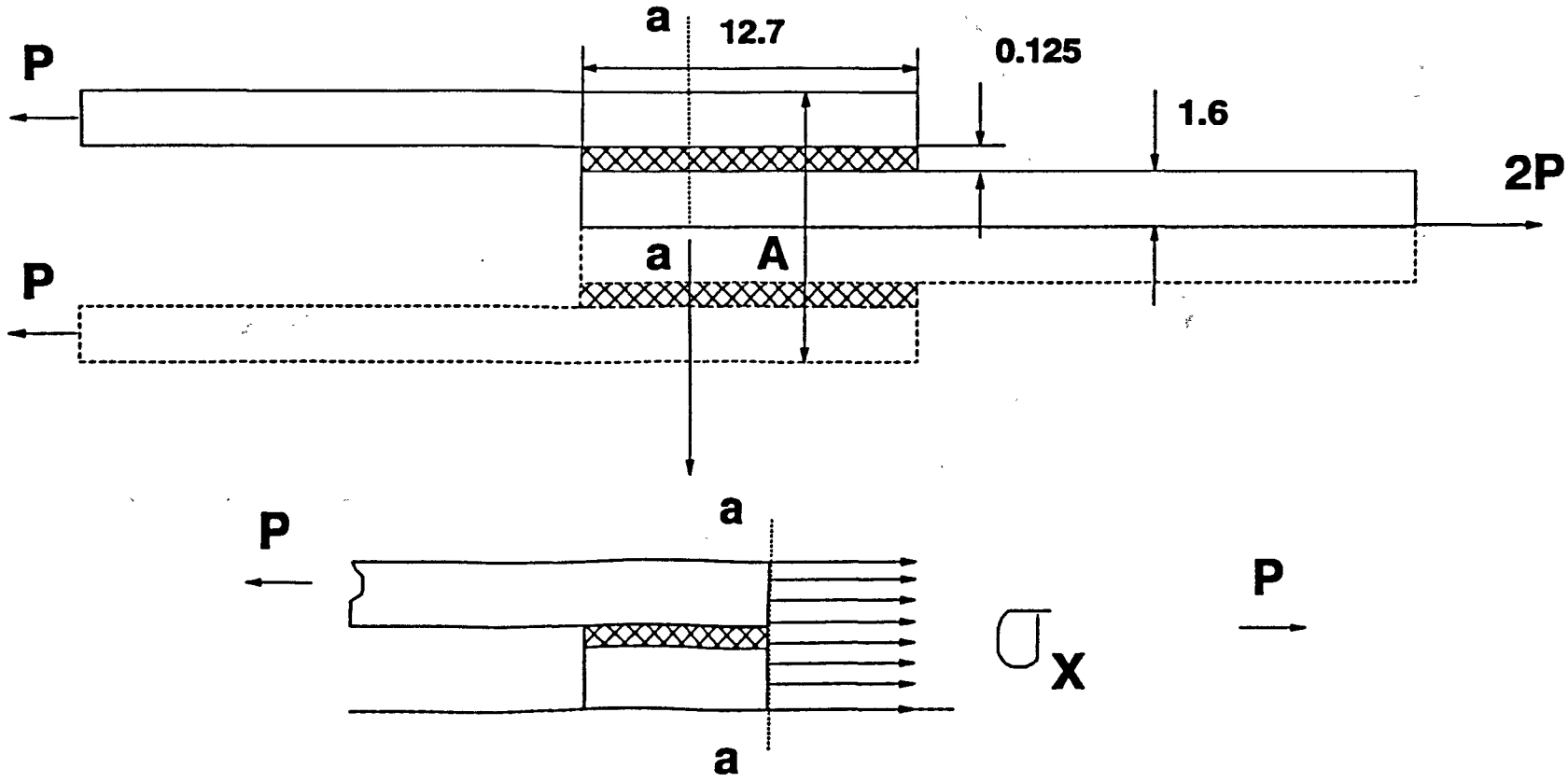

Fig. 6.1 Geometries of joints without spew fillets (not to scale)

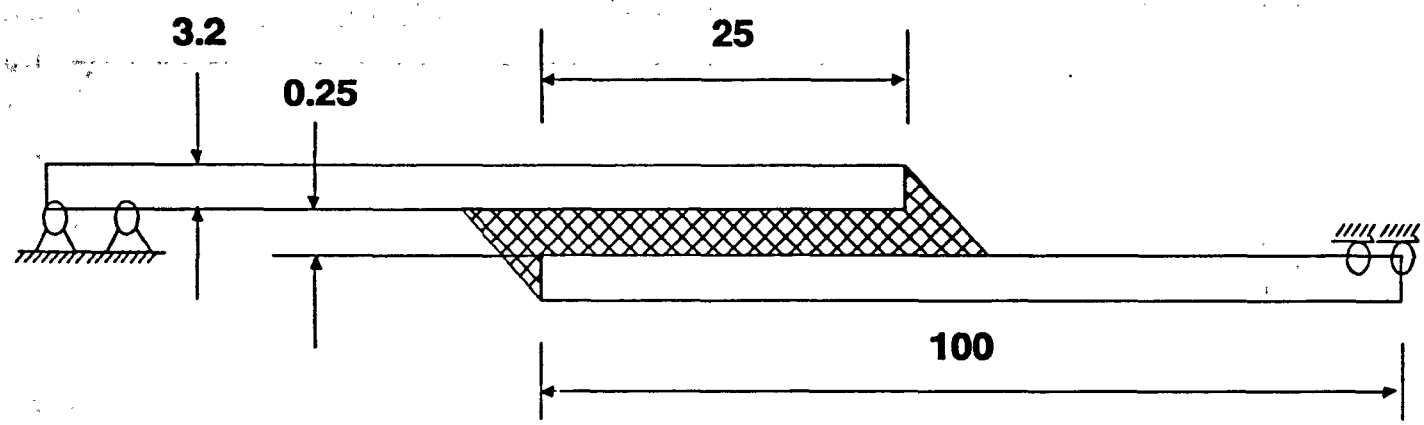

(a). single lap joint geometry (all dimensions in mm)

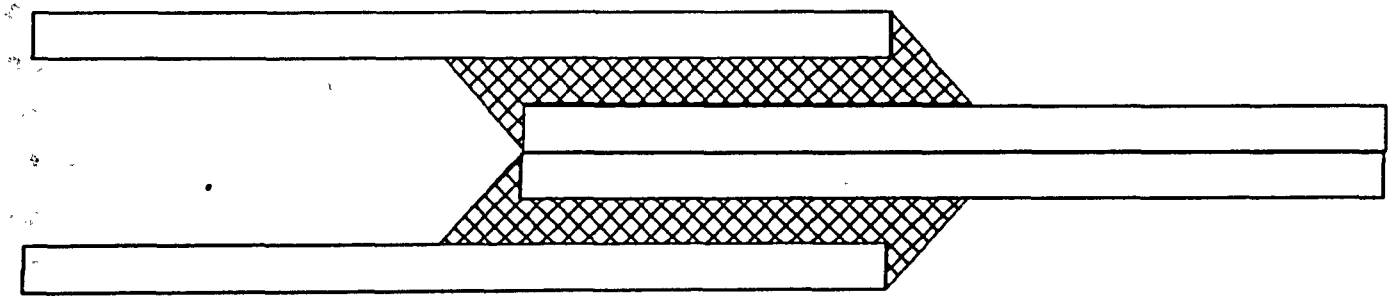

(b). double lap joint geometry (the same dimensions as above)

Fig. 6.2 Geometries for joints with spew fillets

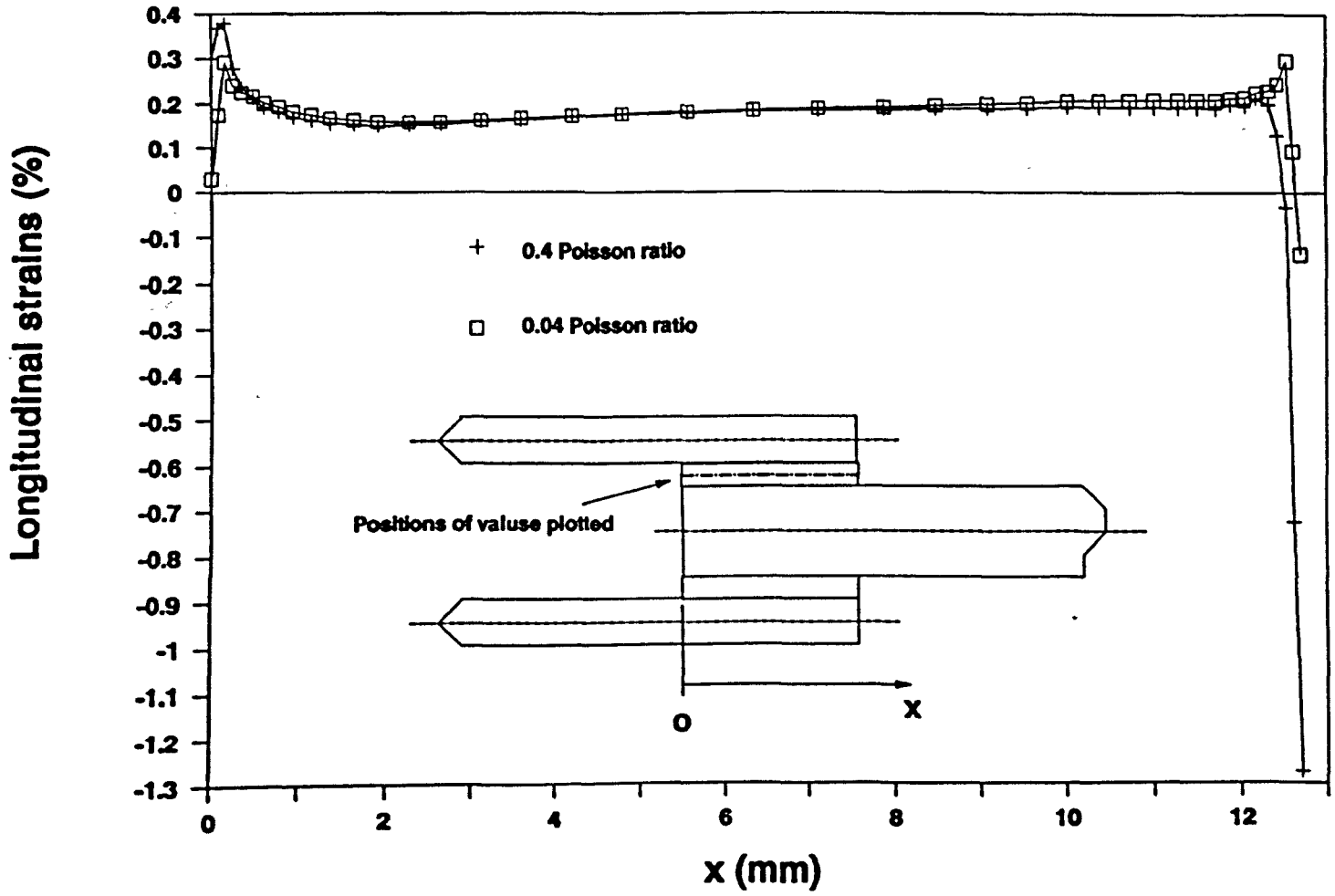

Fig. 6.3 Direct strains (percent) for a double lap joint without fillets

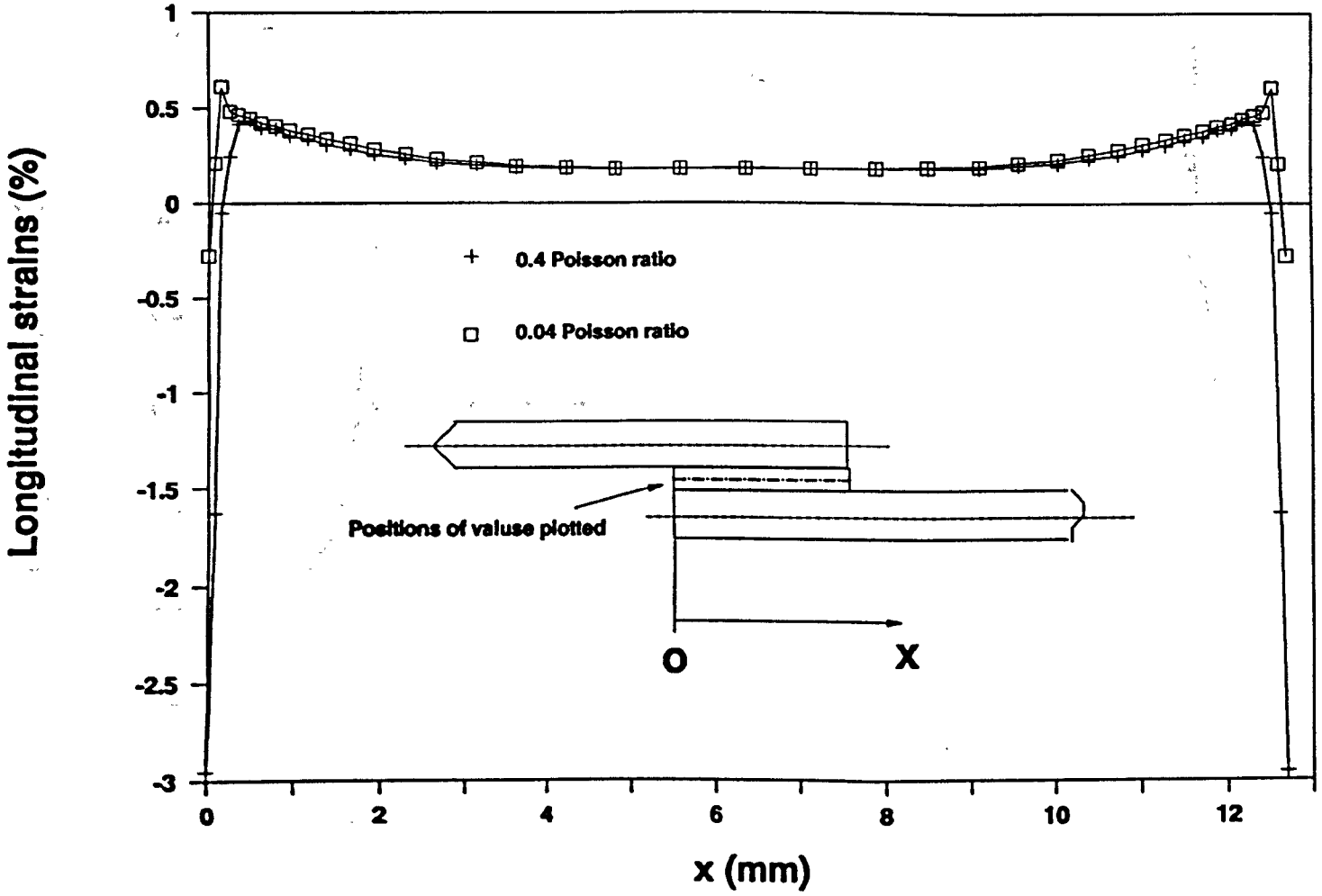

Fig. 6.4 Direct strains (percent) for a single lap joint without fillets

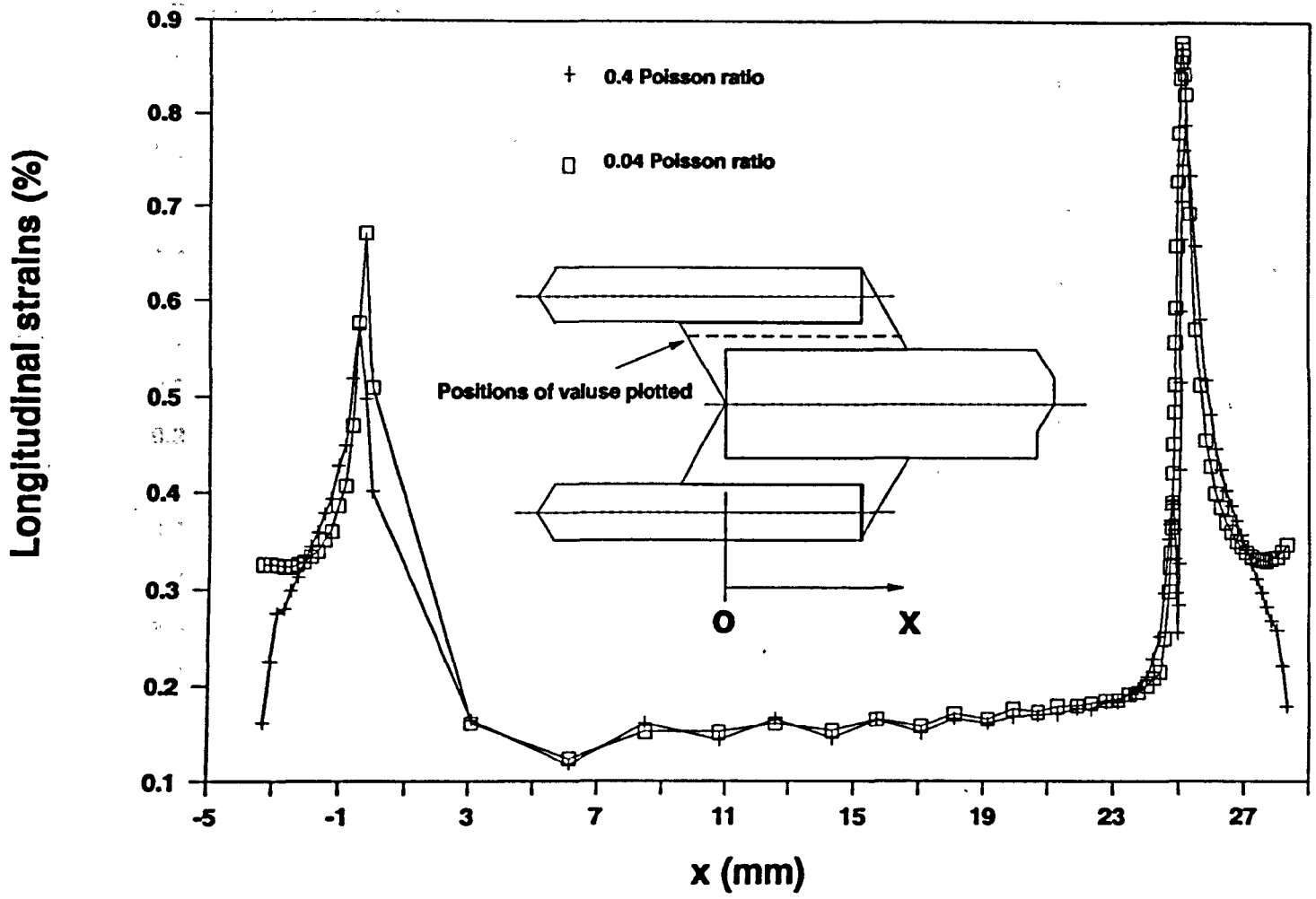

Fig. 6.5 Direct strains (percent) for a double lap joint with spew fillets

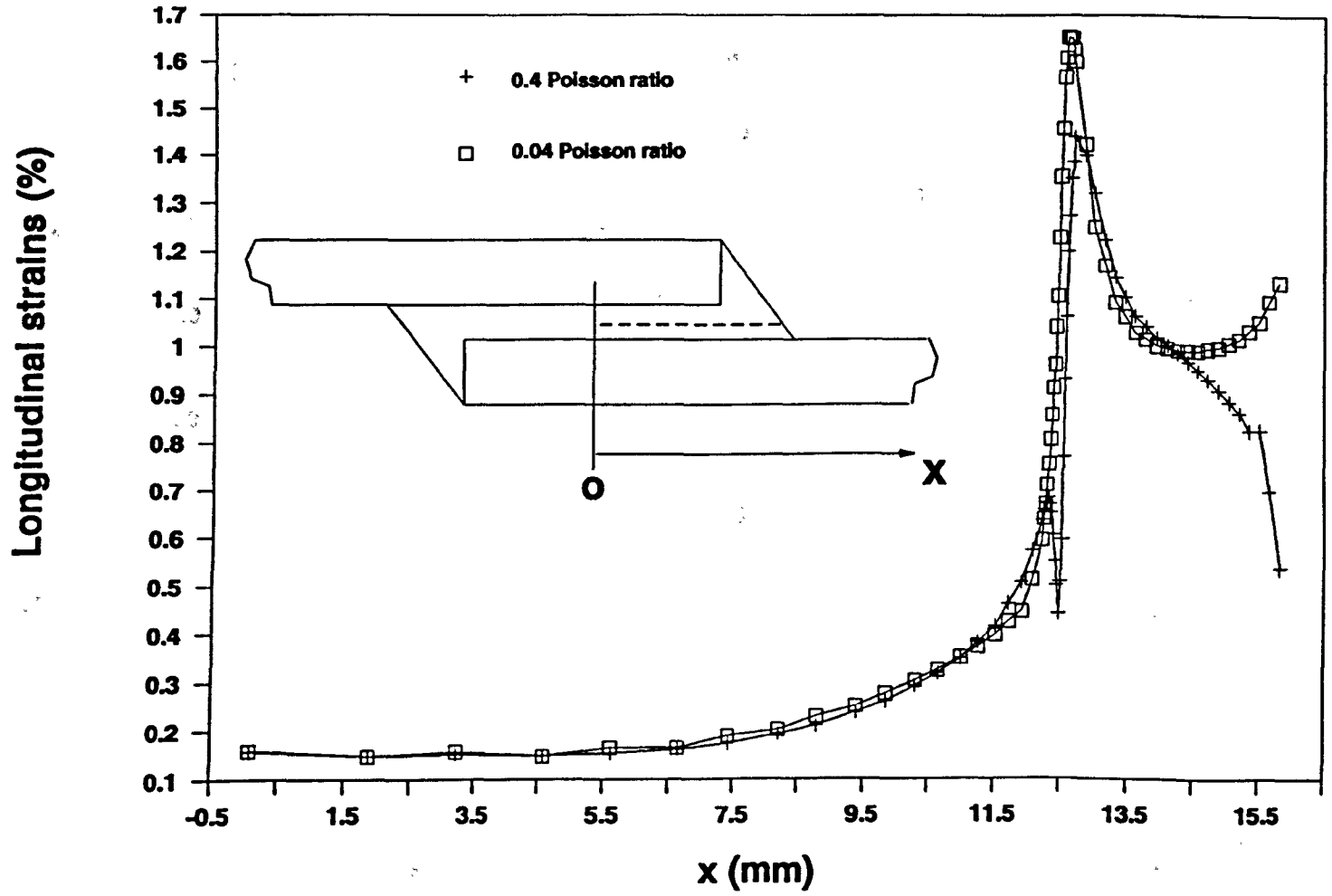

Fig. 6.6 Direct strains (percent) for a single lap joint with spew fillets

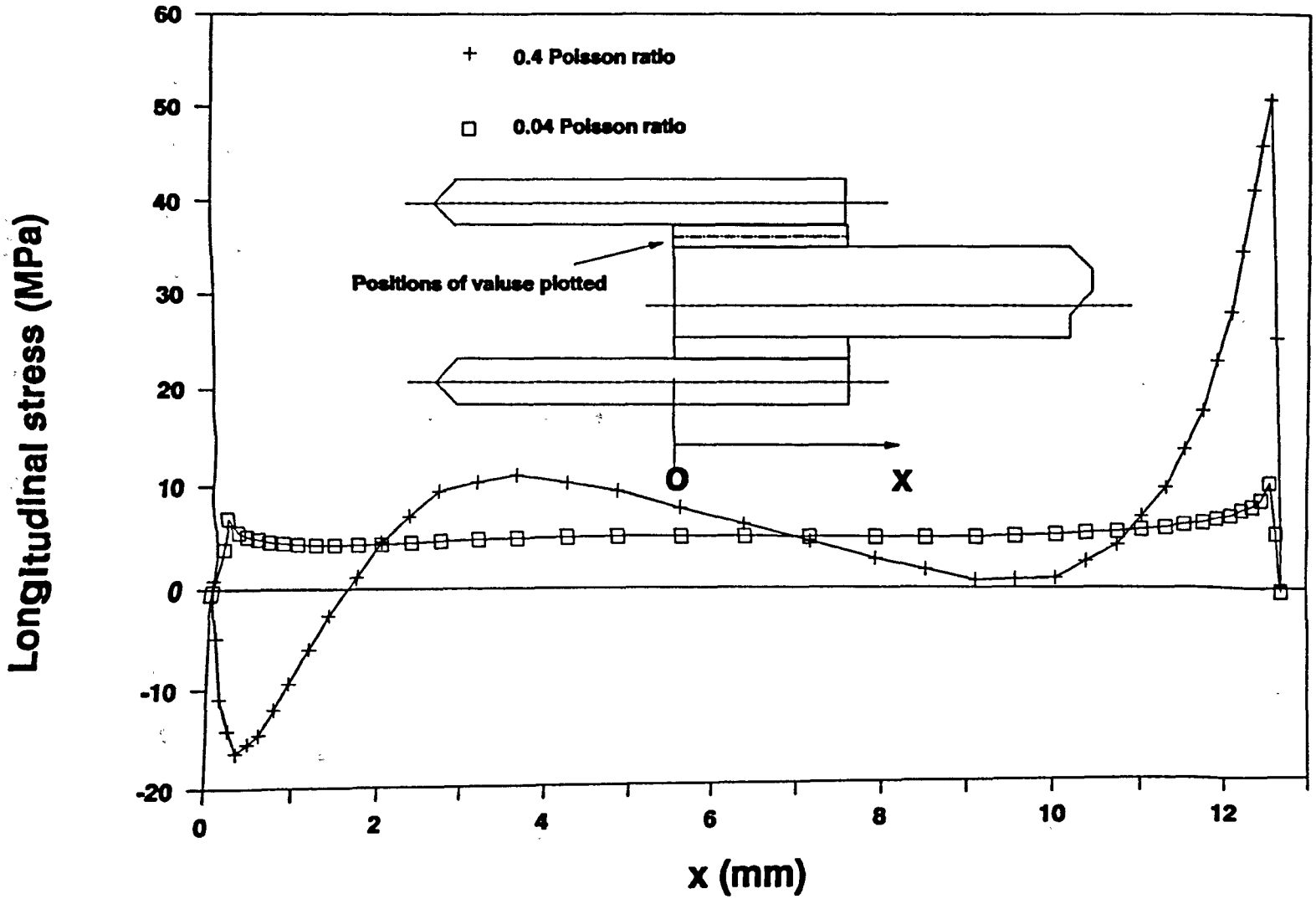

Fig. 6.7 Direct stresses for a double lap joint without fillets

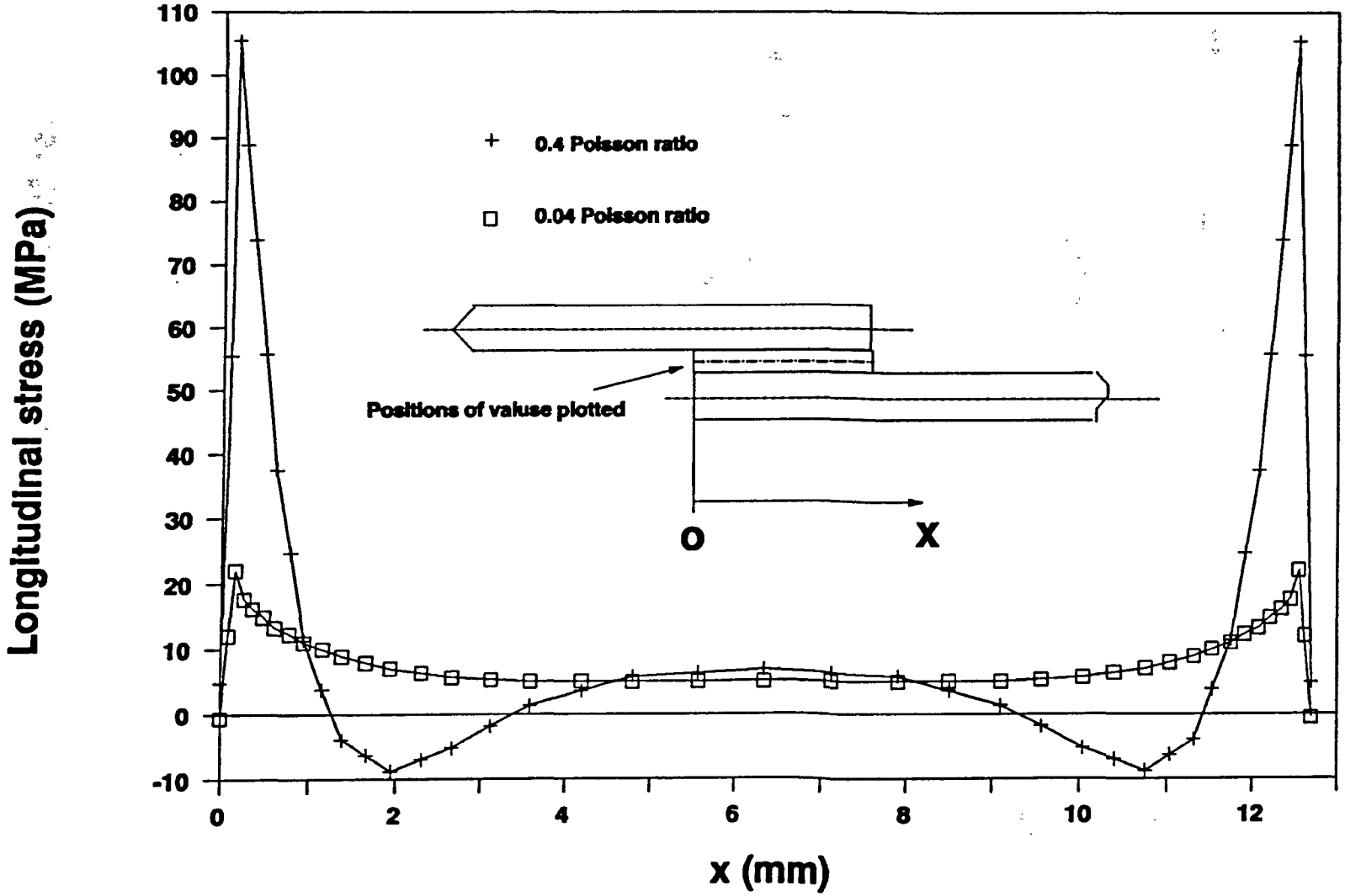

Fig. 6.8 Direct stresses for a single lap joint without fillets

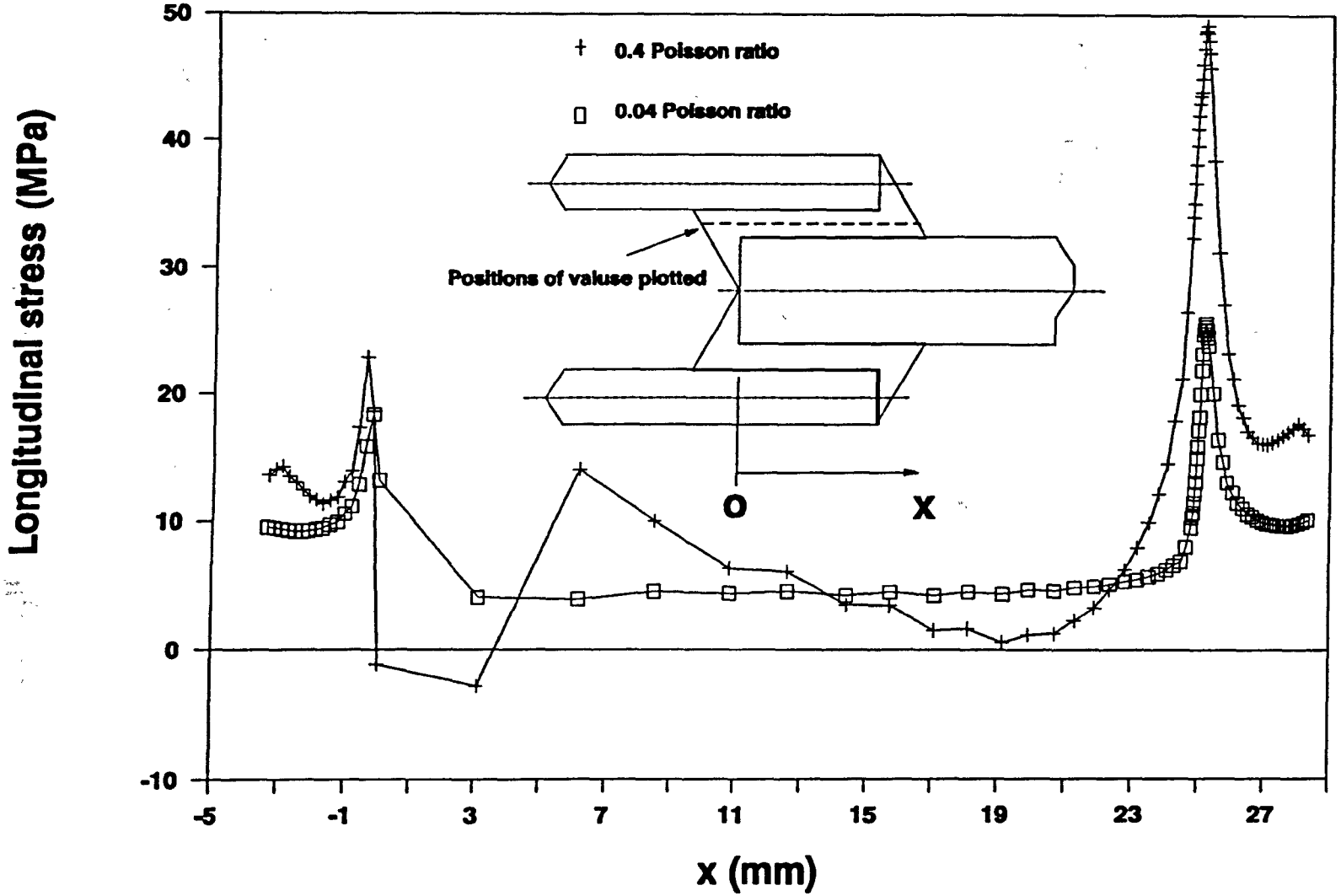

Fig. 6.9 Direct stresses for a double lap joint with spew fillets

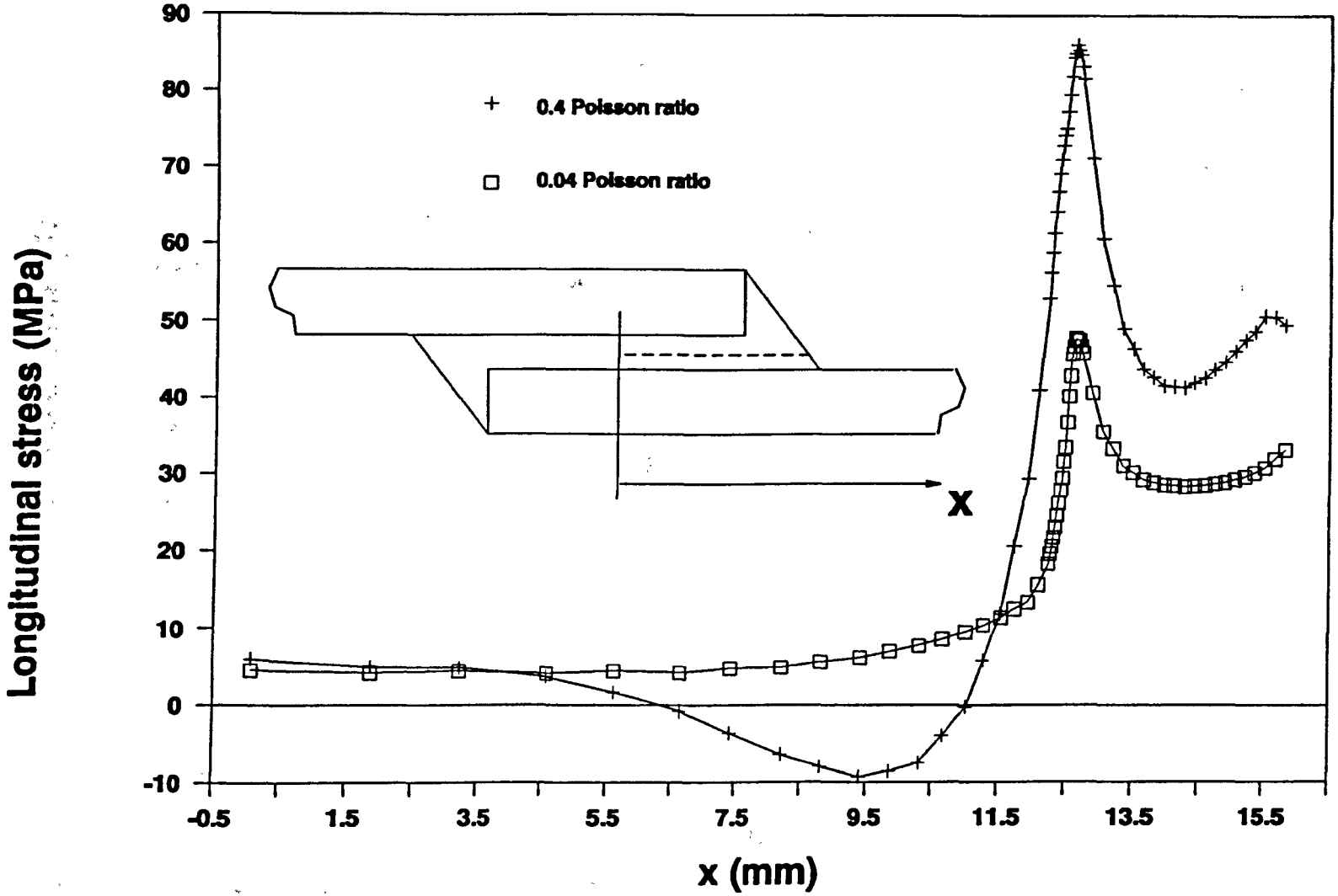

Fig. 6.10 Direct stresses for a single lap joint with spew fillets

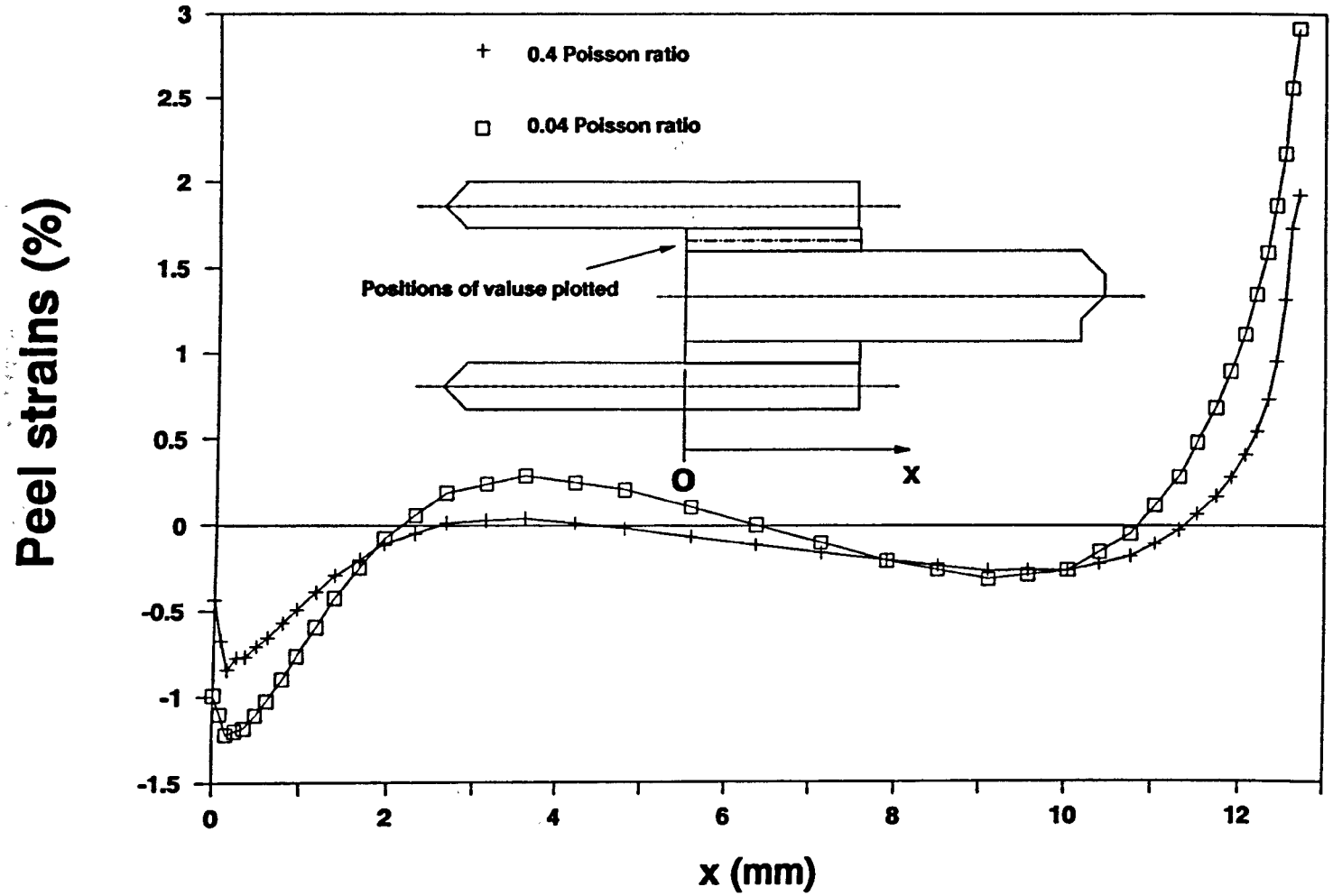

Fig. 6.11 Peel strains (percent) for a double lap joint without fillets

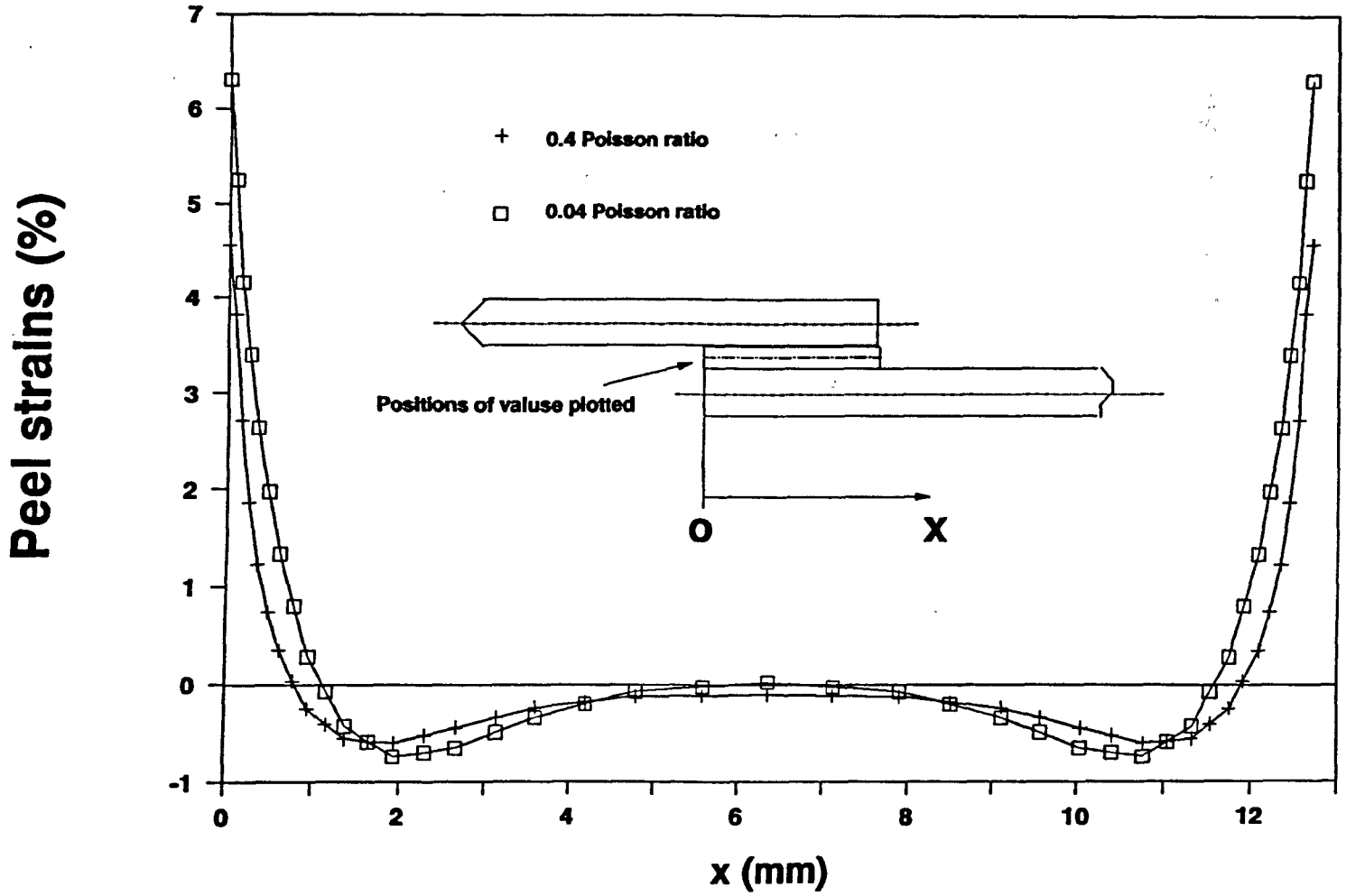

Fig. 6.12 Peel strains (percent) for a single lap joint without fillets

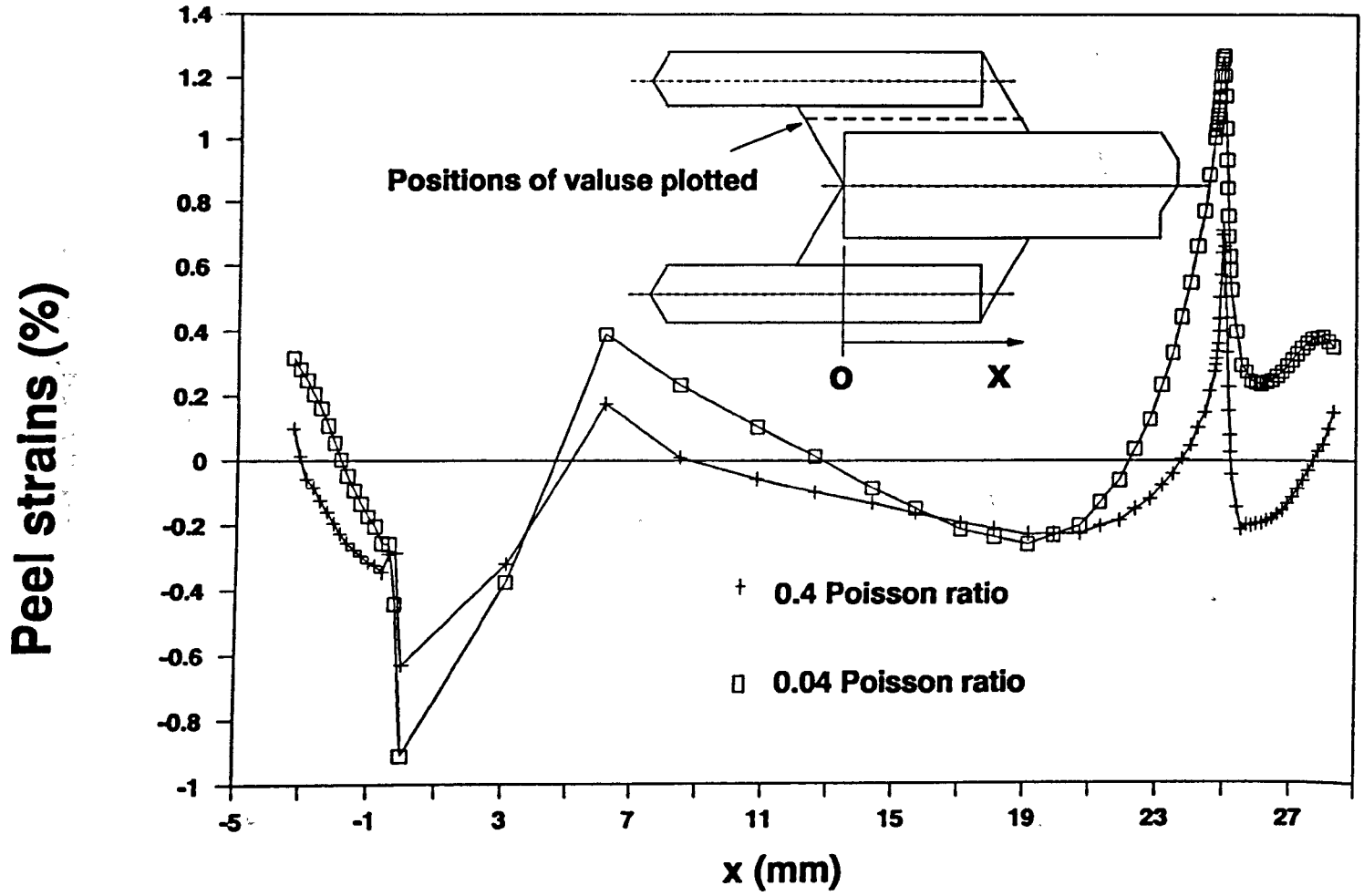

Fig. 6.13 Peel strains (percent) for a double lap joint with spew fillets

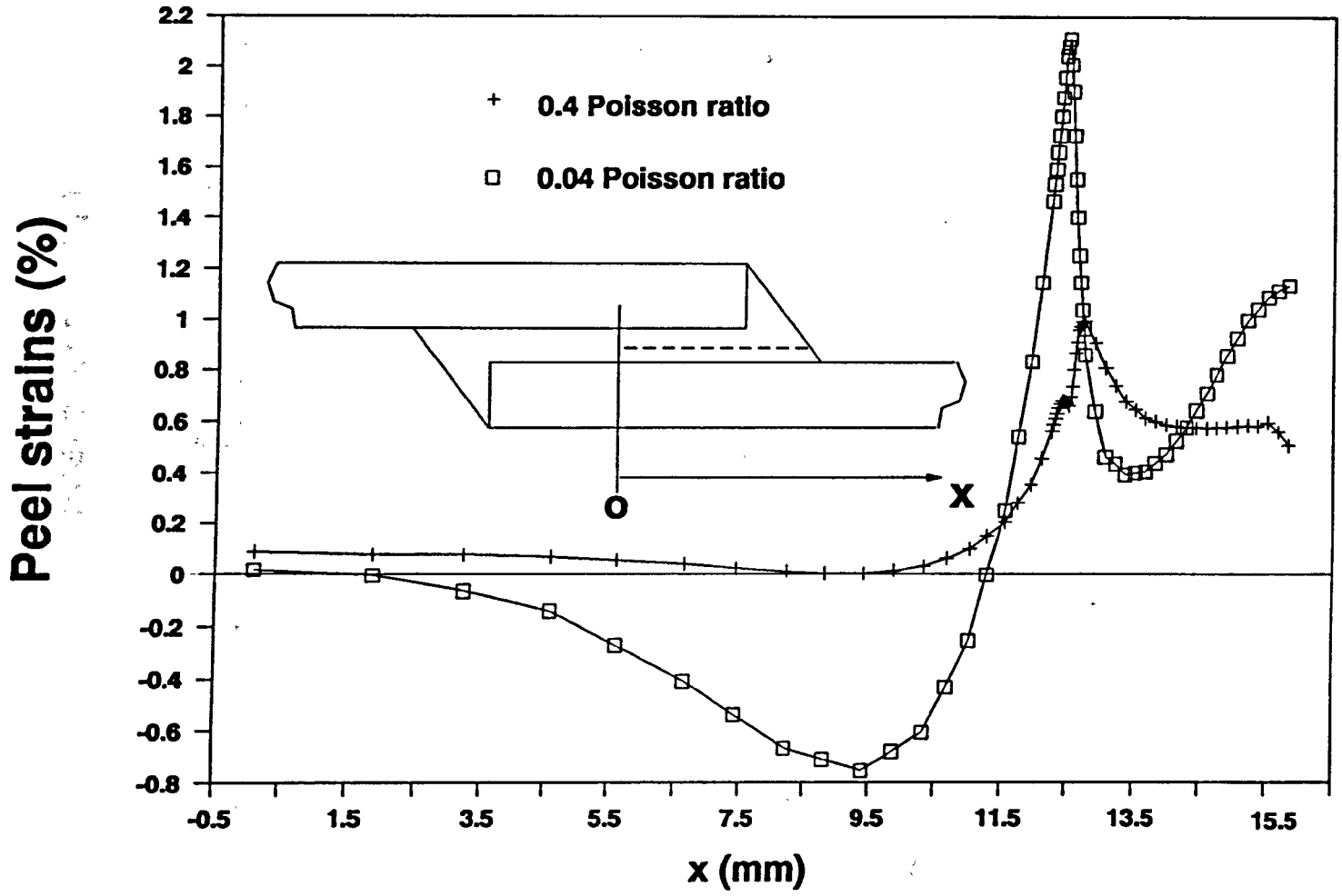

Fig. 6.14 Peel strains (percent) for a single lap joint with spew fillets

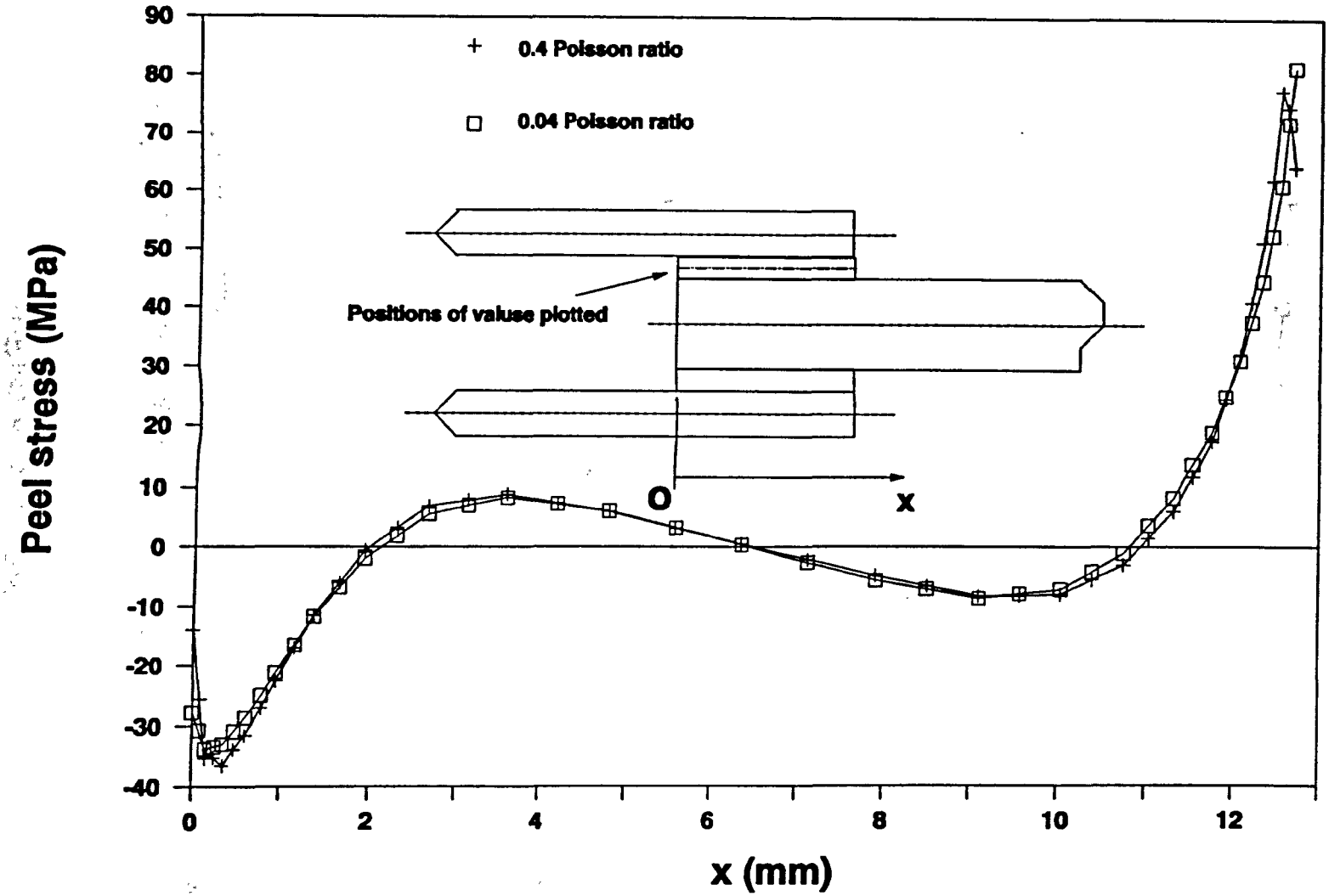

Fig. 6.15 Peel stresses for a double lap joint without spew fillets

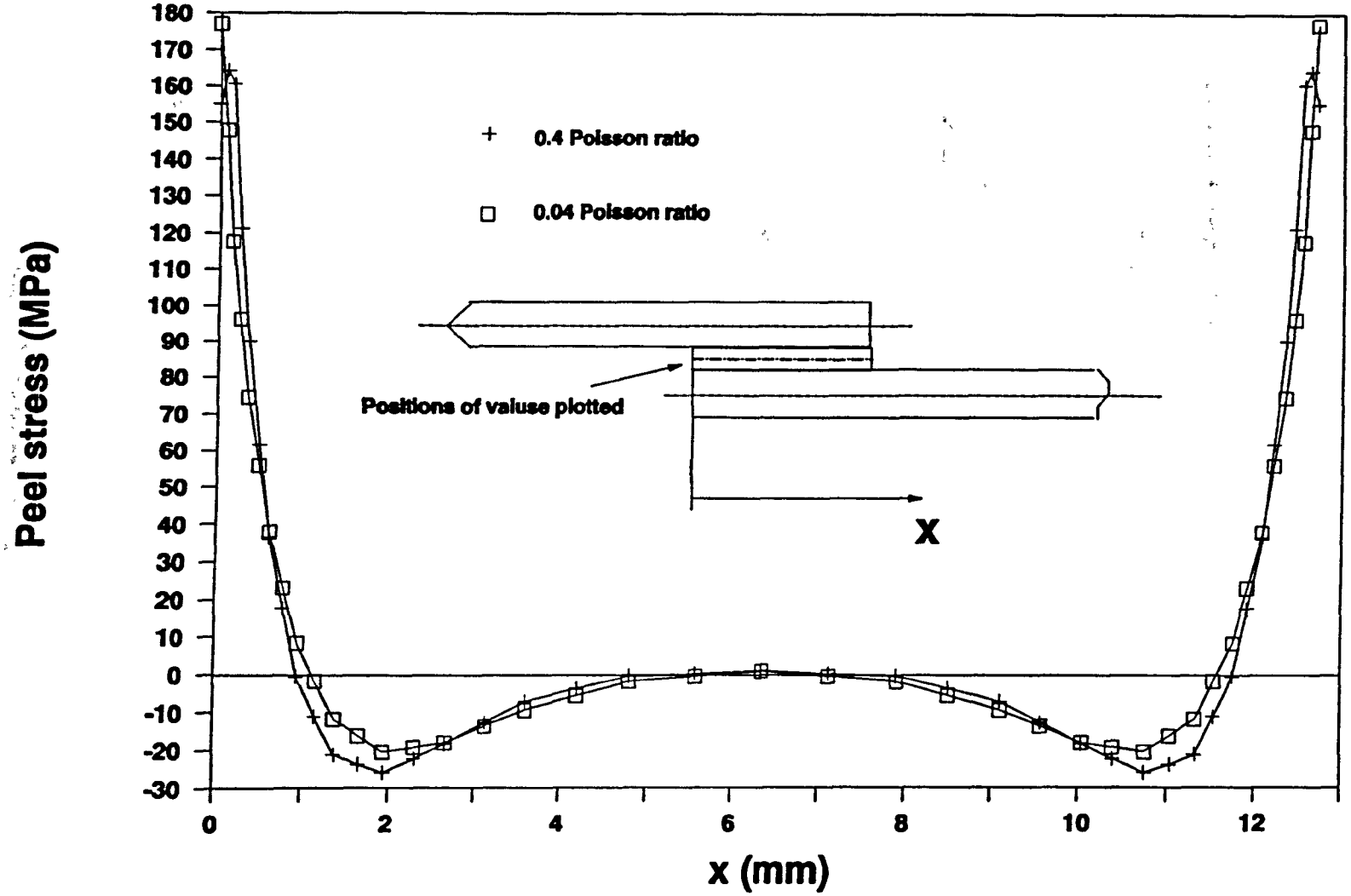

Fig. 6.16 Peel stresses for a single lap joint without spew fillets

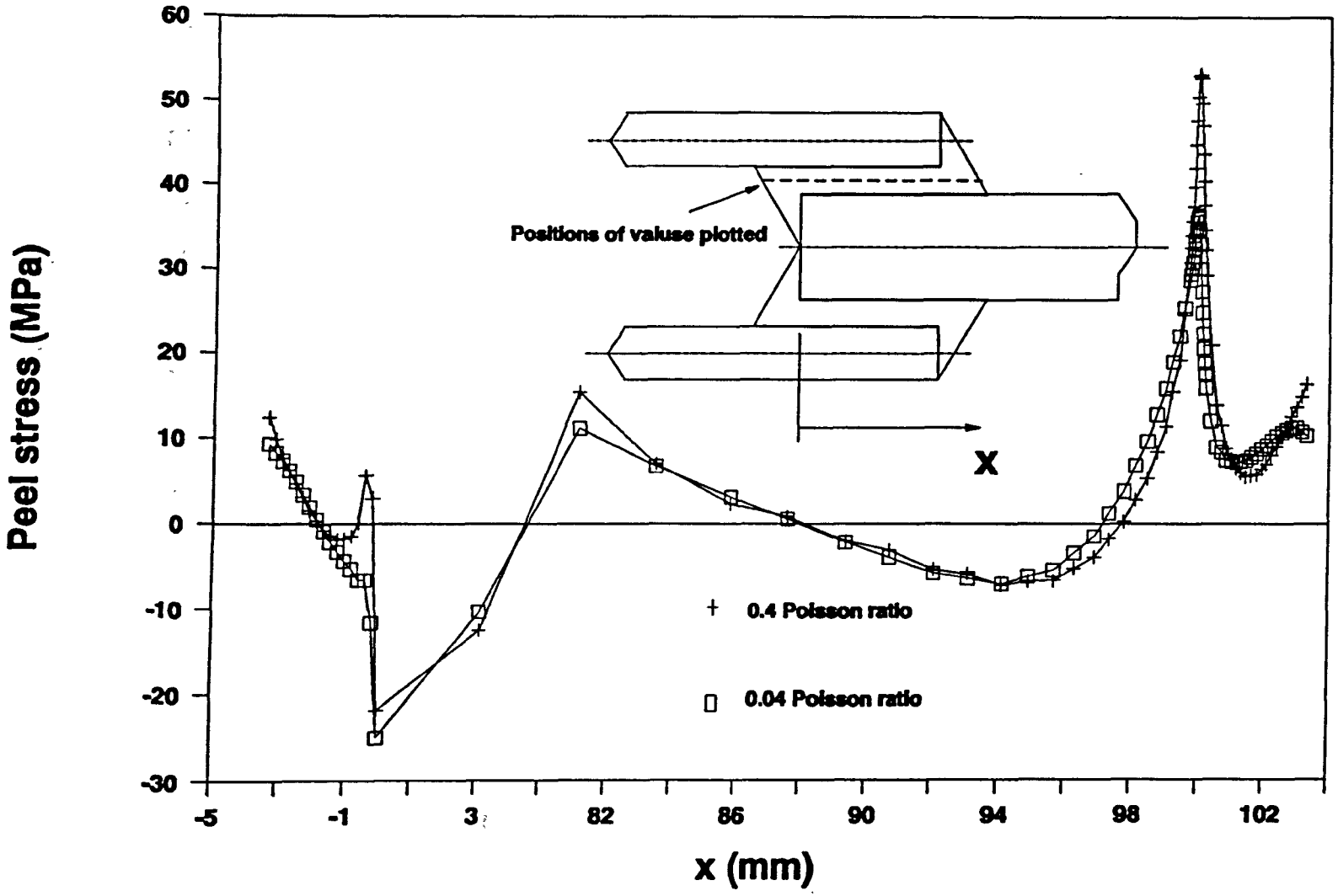

Fig. 6.17 Peel stresses for a double lap joint with spew fillets

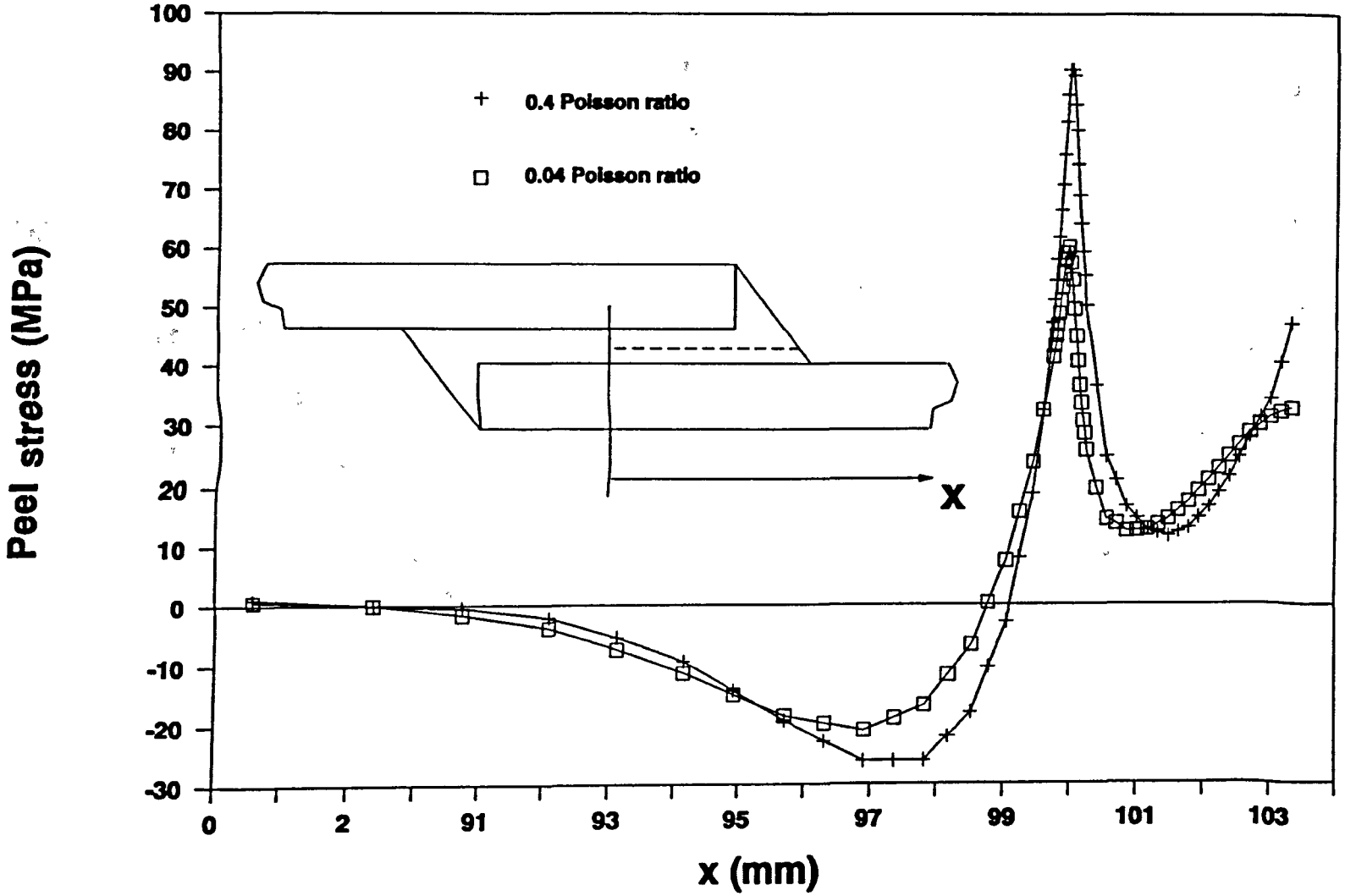

Fig. 6.18 Peel stresses for a single lap joint with spew fillets

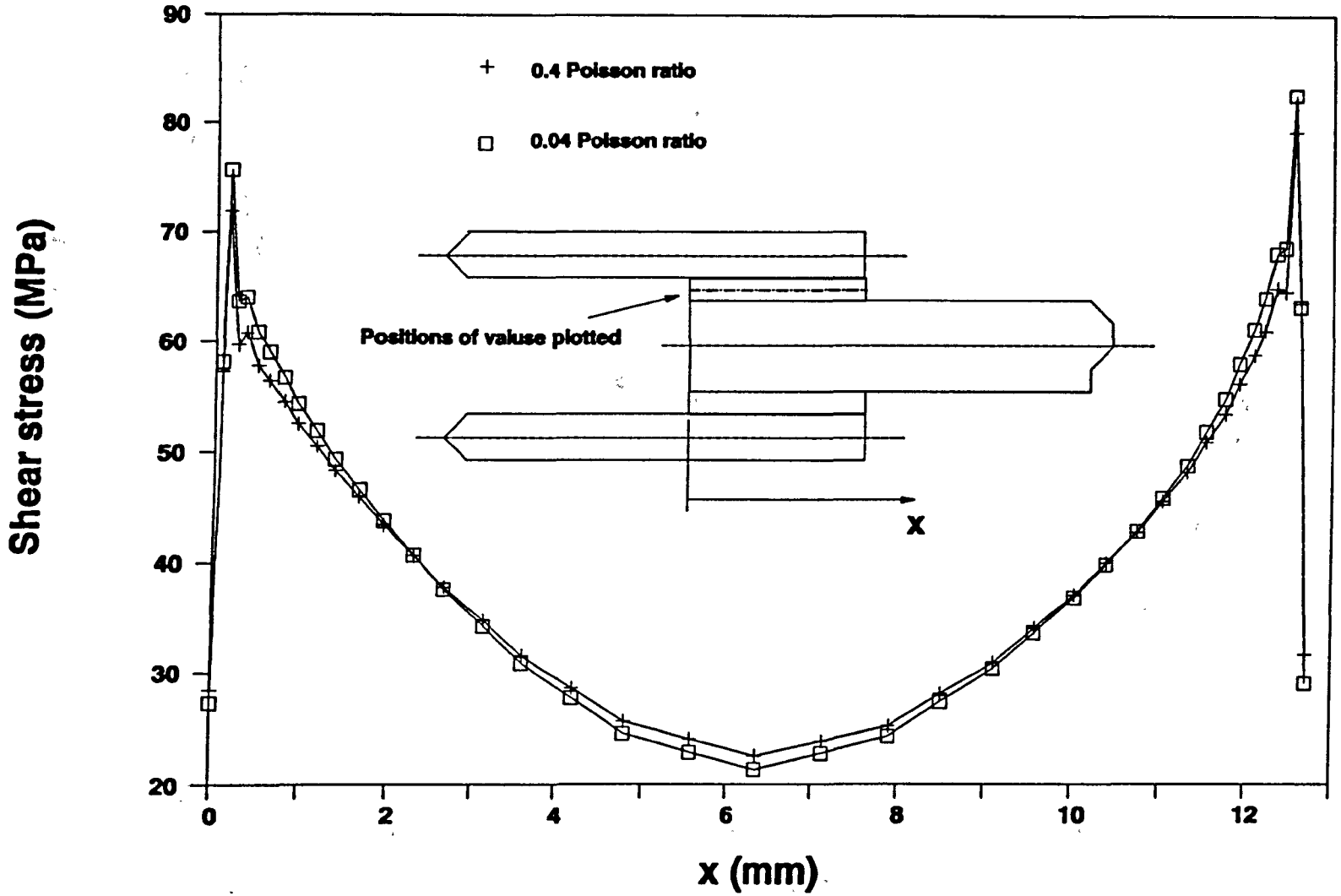

Fig. 6.19 Shear stresses for a double lap joint without spew fillets

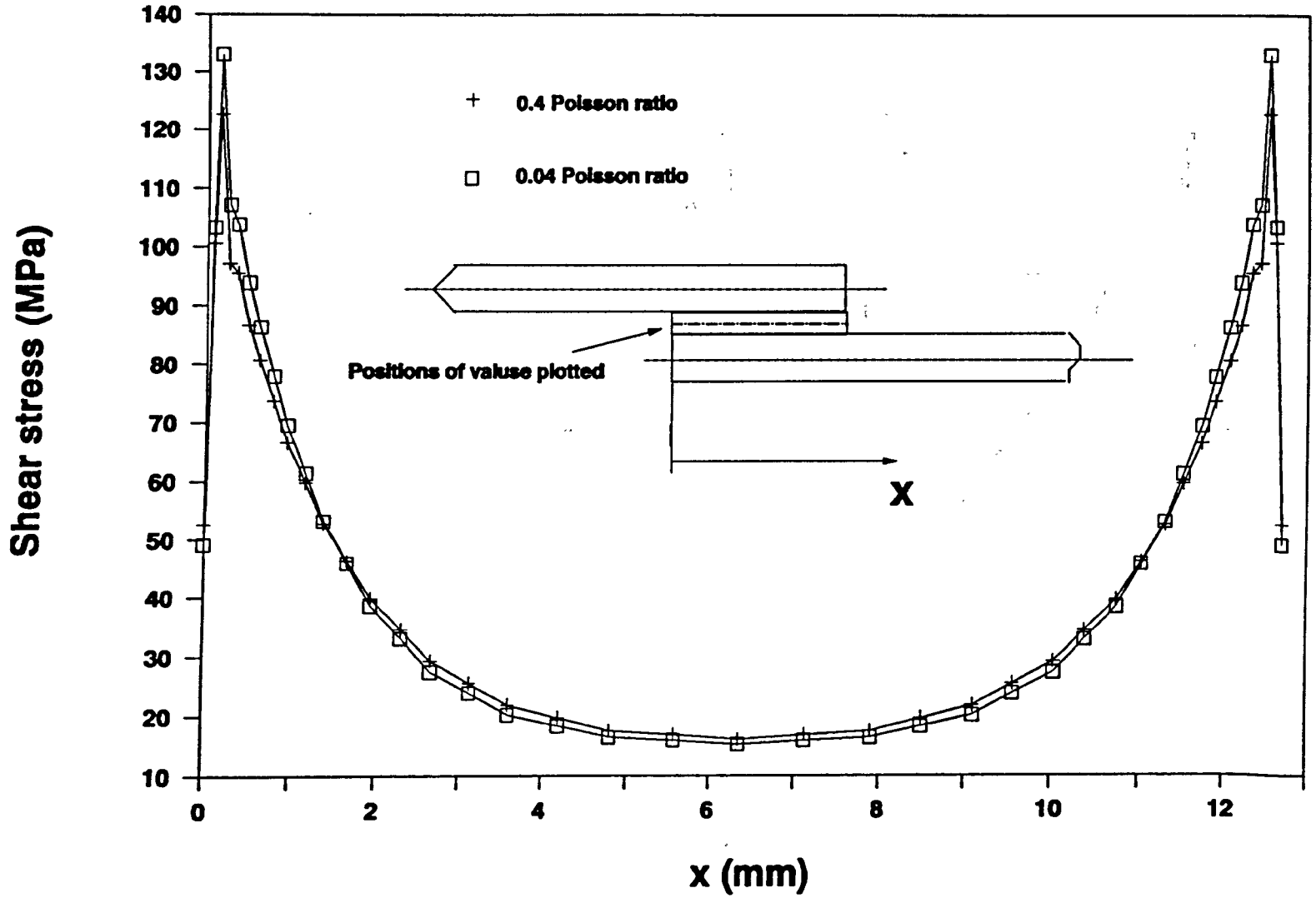

Fig. 6.20 Shear stress for a single lap joint without spew fillets

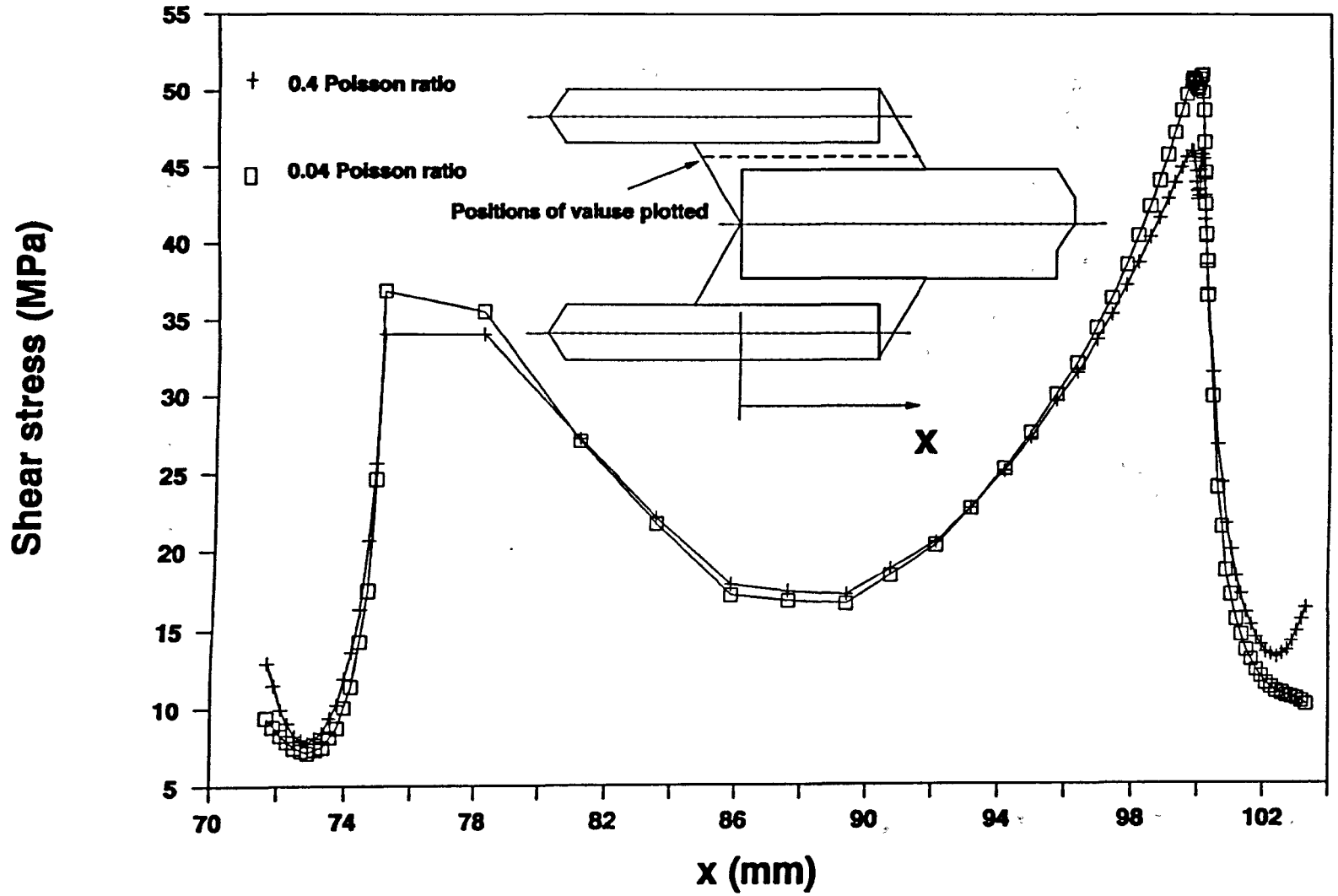

Fig. 6.21 Shear stresses for a double lap joint with spew fillets

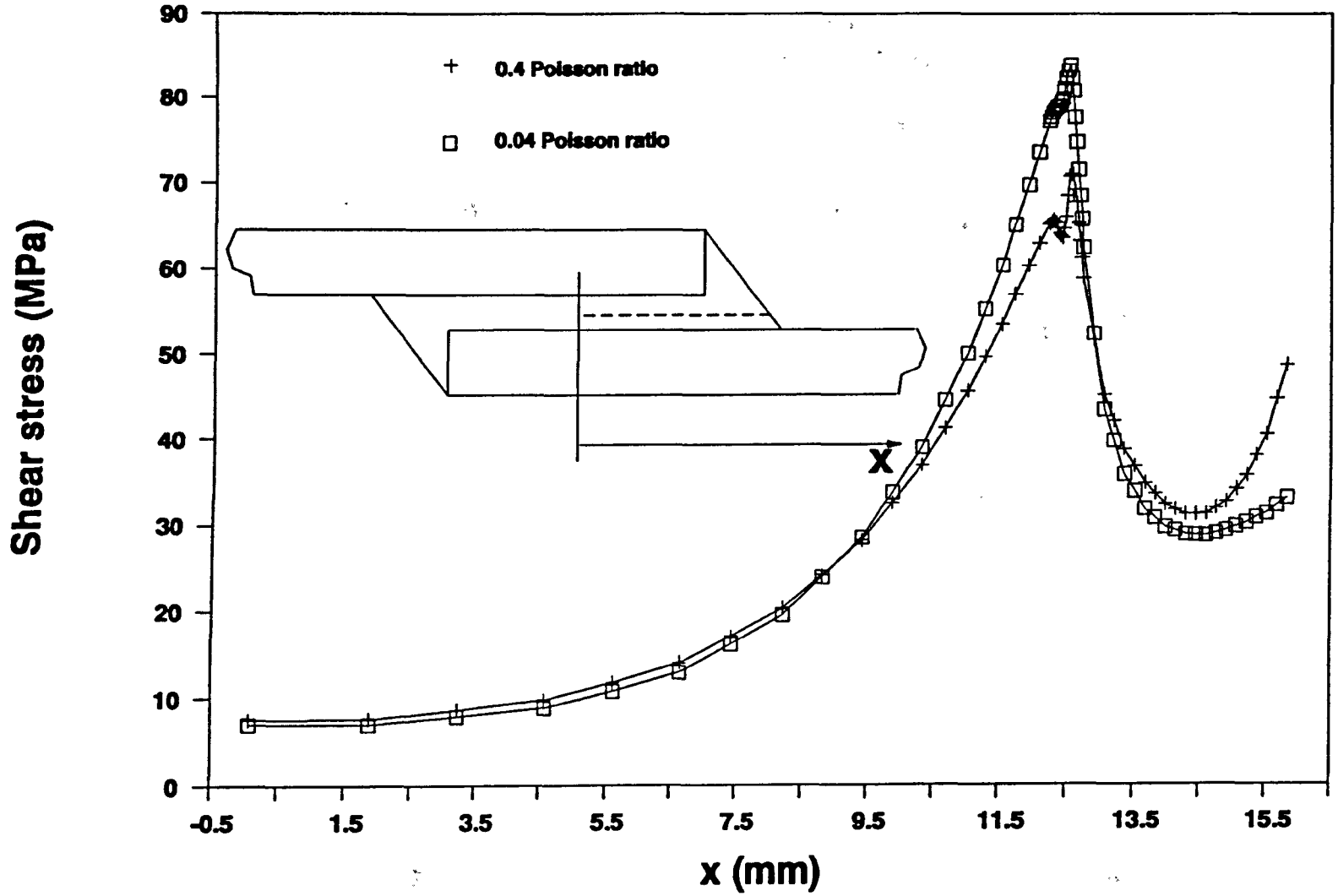

Fig. 6.22 Shear stresses for a single lap joint with spew fillets

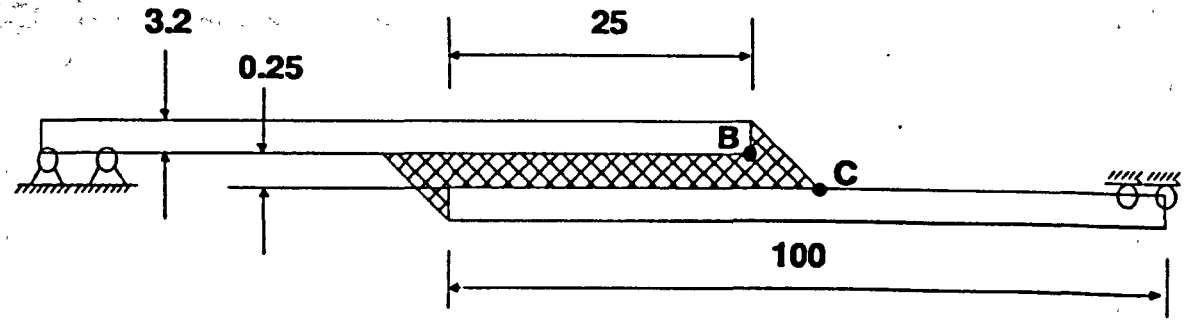

(a). Joint geometry (all dimension in mm)

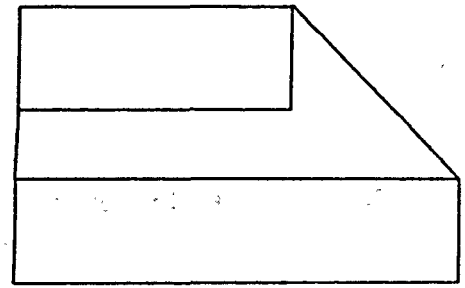

(b). Sharp corner

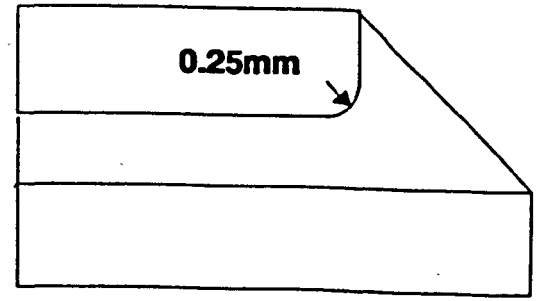

(c). Small radius

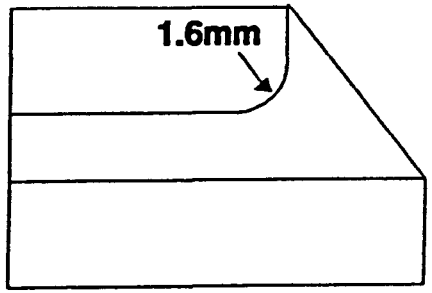

(d). Medium radius

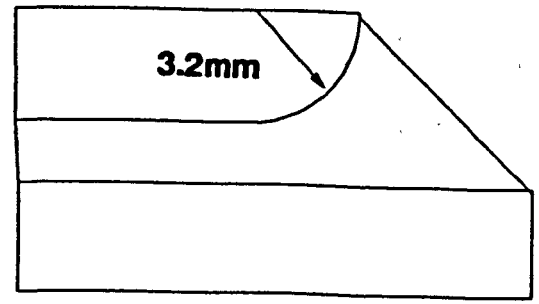

(e). Large radius

Fig. 7.1 Al/Epoxy Single Lap Joints with Different Degrees of Rounding

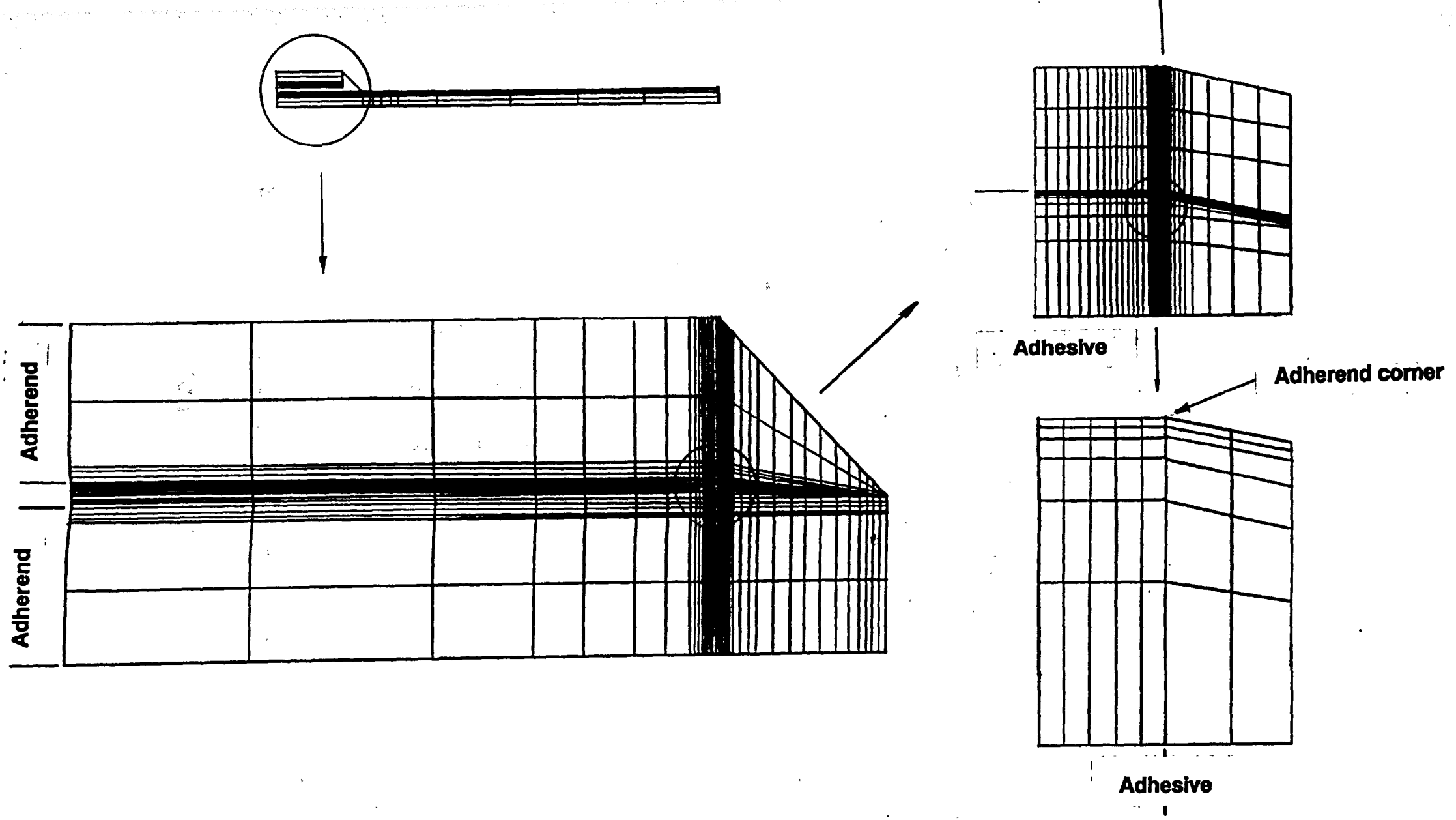

Fig. 7.1A A typical fine mesh around the adherend corner

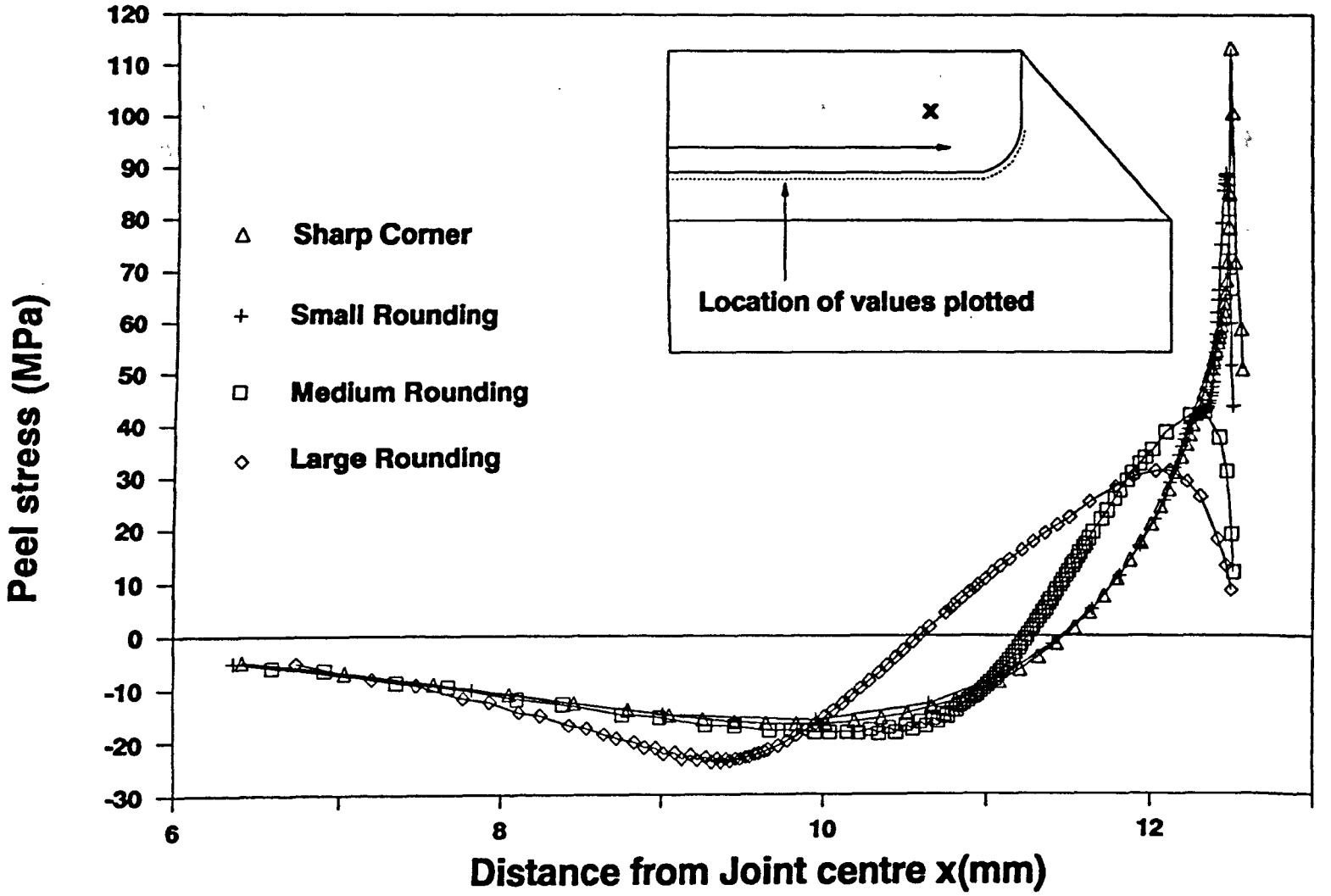

Fig. 7.2 Peel stresses in the adhesive with a 20kN load

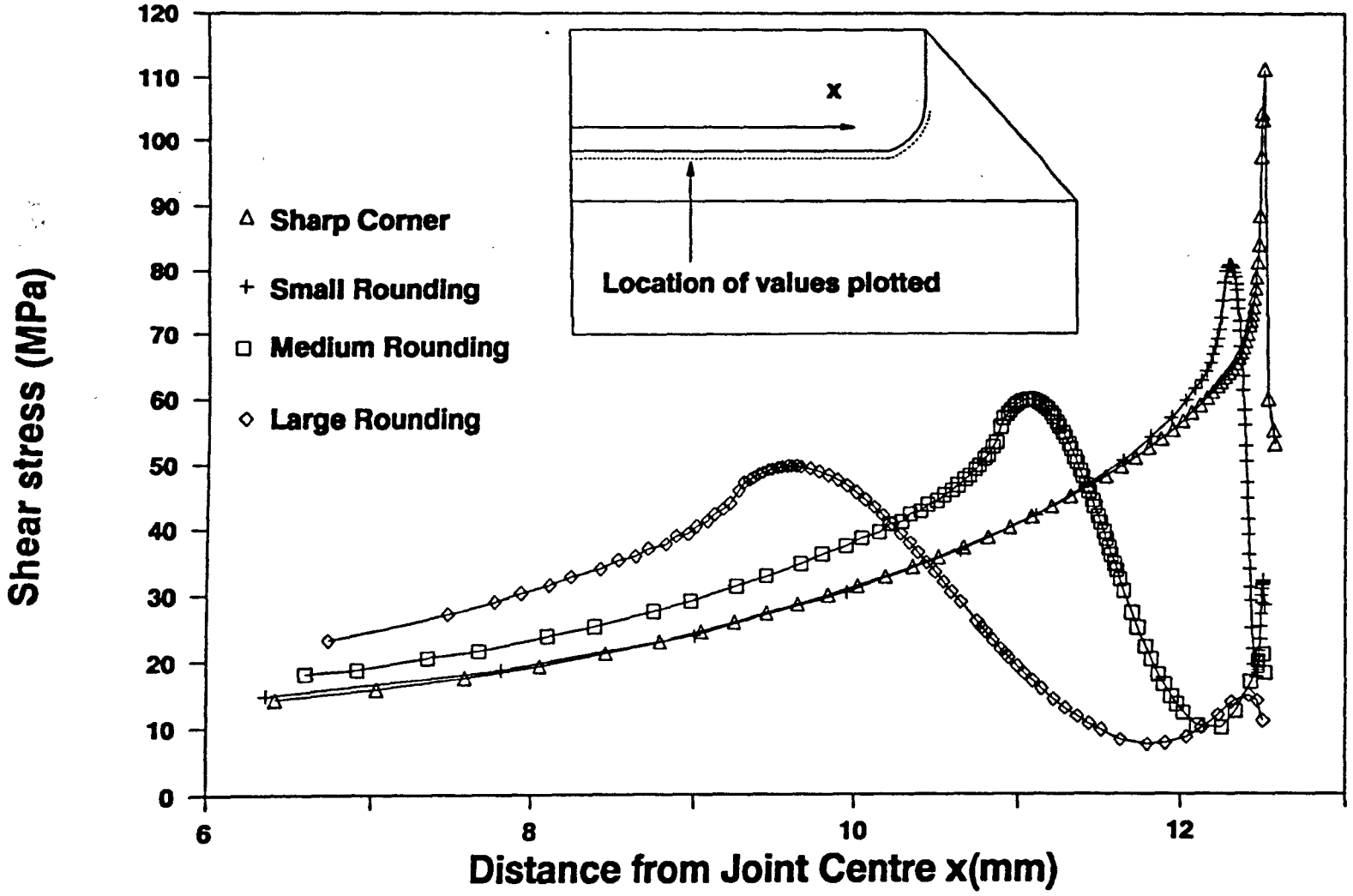

Fig. 7.3 Shear stresses in the adhesive with a 20kN load

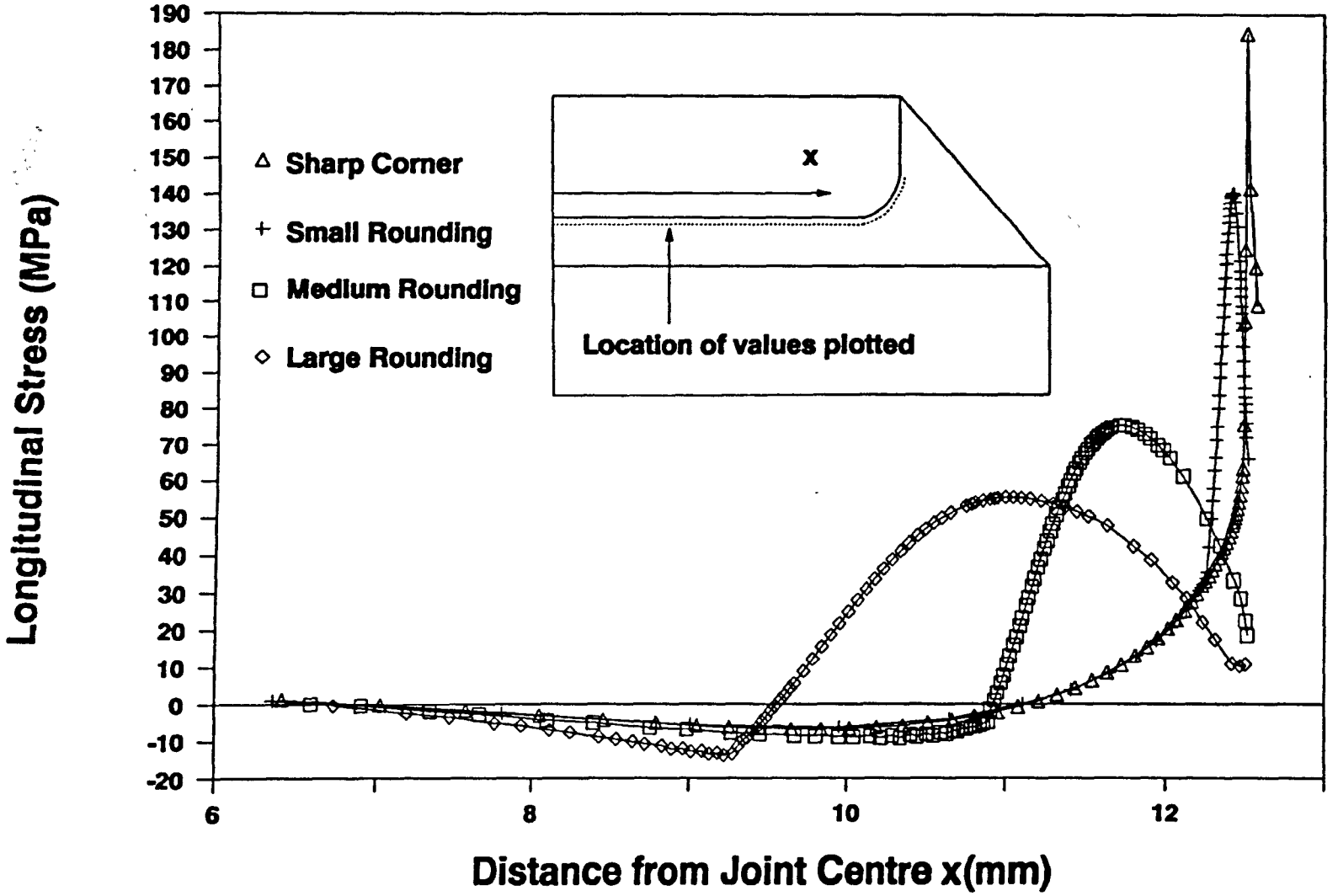

Fig. 7.4 Longitudinal stresses in the adhesive with a 20kN load

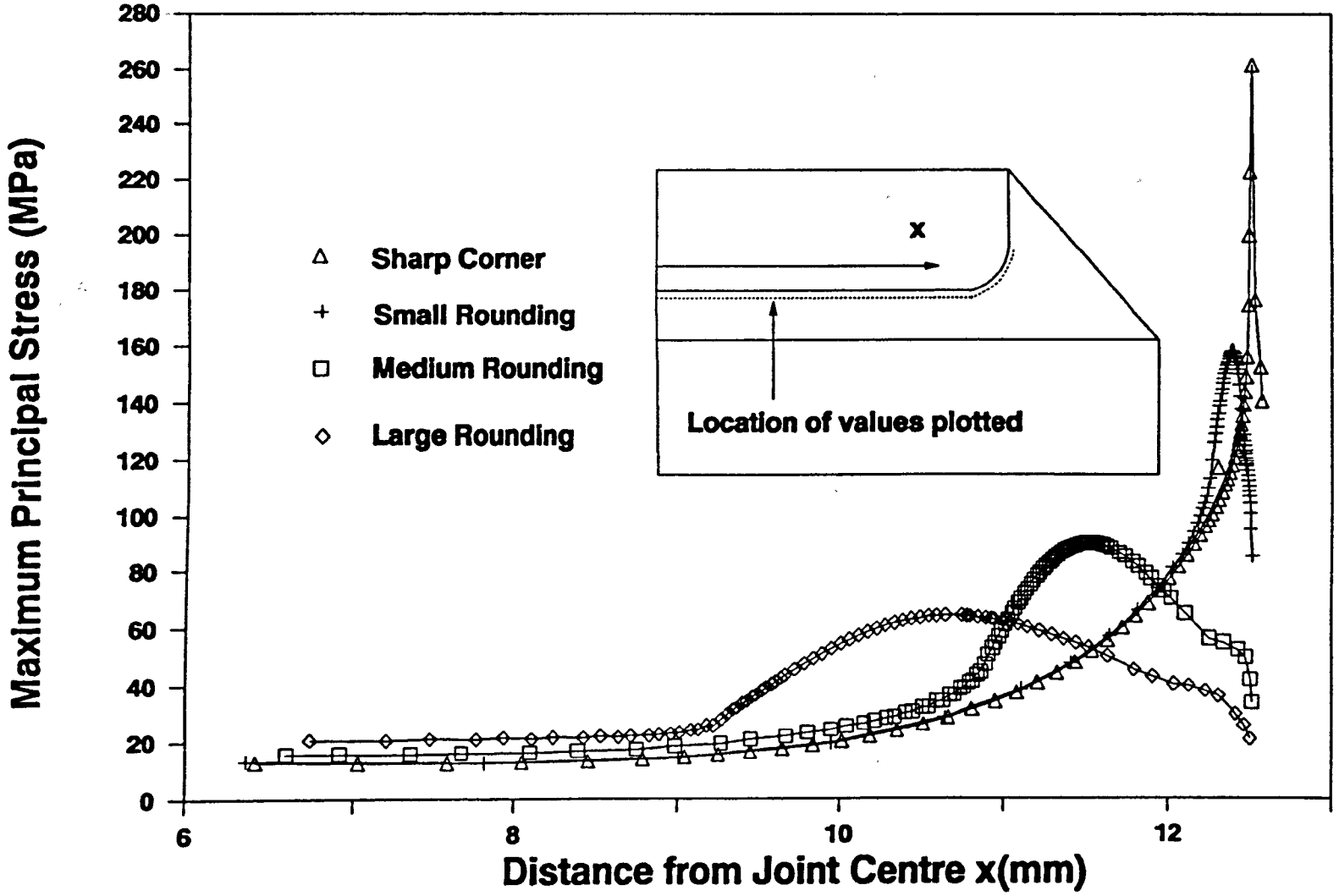

Fig. 7.5 Maximum principal stresses in the adhesive with a 20kN load

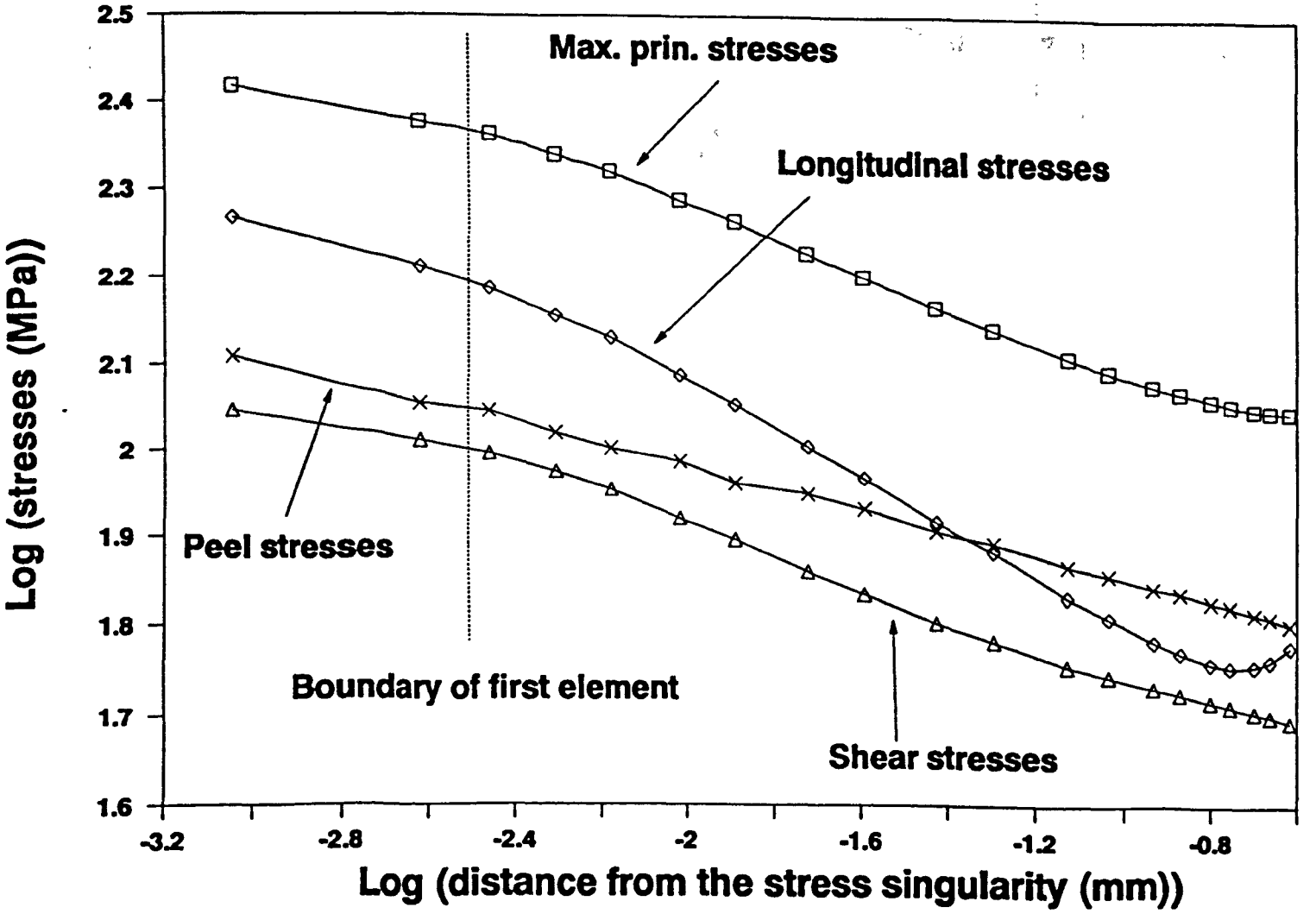

Fig. 7.6 Stresses across the adhesive layer with 20 kN load

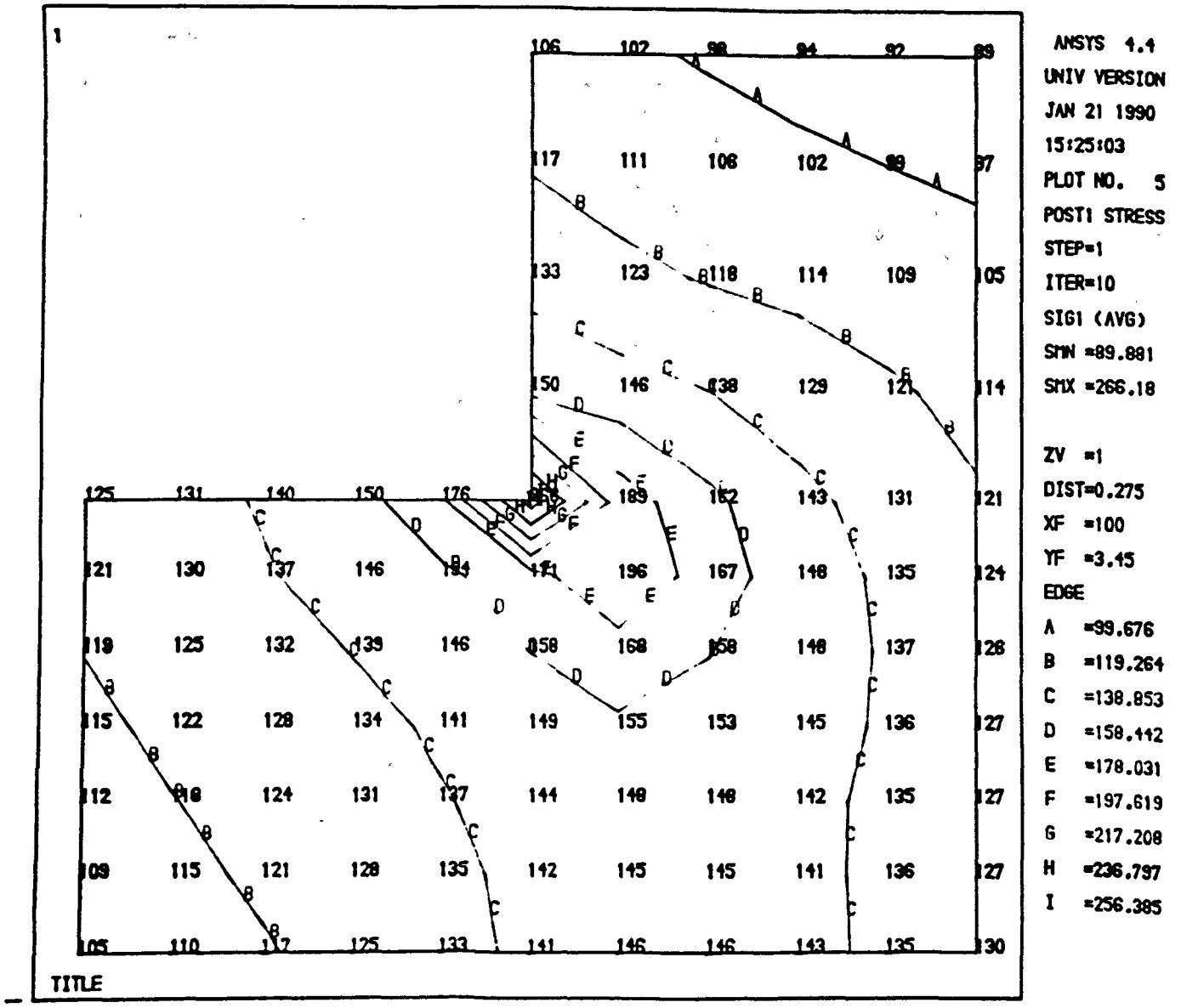

Fig. 7.7 Contour plot of the maximum principal stress in the adhesive around the sharp adherend corner

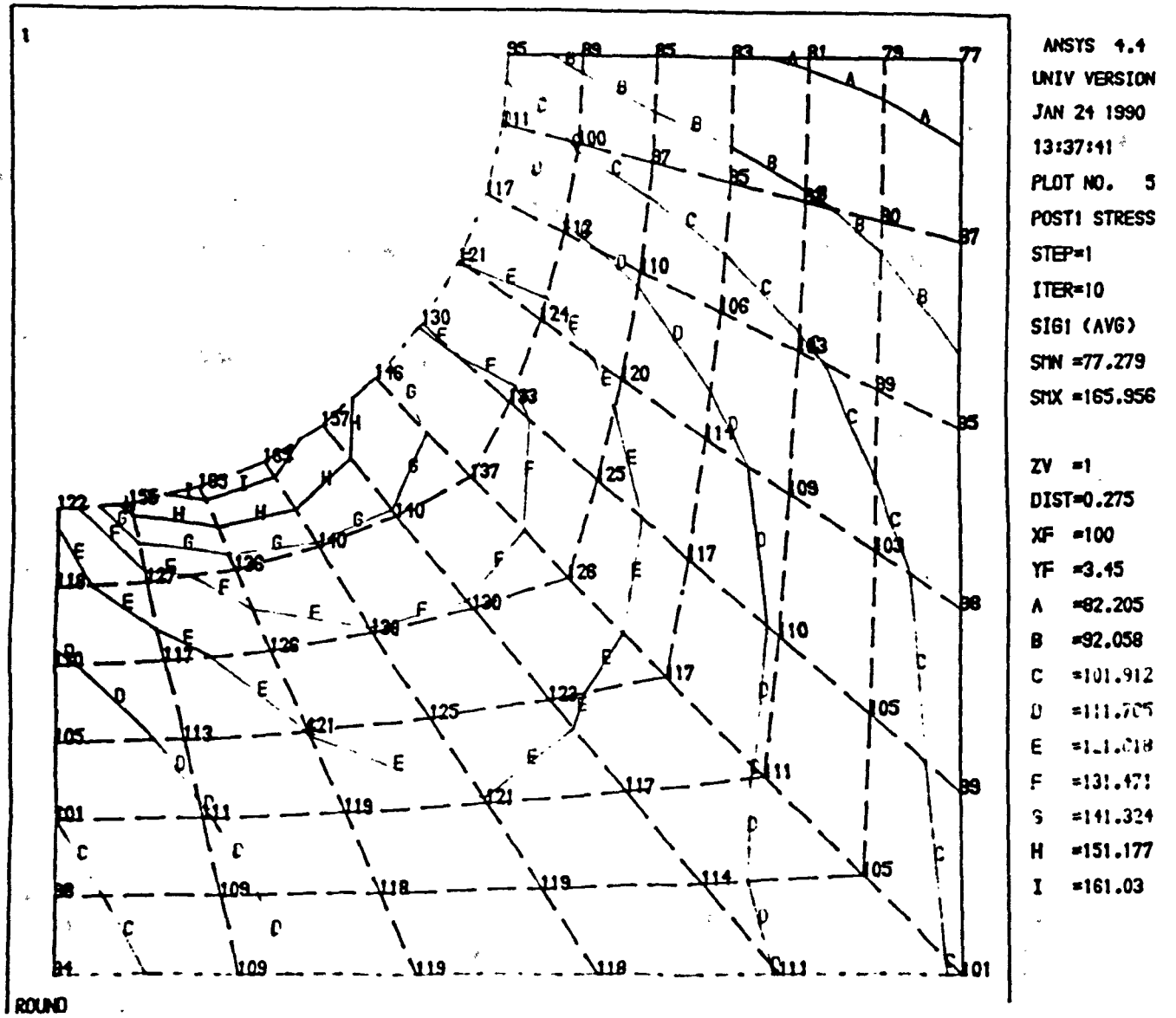

Fig. 7.8 Contour plot of the maximum principal stress in the adhesive around the small rounded adherend corner

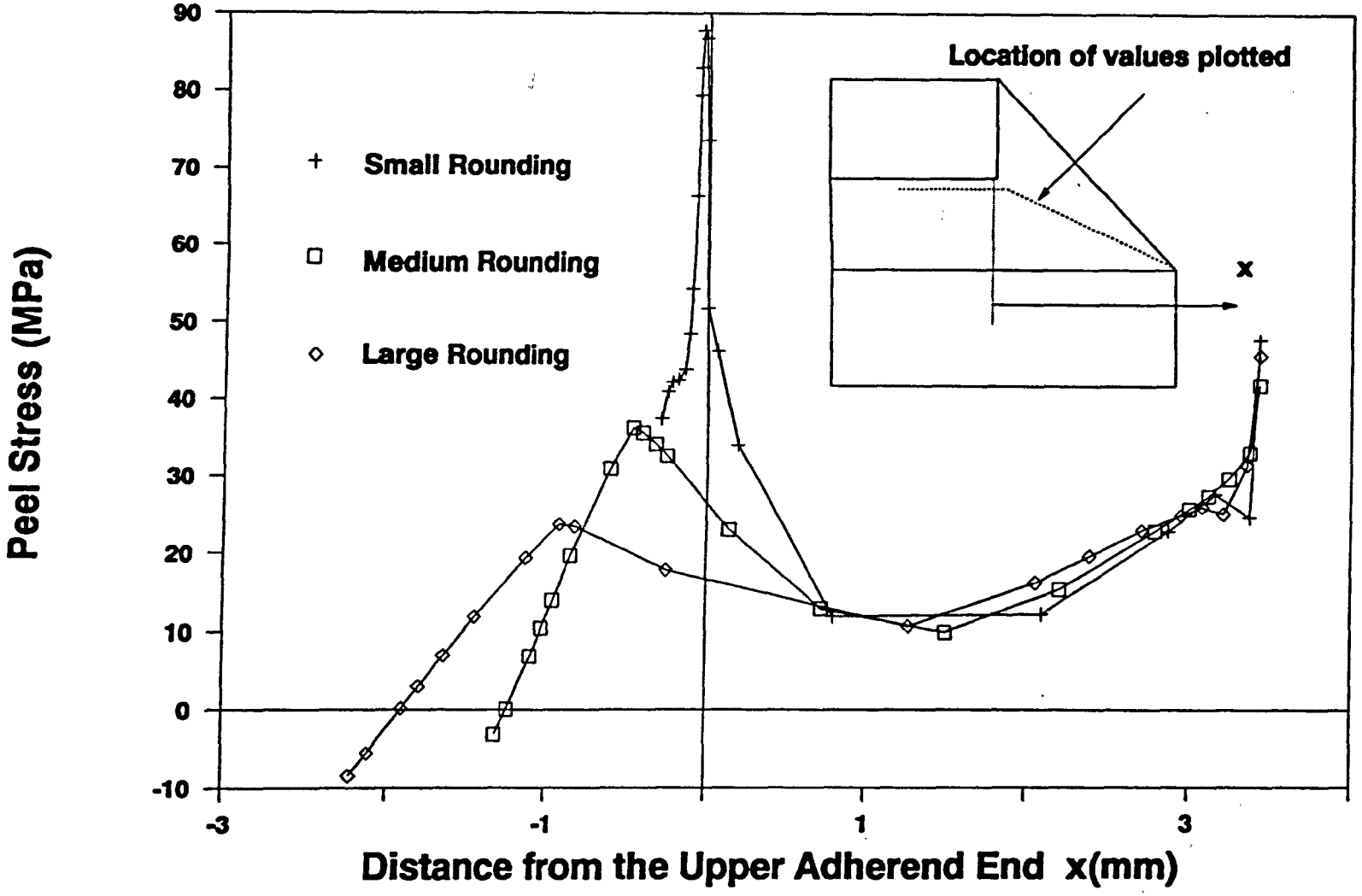

Fig. 7.9 Peel stress comparison inside the Spew Fillet

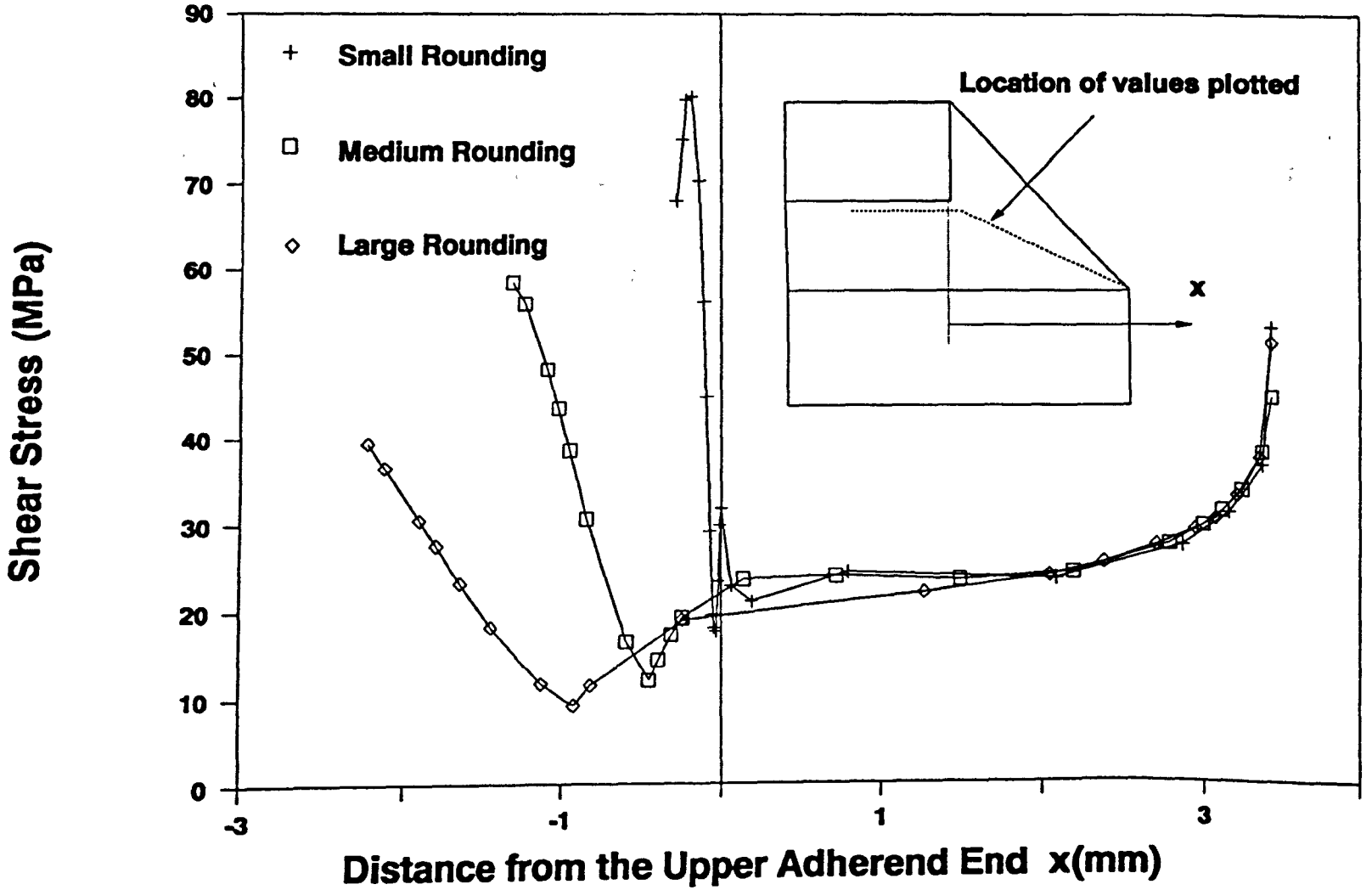

Fig. 7.10 Shear stress comparison inside the spew fillet

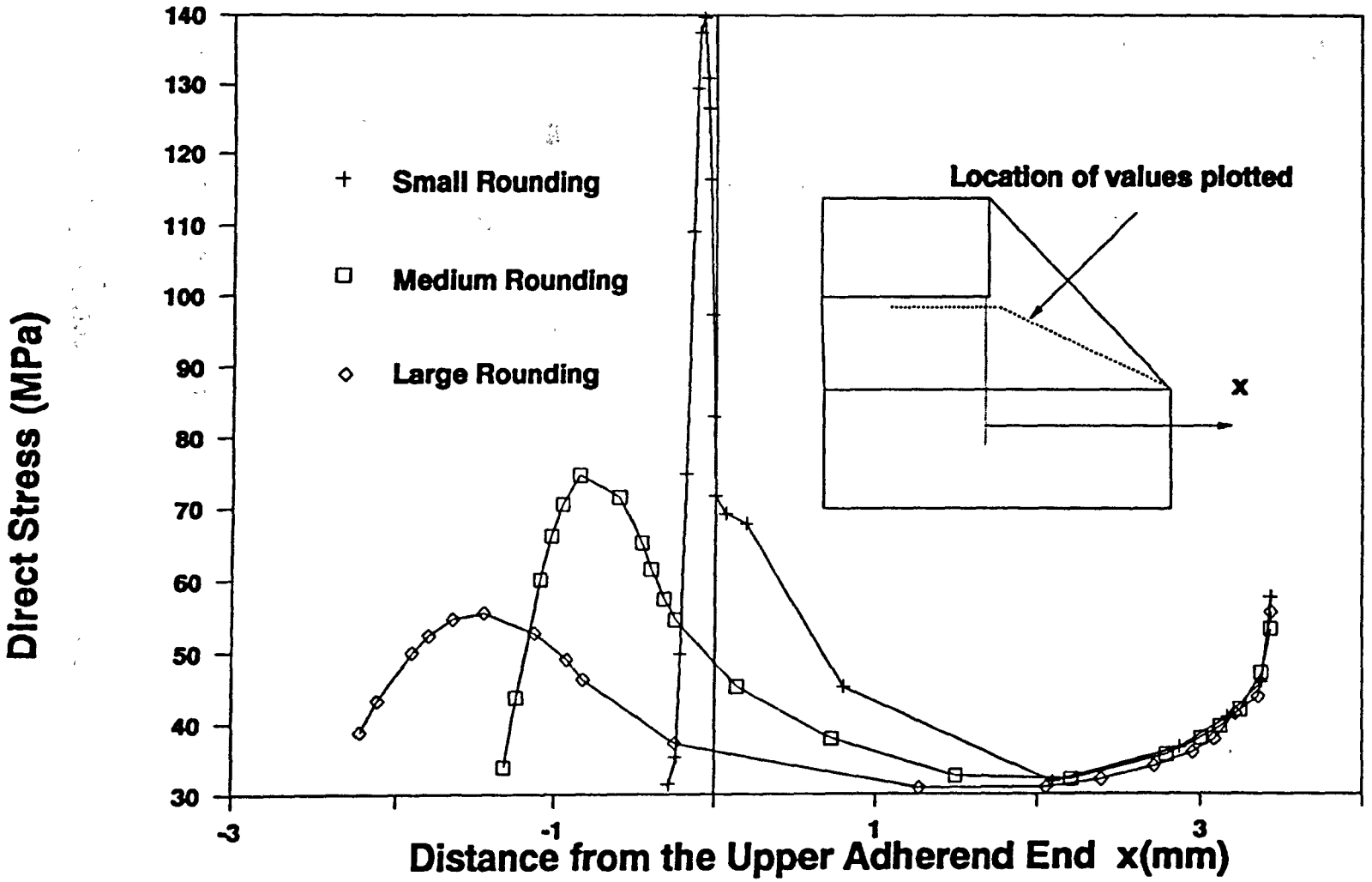

Fig. 7.11 Direct stress comparison inside the spew fillet

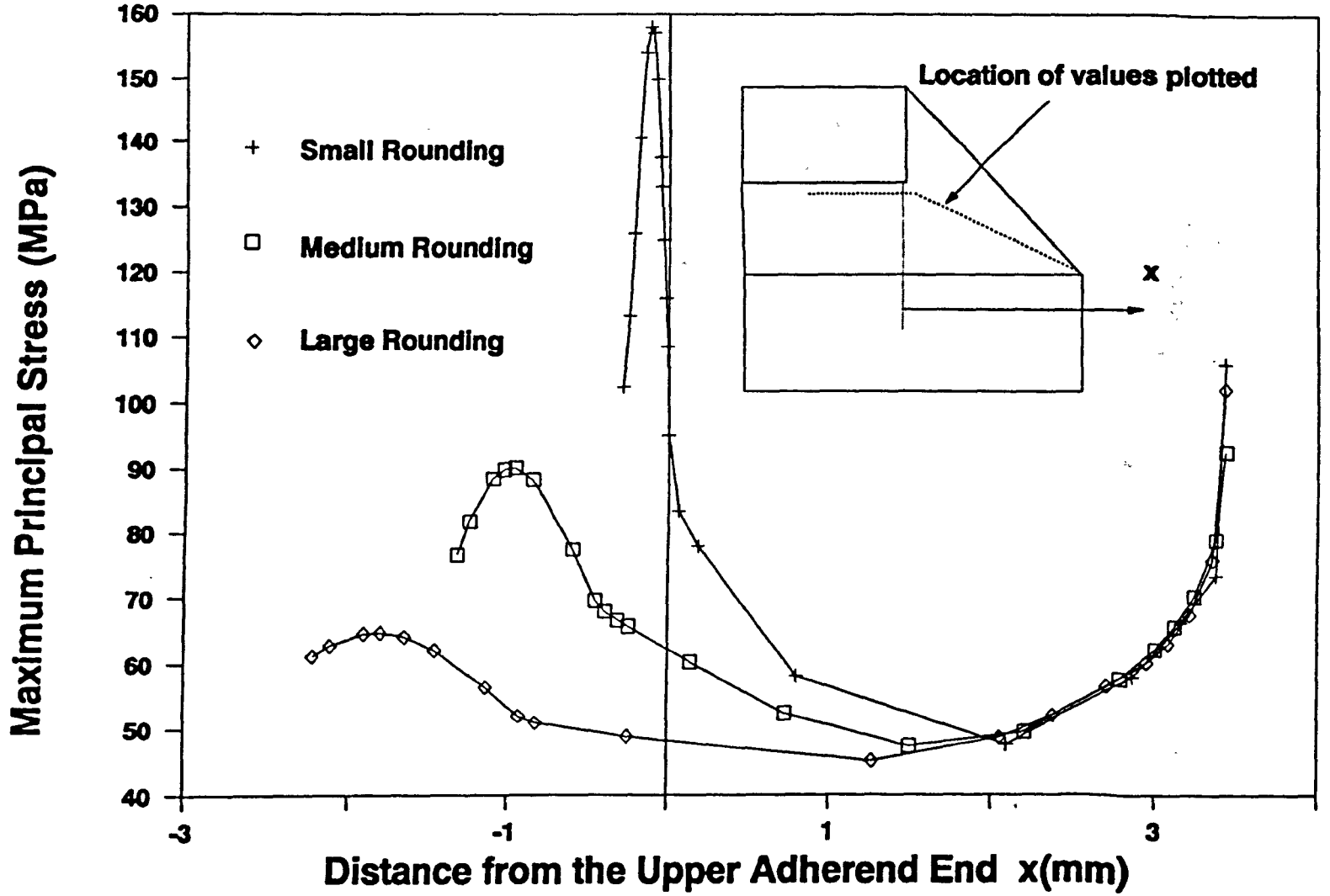

Fig. 7.12 Max. Principal Stress Comparison inside the Spew Fillet

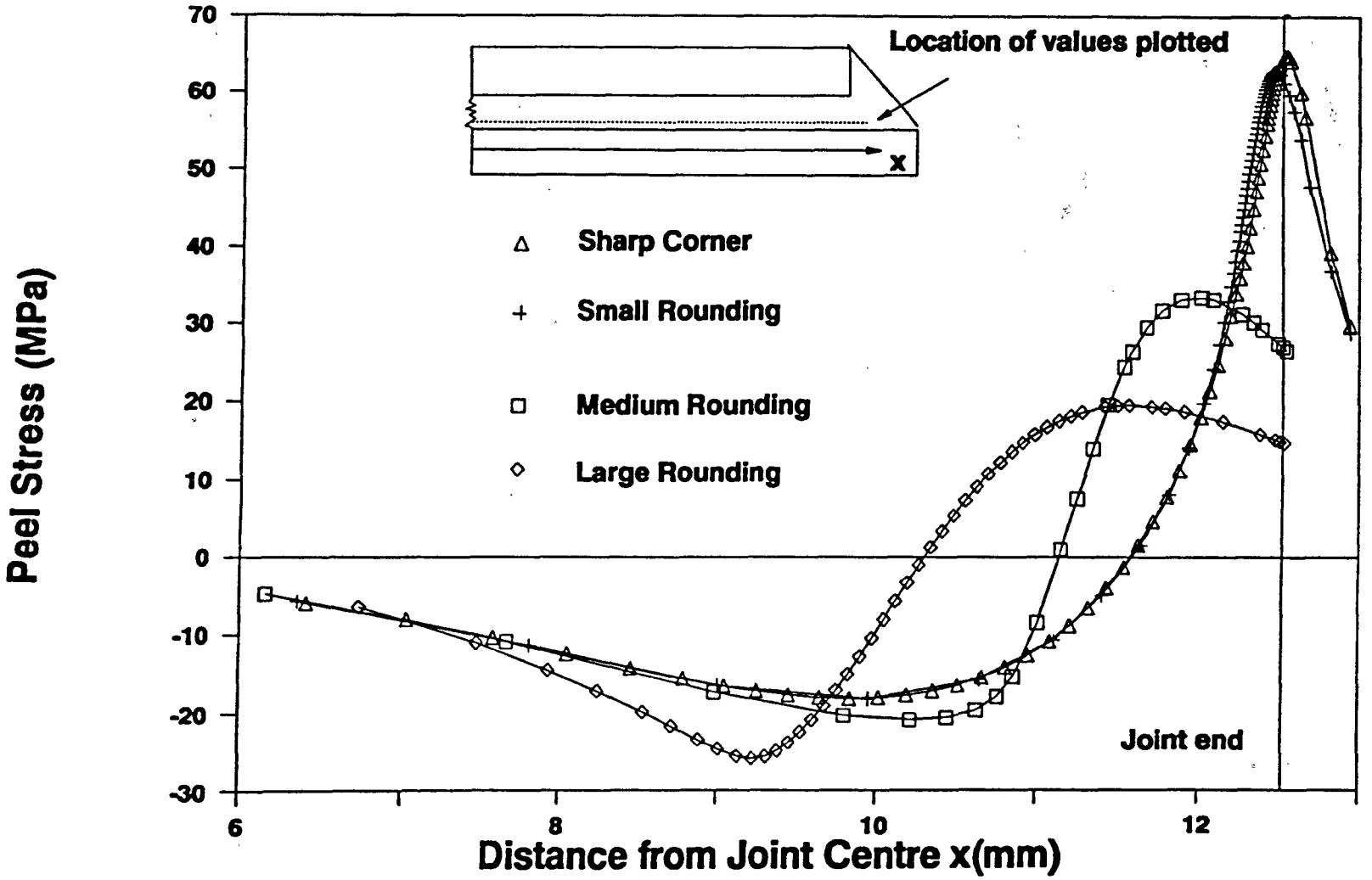

Fig. 7.13 Peel Stresses in the adhesive with a 20kN load

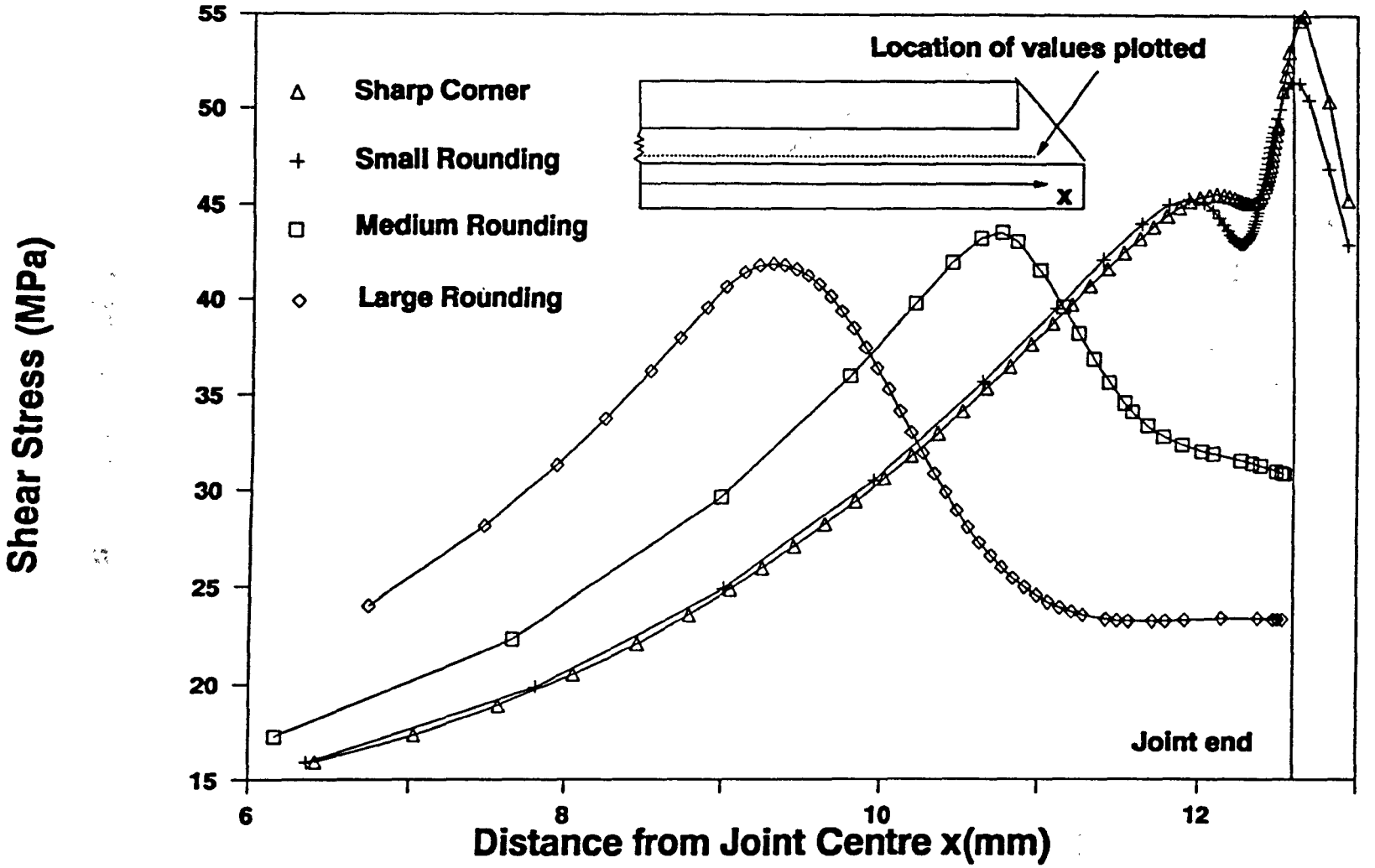

Fig. 7.14 Shear stresses in the adhesive with a 20kN load

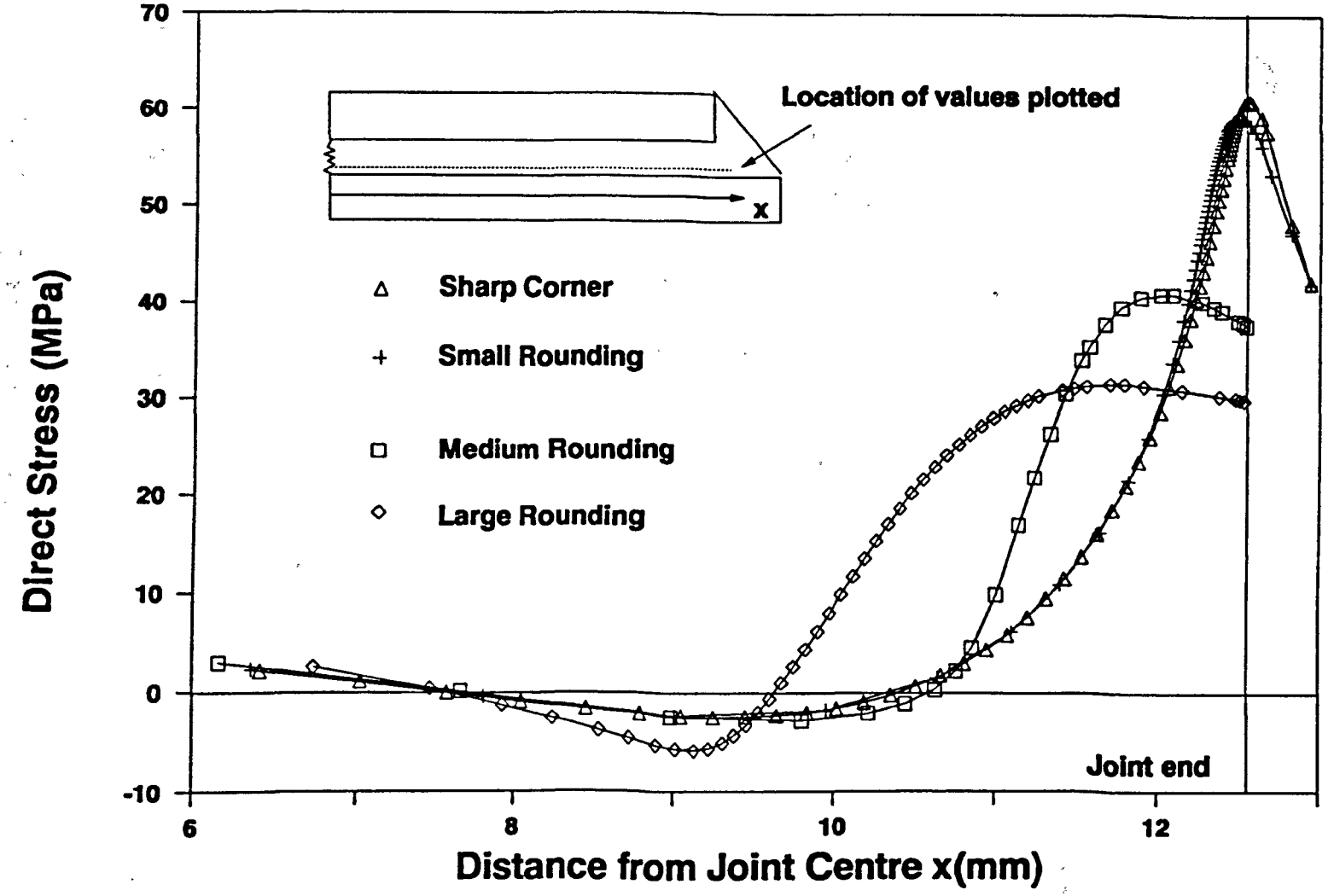

Fig. 7.15 Direct stresses in the adhesive with a 20kN load

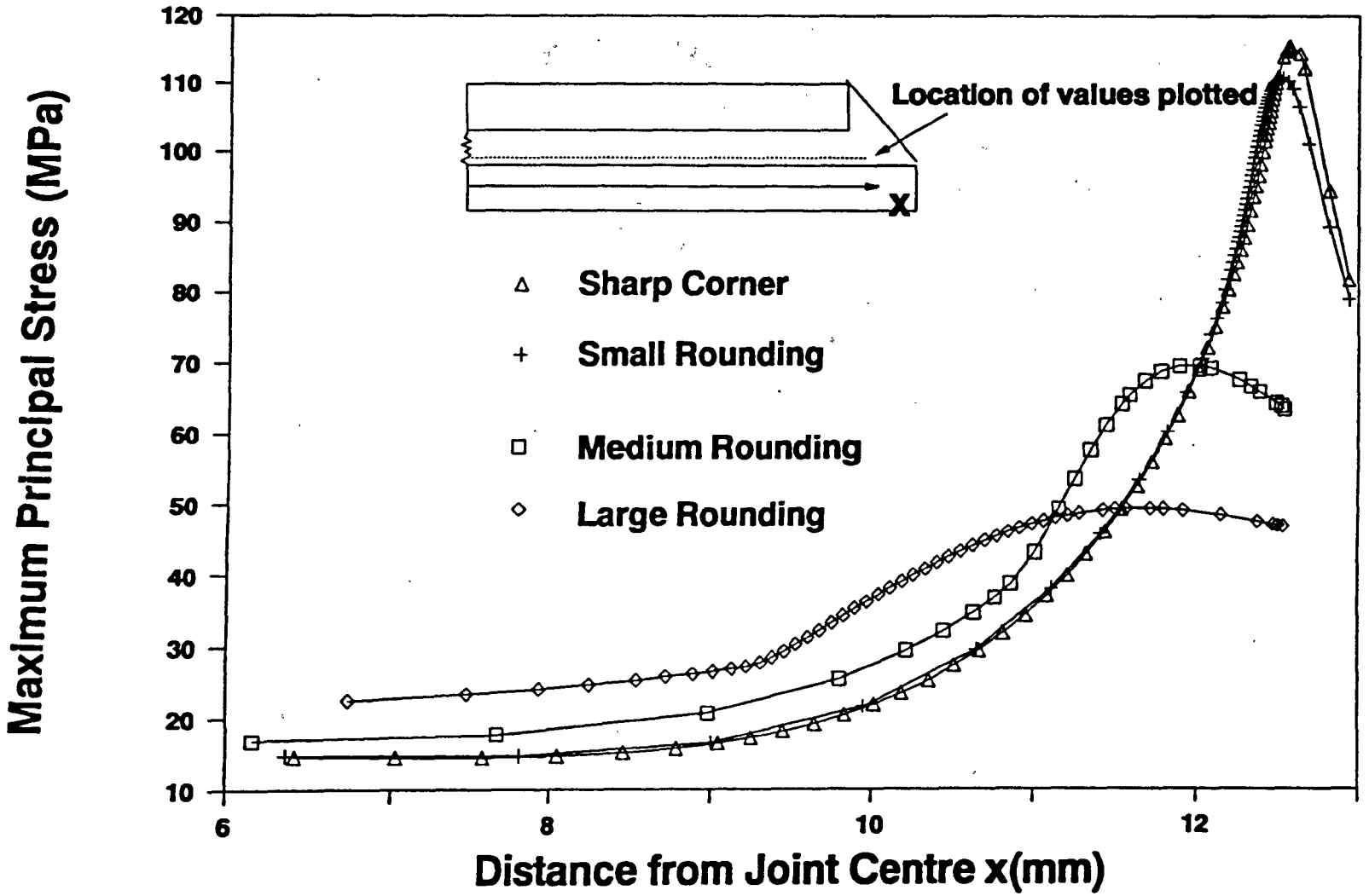

Fig. 7.16 Maximum Principal Stresses in the adhesive with a 20kN load

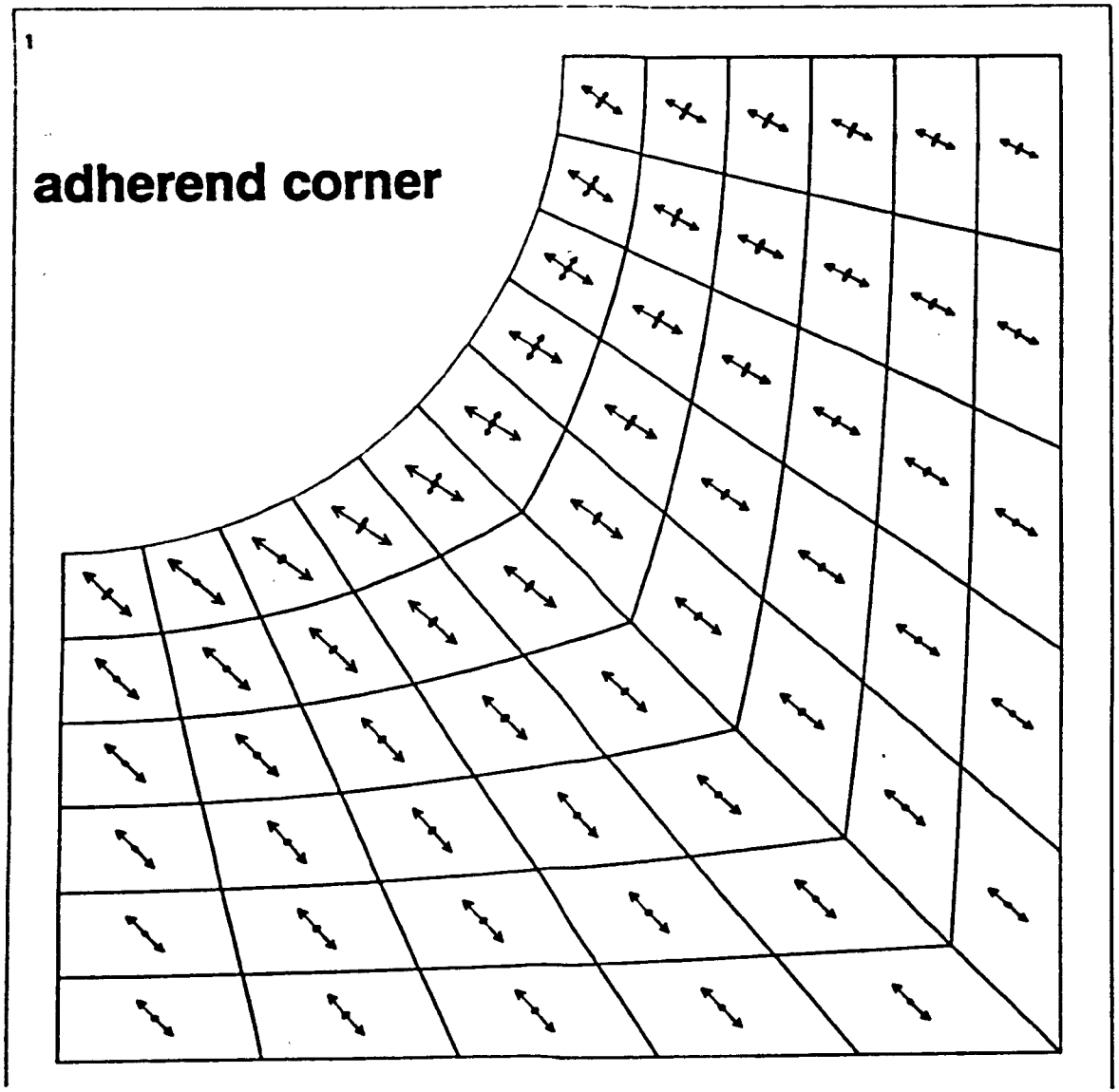

Fig. 7.17 The pattern of the principal stress in the adhesive around the small rounded adherend corner

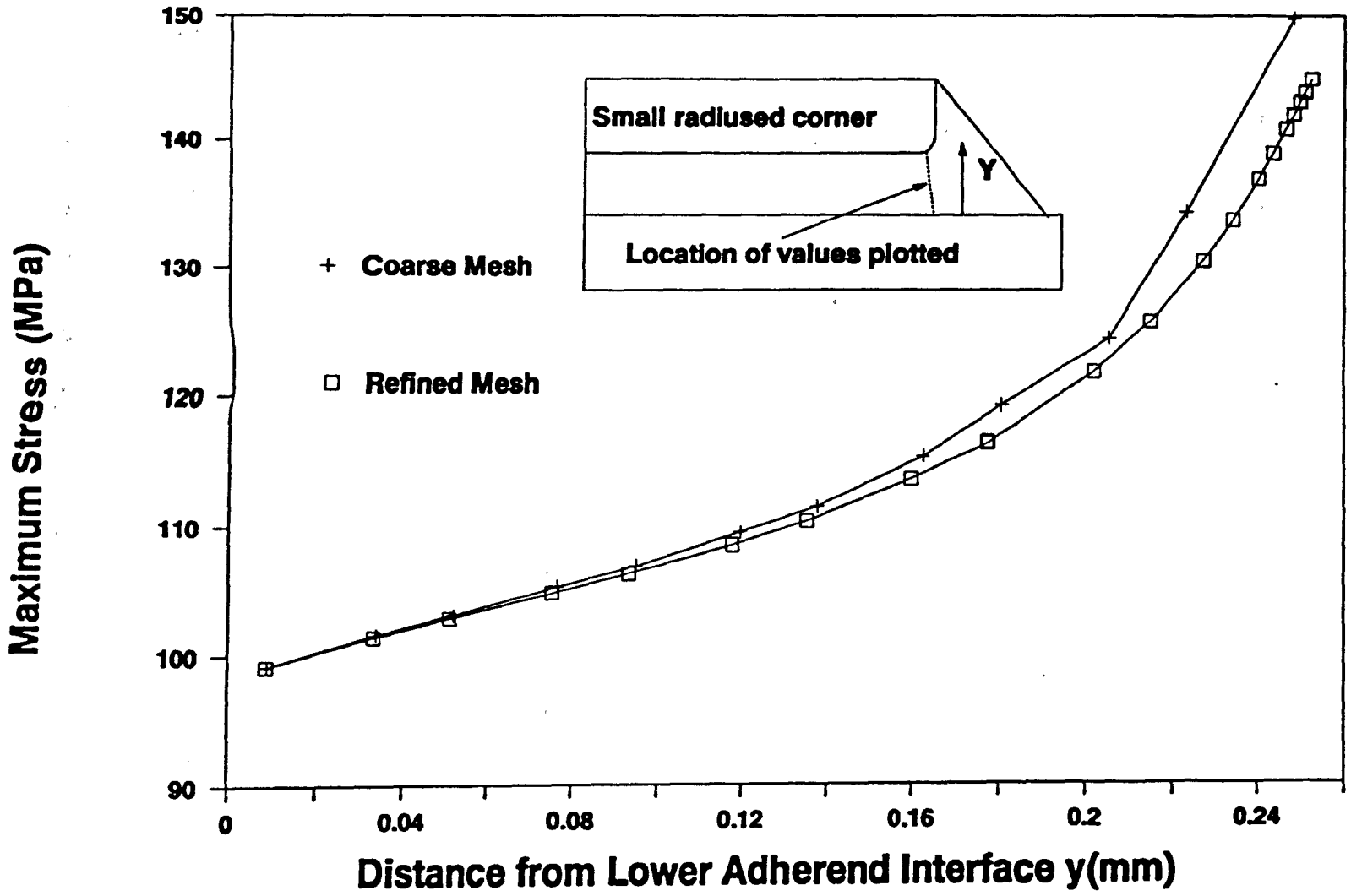

Fig. 7.18 Max. Principal Stress Comparison of Different Meshes

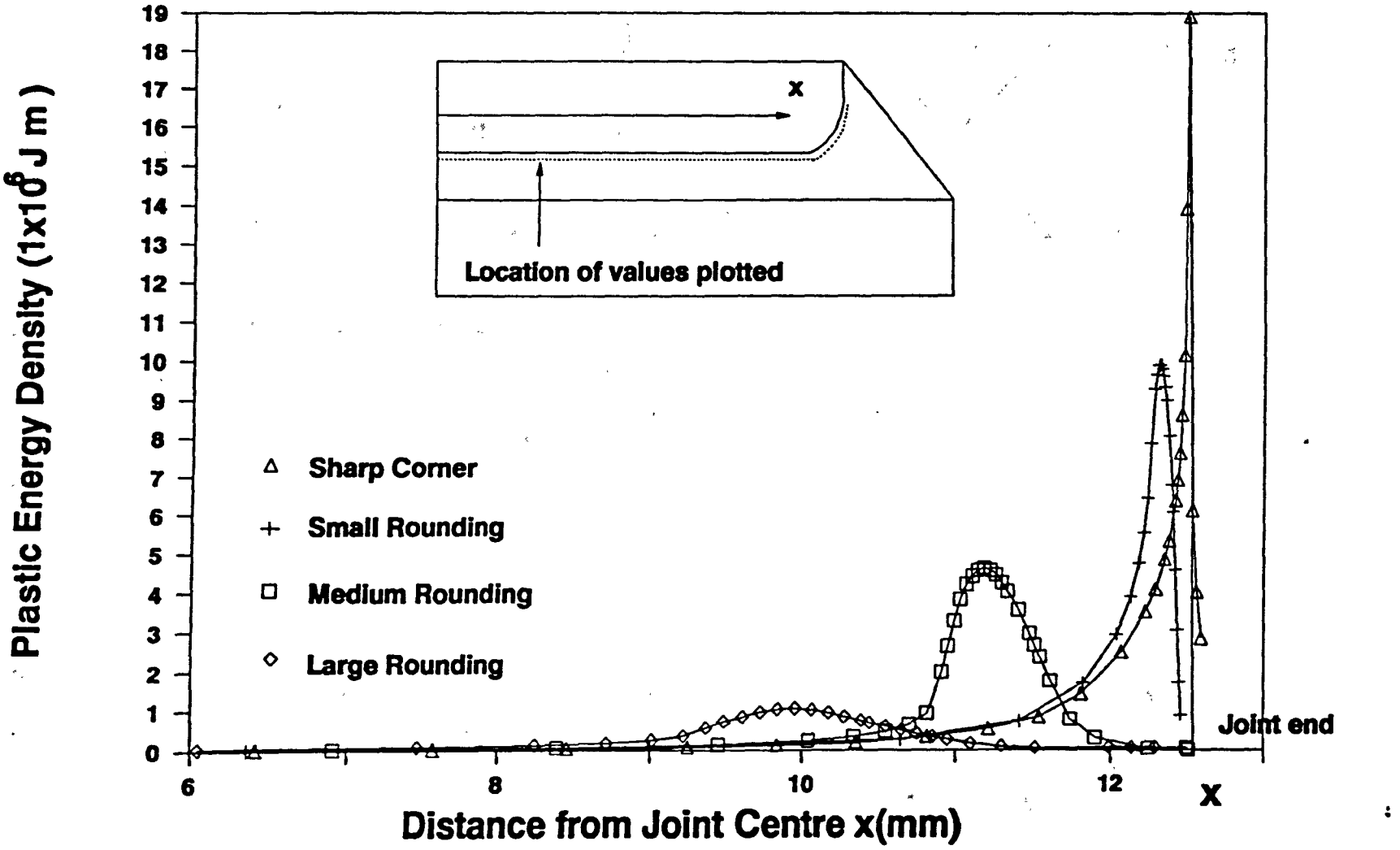

Fig. 7.19 Plastic Energy Density in the adhesive with a 20kN Load

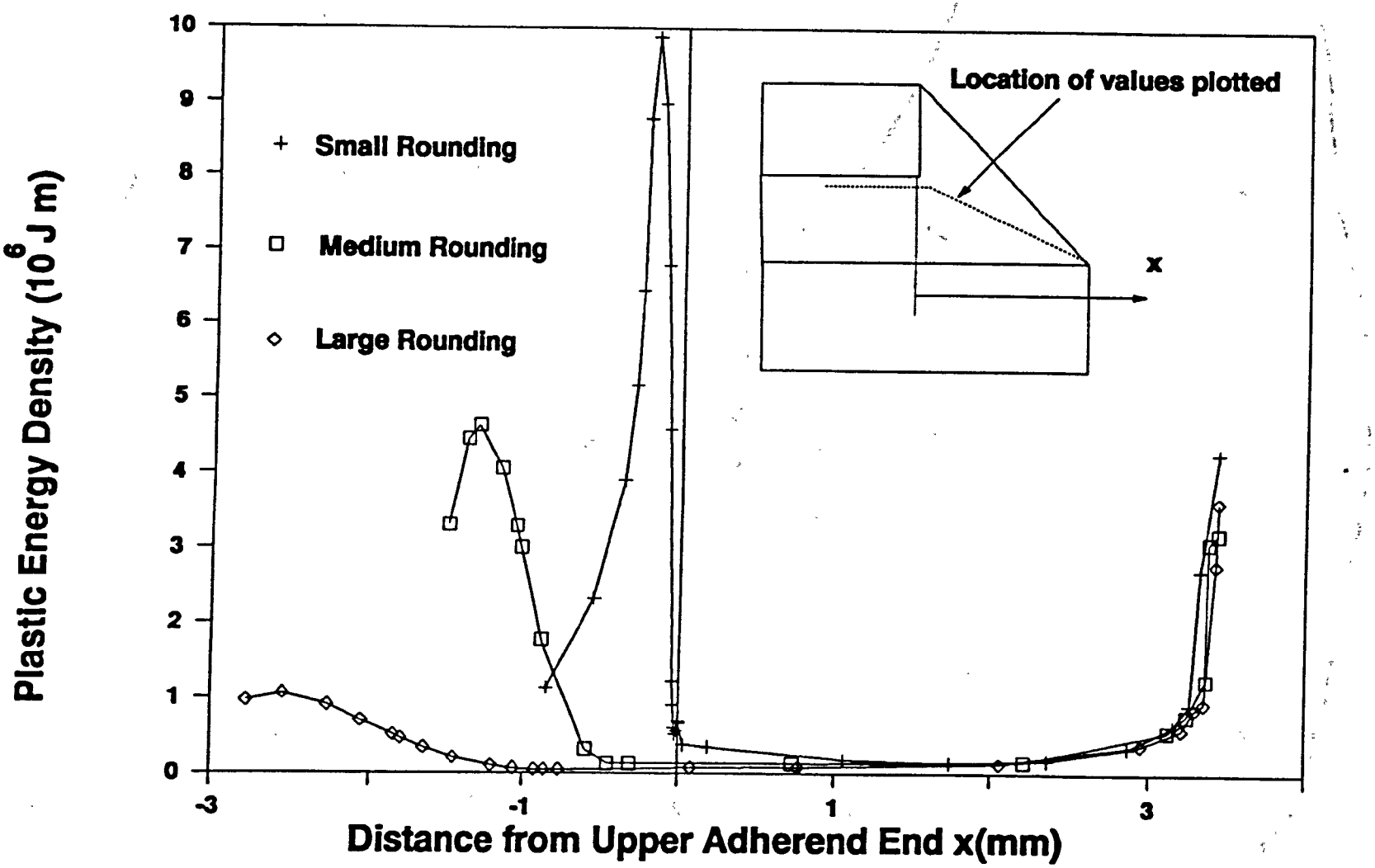

Fig. 7.20 Plastic Energy Density Comparison inside Spew Fillet

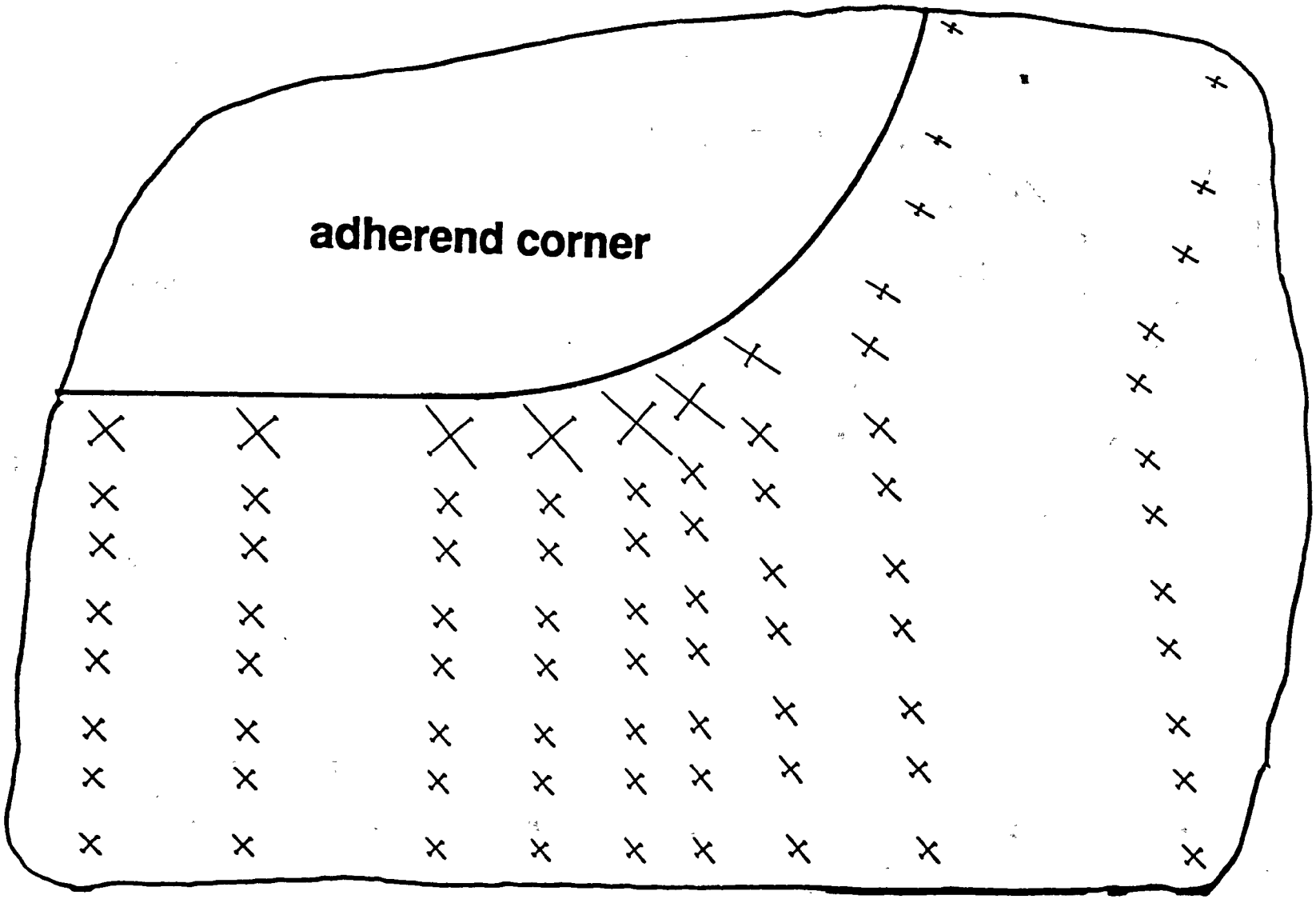

Fig. 7.21 The pattern of the principal strains in the adhesive around the small rounded adherend corner

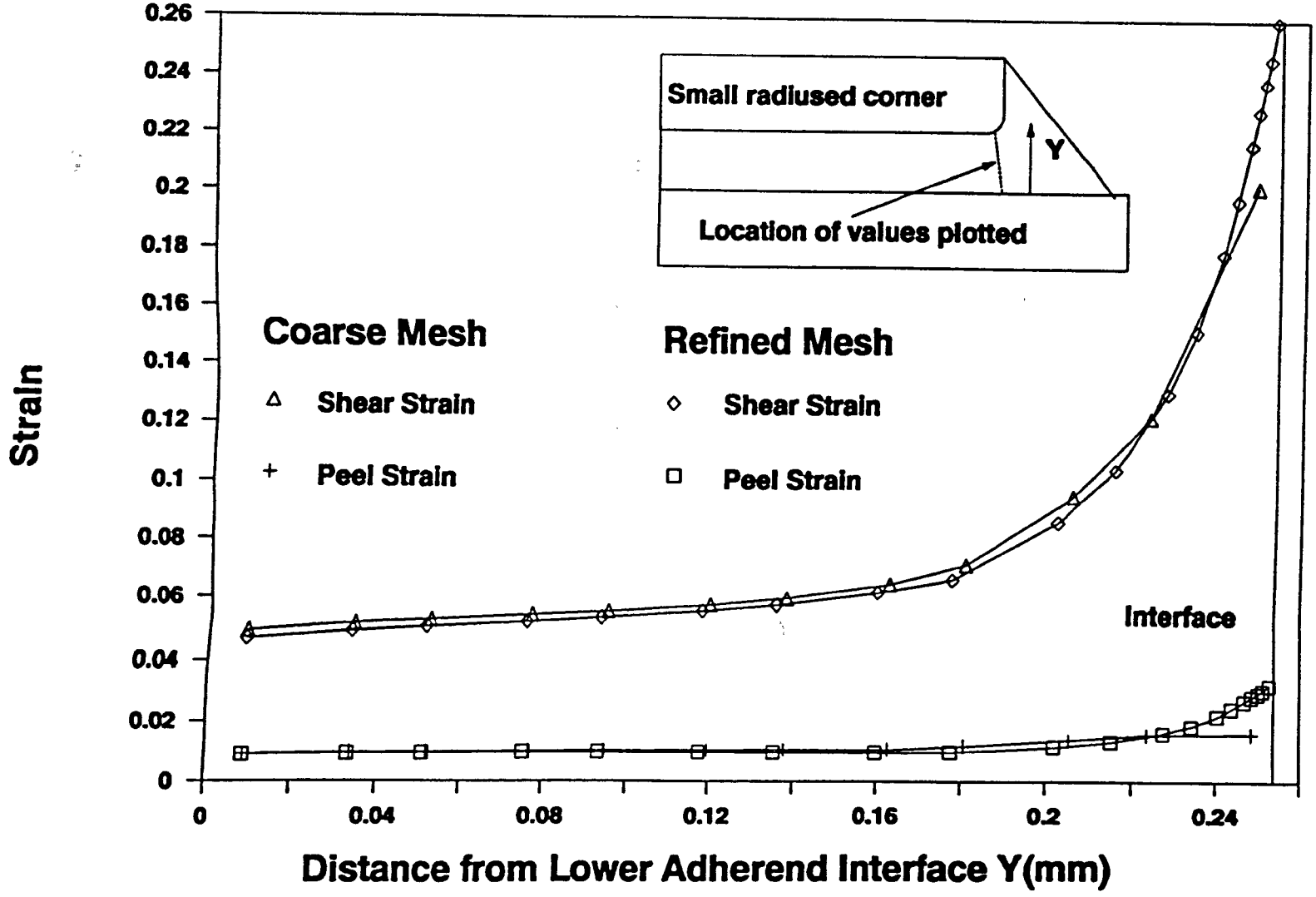

Fig. 7.22 Strains Comparison of Different Meshes

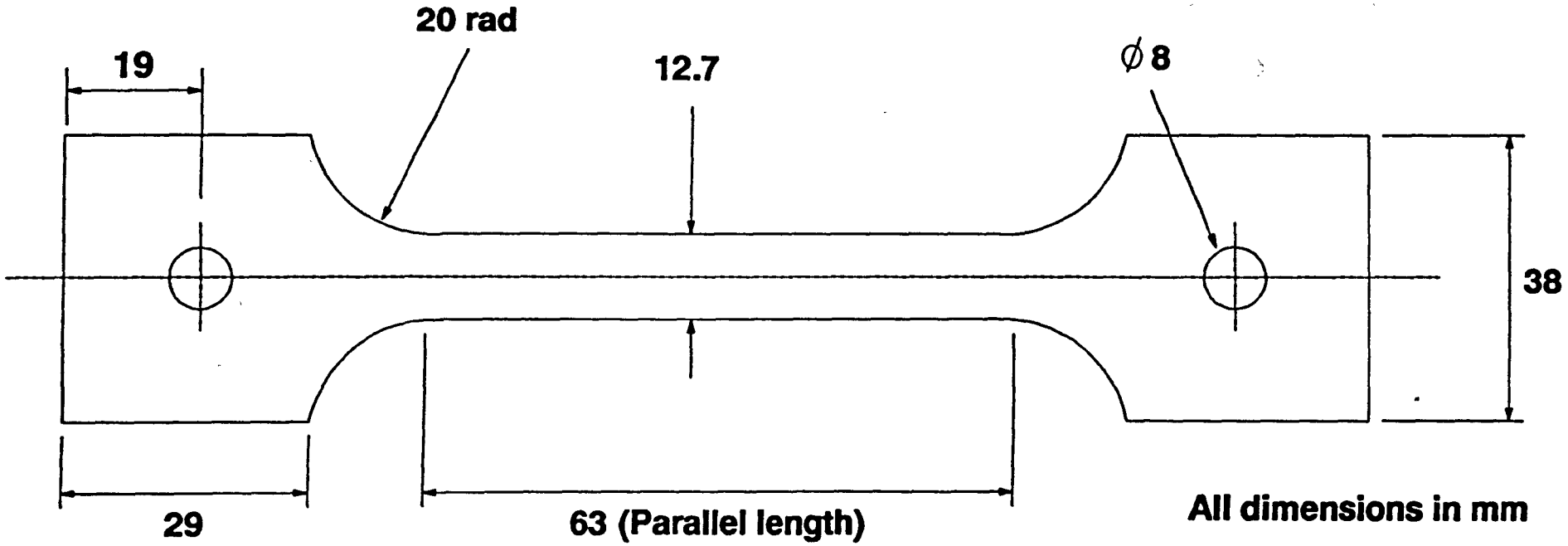

Fig. 8.1 Dimensions of aluminium tensile test specimen

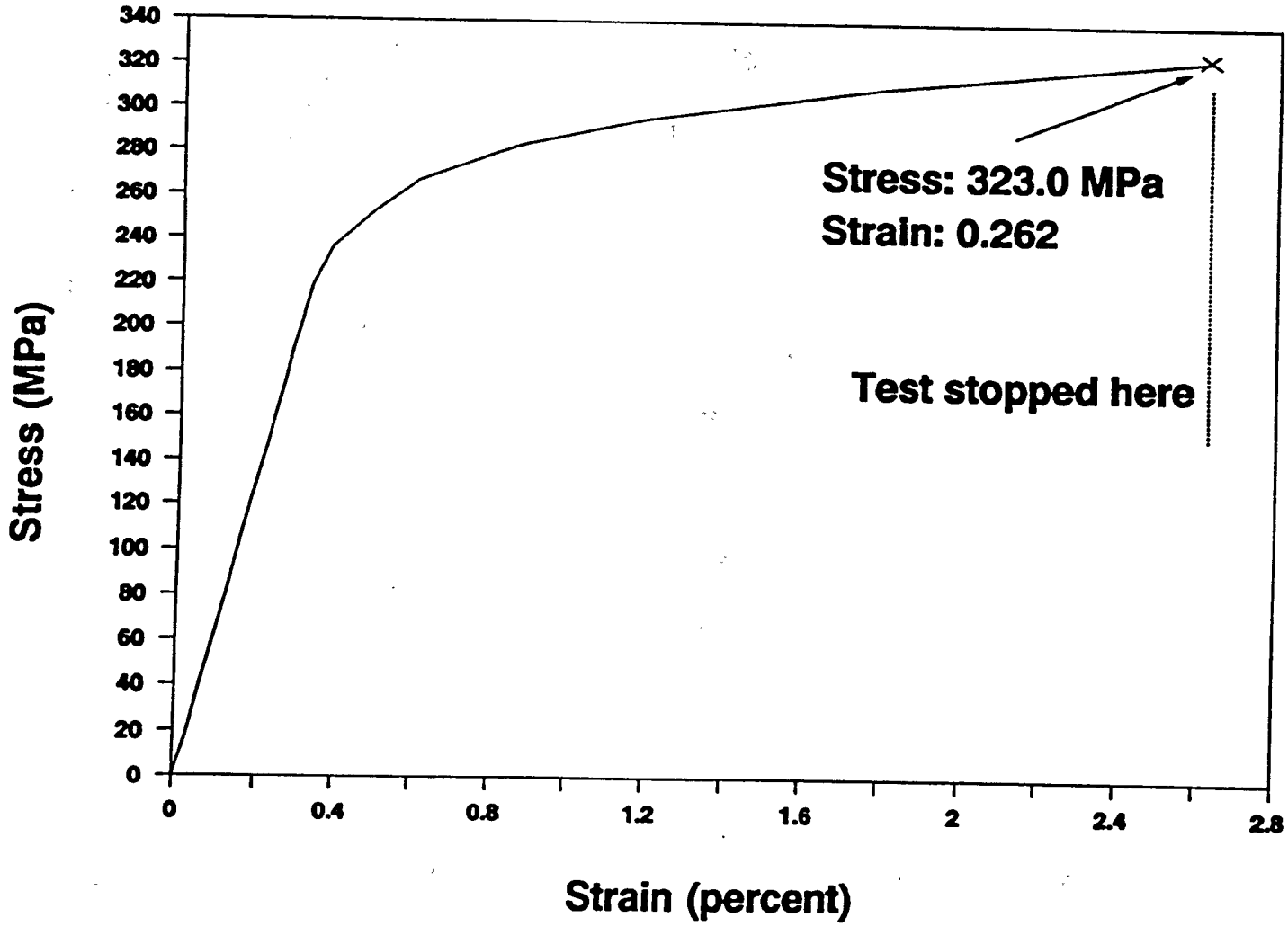

Fig. 8.2 Uniaxial tensile stress-strain curve for aluminium adherends

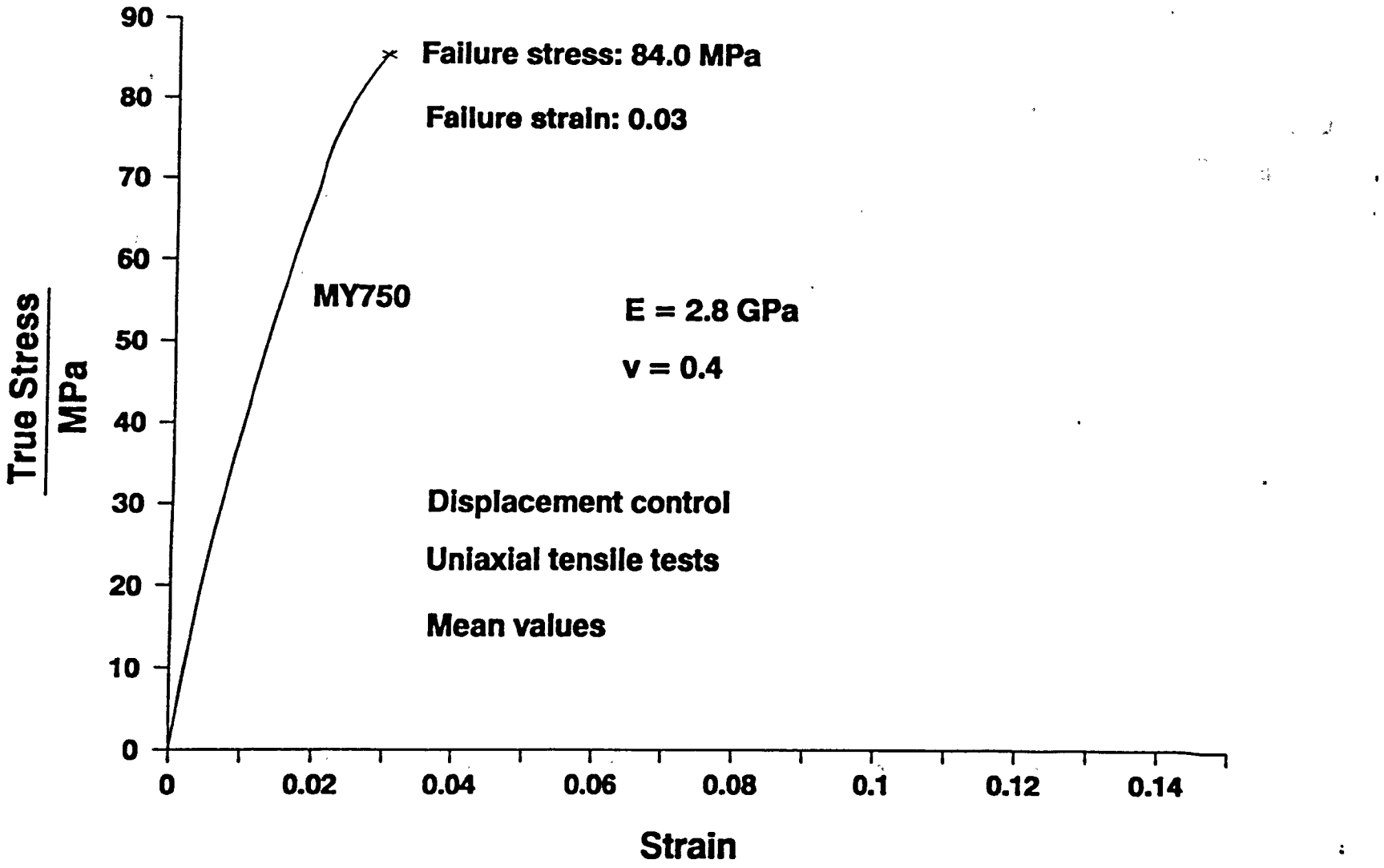

Fig. 8.3 Stress-strain data of MY750 with hardener HY906 from Harris(1985)

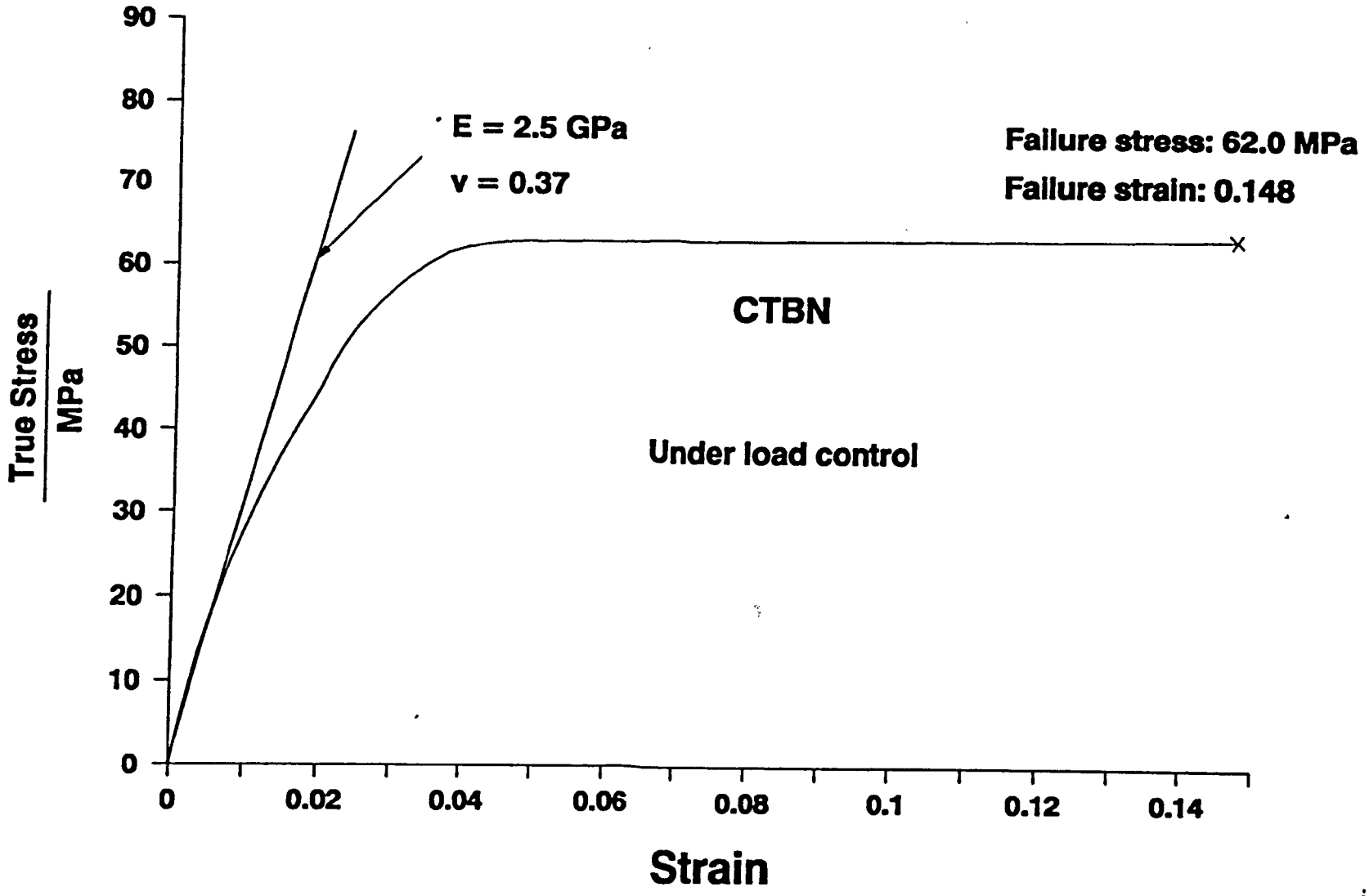

Fig. 8.4 Uniaxial tensile stress-strain data of CTBN from Harris(1985)

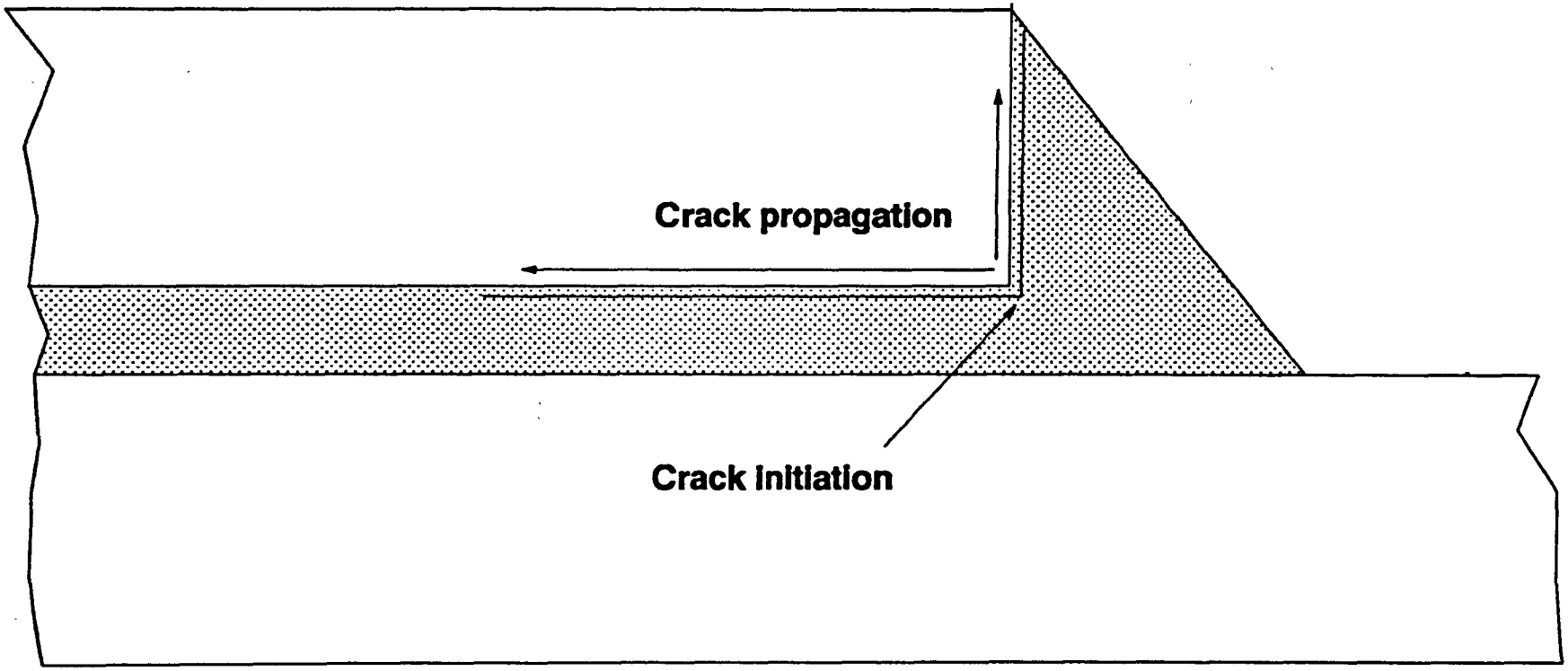

Fig. 8.5 Failure mode of a single lap joint under fatigue load

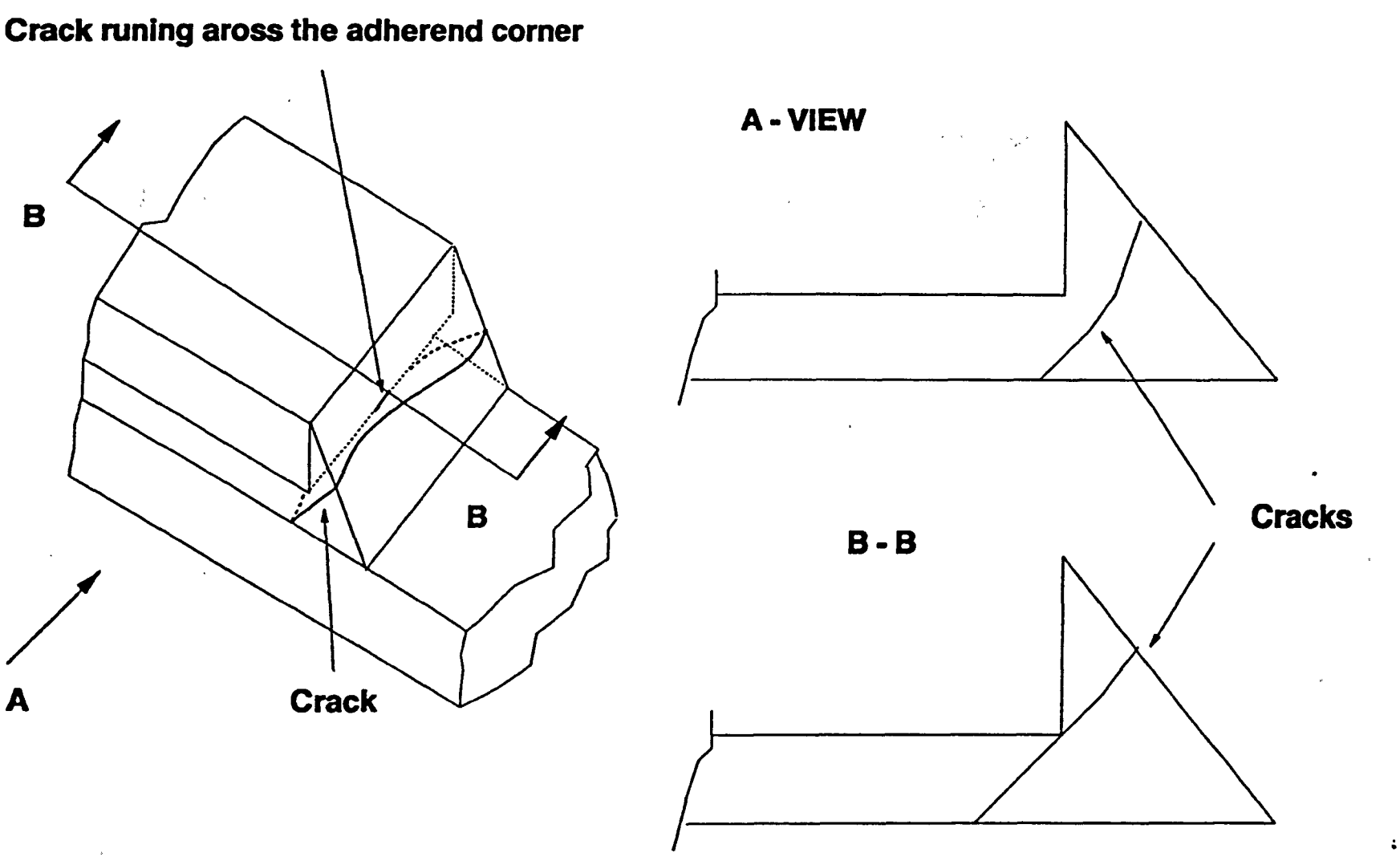

Fig. 8.6 A typical crack shape for a double lap joint

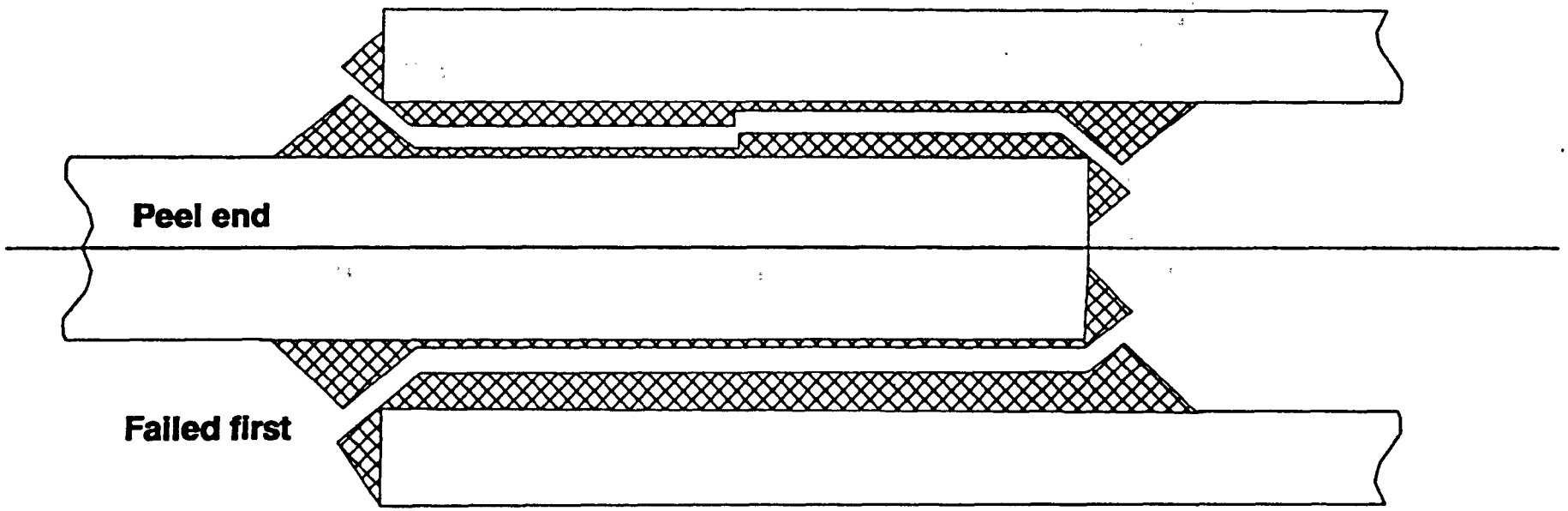

Fig. 8.7 Diagram of failure mode of a double lap joint along overlap

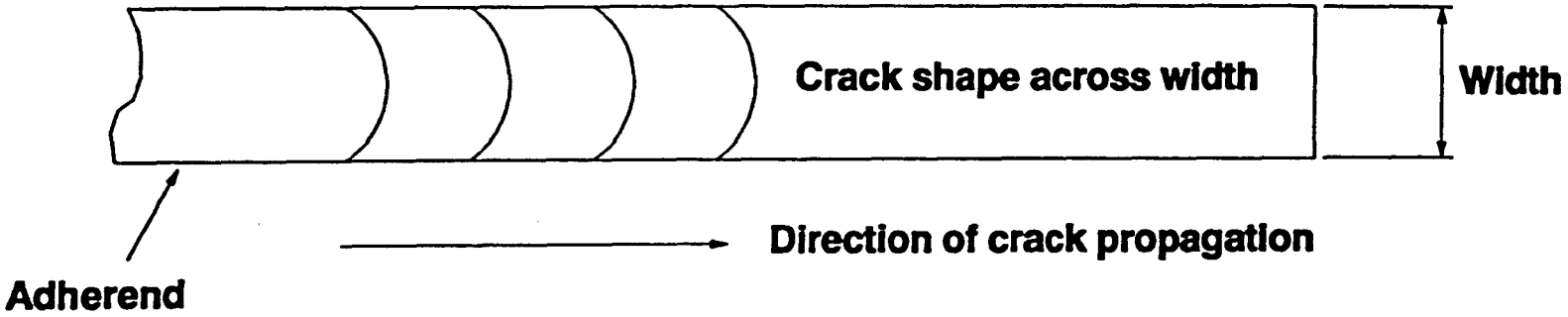

Fig. 8.8 Diagram of crack shape across width

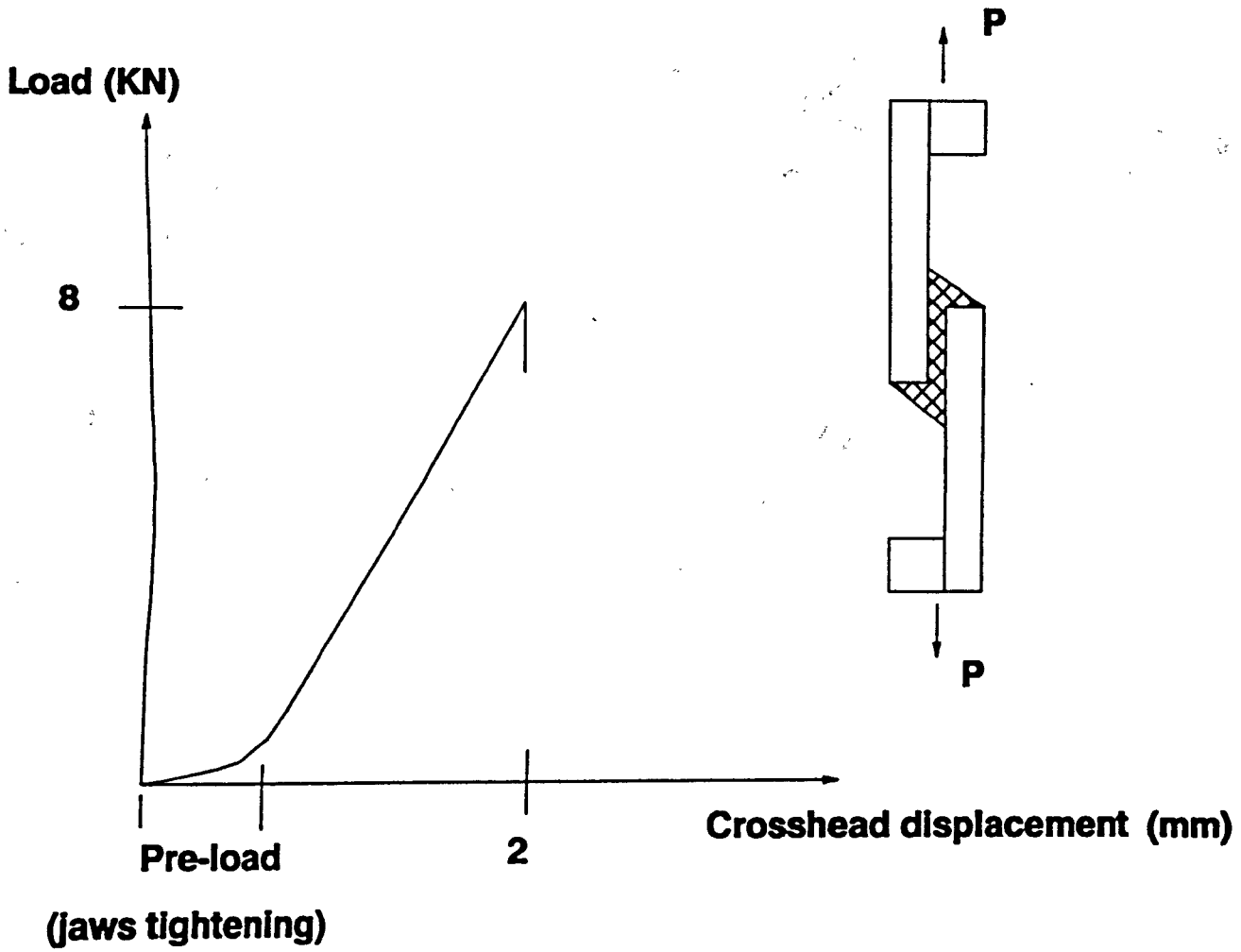

Fig. 8.9 Load versus cross-head curve for a single lap joint with MY750

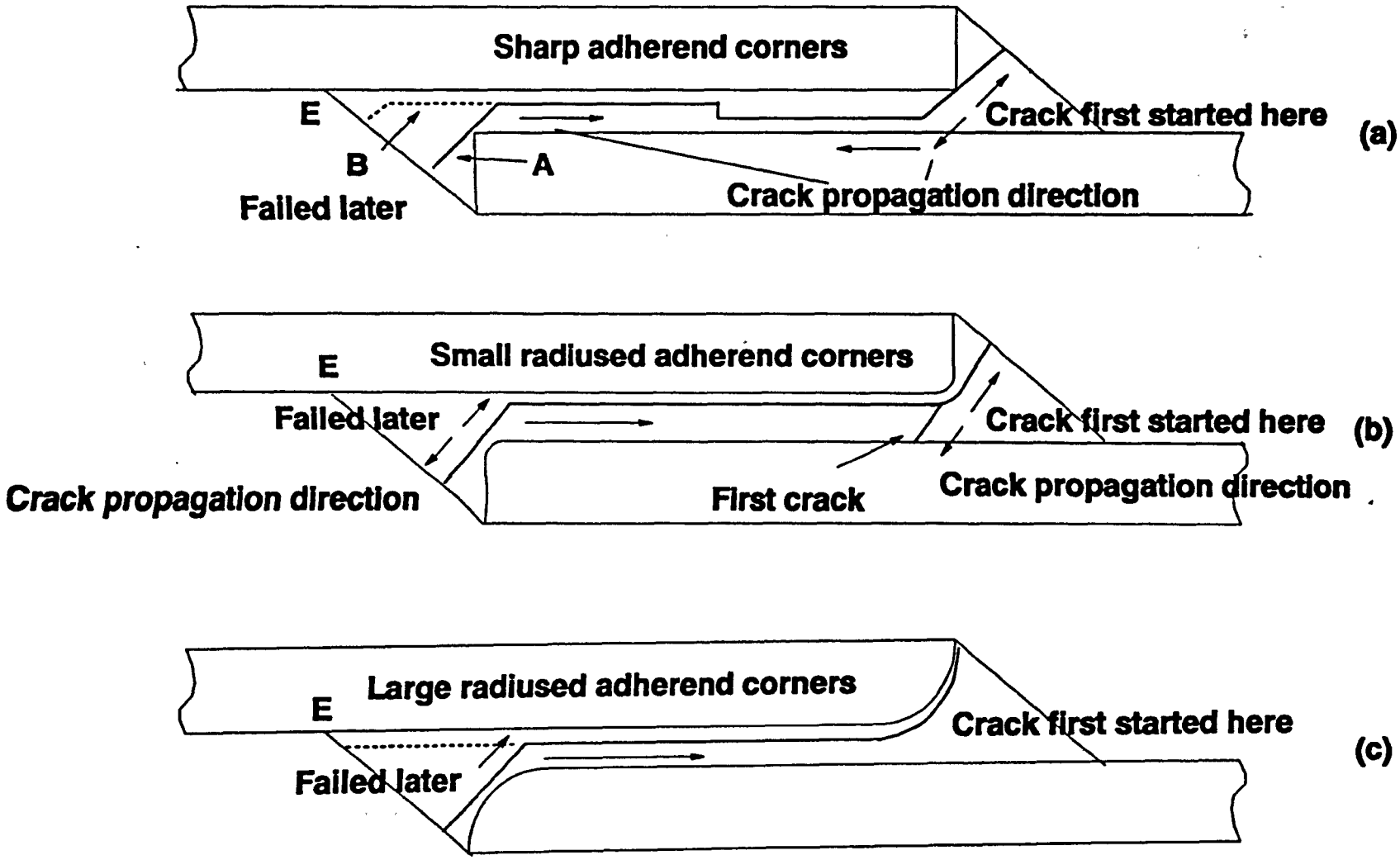

Fig. 8.10 Failure modes of single lap joints

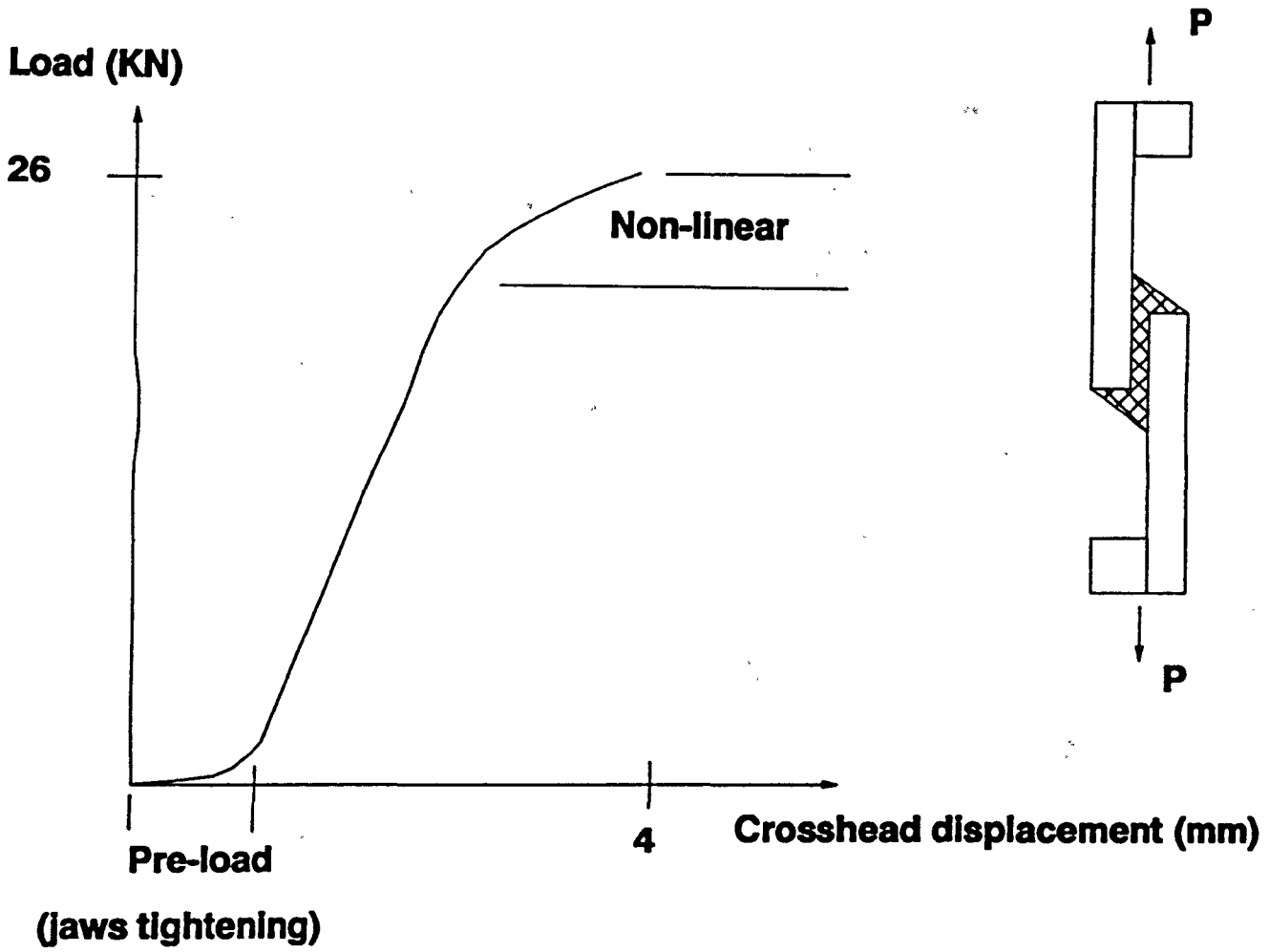

Fig. 8.11 Load versus crosshead curve for a single lap joint with CTBN

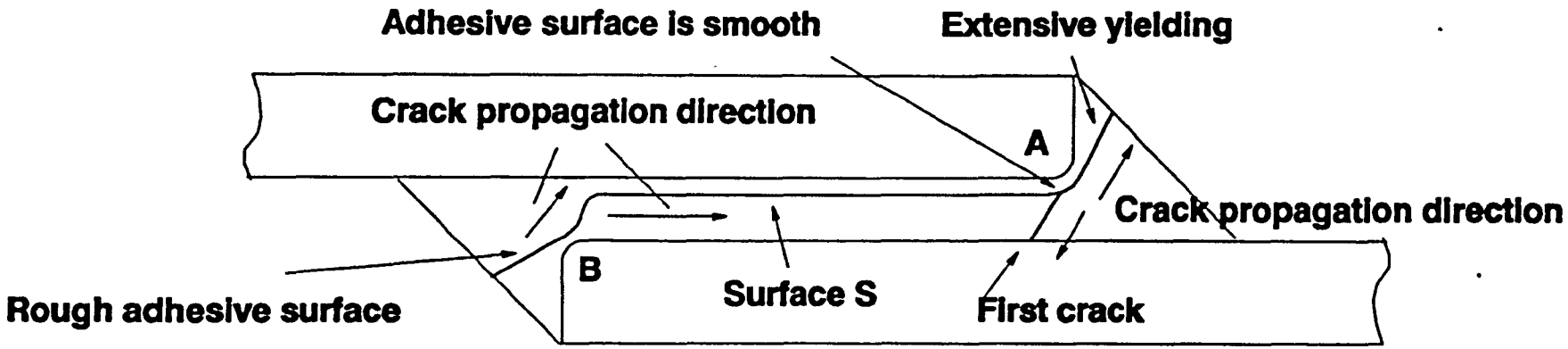

(a) Sharp or small rounded corners

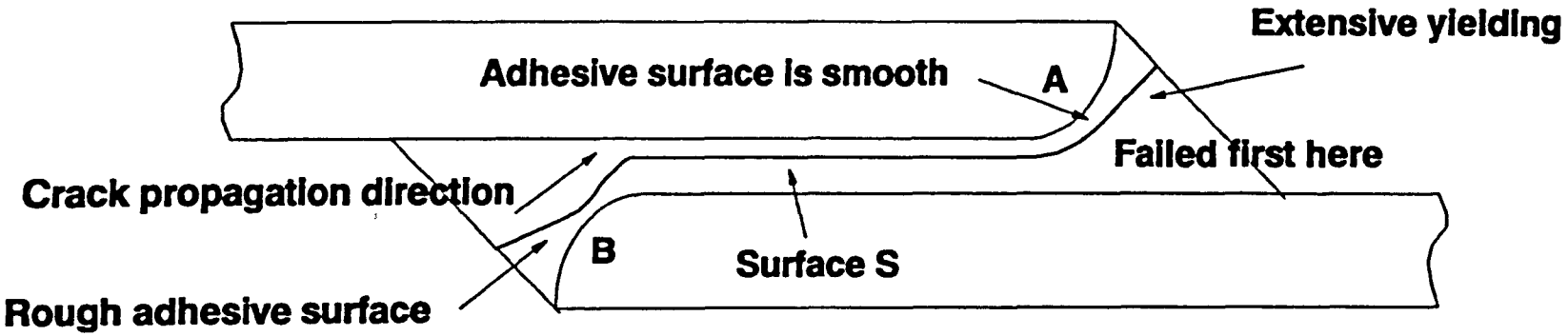

(b) Medium or large rounded corners

Fig. 8.12 Failure modes of single lap joints with CTBN

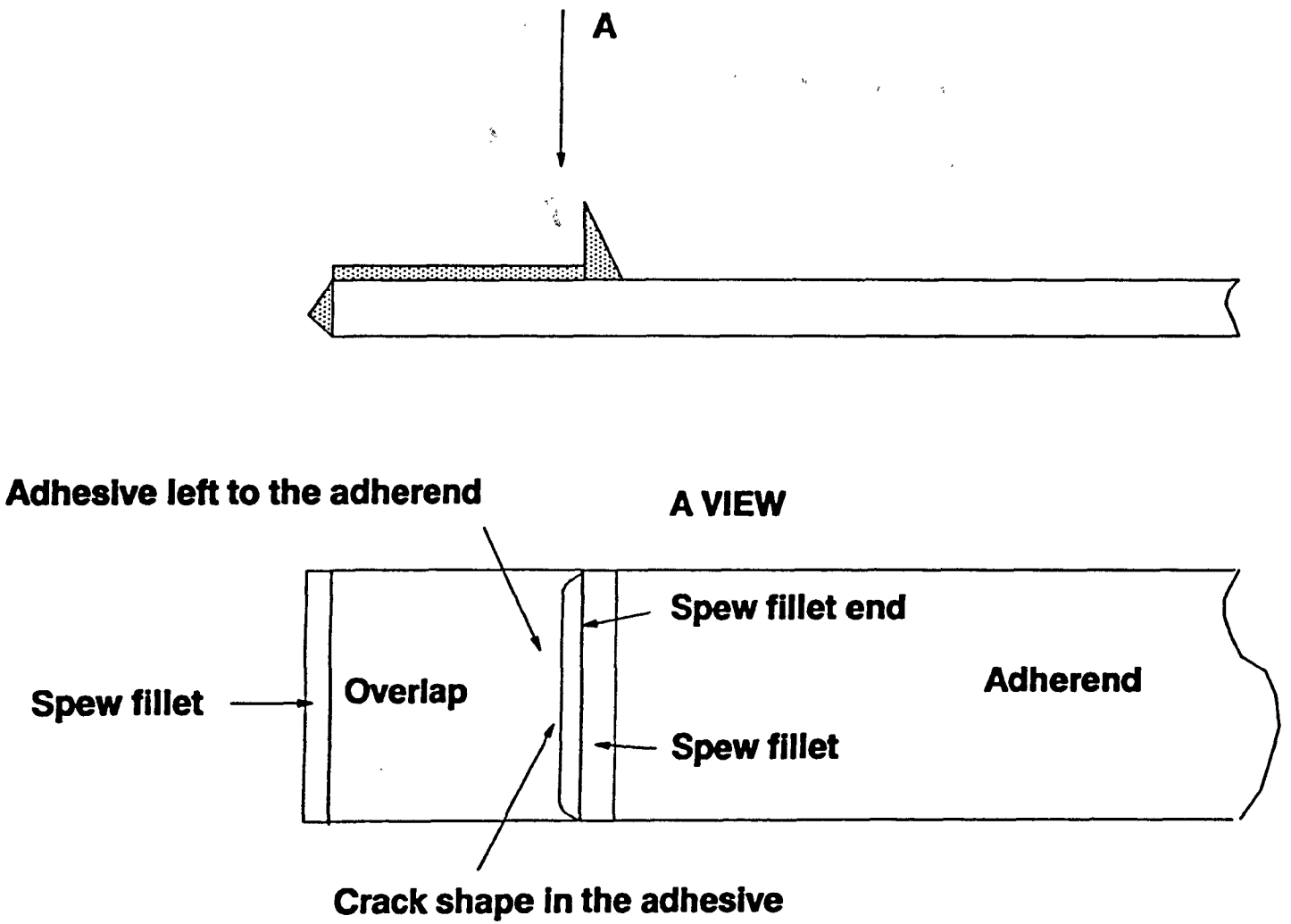

Fig. 8.13 Crack shape across the joint width

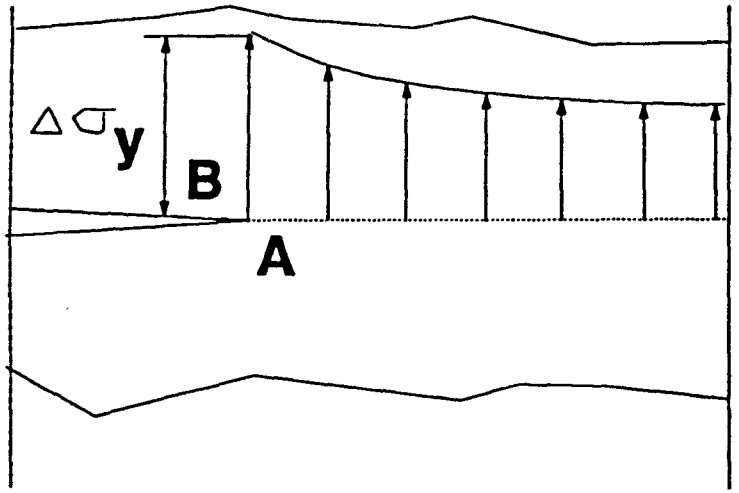

Fig. 9.1a Stress discontinuity around a crack tip

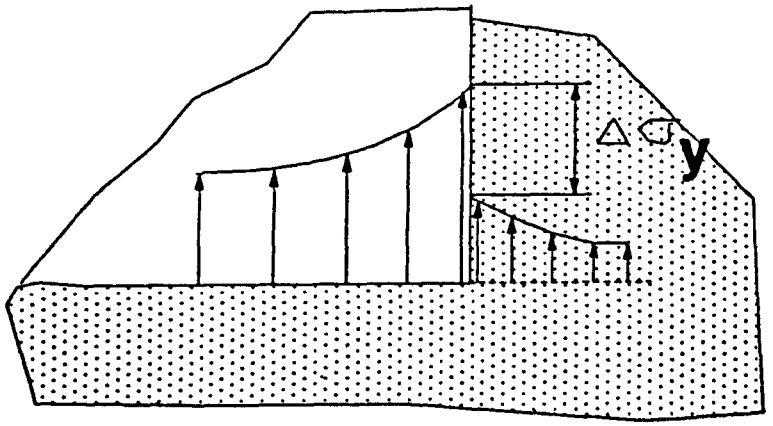

Fig. 9.1b Stress discontinuity around re-entrant corner